

SMALL MOLECULES TO FACILITATE  
CHEMOTHERAPEUTIC DELIVERY

by

Gregory Allen Ellis

A dissertation submitted in partial fulfillment  
of the requirements for the degree of

Doctor of Philosophy  
(Biochemistry)

at the  
UNIVERSITY OF WISCONSIN–MADISON  
2011

SMALL MOLECULES TO FACILITATE  
CHEMOTHERAPEUTIC DELIVERY

submitted to the Graduate School of the  
University of Wisconsin-Madison  
in partial fulfillment of the requirements for the  
degree of Doctor of Philosophy

By

Gregory A. Ellis

Date of final oral examination: October 13, 2011

Month and year degree to be awarded: December 2011

The dissertation is approved by the following members of the Final Oral Committee:

Ronald T. Raines, Professor, Biochemistry and Chemistry

M. Thomas Record, Professor, Biochemistry and Chemistry

Michael R. Sussman, Professor, Biochemistry

John M. Denu, Professor, Biomolecular Chemistry

Samuel H. Gellman, Professor, Chemistry

# SMALL MOLECULES TO FACILITATE CHEMOTHERAPEUTIC DELIVERY

Gregory Allen Ellis

Under the supervision of Professor Ronald T. Raines

at the University of Wisconsin–Madison

The landscape of therapeutics, in particular cancer chemotherapeutics, is limited by ineffective cellular delivery. Controlled and efficient cellular drug delivery involves several stages: first, accumulation of active drug near the cell; second, association with the cell surface; third, internalization into the cell; and fourth, translocation into the cytosol. Not surprisingly, cellular delivery of small-molecule chemotherapeutics, and especially biologic chemotherapeutics, is challenging. Therefore, additional understanding of and strategies to improve chemotherapeutic delivery are desperately needed. This thesis aims to investigate the stages of cellular chemotherapeutic delivery with small molecules, all focused around a ribonuclease model system.

CHAPTER 1 serves as an introduction to cellular drug delivery, the pancreatic-type ribonuclease superfamily, and how members of this superfamily can act as a model system to study and improve drug delivery.

Seeking to optimize the first stage of cellular drug delivery, CHAPTER 2 reports on the attachment of a timed-release ribonucleoside 3'-phosphate pro-moiety to a chemotherapeutic to control accumulation of active drug near a cell. The human pancreatic ribonuclease was used to release an active chemotherapeutic, 4-hydroxytamoxifen, from a pro-moiety, uridine-3'-phosphate, over time. The timed-release of a chemotherapeutic could modulate the near-toxic spikes and near-ineffective troughs normally seen in active drug plasma concentration, leading to safer and more efficacious delivery of chemotherapeutics.

To facilitate the second and third stages of cellular drug delivery, CHAPTER 3 reports on the use of pendant boronic acids to mediate protein association with the cell surface and subsequent internalization into mammalian cells. Boronic acids readily form boronate esters with saccharides, including those on the cell surface. Boronic acids were attached to bovine pancreatic ribonuclease, endowing the ribonuclease with increased affinity for saccharides and enhanced cellular internalization. Notably, this method is distinct from previous methods for enhancing protein cellular delivery.

To enhance the fourth stage of cellular drug delivery, CHAPTER 4 discusses the use of a poly(amidoamine) (PAMAM) dendrimer *in trans* to potentiate the cytotoxicity of bovine pancreatic ribonuclease variants by increasing their translocation into the cytosol after endocytosis. This method differs from previous studies by using the dendrimer as a co-treatment instead of covalently increasing ribonuclease cationicity, thereby lessening destabilizing and inactivating effects. Although this strategy is unlikely to be clinically

useful, it adds to the understanding of how to enhance this inefficient stage of cellular drug delivery.

CHAPTER 5 discusses future directions for additional research, all focused on the pancreatic-type ribonuclease model system. APPENDIX 1 discusses the identification of a small-molecule antagonist of the interaction between a bovine pancreatic ribonuclease variant and the human ribonuclease inhibitor protein. APPENDIX 2 discusses the creation of a ribonuclease zymogen activated by urokinase in efforts to endow this ribonuclease variant with augmented selective toxicity for cancer cells. Together, this thesis describes progress towards understanding and facilitating chemotherapeutic delivery through the use of small molecules.

## Acknowledgments

I would like to express my deepest gratitude to everyone who has provided me guidance and assistance throughout my graduate career. First, I am grateful to my advisor, Professor Ron Raines. His enthusiasm was a major contributor in my decision to pursue graduate studies at UW–Madison. I thank him for his professionalism and for the guidance, insight, and assistance he has provided.

I am grateful for the helpful advice of my thesis committee: Professors Tom Record, Mike Sussman, John Denu, and Sam Gellman. I am thankful for my collaborators at the UW Small Molecule Screening Facility, especially Noël Peters for her kindness, guidance, and extensive knowledge. I also thank Dr. Darrell McCaslin, for his assistance and insightful discussions in the Biophysics Instrumentation Facility, and Professor Aseem Ansari for his friendliness and advice. I also appreciated the mentorship of my undergraduate advisor at the University of Notre Dame, Professor Seth Brown. I am very fortunate to have worked in his lab and to get to know him and his family.

Many individuals in the Raines laboratory have provided invaluable assistance and friendship. I am thankful to those who helped me at the beginning of my graduate career, including Tom Rutkoski, Frank Kotch, Jeremy Johnson, Bryan Smith, Eugene Lee, Steve Fuchs, Jeet Kalia, and Luke Lavis. I also had the privilege to work alongside: John Lukesh, Christine Bradford, Amit Choudhary, Chelcie Eller, Sean Johnston, Mike Levine, Joelle Lomax, Nadia Sundlass, Langdon Martin, Greg Jakubczak, Joe Binder, Cindy Chao, Kelly Gorres, Matt Shoulders, Annie Tam, Rebecca Turcotte, Matt Allen,

Margie Borra, Daniel Gottlieb, Katrina Jensen, Eddie Myers, Moushumi Paul, Lauren Carroll, Nicole McElfresh, Mariëlle Delville, Kristen Andersen, Trish Hoang, Rob Presler, Jim Vasta, Ho-Hsuan Chou, Kevin Desai, Caglar Tanrikulu, and Brett VanVeller. Mentoring Megan Hornung was very rewarding, and she always entered lab with a bright perspective. Rex Watkins and Sayani Chattopadhyay were my “baymates” and great sounding boards. I had fruitful collaborations with Nick McGrath and Mike Palte for which I am very thankful. I am exceptionally grateful to Mike Palte and Ben Caes for their friendship and support both inside and outside of lab.

I am grateful to my friends outside of lab, who have been a constant source of support and laughter. These include Nick Wheeler, Chad Clark, Matt Cook, Mike Miranda, Dave Dean, Rachael Sheridan, and the brothers of Benjamin Franklin Lodge #83.

I cannot express how grateful I am to my parents, Marie and John Ellis, and my brother Brian Ellis. I have always been able to count on their love, support, and encouragement, and for that I consider myself very lucky and blessed. I hope that I can live up to the model my parents have been to me.

Last, and most importantly, I am eternally grateful to my fiancée, Nicole Beauchene. Her love, encouragement, patience, support, and her uncanny ability to make me smile no matter what are absolutely amazing and a constant blessing. I feel lucky and thankful to have gotten to know her parents, Joyce and Dennis Beauchene, as well as her brother, Justin Beauchene. I look forward every day to spending the rest of my life with Nicole, my best friend.

## Table of Contents

Abstract .....	i
Acknowledgments.....	iv
List of Tables .....	xiv
List of Schemes.....	xv
List of Figures .....	xvi
List of Abbreviations .....	xix
CHAPTER 1	
Introduction: Small Molecules to Facilitate Chemotherapeutic Delivery .....	1
1.1 Overview .....	2
1.2 Pancreatic-type Ribonucleases as Model Proteins.....	4
1.3 Pancreatic-type Ribonucleases as Model Biologic Chemotherapeutics .....	7
1.4 Cellular Delivery is Essential for the Model Ribonuclease Chemotherapeutic System.....	10
1.5 Small Molecules to Facilitate Chemotherapeutic Delivery .....	14
1.5.1 Modification of drug for timed-release drug delivery .....	14
1.5.2 Increased cell association and internalization of a model biologic chemotherapeutic .....	16
1.5.3 Enhanced cytotoxicity of a model biologic chemotherapeutic .....	17
1.6 Additional Delivery Methods .....	19



1.6.1 Small-molecule inhibitors of RI–ribonuclease interaction .....	19
1.6.2 Engineering a ribonuclease zymogen activated by urokinase for selective toxicity .....	20
1.7 Prospectus .....	22

## CHAPTER 2

Ribonuclease-Activated Cancer Prodrug .....	32
2.1 Abstract .....	33
2.2 Introduction .....	33
2.3 Results and Discussion .....	36
2.4 Conclusions .....	37
2.5 Experimental Procedures .....	39
2.5.1 Materials .....	39
2.5.2 Instrumentation and statistical calculations .....	40
2.5.3 Determination of partition and distribution coefficients .....	40
2.5.4 Cell cultures .....	41
2.5.5 Recombinant protein production .....	41
2.5.6 Fluorescent assay for ribonuclease activity .....	41
2.5.7 HPLC assay for ribonuclease activity on uridine-3'-(4- hydroxytamoxifen phosphate) .....	42
2.5.8 Cell-proliferation assays .....	44
2.5.9 Syntheses .....	45

2.5.9.1. Protected uridine 3'-(4-Hydroxytamoxifen phosphate).....	45
2.5.9.2. DMT-free, semi-protected uridine 3'-(4-hydroxytamoxifen phosphate).....	46
2.5.9.3. Uridine 3'-(4-Hydroxytamoxifen phosphate).....	47
2.5.10 NMR spectra.....	48
2.5.10.1. 400 MHz $^1\text{H}$ NMR spectrum of 4-Hydroxytamoxifen phosphate in $\text{CD}_3\text{OD}$ .....	49
2.5.10.2. 101 MHz $^{13}\text{C}$ NMR spectrum of 4-Hydroxytamoxifen phosphate in $\text{CD}_3\text{OD}$ .....	50
2.5.10.3. 162 MHz $^{31}\text{P}$ NMR spectrum of 4-Hydroxytamoxifen phosphate in $\text{CD}_3\text{OD}$ .....	51
2.5.10.4. 400 MHz $^1\text{H}$ NMR spectrum of DMT-free 4- Hydroxytamoxifen phosphate in $\text{CD}_3\text{OD}$ .....	52
2.5.10.5. 101 MHz $^{13}\text{C}$ NMR spectrum of DMT-free 4- Hydroxytamoxifen phosphate in $\text{CD}_3\text{OD}$ .....	53
2.5.10.6. 162 MHz $^{31}\text{P}$ NMR spectrum of DMT-free 4- Hydroxytamoxifen phosphate in $\text{CD}_3\text{OD}$ .....	54
2.5.10.7. 400 MHz $^1\text{H}$ NMR spectrum of 4-Hydroxytamoxifen prodrug in $\text{CD}_3\text{OD}$ .....	55
2.5.10.8. 101 MHz $^{13}\text{C}$ NMR spectrum of 4-Hydroxytamoxifen prodrug in $\text{CD}_3\text{OD}$ .....	56

2.5.10.9. 162 MHz $^{31}\text{P}$ NMR spectrum of 4-Hydroxytamoxifen prodrug in $\text{CD}_3\text{OD}$ .....	57
2.6 Acknowledgments.....	58
2.7 Contributions.....	58

## CHAPTER 3

Boronate-mediated Drug Delivery.....	69
3.1 Abstract .....	70
3.2 Introduction.....	70
3.3 Results and Discussion .....	71
3.4 Conclusions.....	74
3.5 Experimental Procedures .....	75
3.5.1 Materials .....	75
3.5.2 Analytical instruments and statistical calculations .....	76
3.5.3 Determination of $K_a$ values by $^1\text{H}$ NMR spectroscopy.....	77
3.5.3.1. Representative procedure for making a boronic acid solution .....	80
3.5.3.2. Determination of the value of $K_a$ for PBA and fructose.....	80
3.5.3.3. Representative procedure for determining the chemical shifts of aryl protons in bound and free boronic acids .....	80
3.5.3.4. Determination of the value of $K_a$ for benzoboroxole and fructose.....	81
3.5.3.5. Determination of the value of $K_a$ for PBA and glucose .....	81

3.5.3.6. Determination of the value of $K_d$ for benzoboroxole and glucose .....	82
3.5.3.7. Determination of the value of $K_d$ for PBA and Neu5Ac .....	82
3.5.3.8. Determination of the value of $K_d$ for benzoboroxole and Neu5Ac .....	83
3.5.4 Preparation of boronated RNase A .....	83
3.5.5 Preparation of inactivated, boronated RNase A.....	85
3.5.6 Preparation of BODIPY FL-labeled ribonucleases .....	86
3.5.7 Heparin-affinity assays .....	87
3.5.8 Fluorescence polarization assays .....	88
3.5.9 Cell culture.....	91
3.5.10 Flow cytometry assays.....	91
3.5.11 Confocal microscopy .....	92
3.5.12 Ribonucleolytic activity assays.....	92
3.5.13 Recombinant protein production .....	93
3.5.13 RI-RNase A competition assays .....	93
3.5.15 Ribonuclease evasion gel.....	95
3.5.16 Cell-proliferation assays .....	95
3.6 Acknowledgments.....	96
3.7 Contributions.....	97

## CHAPTER 4

Potential of Ribonuclease Cytotoxicity by a Poly(amidoamine) Dendrimer .....	132
4.1 Abstract .....	133
4.2 Introduction .....	133
4.3 Results and Discussion .....	136
4.4 Conclusions .....	138
4.5 Experimental Procedures .....	138
4.5.1 Materials .....	138
4.5.2 Analytical instruments and statistical calculations .....	139
4.5.3 Protein production .....	140
4.5.4 Conformational stability assay .....	141
4.5.5 Ribonucleolytic activity assay .....	141
4.5.6 RI-binding assay .....	142
4.5.7 Cell-proliferation assay .....	143
4.5.8 Flow cytometry assay .....	144
4.6 Acknowledgments .....	145
4.7 Contributions .....	145
4.8 Additions/Corrections .....	145

## CHAPTER 5

Future Directions .....	159
-------------------------	-----

5.1 Expanding the Repertoire and Use of Ribonucleotide Pro-moiety Timed-released Prodrugs .....	160
5.2 Further Investigations of Boronate-mediated Drug Delivery .....	161
5.3 Further Investigations of Poly(amidoamine) (PAMAM) Dendrimers.....	161
5.4 Future Ribonuclease-specific Investigations .....	162

## APPENDIX 1

Efforts Towards a Small Molecule Antagonist of the RI–Ribonuclease Interaction.....	164
A1.1 Abstract .....	165
A1.2 Introduction .....	165
A1.3 Results and Discussion.....	168
A1.4 Conclusions .....	175
A1.5 Experimental Procedures .....	175
A1.5.1 Materials .....	175
A1.5.2 Analytical instruments and statistical calculations .....	176
A1.5.3 High-throughput screening libraries .....	177
A1.5.4 Protein production.....	177
A1.5.5 High-throughput screening assay.....	178
A1.5.6 $K_d$ value determination.....	178
A1.5.7 Cell-proliferation assay.....	179
A1.6 Acknowledgements .....	180
A1.7 Contributions.....	181

## APPENDIX 2

### Engineering a Ribonuclease Zymogen Activated by Urokinase for Selective Toxicity 194

A2.1 Abstract .....	195
A2.2 Introduction .....	195
A2.3 Results and Discussion.....	199
A2.4 Conclusions .....	200
A2.5 Ribonuclease Constructs Necessitating Additional Engineering.....	201
A2.6 Experimental Procedures .....	203
A2.6.1 Materials .....	203
A2.6.2 Analytical instruments and statistical calculations .....	204
A2.6.3 Design of zymogens.....	204
A2.6.4 Protein production.....	205
A2.6.5 Activation of RNase A zymogen by urokinase.....	205
A2.5.6 Ribonucleolytic activity assay .....	206
A2.6.7 Cell-proliferation assay.....	207
A2.7 Acknowledgments.....	208
A2.8 Contributions.....	208

## REFERENCES

List of References .....	220
--------------------------	-----

## List of Tables

Table 1.1: Amino-acid sequence alignment of selected pancreatic-type ribonuclease superfamily members.....	23
Table 1.2: Sequence identity/similarity of selected pancreatic-type ribonuclease superfamily members.....	24
Table 1.3: Selected conjugations to enhance RNase A and RNase 1 cellular delivery...	25
Table 2.1: Partition and distribution coefficients of HT and UpHT.....	59
Table 3.1: Values of $K_a$ ( $M^{-1}$ ) for boronic acids and saccharides. ....	98
Table 3.2: Literature values of $K_a$ ( $M^{-1}$ ) for boronic acids and saccharides. ....	99
Table 4.1: Effect of dendrimers on RNase A thermostability, catalytic activity, and cellular internalization. ....	147
Table A2.1: Catalytic efficiency of RNase A zymogen activated by urokinase. ....	208



## List of Schemes

Scheme 2.1: Synthesis of UpHT.....	60
Scheme 3.1: Boronation of RNase A and its putative mechanism for expediting cellular delivery. ....	100

## List of Figures

Figure 1.1: Stages of cellular drug delivery.....	26
Figure 1.2: Selected members of the pancreatic-type ribonuclease superfamily.....	28
Figure 1.3: Putative mechanism of ribonuclease cytotoxicity.....	30
Figure 2.1: Activation of prodrug by RNase 1. ....	61
Figure 2.2: Compilation of HPLC traces from representative UpHT activation experiment.....	63
Figure 2.3: Progress curve of UpHT activation by RNase 1. ....	65
Figure 2.4: MCF-7 cell proliferation upon UpHT activation by RNase 1.....	67
Figure 3.1: Boronate-mediated drug delivery.....	101
Figure 3.2: MALDI-TOF spectrum of unmodified and boronated RNase A. ....	103
Figure 3.3: Elution profile of a mixture of unmodified and boronated RNase A from a column of immobilized heparin. ....	105
Figure 3.4: Fluorescence polarization/anisotropy assay of ribonucleases binding ganglioside-labeled liposomes.....	107
Figure 3.5: Fluorescence polarization/anisotropy data for the binding of boronated RNase A to GD3 ganglioside in liposomes. ....	109
Figure 3.6: Internalization of unmodified and boronated RNase A into Pro-5 and Lec-2 cells.....	111
Figure 3.7: Boronated RNase A evasion of ribonuclease inhibitor protein.....	113

Figure 3.8: Inhibition of K-562 cell proliferation by unmodified and boronated RNase A.....	115
Figure 3.9: Determination of the peaks corresponding to the aryl protons in bound and free boronic acid and example of the $^1\text{H}$ NMR spectrum that was used to determine the $K_a$ value for PBA and fructose.....	117
Figure 3.10: Example of the $^1\text{H}$ NMR spectrum that was used to determine the $K_a$ value for benzoboroxole and fructose.....	119
Figure 3.11: Example of the $^1\text{H}$ NMR spectrum that was used to determine the $K_a$ value for PBA and glucose. ....	121
Figure 3.12: Example of the $^1\text{H}$ NMR spectrum that was used to determine the $K_a$ value for benzoboroxole and glucose. ....	123
Figure 3.13: Example of the $^1\text{H}$ NMR spectrum that was used to determine the $K_a$ value for PBA and Neu5Ac. ....	125
Figure 3.14: Small overlapping peak in Neu5Ac $^1\text{H}$ NMR spectrum.....	127
Figure 3.15: Example of the $^1\text{H}$ NMR spectrum that was used to determine the $K_a$ value for benzoboroxole and Neu5Ac. ....	129
Figure 4.1: The toxicity of a cationic ribonuclease for cancer cells is increased by co-treatment with a cationic dendrimer. ....	148
Figure 4.2: Electrostatic potential map of the RNase A surface.....	150
Figure 4.3: Structure of the generation 2 poly(amidoamine) (PAMAM) dendrimer. ....	152
Figure 4.4: Binding of the ribonuclease inhibitor protein to the generation 2 PAMAM dendrimer. ....	154

Figure 4.5: Effect of generation 2 PAMAM dendrimer on the inhibition of cancer	
cell proliferation by ribonucleases. ....	156
Figure A1.1: Putative mechanism of ribonuclease cytotoxicity. ....	181
Figure A1.2: Determination of the $K_d$ value of KDRNG88C-DEF RNase A for RI. ....	183
Figure A1.3: Development of a high-throughput RI–RNase A binding assay. ....	185
Figure A1.4: Results of the Known Bioactives Library screen. ....	187
Figure A1.5: Determination of the $K_d$ value of triprolidine for inhibiting the	
interaction of KDRNG88C-DEF RNase A with RI. ....	189
Figure A1.6: Investigations of whether triprolidine and G88R RNase A are	
synergistically cytotoxic. ....	191
Figure A2.1: Urokinase and uPAR pathway. ....	209
Figure A2.2: Construction of RNase A zymogen activated by urokinase. ....	211
Figure A2.3: Activation of RNase A zymogen by urokinase <i>in vitro</i> . ....	213
Figure A2.4: Extent of Activation of RNase A zymogen by urokinase <i>in vitro</i> and <i>in</i>	
<i>cellulo</i> . ....	215
Figure A2.5: Construction of genes for other RNase A zymogens and ACPD RNase	
A. ....	217

## List of Abbreviations

$\epsilon$	extinction coefficient
5-IAF	5-iodoacetamidofluorescein
6-FAM	6-carboxyfluorescein
6-TAMRA	6-carboxytetramethylrhodamine
A	adenosine
$A$	anisotropy
$A_B$	anisotropy of bound species
$A_F$	anisotropy of free species
$A_{OBS}$	anisotropy observed (sample)
ADEPT	antibody-directed enzyme prodrug therapy
ADME	absorption, distribution, metabolism, and excretion
Ala or A	alanine
ALS	amyotrophic lateral sclerosis, Lou Gehrig's disease
ANG	angiogenin
Arg or R	arginine
Asp or D	aspartate or aspartic acid
ATCC	American Type Culture Collection
B	boronic acid
BCA	bicinchoninic acid
Benzoboroxole	2-hydroxymethylphenylboronic acid

BSA	bovine serum albumin
BS-RNase	bovine seminal ribonuclease
ca.	circa, approximately
cDNA	complementary deoxyribonucleic acid
CHO	Chinese hamster ovary
CPP	cell-penetrating peptide
d	day
Da	Dalton
ddH <sub>2</sub> O	distilled, deionized water
DCM	dichloromethane
DEPC	diethylpyrocarbonate
DEF	2',7'-diethylfluorescein
DEFIA	2',7'-diethylfluorescein-5-iodoacetamide
DMEM	Dulbecco's modified Eagle's medium
DMF	dimethylformamide
DMSO	dimethylsulfoxide
DNA	deoxyribonucleic acid
DOPC	1,2-dioleoyl- <i>sn</i> -glycero-3-phosphocholine
DPBS	Dulbecco's phosphate-buffered saline
DRNG RNase A	D38R/R39D/N67R/G88R variant of RNase A
DTNB	5,5'-dithiobis(2-nitrobenzoic acid)
DTT	dithiothreitol

E	enzyme
ECP	eosinophilic cationic protein; RNase 3
EDC	<i>N</i> -(3-dimethylaminopropyl)- <i>N'</i> -ethylcarbodiimide hydrochloride
EDN	eosinophil-derived neurotoxin; RNase 2
EDTA	ethylenediaminetetraacetic acid
<i>F</i>	fluorescence
<i>F</i> <sub>SB</sub>	fraction bound
FACS	fluorescence-activated cell sorting
FBS	fetal bovine serum
FDA	United States Food and Drug Administration
FPLC	fast performance liquid chromatography
FRET	Förster resonance energy transfer
GFP	green fluorescent protein
Glu or E	glutamate or glutamic acid
Gly or G	glycine
GSH	reduced glutathione
GSSH	oxidized glutathione
h	hour
HCl	hydrochloric acid
HEPES	2[4-(2-hydroxyethyl)-1-piperazinyl]ethanesulfonic acid
His, H	histidine
HIV	human immunodeficiency virus

HPLC	high performance (pressure) liquid chromatography
HSPG	heparan sulfate proteoglycan
HT	4-hydroxytamoxifen
HTS	high-throughput screen(ing)
I	inhibitor
IC <sub>50</sub>	half maximal inhibitory concentration
IPTG	isoproyl-1-thio-β-D-galactopyranoside
$k_{\text{cat}}$	first-order enzymatic rate constant
$K_{\text{d}}$	equilibrium dissociation constant
kDa	kilodalton
KDRNG RNase A	K31A/D38R/R39D/N67R/G88R variant of RNase A
$K_{\text{i}}$	inhibitor dissociation constant
$K_{\text{M}}$	Michaelis constant
$\lambda_{\text{em}}$	emission wavelength
$\lambda_{\text{ex}}$	excitation wavelength
LB	Luria–Bertani medium
logD	distribution coefficient
logP	partition coefficient
Lys, K	Lysine
MALDI–TOF	matrix-assisted laser desorption/ionization time-of-flight
MEM	minimum essential medium
MeOH	methanol



MES	2-(N-morpholino)-ethanesulfonic acid
Met or M	methionine
MHz	megahertz
microRNA	micro ribonucleic acid
min	minute
MMP	matrix metalloprotease
mRNA	messenger ribonucleic acid
MW	molecular weight
MWCO	molecular weight cutoff
NaCl	sodium chloride
NaOH	sodium hydroxide
NBS	non-binding surface
Neu5Ac	<i>N</i> -acetylneuraminic acid
NMR	nuclear magnetic resonance
OD	optical density
ONC	Onconase®; ranpirnase; P-30; Pannon
OVS	oligo(vinylsulfonic acid)
<i>p</i> value	probability value
PAMAM	poly(amidoamine)
PBA	phenylboronic acid
PBS	phosphate-buffered saline
PCR	polymerase chain reaction

PDB	protein data bank
PEG	poly(ethylene glycol)
$pI$	isoelectric point
$pK_a$	log of the acid dissociation constant
PMSF	phenylmethane sulfonyl fluoride
PPI	protein–protein interaction
pRI	porcine ribonuclease inhibitor
pro-uPa	pro-urokinase-type plasmogen activator
PTD	protein transduction domains; cell-penetrating peptide
$Q$	ratio of fluorescence intensities of bound and free species
R <sub>9</sub> , Arg <sub>9</sub>	nonaarginine
RGD	arginine-glycine-aspartate tripeptide
Rh <sub>110</sub>	rhodamine 110
RI	ribonuclease inhibitor
RNA	ribonucleic acid
RNAi	ribonucleic acid interference
RNase A	bovine pancreatic ribonuclease
RNase 1	human pancreatic ribonuclease
RPMI	Roswell Park Memorial Institute medium
rRNA	ribosomal ribonucleic acid
S	saccharide
s	second

SDS-PAGE	sodium dodecyl sulfate polyacrylamide gel electrophoresis
Ser or S	serine
SMSF	Small Molecule Screening Facility
STP	4-sulfo-2,3,5,6-tetrafluorophenol, sodium salt
<i>t</i>	time
TAT	residues 47–57 of the HIV-1 trans-activator of transcription
TB	terrific broth
$T_m$	temperature at the midpoint of the denaturation curve
TLC	thin-layer chromatography
THF	tetrahydrofuran
TML	trimethyl lock
TMS	tetramethylsilane
TNB	2-nitro-5-thiobenzoate
Tris	2-amino-2-(hydroxymethyl)-1,3-propanediol
U	uridine
U>p	uridine 2',3'-cyclic phosphate
Up	uridine 3'-phosphate
uPa, urokinase	urokinase-type plasminogen activator
UpHT	uridine 3'-(4-hydroxytamoxifen phosphate)
UV	ultraviolet
UW	University of Wisconsin
UWCCC	University of Wisconsin Carbone Cancer Center

v/v	volume per volume
w/v or wt/vol	weight per volume
<i>Z</i>	net molecular charge (Arg + Lys – Asp – Glu)

## **CHAPTER 1**

Introduction:

Small Molecules to Facilitate Chemotherapeutic Delivery

## 1.1 Overview

Drug delivery is an essential element to the success of therapeutics, especially cancer therapeutics (Gennaro, 2000; Wang, *et al.*, 2005a; Kratz, *et al.*, 2008; Rautio, *et al.*, 2008). Cancer therapeutics (i.e., chemotherapeutics) typically have narrow therapeutic indexes, or dosing windows between efficacy and toxic side effects, necessitating exquisite drug delivery (Gennaro, 2000; Wang, *et al.*, 2005a; Kratz, *et al.*, 2008; Rautio, *et al.*, 2008). The body contains several mechanisms to resist exposure to xenobiotics, including biological barriers, which drugs must bypass to reach their site of action (Wang, *et al.*, 2005a). Drug delivery will become even more crucial as new chemotherapeutics, including biologics, are progressively more complex and difficult to deliver (Wang, *et al.*, 2005a; Bildstein, *et al.*, 2011). Therefore, novel methods are desperately needed to enhance the delivery of current and future drugs.

Delivery of a systemically-administered drug initially depends on its absorption, distribution, metabolism, and excretion (ADME) pharmacokinetic properties (Gennaro, 2000). The drug is absorbed into the circulatory system either through the gastrointestinal tract following enteral administration (particularly difficult for biologics) (Gennaro, 2000; Malik, *et al.*, 2007) or directly absorbed following parenteral administration (Gennaro, 2000). After absorption, the plasma concentration of the drug is modulated by: its distribution throughout the circulatory system and other tissues (e.g., adipose); its metabolism (e.g., oxidation by cytochrome P450 enzymes); and its rate of excretion/clearance (Gennaro, 2000). Once systemically dispensed, an extracellular-acting drug may be directly accessible to its site of action.

Many drugs, however, require additional delivery and must be internalized into a cell (cellular delivery) for therapeutic efficacy (Torchilin, 2006). Examples include hormones such as

glucocorticoids for inflammation (Rawat, *et al.*, 2007), lysosomal enzymes for lysosomal storage diseases (Parkinson-Lawrence, *et al.*, 2010), proapoptotic and other chemotherapeutics for cancer, potential gene and RNAi therapies for multiple diseases, and many others (Torchilin, 2006; Rawat, *et al.*, 2007). Cellular delivery of these drugs consists of several stages (Figure 1.1). First, the drugs must accumulate near the cell in an active form. Second, the drugs must associate with the eukaryotic cell surface, comprised of a 5 nm thick, amphipathic plasma membrane (Lu and Oie, 2004) and up to a 500 nm thick glycocalyx consisting of a dense forest of polysaccharides (Vink and Duling, 1996; Varki, *et al.*, 2009). Association with the cell surface is non-trivial — the plasma membrane headgroups and the glycocalyx present a hydrophilic, anionic surface which may repel some drugs (Schultz, 2003; Varki, *et al.*, 2009). Third, the drugs must diffuse through the plasma membrane, be transported by membrane protein pumps, or be internalized into endosomes (Conner and Schmid, 2003; Lu and Oie, 2004). The ability of a molecule to diffuse across the plasma membrane is tightly restricted by size, polarity, charge, and hydration (Lu and Oie, 2004; Rawat, *et al.*, 2007), and membrane protein pumps are specific for essential small molecules (Conner and Schmid, 2003). Therefore, many drugs — especially biologics — must be transported into the cell by either general or receptor-mediated endocytosis (Conner and Schmid, 2003; Lu and Oie, 2004). This process involves the invagination and pinching-off of parts of the plasma membrane into vesicles called endosomes (Conner and Schmid, 2003). Fourth, drugs with cytosolic targets must be able to escape, or translocate, into the cytosol from the endosomes or from the lysosomes with which these endosomes fuse (Lu and Oie, 2004; Luzio, *et al.*, 2007; Rawat, *et al.*, 2007).

Not surprisingly, cytosolic delivery of a small-molecule drug is challenging, and with a biologic drug is formidably arduous. This is likely the reason that of the 41 large peptidic and protein biologics in the top 200 pharmaceutical products in 2009 by worldwide sales, only 1, Sandimmun (ciclosporin) acts cytosolically (3 short peptidic drugs — 2 HIV protease inhibitors and bortezomib — also work cytosolically) (Mack, *et al.*, 2009). Given the plethora of cytosolic drug targets, and the advances of our understanding and engineering of small-molecule and biologic drugs, we now stand poised to develop a multitude of disease treatments if only we could hurdle this barrier of cellular drug delivery. Therefore, we set out to develop innovative methods towards this goal, all centered around a model protein system.

## 1.2 Pancreatic-type Ribonucleases as Model Proteins

Bovine pancreatic ribonuclease (RNase A, EC 3.1.27.5) is the prototypical enzyme of the pancreatic-type ribonuclease superfamily (Raines, 1998). After its discovery in 1920 (Jones, 1920), RNase A became one of the most investigated enzymes of the last century, largely due to a research group at Armour, Inc., purifying over 1 kg of RNase A from leftover bovine pancreata and distributing the enzyme freely to scientists throughout the world (Raines, 1998). RNase A was used as a model enzyme for groundbreaking studies: it was the first enzyme reaction mechanism described (Findlay, *et al.*, 1961; Cuchillo, *et al.*, 2011), it was the first enzyme to have a correct amino acid sequence determined (Hirs, *et al.*, 1960; Smyth, *et al.*, 1963), the third enzyme X-ray structure determined (Karch, 1967), and the first enzyme total synthesis (Gutierrez and Merrifield, 1969; Merrifield, 1986). Researchers from several of these studies have been honored with a Nobel Prize, including Christian B. Anfinsen for studies on protein folding



(Anfinsen, 1973), Stanford Moore and William H. Stein for studies on the chemical structure of proteins (Moore and Stein, 1973), and Robert Bruce Merrifield for studies on solid-phase synthesis (Merrifield, 1986).

RNase A is a small (124 residues, 13.7 kDa), cationic ( $pI$  9.3,  $Z$  +4) (Ui, 1971) enzyme that hydrolyzes RNA with incredible catalytic efficiency; at low salt, this catalytic efficiency approaches the diffusion limit ( $>10^9 \text{ M}^{-1} \text{ s}^{-1}$ ) (Park and Raines, 2000). RNase A cleaves the  $\text{P-O}^{5'}$  bond of RNA with an overall rate enhancement of  $3 \times 10^{11}$  over the uncatalyzed reaction (Thompson, *et al.*, 1995; Raines, 1998). RNase A then hydrolyzes the  $\text{P-O}^{2'}$  bond of the resultant 2',3'-cyclic phosphodiester in a separate, slower reaction (Raines, 1998). For its dramatic catalytic efficiency, RNase A uses two active-site histidines (His12, His119) that act as a general acid/base for catalysis and one active-site lysine (Lys41) that stabilizes the transition state (Raines, 1998). For the cleavage of RNA, RNase A has well-established substrate specificity. RNase A is pyrimidine-specific for the nucleobase prior to the scissile bond; it catalyzes the cleavage of substrates in the following order: cytidine > uridine > adenosine > guanosine (Kelemen, *et al.*, 2000). Conversely, RNase A is purine-specific for the nucleobase following the scissile bond, catalyzing the cleavage of substrates with leaving groups in the following order: adenosine > guanosine > cytidine > uridine (Raines, 1998). While RNase A is sequence-specific for RNA substrates, it will also cleave non-natural substrates; for example, RNase A will cleave several uridine 3'-phosphate aryl esters with rates dependant on the  $pK_a$  of the leaving group (Davis, *et al.*, 1988), and it will cleave chromogenic substrates such as uridine 3'-(5-bromo-4-chloroindol-3-yl) phosphate (Wolf, *et al.*, 1968; Witmer, *et al.*, 1991; Raines, 1998).

In addition to its extreme catalytic efficiency, RNase A is also renowned for its significant stability, with a midpoint of the thermal denaturation curve ( $T_m$ ) of 63 °C (Leland, *et al.*, 1998). This is exemplified by its traditional purification from bovine pancreata, involving first 0.25 N sulfuric acid at 5 °C, then pH 3.0 at 95–100 °C (Kunitz and McDonald, 1953). RNase A is also resilient to proteolysis; incubation of a G88R variant of RNase A with proteinase K resulted in a half-life of over 5 hours, (Klink and Raines, 2000) and incubation of this variant *in cellulo* (K-562 cells) at 37 °C for 100 hours did not result in significant degradation in either cytosolic or lysosomal fractions (Leich, *et al.*, 2007).

While RNase A has been exceedingly well studied, thirteen homologues of RNase A have been identified in humans (Cho, *et al.*, 2005). These homologues (Table 1.1, Table 1.2) include: RNase 1 (human pancreatic ribonuclease), RNase 2 (eosinophil-derived neurotoxin or EDN), RNase 3 (eosinophil-cationic protein or ECP), RNase 4, RNase 5 (angiogenin or ANG), RNase 6, RNase 7, RNase 8, and RNases 9–13 which are less-well characterized (Cho, *et al.*, 2005; Rutkoski and Raines, 2008). RNase 1 is particularly similar to RNase A in terms of protein sequence identity (68%), size (128 residues, 14.6 kDa), charge ( $pI$  9.7,  $Z$  +6) (Cho, *et al.*, 2005), and overall tertiary structure (Johnson, *et al.*, 2007b).

Surprisingly, many of these homologues have special biological roles (Figure 1.2) orthogonal to digestion (Raines, 1998; Sorrentino, 2010). RNase 1 is released by vascular endothelial cells into the plasma and is ubiquitously expressed in several tissues (Weickmann, *et al.*, 1984; Su, *et al.*, 2004; Potenza, *et al.*, 2006; Sorrentino, 2010; Fischer, *et al.*, 2011). The presence of RNase 1 in plasma, coupled with data that implicates extracellular RNA in contributing to blood coagulation, has led to speculation that RNase 1 plays a role in vascular homeostasis (Fischer, *et*

*al.*, 2011). RNases 2 and 3 are released by eosinophils and are thought to have a role in host defense (Rothenberg and Hogan, 2006). This is supported by RNase 2 (EDN) having shown antiviral, alarmin (chemoattractant and activation of dendritic cells), and neurotoxic activities (Rosenberg, 2008), and RNase 3 (ECP) having shown bactericidal, helminthotoxic, antiviral, neurotoxic, and cytotoxic activities (Navarro, *et al.*, 2008; Chang, *et al.*, 2010). RNase 5 (ANG) is a very potent inducer of angiogenesis, and this is dependent on its ribonucleolytic activity (Shapiro, *et al.*, 1986; Tsuji, *et al.*, 2005). Additionally, RNase 5 has been implicated in familial amyotrophic lateral sclerosis (ALS), as RNase 5 gene mutations have been found in several patients (Greenway, *et al.*, 2006). Further, RNase 7 and RNase 8 have demonstrated antimicrobial activities (Zhang, *et al.*, 2003; Rudolph, *et al.*, 2006). Roles for the remaining ribonucleases (RNases 4, 6, 9–13) have yet to be elucidated (Sorrentino, 2010). The wealth of knowledge on RNase A and human pancreatic-type ribonucleases make these enzymes attractive model proteins for studying biologic processes such as drug delivery.

### **1.3 Pancreatic-type Ribonucleases as Model Biologic Chemotherapeutics**

Ribonucleases cleave RNA, molecules not only crucial for the transduction of genetic information as decreed in the central dogma (Voet and Voet, 2004), but also for protein/RNA structural complexes (e.g. ribosomes and spliceosomes) (Korostelev, *et al.*, 2006; Sashital, *et al.*, 2007) and regulatory processes (e.g. microRNAs) (Lagos-Quintana, *et al.*, 2001). Therefore, in the right context, ribonucleases can be extremely cytotoxic: RNase A microinjected into *Xenopus* oocytes is toxic at *picomolar* concentrations (Saxena, *et al.*, 1991). This toxicity has been exploited in the attempt to develop treatments for cancer since the 1950s, though only

recently has this started to show promise in clinical trials. The first attempts to use ribonucleases as chemotherapeutics demonstrated that wild-type RNase A could be toxic to tumors, but only when injected in milligram quantities directly into the tumor (Ledoux and Baltus, 1954; Ledoux, 1955b; Ledoux, 1955a; De Lamirande, 1961; Raines, 1998). A revival of interest in ribonucleases as chemotherapeutics came with the discovery of the anticancer activity of bovine-seminal ribonuclease (for information on bovine-seminal ribonuclease, see (D'Alessio, *et al.*, 1991; Kim, *et al.*, 1995a; Kim, *et al.*, 1995b; Matousek, *et al.*, 2003)) and of amphibian RNase A homologues, in particular one from the Northern leopard frog *Rana pipiens*, hence named Onconase® (ONC) (Shogen and Yoan, 1973; Ardelt, *et al.*, 1991; Lee and Raines, 2008).

RNase A and RNase 1 are similar to ONC (Table 1.1, Table 1.2, Figure 1.2), which has comparable size (104 residues, 11.8 kDa), charge ( $pI > 9.5$ ,  $Z +5$ ) (Ardelt, *et al.*, 1991), and tertiary structure (Mosimann, *et al.*, 1994). ONC is considerably more cytostatic and cytotoxic to cancer cell lines both *in vitro* and *in vivo* than RNase A or RNase 1 (Costanzi, *et al.*, 2005; Ardelt, *et al.*, 2008; Beck, *et al.*, 2008; Ardelt, *et al.*, 2009), and has been investigated in clinical trials for the treatment of unresectable malignant mesothelioma with mixed results (Alfacell, 2009). If ONC and both RNase A and RNase 1 are structurally similar, then why is ONC so dramatically more cytotoxic? ONC is able to significantly evade a cellular ribonuclease inhibitor protein (RI) that binds to and inhibits RNase A and RNase 1 with *femtomolar* affinity (RI has only micromolar affinity for ONC) (Boix, *et al.*, 1996; Cho, *et al.*, 2005; Dickson, *et al.*, 2005; Rutkoski and Raines, 2008; Turcotte and Raines, 2008b). This results in the ability of ONC to be active, and toxic, in cells (D'Alessio and Riordan, 1997).

While ONC is highly cytotoxic, it has met with limited clinical success partly due to reversible dose-limiting renal toxicity and low catalytic activity (Mikulski, *et al.*, 1993; Costanzi, *et al.*, 2005; Pavlakis and Vogelzang, 2006; Rutkoski and Raines, 2008; Ardelt, *et al.*, 2008; Beck, *et al.*, 2008). RNase A and RNase 1 accumulate 50–100 times less than ONC in the kidneys, portending less renal toxicity for mammalian ribonucleases (Vasandani, *et al.*, 1996). RNase A and RNase 1 also have much higher catalytic efficiency for degrading RNA substrates ( $10^2$ – $10^5$  fold higher) (Rutkoski and Raines, 2008; Ardelt, *et al.*, 2008). Therefore, RNase A and RNase 1 would potentially be better chemotherapeutics if they gained cytotoxic abilities comparable to ONC.

To endow cytotoxic abilities to RNase A and RNase 1, variants of these ribonucleases were engineered to evade RI. G88R RNase A demonstrated moderate evasion of RI ( $K_d$  for RI = 1.2 nM) and moderate toxicity to the human erythroleukemia cell line K-562 ( $IC_{50}$  = 4.6–7.0  $\mu$ M) (Leland, *et al.*, 1998; Rutkoski, *et al.*, 2005). A RNase A variant with additional mutations, D38R/R39D/N67R/G88R RNase A (DRNG RNase A), had higher evasion to RI ( $K_d$  for RI = 510 nM) and consequently had higher toxicity to K-562 cells ( $IC_{50}$  = 0.19  $\mu$ M) (Rutkoski, *et al.*, 2005). Both ribonuclease variants were also toxic to several other cancer cell lines, proportional to their RI evasion (Rutkoski, *et al.*, 2005). RI-evasive variants of RNase 1 have also been constructed (Leland, *et al.*, 2001; Johnson, *et al.*, 2007b; Johnson, *et al.*, 2007a), and one RNase 1 variant, QBI-139, is currently in a Phase I clinical trial for patients having advanced, refractory, solid tumors.

RI evasion is not the sole determinant of ribonuclease cytotoxicity. The putative mechanism of ribonuclease cytotoxicity (Figure 1.3) indicates dependence on the efficiency of ribonuclease

association with the cell membrane, internalization into cells, subsequent translocation into the cytosol, ability to evade RI, conformational stability, and ability to catalyze the degradation of cellular RNA (Leland, *et al.*, 1998; Futami, *et al.*, 2001; Leland, *et al.*, 2001; Futami, *et al.*, 2002; Haigis and Raines, 2003; Haigis, *et al.*, 2003; Rutkoski, *et al.*, 2005; Futami, *et al.*, 2005; Benito, *et al.*, 2005; Johnson, *et al.*, 2007b; Johnson, *et al.*, 2007a; Rutkoski and Raines, 2008; Chao, *et al.*, 2010; Chao and Raines, 2011). Importantly, cytotoxic ribonucleases represent some of the first biologic chemotherapeutics that must prevail against the bottleneck of cytosolic delivery for therapeutic action.

#### **1.4 Cellular Delivery is Essential for the Model Ribonuclease Chemotherapeutic System**

The landscape of drugs, in particular macromolecular biologics, is limited by inefficient delivery into cells (Patil, *et al.*, 2005; Malik, *et al.*, 2007; Shim and Kwon, 2010); ribonucleases are no different. For example, RNase A had much higher cytotoxicity ( $> 10^6$ -fold) when injected directly into *Xenopus* oocytes versus applied extracellularly (Saxena, *et al.*, 1991). As an intercellular-acting drug, ribonucleases must undergo several stages for cellular delivery (see section 1.1, Figure 1.1). Ribonucleases are used as active enzymes, thereby completing the first stage for cellular delivery — accumulation of active drug near the cell. The second stage of cellular delivery for RNase A and RNase 1 — association with the cell surface — is non-saturable, indicating that association with the cell surface is also non-receptor-mediated (Haigis and Raines, 2003; Johnson, *et al.*, 2007a; Rutkoski and Raines, 2008). The cationicity of RNase A and RNase 1 is thought to promote non-specific binding to the anionic cell surface through electrostatic interactions (Johnson, *et al.*, 2007a; Chao, *et al.*, 2010; Chao and Raines, 2011). For

RNase A (and presumably RNase 1), these interactions are mediated by heparin sulfate proteoglycans (Fredens, *et al.*, 1991; Soncin, *et al.*, 1997; Fuchs and Raines, 2006; Chao, *et al.*, 2010), sialic acid-containing glycoproteins (Chao, *et al.*, 2010), and/or phospholipid head groups (Notomista, *et al.*, 2006; Rutkoski and Raines, 2008). Similarly, heparin sulfate proteoglycans mediate the binding of cell-penetrating peptides, such as Arg<sub>9</sub> and HIV TAT peptide, to the cell surface (Fuchs and Raines, 2004; Richard, *et al.*, 2005; Chao, *et al.*, 2010; Chao and Raines, 2011). Conversely, cell-surface binding of some ribonuclease amphibian sialic acid-binding lectins is mediated specifically by sialic acid groups, and cell-surface binding of ONC and RNase 5 is thought to be receptor-mediated, though these protein receptors for ONC and RNase 5 are controversial and ill-defined (Rutkoski and Raines, 2008).

Upon binding to the cell surface, ribonucleases undergo the third stage of cellular delivery — endocytosis. RNase A (and presumably RNase 1) is endocytosed in a multi-pathway mechanism (Figure 1.1, insert), including macropinocytosis and cathrin-mediated endocytosis (Chao and Raines, 2011) (phagocytosis is not considered here since it is primarily done by specialized cells) (Conner and Schmid, 2003). Macropinocytosis often utilizes actin-dependant membrane ruffling but not dynamin (Cao, *et al.*, 2007; Chao and Raines, 2011). Dextran, horseradish peroxidase, and some cell-penetrating peptides are also known to use this route for cellular entry (Nakase, *et al.*, 2004; Jones, 2007; Cao, *et al.*, 2007; Chao and Raines, 2011). Cathrin-mediated endocytosis occurs constitutively in all mammalian cells (Conner and Schmid, 2003; Chao and Raines, 2011) and uses recruitment of cargo by adaptor protein complex AP2 to clathrin-coated pits followed by fission of these vesicles by the GTPase dynamin (Mukherjee, *et al.*, 1997; Chao and Raines, 2011). Transferrin is known to enter cells by this route (Conner and Schmid, 2003; Chao and

Raines, 2011). Regardless of which pathway is employed, endocytosis has been shown to be a crucial factor for RNase A and RNase 1 cytotoxicity (Johnson, *et al.*, 2007a; Leich, *et al.*, 2007).

Following endocytosis, ribonucleases are still excluded from the cytosol; they have not completed the fourth stage of cellular delivery — translocation from the endosomes into the cytosol. This translocation step is particularly difficult to analyze, and the mechanism is still unknown. However, it is thought that RNase A (and presumably RNase 1) translocation occurs prior to the trans-Golgi network (Haigis and Raines, 2003). Ribonuclease destabilization of membrane vesicles (representing endosomes) correlates with the cationicity of the ribonuclease, indicating the possible importance of charge in this stage (though this is convoluted by the use of dimeric ribonucleases in the analysis) (Notomista, *et al.*, 2006). Supporting this, immunoblot analysis of fractionated K-562 cells showed that more G88R RNase A (Z +5) was delivered to the cytosol versus wild-type RNase A (Z +4) (Leich, *et al.*, 2007). Finally, ribonuclease translocation is thought to be very inefficient, as only approximately 5% of the ribonuclease escapes into the cytosol, with 95% remaining in the endosomes/lysosomes (Rutkoski and Raines, 2008).

Given this major bottleneck of cellular delivery in ribonuclease cytotoxicity, which can be considered a model for future intercellular biologic chemotherapeutics, several methods have been employed to increase ribonuclease cellular delivery (Table 1.3). One method includes increasing ribonuclease cationization for enhanced binding to the anionic cell surface and subsequent internalization/translocation. This has been engineered chemically (Futami, *et al.*, 2001; Futami, *et al.*, 2005), through mutagenesis (Fuchs, *et al.*, 2007; Johnson, *et al.*, 2007a), and with tags (Fuchs and Raines, 2005). However, these methods tend to decrease the conformational



stability and/or activity of the ribonuclease, abrogating some of the benefit from the increased cytosolic delivery (Futami, *et al.*, 2001; Fuchs and Raines, 2005; Fuchs, *et al.*, 2007). Another method to increase ribonuclease internalization is to conjugate ribonuclease to ligands or antibodies which bind to cell-surface receptors overexpressed in cancer cells (for lists of several conjugates, see (Benito, *et al.*, 2008; Rutkoski and Raines, 2008; Krauss, *et al.*, 2008)). This can result in very potent cytotoxic ribonucleases. However, these constructs only target cells with the corresponding receptors up-regulated, potentially leading to easy mechanisms for cancer cell resistance (by down-regulation of these receptors) or off-target toxicity to normal cells that overexpress these receptors. Further, receptor-mediated endocytosis can lead ribonucleases down less-productive pathways for translocation or even down pathways to the lysosome (Erickson, *et al.*, 2006; Benito, *et al.*, 2008). Finally, if the ribonuclease–ligand or ribonuclease–antibody conjugate binds too tightly to its receptor, after endocytosis it may not be able to “let go” in order to translocate into the cytosol and/or the extra size of the ligand/antibody may hinder translocation (Borra, M. and Raines, R.T., personal communication). Therefore, additional cellular delivery strategies are still desperately needed.

For studies seeking to improve cytosolic delivery of biologic chemotherapeutics, RNase A and RNase 1 have proven to be robust protein models. Given their high conformational stability, RNase A and RNase 1 are readily chemically conjugated or mutated. While these changes may hinder their stability and cytotoxicity (see above), the constructs typically retain enough stability for cellular delivery analysis. Further, using these ribonucleases makes delivery analysis relatively facile. By attachment of a fluorophore and subsequent flow cytometry experiments, RNase A and RNase 1 can report on the efficiency of their internalization (Johnson, *et al.*,

2007a; Chao, *et al.*, 2010). RI-evasive variants of RNase A and RNase 1 can also report on the efficiency of their translocation by monitoring their cytotoxic potency, which correlates with their ability to reach the cytosol and degrade cellular RNA (Johnson, *et al.*, 2007a; Chao, *et al.*, 2010). Consequently, RNase A and RNase 1 are ideal models for drug delivery.

## **1.5 Small Molecules to Facilitate Chemotherapeutic Delivery**

This thesis aims to investigate and facilitate the stages of chemotherapeutic cellular delivery with small molecules, all focused around the ribonuclease model system.

### *1.5.1. Modification of drug for timed-release drug delivery*

Modulation of the first stage of cellular delivery, accumulation of active drug near the cell, is crucial for cancer chemotherapeutic drugs, since these drugs often have narrow therapeutic indexes that make maintaining a safe and effective dose challenging (Gennaro, 2000; Kratz, *et al.*, 2008). Using a timed-release prodrug strategy, where pro-moieties inactivate a drug until it is released enzymatically or chemically over time, consistent plasma concentrations of the drug can be obtained. This modulates the near-toxic spikes or near-ineffective troughs in active drug plasma concentration (Langer, 1990; Gennaro, 2000; Testa and Mayer, 2003; Brown, 2004; Wang, *et al.*, 2005a). While many pro-moieties exist, the current landscape of timed-release pro-moieties is limited, particularly ones with tunable release kinetics for precise regulation of active drug plasma concentration (Langer, 1990; Gennaro, 2000; Testa and Mayer, 2003; Brown, 2004; Wang, *et al.*, 2005a; Kratz, *et al.*, 2008; Rautio, *et al.*, 2008). The discovery of additional pro-moieties would enhance the ability to optimize the accumulation of active drug near the cell.

An ideal timed-release pro-moiety would not only inactivate the parent drug, but also be released by an endogenous plasma enzyme with promiscuous substrate tolerability. Fulfilling these criteria is non-trivial: most enzymes are by necessity very substrate specific, or are not found in abundant concentration in the plasma. Even if an enzyme is mildly promiscuous, that does not guarantee it will act on a non-natural substrate. Human pancreatic ribonuclease (RNase 1) is an attractive prodrug-activating enzyme as it is expressed in many tissues and circulates in the plasma at approximately 0.4 mg/L (Weickmann, *et al.*, 1984; Su, *et al.*, 2004; Potenza, *et al.*, 2006; Sorrentino, 2010). While RNase 1 is an extremely efficient catalyst for RNA cleavage (Johnson, *et al.*, 2007b), it, along with its more studied bovine homolog RNase A, are also known to promiscuously catalyze the hydrolysis of other phosphate aryl esters attached to the 3'-end of ribonucleotides (Taylorson, *et al.*; Davis, *et al.*, 1988; Witmer, *et al.*, 1991; Thompson and Raines, 1994; delCardayré, *et al.*, 1995). In fact, this was the basis for a patent describing tumor-targeted activation of a phenolic nitrogen mustard from a ribonuclease 3'-phosphate pro-moiety using an antibody–RNase 1 variant in an antibody-directed enzyme prodrug therapy (ADEPT) strategy (Taylorson, *et al.*).

In CHAPTER 2 we hypothesized that a ribonucleoside 3'-phosphate pro-moiety attached to a chemotherapeutic drug would be released by RNase 1 as a novel timed-release prodrug strategy. For our proof-of-concept studies, we chose the model parent drug 4-hydroxytamoxifen (HT). HT is the activated form of tamoxifen (oxidized by cytochrome P450 enzymes) (Desta, *et al.*, 2004) and is significantly more potent than tamoxifen as an anti-proliferative agent against breast cancer cells (Coezy, *et al.*, 1982). We attached HT to the uridine 3'-phosphate to synthesize uridine 3'-(4-hydroxytamoxifen phosphate) (UpHT). Given the hydrophilicity of uridine-

phosphate, we computationally analyzed UpHT to determine if the prodrug had increased hydrophilicity, which may improve its pharmacokinetics (Stella and Nti-Addae, 2007). The ability of RNase 1 to cleave UpHT was analyzed *in vitro* to determine if the prodrug had timed-release kinetics. Finally, a breast cancer cell line (MCF-7) was co-treated with UpHT and RNase 1 to determine if RNase 1 could release active HT to accumulate near the cell and ultimately decrease cell proliferation.

#### 1.5.2. *Increased cell association and internalization of a model biologic chemotherapeutic*

The utility of many biologic drugs is limited by inefficient cellular delivery (Patil, *et al.*, 2005; Malik, *et al.*, 2007; Shim and Kwon, 2010). Previous methods to improve the second and third stages of cellular delivery, association with the cell surface and subsequent internalization into the cell, of RNase A and RNase 1 have focused on increasing cell-surface binding by the use of cationic domains or conjugating these enzymes with antibodies and natural ligands (see above and Table 1.3). While these methods have had moderate success, additional delivery strategies are urgently needed for biologics with intractable delivery.

In CHAPTER 3, we investigated the use of boronic acids for boronate-mediated drug delivery. The cell surface is coated with a dense forest of polysaccharides known as the glycocalyx (Varki, *et al.*, 2009). We anticipated that targeting therapeutic agents to these abundant saccharides would enhance their cellular delivery. Boronic acids readily form boronate esters with the 1,2- and 1,3-diols found in saccharides (James, *et al.*, 2006), including the polysaccharides found in the glycocalyx (Vandenburg, *et al.*, 2000; Yang, *et al.*, 2004; Polsky, *et al.*, 2008; Matsumoto, *et al.*, 2009; Zhong, *et al.*, 2010; Matsumoto, *et al.*, 2010). In addition,

boronic acids are biologically compatible as they are used as therapeutic agents and for other biomedical applications (Westmark and Smith, 1996; Jay, *et al.*, 2009; Barth, 2009; Wu, *et al.*, 2010; Peng, *et al.*, 2010; Kumar, *et al.*, 2011). Further, pendant boronic acids conjugated to polyethylenimine have been shown to enhance gene transfection (Peng, *et al.*, 2010). Hence, we reasoned that boronic acids would enhance drug delivery through boronate–glycocalyx complexation. A boronic acid was chosen through small molecule NMR analysis and coupled to RNase A as a biologic chemotherapeutic model. This conjugate was analyzed for its affinity for saccharides *in vitro*. Importantly, the ability for the boronic acid to facilitate internalization into a cell was then measured. The cytotoxicity of this conjugate was also measured, thereby indicating whether it was still able to translocate to the cytosol to degrade cellular RNA. A competing saccharide, fructose, was used to indicate that the increased saccharide affinity of the conjugate was due, at least in part, to boron–saccharide complexation. Demonstration that boronates not only facilitate the cellular uptake of proteins, but also allow for protein cytosolic delivery and maintenance of therapeutic activity, opens new doors in biologic drug delivery.

### 1.5.3. *Enhanced cytotoxicity of a model biologic chemotherapeutic*

RNase A is very inefficient at the fourth stage of cellular delivery, translocating from the endosomes into the cytosol, limiting its cytotoxic potential (Rutkoski and Raines, 2008). To improve the translocation (and internalization) of RNase A, the Yamada lab increased its cationicity chemically by condensing the side chains of aspartate and glutamate residues with either ethylenediamine (Futami, *et al.*, 2001; Futami, *et al.*, 2002) or with cationic polymers of poly(ethyleneimine) (Futami, *et al.*, 2005). While these covalent modifications increased

cytotoxicity, they also diminished catalytic activity (Futami, *et al.*, 2001; Futami, *et al.*, 2005). The Raines lab increased the cationicity of proteins by using ‘arginine-grafting’, where specific anionic residues were mutated to cationic residues. This technique increased the internalization of both GFP (Fuchs and Raines, 2007) and RNase A (Fuchs, *et al.*, 2007) and led to an increase in cytotoxicity of a RI-evasive variant of RNase A, but at the cost of conformational stability (Fuchs, *et al.*, 2007). A genetically-encoded nonaarginine tag (Arg<sub>9</sub>) attached to RNase A increased internalization but also had detrimental effects on stability (Fuchs and Raines, 2005).

In CHAPTER 4, we investigated the potentiation of ribonuclease cytotoxicity by a poly(amidoamine) (PAMAM) dendrimer *in trans*, likely by improved translocation into the cytosol after endocytosis (Ellis, *et al.*, 2011). This was supported by recent observations that co-treatment with a cationic peptide or PEI could enhance the cellular uptake of proteins (Didenko, *et al.*, 2005; Loudet, *et al.*, 2008) and by recent work from the Pellois laboratory (Lee, *et al.*, 2010; Angeles-Boza, *et al.*, 2010). Notably, this work differed from previous methods of directly increasing RNase A cationicity in that the dendrimer was added as a co-treatment, or *in trans*, and not directly conjugated to the ribonuclease. This was hypothesized to lessen any destabilizing and inactivating effects. PAMAM dendrimers are monodisperse, branched polymers with a high density of cationic charge (Tomalia, *et al.*, 1985; Esfand and Tomalia, 2001). They are commercially available and have been employed as drug and gene delivery vehicles, as they have the ability to transport encapsulated small molecules and enwrapped DNA into cells (Cloninger, 2002; Guillot-Nieckowski, *et al.*, 2007; Navarro, *et al.*, 2010). Specifically, the relatively small generation 2 dendrimer was investigated due to its low inherent cytotoxicity compared to higher generation dendrimers and other cationic polymers such as polyethylenimine

(Roberts, *et al.*, 1996; Malik, *et al.*, 2000; Fischer, *et al.*, 2003). Not only were the effects of dendrimers on internalization and cytotoxicity of ribonucleases measured, but also the effects of dendrimers on ribonuclease thermostability and catalytic activity. Although it is unlikely that this dendrimer strategy could be used in a clinical setting, its investigation encourages further exploration of cationic dendrimers as co-treatments with chemotherapeutic agents and their mechanism of action.

## 1.6 Additional Delivery Methods

In addition to the investigations mentioned above, further investigations have been conducted that are specific to RNase A.

### 1.6.1. *Small-molecule inhibitors of RI—ribonuclease interaction*

Human ribonuclease inhibitor (RI) is found at a concentration of 4  $\mu\text{M}$  in the cytosol of all mammalian cells studied (Dickson, *et al.*, 2005). Remarkably, RI binds to and inhibits several mammalian ribonucleases in 1:1 stoichiometric interactions with *femtomolar* affinity by burying approximately 2900  $\text{\AA}^2$  of surface area. These ribonucleases include RNase A, RNase 1, RNase 2 (EDN), RNase 4, and RNase 5 (ANG), even though these proteins only share 20–68% protein sequence identity (RNases 3, 6, and 7 have also been demonstrated to be sensitive to RI) (Cho, *et al.*, 2005; Dickson, *et al.*, 2005; Rutkoski and Raines, 2008). Variants of RNase A and RNase 1 have been engineered to evade RI and are toxic to several cancer cell lines proportional to their ability to evade RI (Leland, *et al.*, 1998; Leland, *et al.*, 2001; Rutkoski, *et al.*, 2005; Johnson, *et*

*al.*, 2007b). In this way, RI acts to inhibit delivery, albeit intracellular delivery, of ribonucleases to their site of action, cellular RNA.

In APPENDIX 1, it was hypothesized that small-molecule antagonists of the RI–ribonuclease interaction, identified through a high-throughput screen (HTS), would potentiate the cytotoxicity of modestly RI-evasive ribonucleases. These small-molecule RI antagonists could augment the cytotoxicity of RNase A or RNase 1 variants which are hindered by weak RI-evasiveness but possess other desirable attributes for ribonuclease cytotoxicity, such as high stability (Klink and Raines, 2000) or enhanced ability to internalize into cells (Johnson, *et al.*, 2007a). In addition to cytotoxicity, RNase A homologues have been implicated in other important biological processes, including neovascularization (ANG) and host defense (EDN) (D'Alessio and Riordan, 1997; Rosenberg, 1998; Dickson, *et al.*, 2005). Inhibitors of the RI–ribonuclease interaction could be used to probe the biological activities of these ribonucleases, and the role that RI plays in these processes. Therefore, we optimized a HTS assay for identifying inhibitors of the interaction between RI and a RNase A variant interaction and screened two compound libraries (4,160 compound Known Bioactives Library; 16,000 compound Chembridge Library). Initial hits were analyzed and screened in a secondary assay. While these compounds did not show utility *in cellulo*, future development of these hits could lead to more potent antagonists.

#### 1.6.2. *Engineering a ribonuclease zymogen activated by urokinase for selective toxicity*

A crucial issue for the body in the design of proteases is how to produce them without significant off-target activity and consequent toxicity. One evolved solution is the use of zymogens: precursor enzymes that are produced to be inactive until a region, such as a domain



blocking the active site, is cleaved by another protease, thereby activating the enzyme at its needed site of action (Khan and James, 1998). The ability of zymogens to regulate enzyme activity was used as a model to engineer three previously published RNase A zymogens (Plainkum, *et al.*, 2003; Johnson, *et al.*, 2006; Turcotte and Raines, 2008a). These zymogens were engineered using circular permutation, where new N- and C- termini were produced and a peptide linker spanned the old N- and C- terminus, blocking the active site. The RNase A zymogens were relatively inactive until the linker regions were cleaved by disease-associated proteases: plasmepsin II from *Plasmodium falciparum*, the organism responsible for most cases of malaria; NS3 protease from the hepatitis C virus; or the HIV-1 protease (Plainkum, *et al.*, 2003; Johnson, *et al.*, 2006; Turcotte and Raines, 2008a). Hypothetically, by RNase A only becoming activated when in the presence of these proteases, only infected cells would undergo cell death. Unfortunately, no previously published RNase A zymogen has been effective *in cellulo*.

In an attempt to produce a novel RNase A zymogen, in APPENDIX 2 a ribonuclease zymogen activated by urokinase is investigated. Urokinase-type plasminogen activator (urokinase) is a serine protease overexpressed in many tumors, and is part of a cascade towards matrix-metalloprotease activation (Andreasen, *et al.*, 1997; Sidenius and Blasi, 2003). A RI-evasive RNase A zymogen activated by urokinase could therefore have an increased therapeutic index compared to normal RNase A variants, if it were preferentially activated near tumors overexpressing urokinase. Using urokinase to activate cytotoxins is predicated by work from Leppla, Bugge, and coworkers using an urokinase-activated cytotoxin based on anthrax toxin (Liu, *et al.*, 2001). A RNase A zymogen was produced using circular permutation with a new

urokinase-cleavable linker over the active site, and it was analyzed both *in vitro* and *in cellulo*.

While the zymogen was activated by urokinase *in vitro*, it did not demonstrate *in cellulo* toxicity.

Two other novel engineered RNase A zymogen methods were also attempted, but did not produce any usable protein. Additional engineering of RNase A zymogens activated by urokinase may lead to viable *in cellulo* zymogens that can be analyzed biologically.

## 1.7 Prospectus

Ribonucleases show promise as a rare class of biologic chemotherapeutics; a biologic that works in the *cytosol*, not in lysosomes or outside of a cell. While these enzymes may help patients clinically, perhaps just as important will be their role to serve as models. The potential for intercellular-acting biologic therapeutics is enormous if the barriers to delivery can be surmounted. Hopefully, scientists will reference studies on the delivery of ribonuclease chemotherapeutics and apply the lessons learned from this system to other biologic chemotherapeutics.

**Table 1.1** Amino-acid sequence alignment of selected pancreatic-type ribonuclease superfamily members. The alignment is modified from the Raines Lab Archive.

	1	10	20	30	40	
RNase A ( <i>Bos taurus</i> )	- - - K E T A A A K F E R Q	M D S S T S A A S S S N Y	C N Q M M K S R N L T K D R	C P V N T F V H E		
Onconase ( <i>Rana pipiens</i> )	- - - Q D W L T - F Q K K	I T N T R D V D - - - -	C D N I M - S T N L - - F H	C D K N T F I Y S		
RNase 1 ( <i>Homo sapiens</i> )	- - - K E S R A K K F Q R Q	M D S D S S P S S S S T Y	C N Q M M R R R N M T Q G R	C P V N T F V H E		
RNase 2, EDN ( <i>Homo sapiens</i> )	K P P Q F T W A Q W F E T Q	I N M T S Q Q - - - - -	C T N A M Q V I N N Y Q R R	C N Q N T F L L T		
RNase 3, ECP ( <i>Homo sapiens</i> )	R P P Q F T R A Q W F A I Q	I S L N P P R - - - - -	C T I A M R A I N N Y R W R	C N Q N T F L R T		
RNase 4 ( <i>Homo sapiens</i> )	- - - Q D G M Y Q R F L R Q	V H P E E - T G G S D R Y	C D L M M Q R R K M T L Y H	C R F N T F I H E		
RNase 5, ANG ( <i>Homo sapiens</i> )	- - - Q D N S R Y T H F L T Q	Y D - A K P Q G R D D R Y	C E S I M R R R G L T - S P	C D I N T F I H G		
	P2	P2		B1		
	50	60	70	80		
RNase A ( <i>Bos taurus</i> )	S L A D V Q A V C S Q K N V A C K N G Q T - - N C Y Q - - - - S Y S T M S I T D C R E T G S					
Onconase ( <i>Rana pipiens</i> )	R P E P V K A I C - K G I I A S K N V L T - - T - - - - - S E F Y L S D C N V T - -					
RNase 1 ( <i>Homo sapiens</i> )	P L V D V Q N V C F Q E K V T C K N G Q G - - N C Y K - - - - S N S S M H I T D C R L T N G					
RNase 2, EDN ( <i>Homo sapiens</i> )	T F A N V V N V C G N P N M T C P S N K T R K N C H H - - - - S G S Q V P L I H C N L T T P					
RNase 3, ECP ( <i>Homo sapiens</i> )	T F A N V V N V C G N Q S I R C P H N R T L N N C H R - - - - S R F R V P L L H C D L I N P					
RNase 4 ( <i>Homo sapiens</i> )	D I W N I R S I C S T T N I Q C K N G K M - - N C H E - - - - G - - V V K V T D C R D T G S					
RNase 5, ANG ( <i>Homo sapiens</i> )	N K R S I K A I C - - E N - - - K N G - - - - N P H R E N I R I S K S S F Q V T T C K L H G G					
		P0	B2	B1	Pt-1	
	90	100	110	120	124	
RNase A ( <i>Bos taurus</i> )	S K - - Y P N C A Y K T T Q A N K H I I V A C E G N - - - - - P Y V P V F D A S V - - - -					
Onconase ( <i>Rana pipiens</i> )	S R - - - P - C K Y K L K K S T N K F C V T C E N Q - - - - - A - - P V F - V G V G S C -					
RNase 1 ( <i>Homo sapiens</i> )	S R - - Y P N C A Y R T S P K E R H I I V A C E G S - - - - - P Y V P V F D A S V E D S T					
RNase 2, EDN ( <i>Homo sapiens</i> )	S P Q N I S N C R Y A Q T P A N M F Y I V A C D N R D Q R R D P P Q Y P V V P V L D R I I - - - -					
RNase 3, ECP ( <i>Homo sapiens</i> )	G A Q N I S N C R Y A D R P G R R F Y V V A C D N R D - P R D S P R Y P V V P V L D T T I - - - -					
RNase 4 ( <i>Homo sapiens</i> )	S R - - A P N C R Y R A I A S T R R V V I A C E G N - - - - - P Q V P V F D G - - - - -					
RNase 5, ANG ( <i>Homo sapiens</i> )	S P - - W P P C Q Y R A T A G F R N V V V A C E N G - - - - - - L P V L D Q S I F R R P					
			B2	B1		

**C** Cysteine Residue  
**■** Active Site  
**hst** helix, sheet, turn in RNase A

*Pt-1* 5"-Phosphate Binding Site  
*P0* 5'-Phosphate Binding Site  
*P2* 3'-Phosphate Binding Site  
*B1* CytUra Binding Site  
*B2* Ade Binding Site

**Table 1.2** Sequence identity/similarity of selected pancreatic-type ribonuclease superfamily members. Sequence identities (%) are to the left of the diagonal and sequence similarities (%) are to the right of the diagonal. These were calculated with MacVector v9.5 (MacVector, Inc., Cary, NC) in a previous publication from which the table was modified (Rutkoski and Raines, 2008).

Sequence Similarities (%)											
Sequence Identities (%)		RNase A	RNase 1	RNase 2 (EDN)	RNase 3 (ECP)	RNase 4	RNase 5 (ANG)	RNase 6	RNase 7	RNase 8	ONC
	RNase A	100	80.5	44.5	44.9	66.1	51.2	45.5	45.5	43.9	36.2
	RNase 1	68.0	100	42.6	44.3	60.2	52.7	46.3	45.6	41.2	33.3
	RNase 2 (EDN)	29.2	28.4	100	75.4	38.7	35.9	60.4	57.5	58.2	31.4
	RNase 3 (ECP)	23.5	27.9	64.9	100	37.5	35.5	58.2	52.2	50.0	25.0
	RNase 4	41.9	40.6	24.1	22.8	100	49.2	44.7	41.7	39.4	36.5
	RNase 5 (ANG)	30.2	33.3	19.7	22.7	35.9	100	38.7	40.9	36.5	31.2
	RNase 6	33.3	30.9	44.0	41.8	31.1	22.6	100	68.8	66.9	31.1
	RNase 7	35.6	31.6	41.0	37.3	28.8	23.4	55.5	100	82.8	29.3
	RNase 8	35.6	32.4	44.0	36.6	27.3	20.4	55.1	76.6	100	30.3
	ONC	20.5	19.4	18.2	14.7	23.8	22.7	19.7	18.8	18.2	100

**Table 1.3** Selected conjugations to enhance RNase A and RNase 1 cellular delivery.

Methods above the double line use cationization; methods below the double line use targeting of cell-surface receptors. The table is partially adapted from previous publications (Benito, *et al.*, 2008; Rutkoski and Raines, 2008).

	Ribonuclease	Conjugate	Design	Cytotoxicity/IC50 (cell line)	Ref
Cationization	RNase A	Ethylenediamine	Carboxyl group amidation using EDC	0.17 $\mu$ M (3T3-SV40); 3.6 nM with Endoportor (HeLa)	(Futami, <i>et al.</i> , 2001; Futami and Yamada, 2008)
	RNase A	Ethylenediamine	Limited carboxyl group amidation using EDC	0.085 $\mu$ M (MCF-7), 0.075 $\mu$ M (3T3-SV40)	(Futami, <i>et al.</i> , 2002)
	RNase A	Polyethylenimine (PEI), 250–1800 Da	Carboxyl group amidation using EDC	0.33–3.3 $\mu$ M (3T3-SV40)	(Futami, <i>et al.</i> , 2005)
	RNase 1	Ethylenediamine	Carboxyl group amidation using EDC	0.13 $\mu$ M (3T3-SV40)	(Futami, <i>et al.</i> , 2001)
	RNase A	Nonaarginine tag	Genetic fusion with tag to RI-evasive RNase	2.0 $\mu$ M (K-562)	(Fuchs and Raines, 2005)
	RNase A	Arginine	Mutating selected Asp/Glu with Arg ("arginine grafting") on RI-evasive RNase	1.9 $\mu$ M, 0.58 $\mu$ M with Arg tag (K-562)	(Fuchs and Raines, 2007)
	RNase 1	Arginine/Lysine; Aspartate/Glutamate removal	Site-directed mutagenesis for RI-evasion and charge	5.7 $\mu$ M (K-562)	(Johnson, <i>et al.</i> , 2007)
Targeting Cell-Surface Receptors	RNase 1	Transferrin (Tf) or anti-human Tf receptor	Site-specific attachment to free cysteine variant	1–2 nM (human glioma)	(Suzuki, <i>et al.</i> , 1999)
	RNase 1	C-terminus of Human anti-ErbB-2 receptor scFv	Genetic fusion to N-terminus of RNase	12.5–60 nM (cell lines displaying ErbB-2)	(De Lorenzo, <i>et al.</i> , 2004)
	RNase 1	C-terminus of Human Her-2 scFv (binds to CD30)	Genetic fusion to N-terminus of RNase	Cytotoxic (CD30+ cell lines)	(Braschoss, <i>et al.</i> , 2007)
	RNase 1	N-terminus of EGF	Genetic fusion to C-terminus of $\Delta$ 1–7 RNase	0.35 $\mu$ M (A431)	(Hoshimoto, <i>et al.</i> , 2006)
	RNase 1	N-terminus of FGF	Genetic fusion to C-terminus of $\Delta$ 1–7 RNase	ca. 2 $\mu$ M (B16/BL6)	(Futami, <i>et al.</i> , 1999)
	RNase 1	C-terminus of human bFGF	Genetic fusion to N-terminus of RNase	1.6 $\mu$ M (B16/BL6)	(Tada, <i>et al.</i> , 2004)
	RNase 1	$\beta$ -trefoil core region (residues 19–146) of bFGF	Genetic insertion into a RNase (with extra disulfide) loop	0.23 $\mu$ M to > 3 $\mu$ M (Mice with human A431 SCC tumors)	(Tada, <i>et al.</i> , 2004)
	RNase 1	N-terminus of human IL2	Genetic fusion to C-terminus of RNase	20 nM (T-cells infected to overproduce IL2 receptor)	(Psarras, <i>et al.</i> , 2000)
	RNase A	Anti-human $\alpha$ -IL2 receptor	Chemical conjugation	50 nM (T-cells infected to overproduce IL2 receptor)	(Yamamura, <i>et al.</i> , 2002)
	RNase 1	N-terminus of scFv for CD7	Genetic fusion to C-terminus of RNase	Not toxic to CD7+ T cells	(Erickson, <i>et al.</i> , 2006)
	RNase A	Folate	Chemical conjugation to RI-evasive RNase	9–11 $\mu$ M (K-562)	(Smith, <i>et al.</i> , 2011)

**Figure 1.1** Stages of cellular drug delivery. For therapeutic action, intercellular-acting drugs must (1) accumulate near the cell in an active form, (2) associate with the cell surface, and (3) internalize by endocytosis or other mechanisms. If the drug is internalized by endocytosis and must reach the cytosol for therapeutic action, it must also (4) undergo translocation. The figure is modified from previous publications (Conner and Schmid, 2003; Bildstein, *et al.*, 2011).

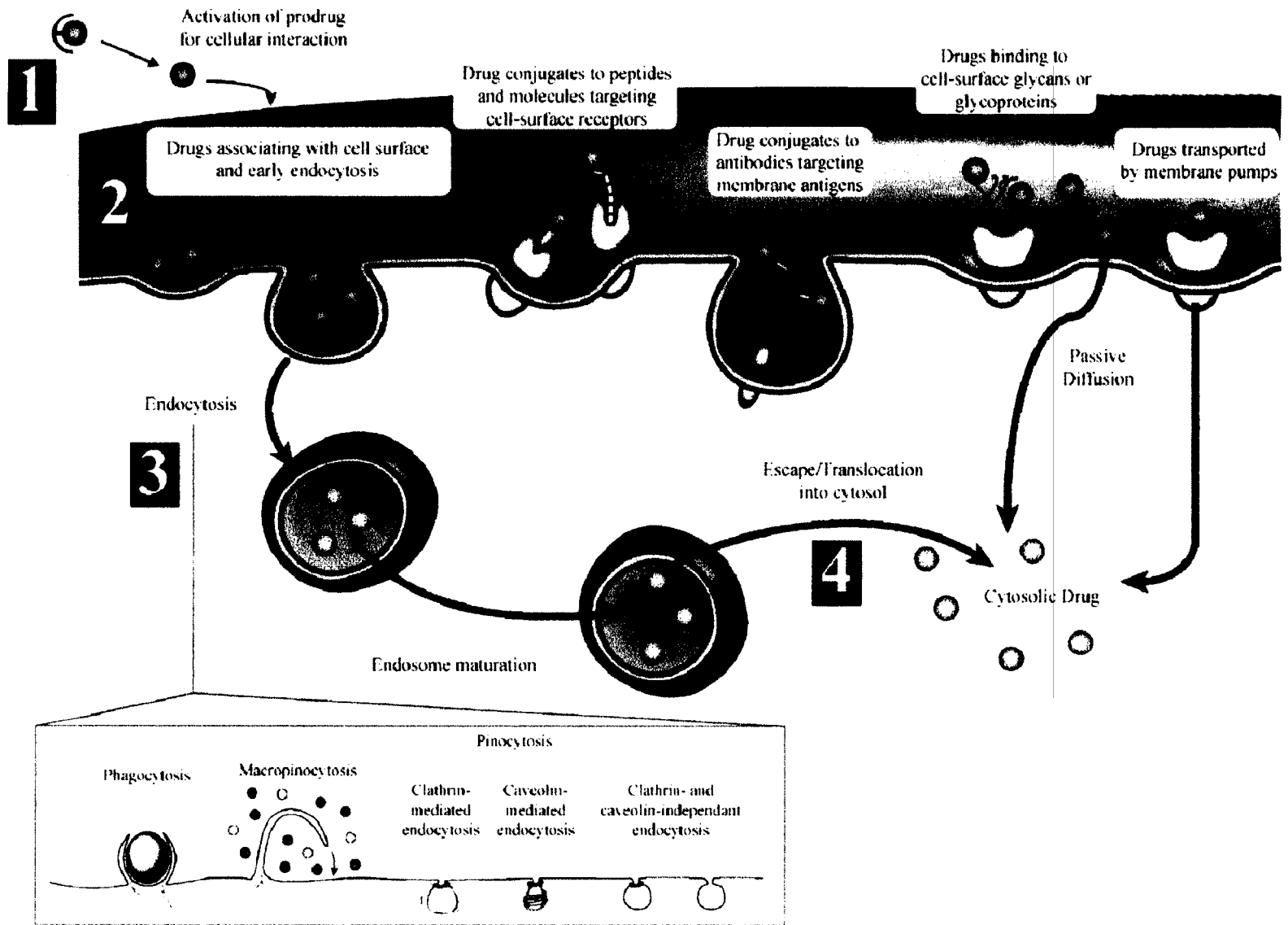


**Figure 1.2** Selected members of the pancreatic-type ribonuclease superfamily. Six selected ribonucleases are aligned to RNase 1 (top) to emphasize similarities in tertiary structure. The ribonucleases are RNase A (red): PDB entry 7rsa (Wlodawer, *et al.*, 1988); Onconase or ONC (orange): 1ONC (Mosimann, *et al.*, 1994); RNase 1 (yellow): chain Z of 1z7x (Johnson, *et al.*, 2007b); RNase 2 or EDN (blue): chain C of 2bex (Iyer, *et al.*, 2005); RNase 3 or ECP (green): 1qmt (Boix, *et al.*, 1999); RNase 4 (cyan): 1rmf (Terzyan, *et al.*, 1999); and RNase 5 or ANG (magenta): chain B of 1a4y (Papageorgiou, *et al.*, 1997). Organism source and selected putative biological roles are given for each ribonuclease (bottom, excludes neurotoxicity for EDN and ECP). The figure is adapted from a previous publication (Rutkoski and Raines, 2008).



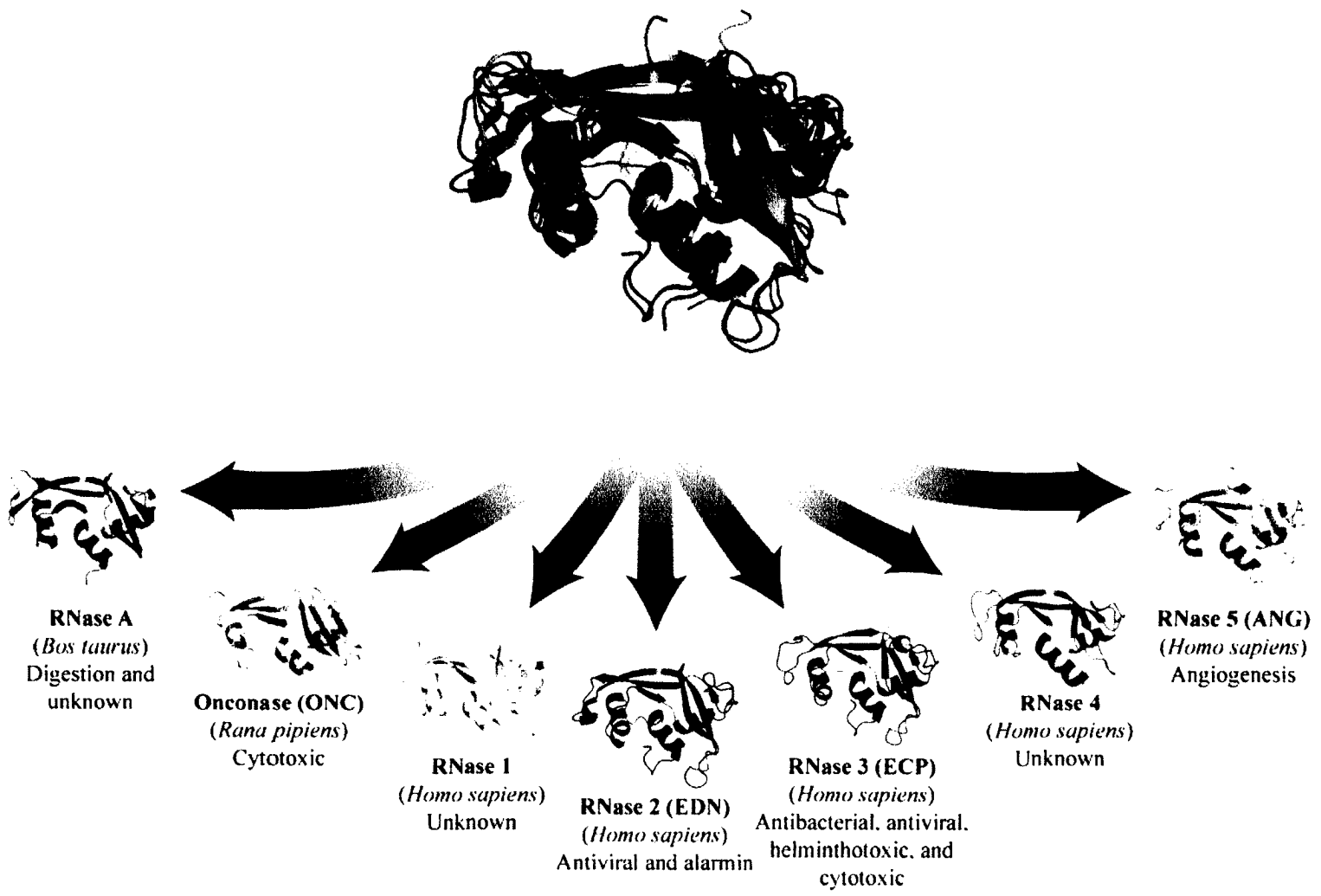
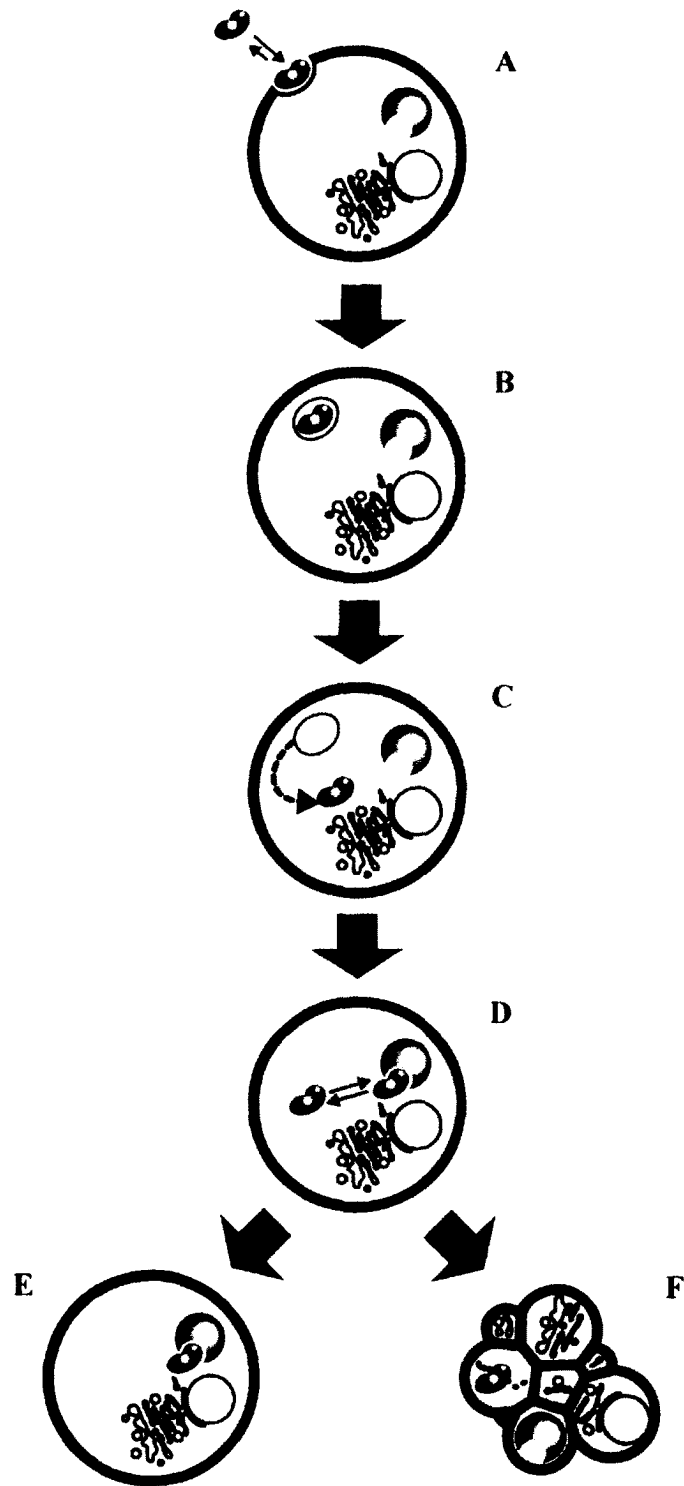


**Figure 1.3** Putative mechanism of ribonuclease cytotoxicity. (A) Ribonucleases (blue) reversibly bind to the anionic cell surface. This binding is needed to facilitate (B) endocytosis. Following endocytosis, ribonucleases (C) translocate from endosomes into the cytosol where they (D) encounter RI (red). Ribonucleases are either (E) bound and inhibited by RI, maintaining cell status, or (F) able to evade RI and degrade cellular RNA, causing cell death. The figure is adapted from a previous publication (Rutkoski and Raines, 2008).



## **CHAPTER 2**

### **Ribonuclease-Activated Cancer Prodrug**

This chapter is in preparation for publication as:

Ellis, G.A.\*, McGrath, N.A.\*, Palte, M.J., and Raines, R.T. (2011) Ribonuclease-activated cancer prodrug. (\* denotes equal contribution)

## 2.1 Abstract

Cancer chemotherapeutic agents often have a narrow therapeutic index that challenges the maintenance of a safe and effective dose. Consistent plasma concentrations of the drug can be obtained by using a prodrug strategy. We reasoned that a ribonucleoside 3'-phosphate could serve as a timed-release pro-moiety that also serves to increase the hydrophilicity of a cancer chemotherapeutic agent. Herein, we report an efficient route for the synthesis of the prodrug uridine 3'-(4-hydroxytamoxifen phosphate) (UpHT). UpHT demonstrates timed-released activation kinetics with a half-life of approximately 4 h near the approximate plasma concentration of human pancreatic ribonuclease (RNase 1). MCF-7 breast cancer cells treated with UpHT showed decreased proliferation when co-incubated with RNase 1, consistent with their release of the active drug 4-hydroxytamoxifen. These data demonstrate the utility of plasma ribonuclease as a useful activator of a prodrug.

## 2.2 Introduction

Many drug candidates have demonstrable therapeutic potential *in vitro* but fail *in vivo* due to poor pharmacokinetic behavior (Wang, *et al.*, 2005a; Rautio, *et al.*, 2008). Dosing of cancer chemotherapeutic agents, in particular, is made difficult by narrow therapeutic indices (Gennaro, 2000; Kratz, *et al.*, 2008). Following parenteral administration of a drug, there is a spike in drug plasma concentration, followed by a slow decline in concentration as the drug is eliminated or metabolized, complicating the maintenance of the drug concentration within its therapeutic index (Langer, 1990; Gennaro, 2000). Timed-release prodrug technology provides one potential means to overcome this problem. A pro-moiety renders the drug inactive until liberation by an enzyme-

catalyzed or non-enzymic process. Ideally, such timed-release modulates near-toxic peaks or near-ineffective troughs in the concentration of active drug in plasma (Langer, 1990; Gennaro, 2000; Testa and Mayer, 2003; Brown, 2004; Wang, *et al.*, 2005a). Although many pro-moieties exist, few provide timed-release in plasma, particularly with tunable release kinetics (Langer, 1990; Gennaro, 2000; Testa and Mayer, 2003; Brown, 2004; Wang, *et al.*, 2005a; Kratz, *et al.*, 2008; Rautio, *et al.*, 2008).

We sought a pro-moiety that would not only inactivate the parent drug, but also be released by an endogenous plasma enzyme. Fulfilling these criteria is difficult, as few enzymes have high plasma concentrations and many are highly specific to their native substrate. Human pancreatic ribonuclease (RNase 1) is an exception. Contrary to its name, RNase 1 is expressed in tissues other than pancreas, and circulates in human plasma at a concentration of ~0.4 mg/L (Weickmann, *et al.*, 1984; Su, *et al.*, 2004; Potenza, *et al.*, 2006; Sorrentino, 2010). Although RNase 1 is an extremely efficient catalyst of RNA cleavage (Johnson, *et al.*, 2007b), it, like its renowned homolog bovine pancreatic ribonuclease (RNase A), is a promiscuous enzyme that can also catalyze the cleavage of other aryl phosphate esters attached to the 3'-end of ribonucleotides (Taylorson, *et al.*; Davis, *et al.*, 1988; Witmer, *et al.*, 1991; Thompson and Raines, 1994; delCardayré, *et al.*, 1995). This promiscuity is the basis for the tumor-targeted activation of a phenolic nitrogen mustard from a ribonucleoside 3'-phosphate pro-moiety using an antibody–RNase 1 variant in an antibody-directed enzyme prodrug therapy (ADEPT) strategy (Taylorson, *et al.*).

Due to the promiscuous activity of ribonucleases, we reasoned that a chemotherapeutic drug condensed with a ribonucleoside 3'-phosphate pro-moiety would be released upon catalysis by

RNase 1. We were aware that the use of a ribonucleoside 3'-phosphate as a pro-moiety would be facilitated by highly optimized phosphoramidite chemistry, making the prodrug readily accessible on a laboratory or industrial scale (Beaucage and Caruthers, 1981). A pendant ribonucleoside 3'-phosphate could inactivate a small-molecule drug by hindering the interaction with its target. The hydrophilicity of a ribonucleoside 3'-phosphate could impart improved pharmacokinetics to hydrophobic drugs (Stella and Nti-Addae, 2007). Additionally, the anionic phosphoryl group could deter cellular uptake prior to activation (Schultz, 2003).

For our proof-of-concept studies, we chose the model parent drug 4-hydroxytamoxifen (HT). HT is the activated form of tamoxifen (oxidized by cytochrome P450 enzymes) (Desta, *et al.*, 2004) and is significantly more potent than tamoxifen as an anti-proliferative agent against breast cancer cells (Coezy, *et al.*, 1982). Tamoxifen acts as an anti-estrogen and is one of the most commonly used hormonal drugs for the prevention and treatment of breast cancer (O'Regan and Jordan, 2002; Powles, 2003). Unfortunately, tamoxifen can have off-target effects and is linked to an increased risk of endometrial carcinoma and pulmonary embolism (~2–3% risk) (Fisher, *et al.*, 2005). Presumably, some of tamoxifen's side effects might be attenuated by delivering tamoxifen at a consistent, low dose over time (Bergman, *et al.*, 2000; Decensi, *et al.*, 2003; Vitseva, *et al.*, 2005; Veronesi, *et al.*, 2007). A system using tamoxifen-encapsulated liposomes has been developed for this purpose, (Layek and Mukherjee, 2010) but liposomal delivery systems have demonstrated only modest efficacy in the clinic (Andresen, *et al.*, 2005). Hence, we elected to attach HT to uridine 3'-phosphate and analyze the activation of this model prodrug by RNase 1 (Figure 2.1).

## 2.3 Results and Discussion

Uridine 3'-(4-hydroxytamoxifen phosphate) (UpHT) was synthesized from commercially available HT ( $\geq 70\%$  *Z* isomer, which is the more active form) (Murphy, *et al.*, 1990) and uridine phosphoramidite. HT was coupled to uridine phosphoramidite by standard coupling chemistry using methylbenzimidazolium triflate as a catalyst (Hayakawa, *et al.*, 2001). The coupled product was oxidized with iodine and deprotected stepwise, and the final product was purified by reverse-phase HPLC on C18 resin to provide UpHT with an overall yield of 58% (Scheme 2.1).

We expected the uridine 3'-phosphate moiety to endow the prodrug with greater hydrophilicity than the parent drug, which could improve pharmacokinetic behavior. To investigate this issue, we calculated the partition (logP) and distribution (logD) coefficients of UpHT and HT with the program MarvinView (ChemAxon, Budapest, Hungary) (ChemAxon, 2011). The calculated logP and logD values of UpHT were significantly lower than those of the parent drug HT (Table 2.1), indicative of increased hydrophilicity.

To be the basis for an effective timed-release prodrug strategy, the pro-moiety needs to be released by the activating enzyme over time. Hence, we used an HPLC assay to determine the rate of HT release from UpHT by RNase 1 at 37 °C (Figure 2.2). UpHT (90.45  $\mu\text{M}$ ) was dissolved in 100 mM MES–NaOH buffer, pH 6.0, containing NaCl (100 mM) (Kelemen, *et al.*, 1999; Smith, *et al.*, 2003; Johnson, *et al.*, 2007b). The concentration of RNase 1 ( $\sim 0.15$  mg/L) was similar to its plasma concentration ( $\sim 0.4$  mg/L). The half-life of HT release by RNase 1 was determined to be  $\sim 4$  h (Figure 2.3). Importantly, UpHT was stable in the absence of RNase 1; after  $\sim 11$  h at 37 °C,  $<6\%$  of UpHT had degraded to HT.



To demonstrate the efficacy of UpHT *in cellulo*, we used a cell-proliferation assay with a MCF-7 breast cancer cell line, which are known to be vulnerable to HT (Coezy, *et al.*, 1982). UpHT was made ~3-fold more anti-proliferative by the presence of added RNase 1, indicating that HT was released and UpHT was acting as a prodrug (Figure 2.4).

## 2.4 Conclusions

Thus, we have demonstrated proof-of-concept for a prodrug strategy that employs RNase 1 to release a cancer chemotherapeutic agent in a timed-release manner (Figure 2.1). UpHT is more hydrophilic than the parent HT due to its ribonucleoside 3'-phosphate moiety (Table 2.1). UpHT was activated by RNase 1 over time *in vitro* (Figure 2.3), and was activated *in cellulo* as indicated by decreased proliferation of MCF-7 cells when co-incubated with RNase 1 (Figure 2.4).

In addition to the features demonstrated with UpHT, the RNase 1/ribonucleoside 3'-phosphate prodrug system has versatile modularity. For example, the leaving group need not be an aryloxy group. Pancreatic-type ribonucleases cleave the P–O bonds to alkoxy groups, which could include a self-immolative linker to an amino group (Kratz, *et al.*, 2008). RNase 1 is known to cleave poly(cytidine) faster than poly(uridine), which is cleaved faster than poly(adenosine) (Sorrentino and Libonati, 1994). Hence, cytidine- and uridine-masked drugs are likely to be activated more rapidly than adenosine- and guanosine-masked drugs, leading to potential tunable kinetics of pro-moiety release. In addition, synergistic drugs could be conjugated to different ribonucleoside 3'-phosphates to achieve simultaneous release of drugs at desired concentrations. These same effects could be used to optimize simultaneous plasma concentrations of

chemoprotective drugs and chemotherapeutic drugs. The pharmacokinetics of the drug could be tuned by modification of the ribose 5'-hydroxyl group. For instance, this hydroxyl group could be PEGylated to enhance serum half-life, extended with additional nucleoside 3'-phosphates to increase hydrophilicity, or alkylated to increase hydrophobicity.

Finally, we note that nucleoside 3'-phosphate pro-moieties could impart selective activation of chemotherapeutic agents near tumor sites. Although RNase 1 was employed herein due to its abundance in plasma, (Weickmann, *et al.*, 1984; Su, *et al.*, 2004; Potenza, *et al.*, 2006; Sorrentino, 2010) RNase 1 homologues are also likely to activate prodrugs like UpHT (Sorrentino, 2010). One such homologue is eosinophil-derived neurotoxin (RNase 2), which is carried and released by eosinophils (Sorrentino, 2010) (another eosinophil ribonuclease, eosinophil cationic protein or RNase 3, was not shown to activate UpHT, data not shown). These cells are known to accumulate and degranulate at tumor sites (Munitz and Levi-Schaffer, 2004; Cormier, *et al.*, 2006; Lotfi, *et al.*, 2007). We anticipate that, akin to prodrug monotherapy (PMT) in which prodrugs are activated by endogenous enzymes found in abundance specifically near tumors (Bosslet, *et al.*, 1998), a prodrug strategy reliant on RNase 2 could be used to generate active drugs at adventitious sites. This would only work, however, if significant amounts of RNase 2 are released near tumors relative to RNase 1 serum levels.

## 2.5 Experimental Procedures

### 2.5.1 Materials

Uridine phosphoramidite and iodine oxidizing solution were purchased from Glen Research (Sterling, VA). Minimum 70% Z isomer of 4-hydroxytamoxifen (remainder primarily E-isomer), 3 Å molecular sieves, tetrabutylammonium fluoride (TBAF), methylbenzimidazole, and all other commercial reagents were purchased from Sigma–Aldrich (St. Louis, MO).

Methylbenzimidazole triflate was made according to literature precedent from methylbenzimidazole (Hayakawa, *et al.*, 2001). Spectra/Por<sup>®</sup> dialysis bags (3500 MWCO) were purchased from Fisher Scientific (Thermo Fisher Scientific, Walham, MA). *Escherichia coli* BL21(DE3) cells were from Novagen (Madison, WI). Cell culture medium and supplements, as well as Delbecco's PBS (DPBS) were from Invitrogen (Carlsbad, CA). [*methyl*-<sup>3</sup>H]Thymidine (6.7 Ci/mmol) was from Perkin-Elmer (Boston, MA). HiTrap columns were from GE Biosciences (Piscataway, NJ). MES buffer was from Sigma–Aldrich (St. Louis, MO) and purified by anion-exchange chromatography to remove trace amounts of oligomeric vinylsulfonic acid (Smith, *et al.*, 2003). Ribonuclease substrate 6-FAM-dArUdAdA-6-TAMRA was from Integrated DNA Technologies (Coralville, IA). Terrific Broth (TB) was from Research Products International Corp (Mt. Prospect, IL). SDS-PAGE gels were from Bio-Rad Laboratories (Hercules, CA).

### 2.5.2 *Instrumentation and statistical calculations*

$^1\text{H}$  NMRs were acquired at the National Magnetic Resonance Facility at Madison (NMRFAM) at 298 °K with a Bruker DMX-400 Avance spectrometer (Bruker AXS, Madison, WI,  $^1\text{H}$ , 400 MHz;  $^{13}\text{C}$ , 101 MHz;  $^{31}\text{P}$ , 162 MHz).  $^{13}\text{C}$  and  $^{31}\text{P}$  spectra were proton decoupled. All  $^1\text{H}$  and  $^{13}\text{C}$  NMR spectra were referenced to TMS. All  $^{31}\text{P}$  NMR spectra were referenced to an internal insert standard of  $\text{H}_3\text{PO}_4$ . Preparatory HPLC was performed on a Shimadzu Prominence HPLC (Kyoto, Japan) equipped with two LC-20AP pumps, a SPD-M20A photodiode array detector, and a CTO-20A column oven. Analytical HPLC was performed on a Waters HPLC (Milford, MA) equipped with two 515 pumps, a 717 plus autosampler, and a 996 photodiode array detector. Protein absorbance values were measured on a Varian Cary 50 UV-Vis Spectrometer (Agilent Technologies, Santa Clara, CA). [*methyl*- $^3\text{H}$ ]Thymidine incorporation into K-562 genomic DNA was quantified by scintillation counting using a Microbeta TriLux liquid scintillation and luminescence counter (Perkin-Elmer, Wellesley, MA). Fluorescence measurements were made on a QuantaMaster1 photon counting cuvette fluorometer from Photon Technology Internationalization (South Brunswick, NJ). Calculations for cell-proliferation assays were performed using GraphPad Prism version 5.02 (GraphPad Software, Inc., La Jolla, CA).

### 2.5.3 *Determination of partition and distribution coefficients*

LogP and LogD values were calculated using calculator plugins in the program MartinView 5.4.1.1, 2011 (ChemAxon Ltd., Budapest, Hungary) (ChemAxon, 2011). All values were set at default: calculations used equal weights (1) of VG, KLOP, and PHYS methods and the electrolyte concentrations ( $\text{Cl}^-$ ) and ( $\text{Na}^+$ ,  $\text{K}^+$ ) were set to 0.1 mol/dm<sup>3</sup>.

#### 2.5.4 *Cell cultures*

The MCF-7 cell line was a generous gift from the laboratory of Prof. Wes Pike at the University of Wisconsin–Madison. Cells were grown in a cell culture incubator at 37 °C and 5% CO<sub>2</sub> in flat-bottomed culture flasks. Cell media for growth and initial plating in assays was Dulbecco's Modified Eagle Medium (DMEM) containing phenol red and supplemented with 10% (v/v) GIBCO fetal bovine serum (FBS), 100 units/mL penicillin, 100 µg/mL streptomycin, 10 µg/mL human recombinant insulin, and 100 µM MEM non-essential amino acids solution (medium A). Cell media for cell proliferation experiments was DMEM without phenol red and without FBS, supplemented with 100 units/mL penicillin, 100 µg/mL streptomycin, 10 µg/mL human recombinant insulin, 100 µM MEM non-essential amino acids solution, and 1 mM sodium pyruvate (medium B). Values do not account for dilution.

#### 2.5.5 *Recombinant protein production*

Human pancreatic ribonuclease (RNase 1) was produced similar to previously described methods, (Johnson, *et al.*, 2007b) except that after purification over two chromatographic steps, the protein was re-purified over both steps to ensure purity. Following purification, purity and apparent molecular mass of RNase 1 was verified with SDS-PAGE.

#### 2.5.6 *Fluorescent assay for ribonuclease activity*

To ensure RNase 1 was active, the ribonucleolytic activity of RNase 1 was determined by quantitating its ability to cleave 6-FAM–dArUdAdA–6-TAMRA as described previously (Kelemen, *et al.*, 1999; Johnson, *et al.*, 2007b). Assays were carried out at ambient temperature

in 2 mL of 0.1 M MES–NaOH buffer containing 0.1 M NaCl, pH 6.0. Fluorescence data were fitted to equation 2.1, in which  $\Delta I/\Delta t$  is the initial reaction velocity,  $I_0$  is the fluorescence intensity before addition of ribonuclease,  $I_f$  is the fluorescence intensity after complete substrate hydrolysis, and  $[E]$  is the total ribonuclease concentration. Data were the average of three experiments. The activity of RNase 1 was  $(6.0 \pm 0.7) \times 10^6 \text{ M}^{-1} \text{ s}^{-1}$ . This is similar to previous values (29% of reference (Johnson, *et al.*, 2007b), though this reference lacked residue 128; 21% of reference (Rutkoski, *et al.*, 2010), though this reference used DPBS and 0.1 mg/mL BSA).

$$k_{\text{cat}}/K_{\text{M}} = \frac{\Delta I/\Delta t}{(I_f - I_0)[E]} \quad (2.1)$$

#### 2.5.7 HPLC assay for ribonuclease activity on uridine-3'-(4-hydroxytamoxifen phosphate)

Uridine 3'-(4-hydroxytamoxifen phosphate) (UpHT) was dissolved in standard ribonuclease activity buffer, 0.1 M MES–NaOH buffer, 0.1 M NaCl, pH 6.0, (Kelemen, *et al.*, 1999; Johnson, *et al.*, 2007b) plus 0.19% methanol (for solubility) to a final concentration of 90.45  $\mu\text{M}$ . One aliquot (900  $\mu\text{L}$ ) of this solution was placed in HPLC vial 1, and another aliquot (300  $\mu\text{L}$ ) was placed in HPLC vial 2. Vials with UpHT were pre-incubated at 37 °C in the HPLC autosampler. Buffer A was 0.1 M triethylammonium acetate (TEAA) diluted from 2 M TEAA stock (5% of vol final) in  $\text{H}_2\text{O}$  (95% of vol final). Buffer B was 0.1 M TEAA diluted from 2 M TEAA stock (5% of vol final) in acetonitrile (95% of vol final). RNase 1 was diluted in 0.1 M MES–NaOH buffer, pH 6.0, to a concentration of 8.526  $\mu\text{M}$  (~125 mg/L). A Varian 150/4.6 Microsorb-MV 100-5 C18 reverse-phase column was equilibrated with 30% Buffer A and 70% Buffer B. All

assays were performed isocratically with the same solution, 30% Buffer A and 70% Buffer B, at 1 mL/min for 5 min. First, 50  $\mu$ L from vial 1 was analyzed to obtain a baseline reading. Then, an aliquot (1  $\mu$ L) of the RNase 1 solution was added to the remaining 850  $\mu$ L of vial 1 (final RNase 1 concentration: 10 nM,  $\sim$ 0.15 mg/L). Twelve assays of 50  $\mu$ L each were then performed at specified times. After a blank sample of 50  $\mu$ L of Buffer B was assayed, an aliquot (50  $\mu$ L) of vial 2 was assayed to assess the amount of UpHT activated under the same experimental conditions but in the absence of RNase 1. An aliquot (9  $\mu$ L) of an excess RNase 1 solution (143.89  $\mu$ M RNase) was then added to the remaining 250  $\mu$ L in vial 1 for a final RNase 1 concentration of 5  $\mu$ M ( $\sim$ 74 mg/L) to cleave >95% of the UpHT. After  $\sim$ 1.5 h, 50  $\mu$ L was assayed and set as 100% UpHT activated (adjusted for dilution by excess RNase 1; <5% of the original prodrug peak remained). The entire experiment was run in triplicate. Overlaid HPLC traces are from one experiment (Figure 2.2). Baseline readings (the UpHT sample ran prior to RNase 1 addition) were subtracted from peaks at approximately the same elution time to obtain HT concentrations at each timepoint (<2% of 100% UpHT activated HT peak areas were seen in baseline readings). Any other small peaks that overlapped with the elution times of the HT peaks in the baseline reading (UpHT sample prior to RNase 1 addition) were subtracted from HT peaks to obtain HT concentrations at each timepoint. To determine the amount of free 4-hydroxytamoxifen (HT) released, the area for the two HT peaks for each assay was divided by the 100% UpHT activated area of the two HT peaks (adjusted for dilution) and multiplied by the concentration of UpHT used (90.45  $\mu$ M). The kinetic graph data points represent the mean  $\pm$  standard error for each timepoint. All data accounted for the dilution that accompanies the addition of RNase 1.

### 2.5.8 Cell-proliferation assays

The effect of UpHT and HT on the proliferation of MCF-7 cells was assayed using a [*methyl*-<sup>3</sup>H]thymidine incorporation assay, similar to a [*methyl*-<sup>3</sup>H]thymidine incorporation assay described previously (Leland, *et al.*, 1998). The assay was also modified from a previous publication that studied rapid death of MCF-7 cells by tamoxifen (Zheng, *et al.*, 2007). For assays, MCF-7 cells (100  $\mu$ L of a solution of  $5.0 \times 10^4$  cells/mL) in medium A were plated in each well of 96-well plates and incubated for 22 h to allow for cell adherence. Medium was removed, cells were washed with DPBS, and medium B (50  $\mu$ L) was then added. UpHT and HT were first dissolved in DMSO, and then diluted 1000-fold with medium B, resulting in a final DMSO concentration of 0.1% v/v. This was serially diluted with medium B with an equal percentage of final DMSO (0.1%). The highest concentration HT dilutions appeared to be cloudy, indicating that these concentrations may be reaching the solubility limit of HT in medium. Aliquots (50  $\mu$ L) of these serial dilutions were added to wells (final DMSO concentration: 0.05% v/v). Cell growth control wells received medium B and 0.1% DMSO but no drug (final DMSO concentration: 0.05% v/v). RNase 1 was diluted in medium B, and wells either received 1  $\mu$ L of stock RNase 1 for a final concentration of 0.42  $\mu$ M ( $\sim 6.2$  mg/L,  $\sim 15.5\times$  plasma concentration of  $\sim 0.4$  mg/L) or 1  $\mu$ L of medium B, and the analyzed drug concentrations take into account this dilution. RNase 1 control wells received no drug but did receive RNase 1. After a 2 h incubation with treatments, MCF-7 cells were treated with [*methyl*-<sup>3</sup>H]thymidine for 4 h, and the incorporation of radioactive thymidine into cellular DNA was then quantitated by liquid scintillation counting. The results are shown as the percentage of [*methyl*-<sup>3</sup>H]-thymidine incorporated relative to control cells treated with medium B and 0.1% DMSO (final DMSO concentration: 0.05% v/v). Data are the average



of three measurements for each concentration, excluding those measurements that were determined to be outliers by the Grubb's test for outliers with  $p$  value = 0.05 (Grubbs, 1969). The entire experiment was repeated in triplicate. Values for  $IC_{50}$  were calculated by fitting the curves by nonlinear regression with equation 2.2, in which  $y$  is the total DNA synthesis following the [*methyl*- $^3H$ ]thymidine pulse, and  $h$  is the slope of the curve.

$$y = \frac{100\%}{1 + 10^{(\log(IC_{50}) - \log[ribonuclease])h}} \quad (2.2)$$

## 2.5.9 Syntheses

### 2.5.9.1 Protected uridine 3'-(4-hydroxytamoxifen phosphate)

A 20 mL scintillation vial was flame-dried under vacuum and to this was added 3 Å molecular sieves (10 beads) followed by 4-hydroxytamoxifen (0.100 g, 0.258 mmol), phosphoramidite (0.222 g, 0.258 mmol), and anhydrous acetonitrile (2.58 mL, 0.1 M). After stirring at room temperature 5 minutes, methylbenzimidazole triflate (0.073 g, 0.258 mmol) was added and the reaction was allowed to stir for 2.5 h at room temperature. The solution was then decanted from the sieves into a new scintillation vial, concentrated to remove the acetonitrile, and treated with a 0.02 M  $I_2$  solution (12.6 mL, 2.52 mmol) in tetrahydrofuran, pyridine, and water (Glen Research Oxidizing Solution) for 1 h. The reaction was then concentrated under vacuum and purified by flash silica gel chromatography (10% MeOH, 90% DCM) to give protected uridine 3'-(4-hydroxytamoxifen phosphate) as a mixture of isomers (0.279 g, 93%).

**<sup>1</sup>H NMR (400 MHz, CD<sub>3</sub>OD)**(Mixture of isomers)  $\delta$ = 7.91–7.83 (m, 1H), 7.43–7.35 (m, 2H), 7.34–7.20 (m, 8H), 7.19–7.01 (m, 8H), 6.91–6.82 (m, 4H), 6.80–6.73 (m, 2H), 6.65–6.56 (m, 2H), 6.00–5.85 (m, 1H), 5.43–5.31 (m, 1H), 5.08–4.96 (m, 1H), 4.64–4.50 (m, 1H), 4.48–4.36 (m, 2H), 4.34–4.21 (m, 1H), 4.15–4.01 (m, 3H), 3.76 (as, 6H), 3.65–3.45 (m, 2H), 3.40–3.30 (m, 1H), 2.95–2.85 (m, 2H), 2.74 (as, 6H), 2.51–2.30 (m, 2H), 0.95–0.82 (m, 12H), 0.20–0.06 (m, 6H). **<sup>13</sup>C NMR (101 MHz, CD<sub>3</sub>OD)**(Major Isomer)  $\delta$ = 165.6, 160.3, 157.2, 152.1, 150.0, 145.8, 143.8, 143.3, 142.7, 141.7, 138.2, 137.6, 136.3, 133.2, 132.2, 131.5, 130.8, 129.3, 129.2, 129.0, 128.3, 127.4, 121.2, 118.2, 115.6, 114.7, 114.5, 103.3, 88.8, 83.4, 79.4, 75.7, 65.3, 63.7, 63.3, 57.9, 55.9, 44.3, 30.0, 26.2, 20.2, 19.0, 13.8, –4.7. **<sup>31</sup>P NMR (162 MHz, CD<sub>3</sub>OD)**(Mixture of isomers)  $\delta$  = –8.57, –8.82, –9.02. **HRMS (ESI)  $m/z$**  1163.4998 [calc'd for C<sub>65</sub>H<sub>76</sub>N<sub>4</sub>O<sub>12</sub>PSi (M+H) 1163.4962].

#### 2.5.9.2 DMT-free, semi-protected uridine 3'-(4-hydroxytamoxifen phosphate)

An acetic acid : distilled water mixture (60 : 40, 4.6 mL, 0.05 M) was added to a 20 mL scintillation vial containing 4-hydroxytamoxifen phosphate (0.270 g, 0.232 mmol) and the reaction was allowed to stir at room temperature for 5 h until starting material was consumed as determined by TLC (10% MeOH, 90% DCM). The reaction was then quenched by adding saturated sodium bicarbonate (5 mL), extracted with ethyl acetate (4 x 5 mL), dried over sodium sulfate, and concentrated under vacuum. The resulting residue was purified using flash silica gel chromatography (10% MeOH, 90% DCM) to give DMT-free, semi-protected uridine 3'-(4-hydroxytamoxifen phosphate) (0.180 g, 90%).

**<sup>1</sup>H NMR (400 MHz, CD<sub>3</sub>OD)**(Mixture of isomers)  $\delta$ = 8.17–7.95 (m, 1H), 7.35–7.21 (m, 3H), 7.20–7.05 (m, 6H), 6.81 (d,  $J$  = 8.6, 2H), 6.64 (d,  $J$ = 8.6, 2H), 6.09–5.89 (m, 1H), 5.82–5.66 (m, 1H), 4.63–4.25 (m, 4H), 4.20–4.07 (m, 2H), 3.75–3.53 (m, 2H), 3.43–3.33 (m, 1H), 2.97–2.90 (m, 2H), 2.87–2.74 (m, 8H), 2.50–2.40 (m, 2H), 0.97–0.79 (m, 12H), 0.15–0.01 (m, 6H). **<sup>13</sup>C NMR (101 MHz, CD<sub>3</sub>OD)**(Major Isomer)  $\delta$  = 164.4, 156.1, 151.0, 148.7, 141.9, 140.7, 137.0, 136.1, 130.8, 130.3, 129.4, 127.6, 125.9, 119.9, 118.8, 116.8, 114.1, 113.3, 102.1, 87.2, 83.7, 78.9, 74.3, 63.9, 62.3, 60.7, 56.5, 42.9, 28.5, 24.8, 18.8, 17.6, 12.4, –6.0. **<sup>31</sup>P NMR (162 MHz, CD<sub>3</sub>OD)**(Mixture of Isomers)  $\delta$  = –8.53, –8.64, –8.71, –8.81. **HRMS (ESI)**  $m/z$  861.3652 [calc'd for C<sub>44</sub>H<sub>58</sub>N<sub>4</sub>O<sub>10</sub>PSi (M+H) 861.3655].

#### 2.5.9.3 *Uridine 3'-(4-Hydroxytamoxifen phosphate)*

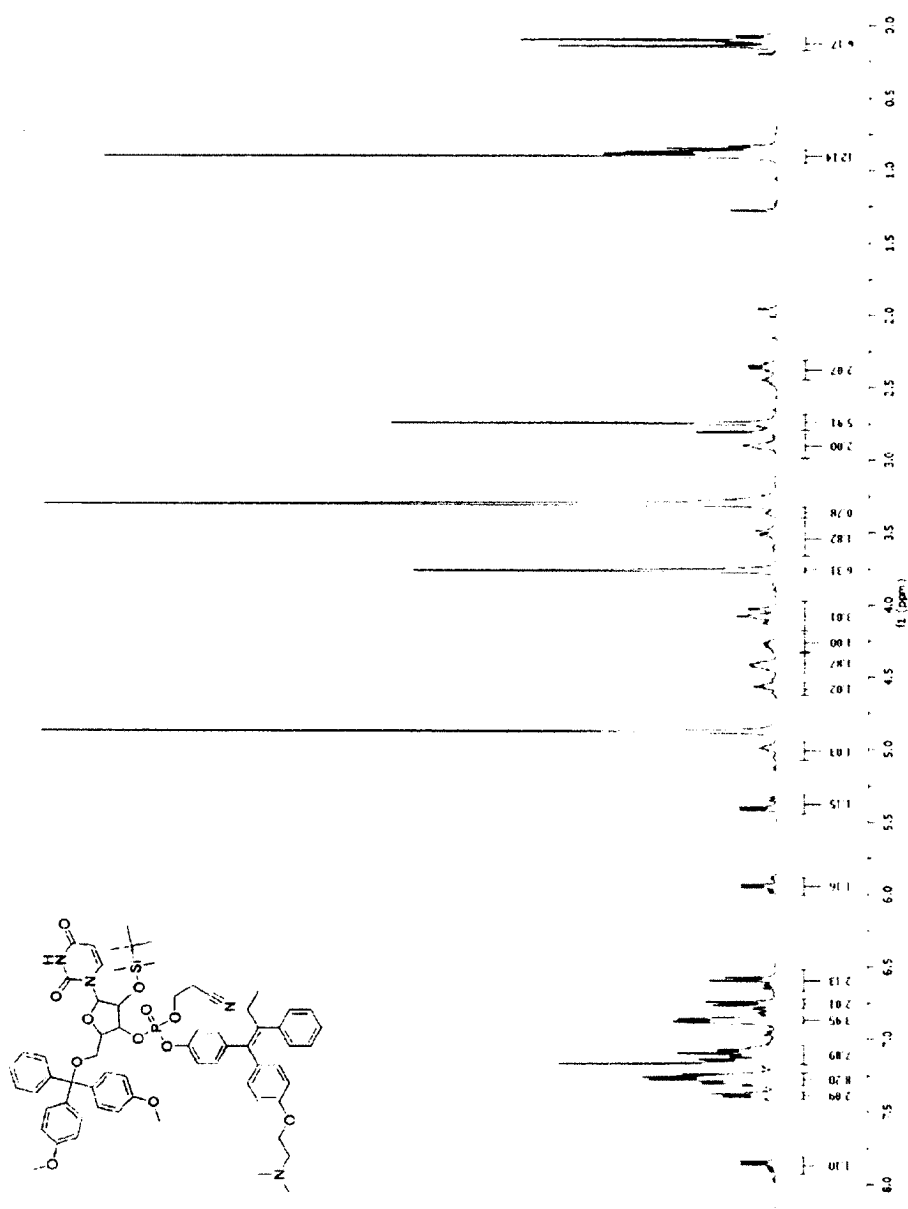
Anhydrous ethanol (1.2 mL, 0.05 M) was added to a 20 mL scintillation vial containing DMT-free 4-hydroxytamoxifen phosphate (0.051 g, 0.059 mmol) at room temperature followed by ammonium hydroxide (0.04 mL, 1.185 mmol) and the reaction was allowed to stir 3 h before concentrating under vacuum to give a crude residue (0.047 g, 98%) that was used directly in the next step.

A portion of the resulting crude residue (0.030 g, 0.037 mmol) was dissolved in anhydrous acetonitrile (4.3 mL, 0.009 M) at 0 °C and tetrabutylammonium fluoride solution (0.04 mL, 0.040 mmol, 1 M) was added in one portion and the reaction was warmed to room temperature and allowed to stir for a total of 5 h. The reaction was then diluted with 4.3 mL of distilled water and stored in the freezer for HPLC purification. After thawing, the sample was loaded onto a Macherey-Nagel VP 250/21 Nucleosil 100-5 C18 reverse-phase column incubated at 35 °C (also

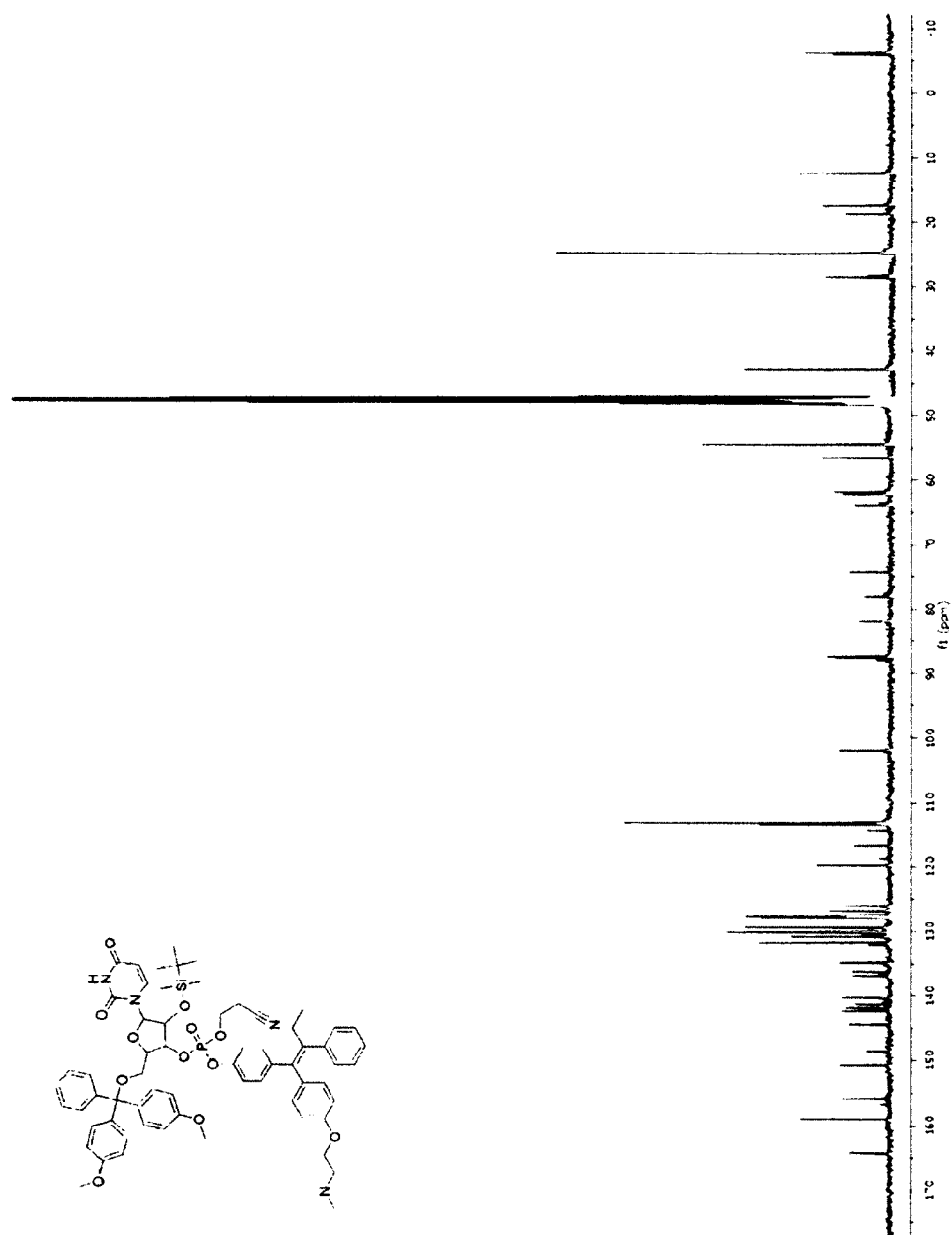
for duration of run) and pre-equilibrated in 25% acetonitrile in H<sub>2</sub>O. Sample was washed with the same solution, 25% acetonitrile in H<sub>2</sub>O, for 13 min. Product was then eluted with a linear gradient from 25% to 100% acetonitrile in H<sub>2</sub>O for 68 minutes and then concentrated under vacuum, providing the uridine 3'-(4-hydroxytamoxifen phosphate) (0.020 g, 77%, 69% corrected for Bu<sub>4</sub>N<sup>+</sup> salt).

**<sup>1</sup>H NMR (400 MHz, CD<sub>3</sub>OD)**(Both Olefin Isomers)  $\delta$  = 8.03 (d,  $J$  = 8.1, 0.77H), 7.99 (d,  $J$  = 8.2, 0.23H), 7.23 (d,  $J$  = 8.2, 1.54H), 7.17–7.03 (m, 7.00H), 6.97 (d,  $J$  = 8.5, 0.46H), 6.87 (d,  $J$  = 8.5, 0.46H), 6.77 (at,  $J$  = 8.6, 2.00H), 6.61 (d,  $J$  = 8.6, 1.54H), 5.96 (d,  $J$  = 5.5, 0.77H), 5.90 (d,  $J$  = 5.5, 0.23H), 5.69 (at,  $J$  = 6.8, 1.00H), 4.77–4.66 (m, 0.77H), 4.64–4.56 (m, 0.23H), 4.35–4.05 (m, 4.00H), 3.80–3.66 (m, 2.00H), 3.31–3.17 (m, 2.00H), 2.80 (s, 1.38H), 2.74 (s, 4.62H), 2.46 (q,  $J$  = 7.3, 2.00H), 0.90 (t,  $J$  = 7.3, 3.00H). (Bu<sub>4</sub>N<sup>+</sup> Signals)  $\delta$  = 3.31–3.17 (m, 2.42H), 1.70–1.60 (m, 2.53H), 1.47–1.37 (m, 2.60H), 1.02 (t,  $J$  = 7.3, 3.62H). **<sup>13</sup>C NMR (101 MHz, CD<sub>3</sub>OD)**(Major Isomer Peaks + 4 Bu<sub>4</sub>N<sup>+</sup> Salt Signals)  $\delta$  = 164.7, 155.9, 151.4, 151.0, 142.3, 141.6, 141.1, 138.8, 137.7, 136.5, 131.7, 130.0, 129.5, 127.5, 125.8, 119.8, 113.1, 101.4, 88.5, 84.0, 74.6, 73.9, 62.4, 60.8, 58.1, 56.6, 42.9, 28.5, 23.4, 19.3, 12.5, 12.4. **<sup>31</sup>P NMR (162 MHz, CD<sub>3</sub>OD)** (Both Olefin Isomers)  $\delta$  = –5.90, –6.09. **HRMS (ESI)  $m/z$**  716.2324 [calc'd for C<sub>35</sub>H<sub>40</sub>N<sub>3</sub>O<sub>10</sub>PNa (M+Na) 716.2344].

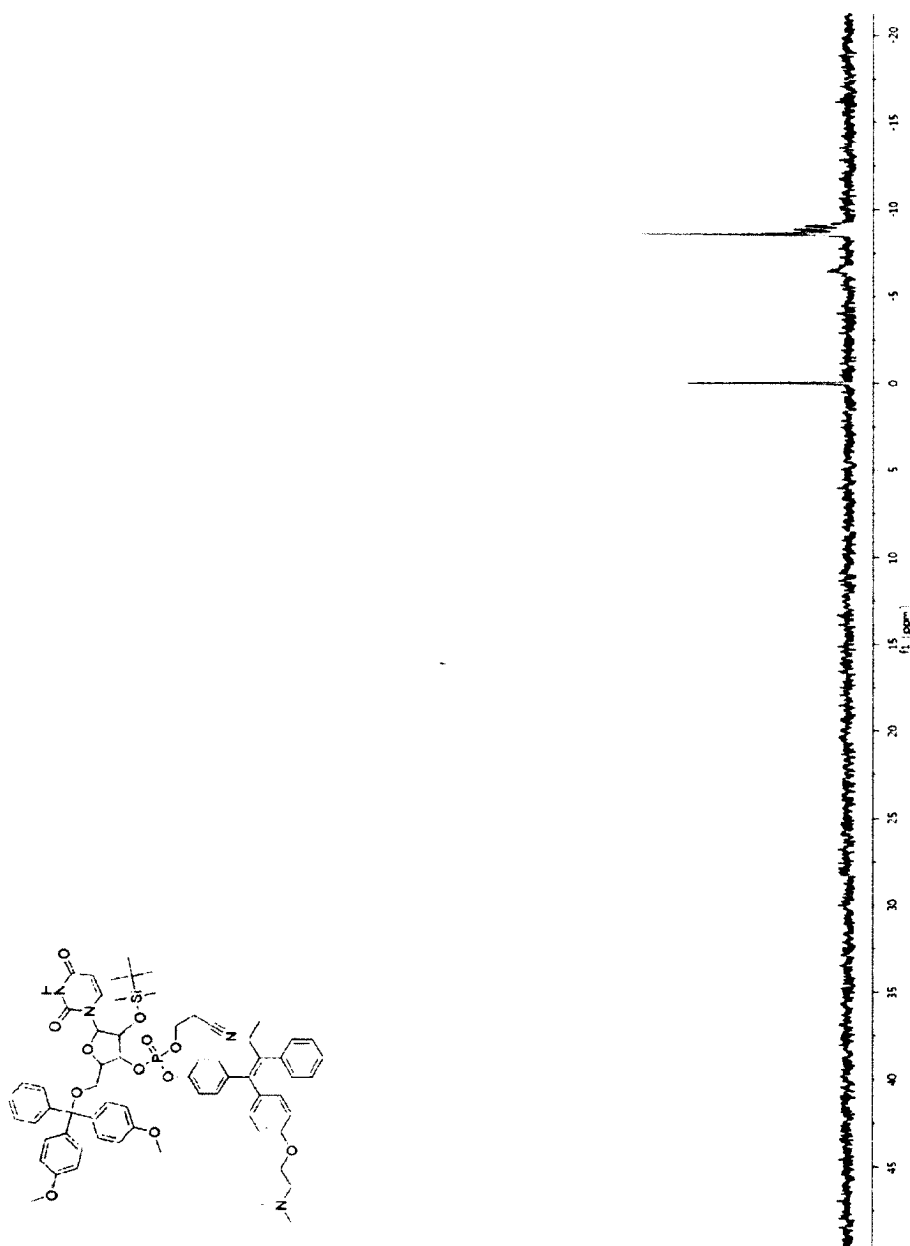
#### 2.5.10 NMR spectra

2.5.10.1 400 MHz  $^1\text{H}$  NMR spectrum of 4-Hydroxytamoxifen phosphate in  $\text{CD}_3\text{OD}$ 

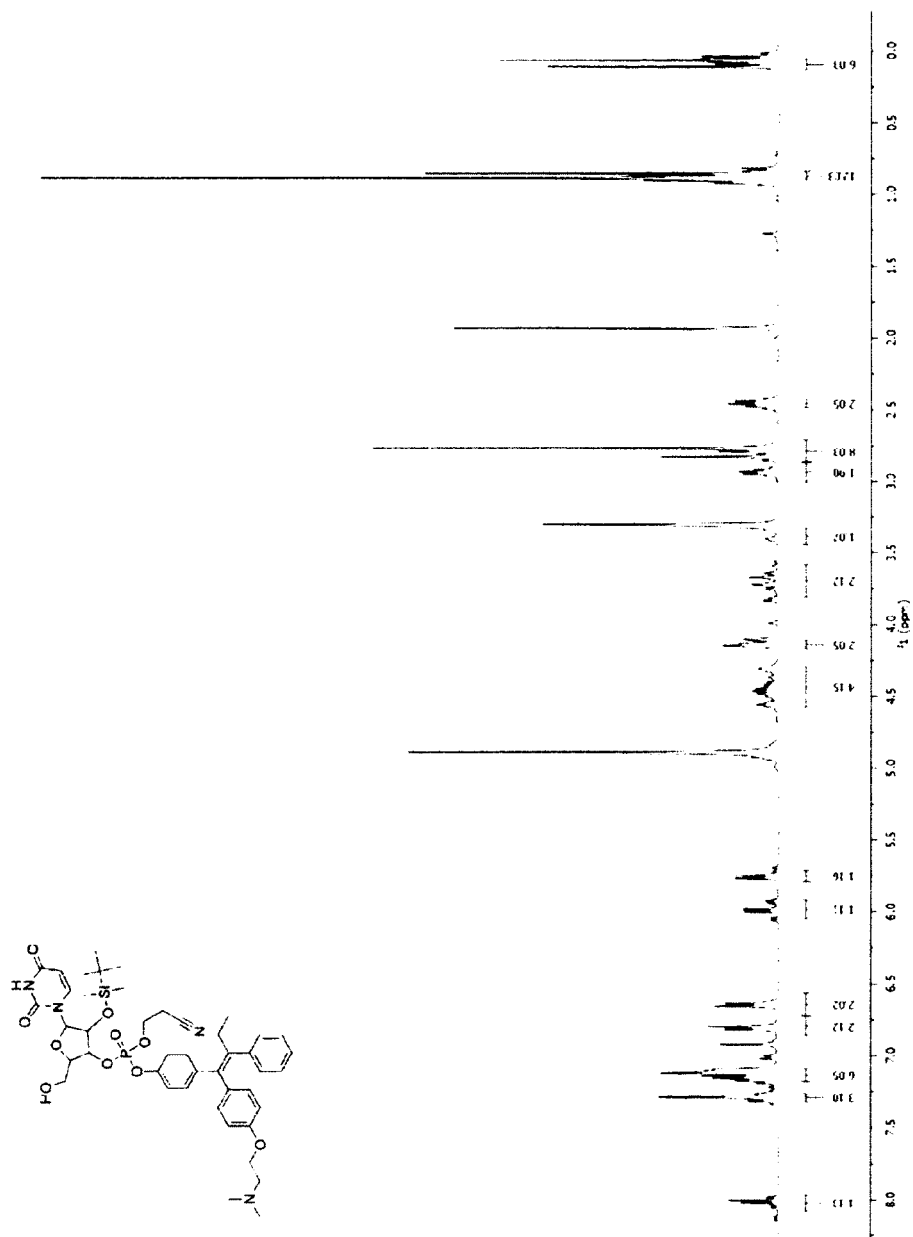
2.5.10.2 101 MHz  $^{13}\text{C}$  NMR spectrum of 4-Hydroxytamoxifen phosphate in  $\text{CD}_3\text{OD}$



2.5.10.3 162 MHz  $^{31}\text{P}$  NMR spectrum of 4-Hydroxytamoxifen phosphate in  $\text{CD}_3\text{OD}$

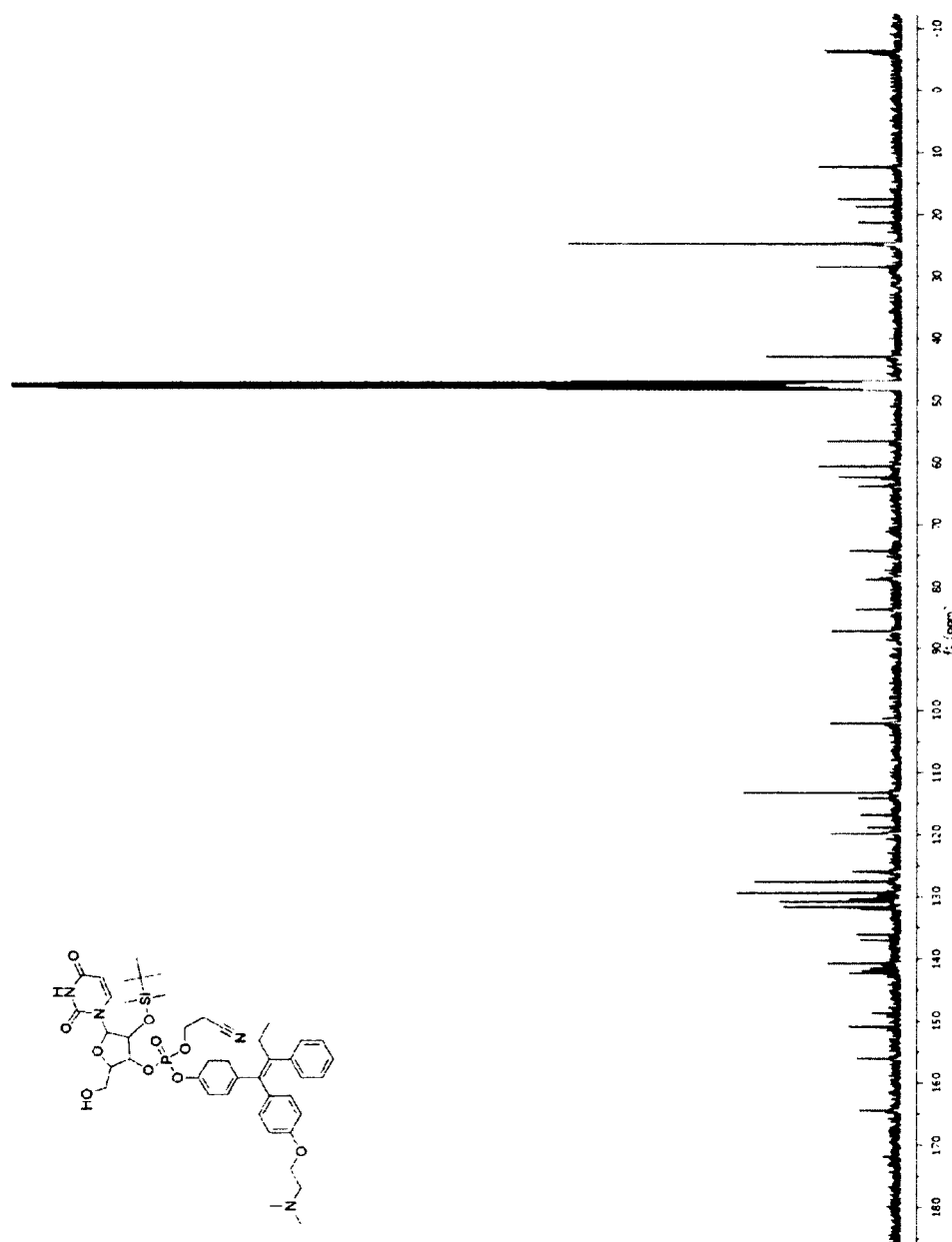


2.5.10.4 400 MHz  $^1\text{H}$  NMR spectrum of DMT-free 4-hydroxytamoxifen phosphate in  $\text{CD}_3\text{OD}$

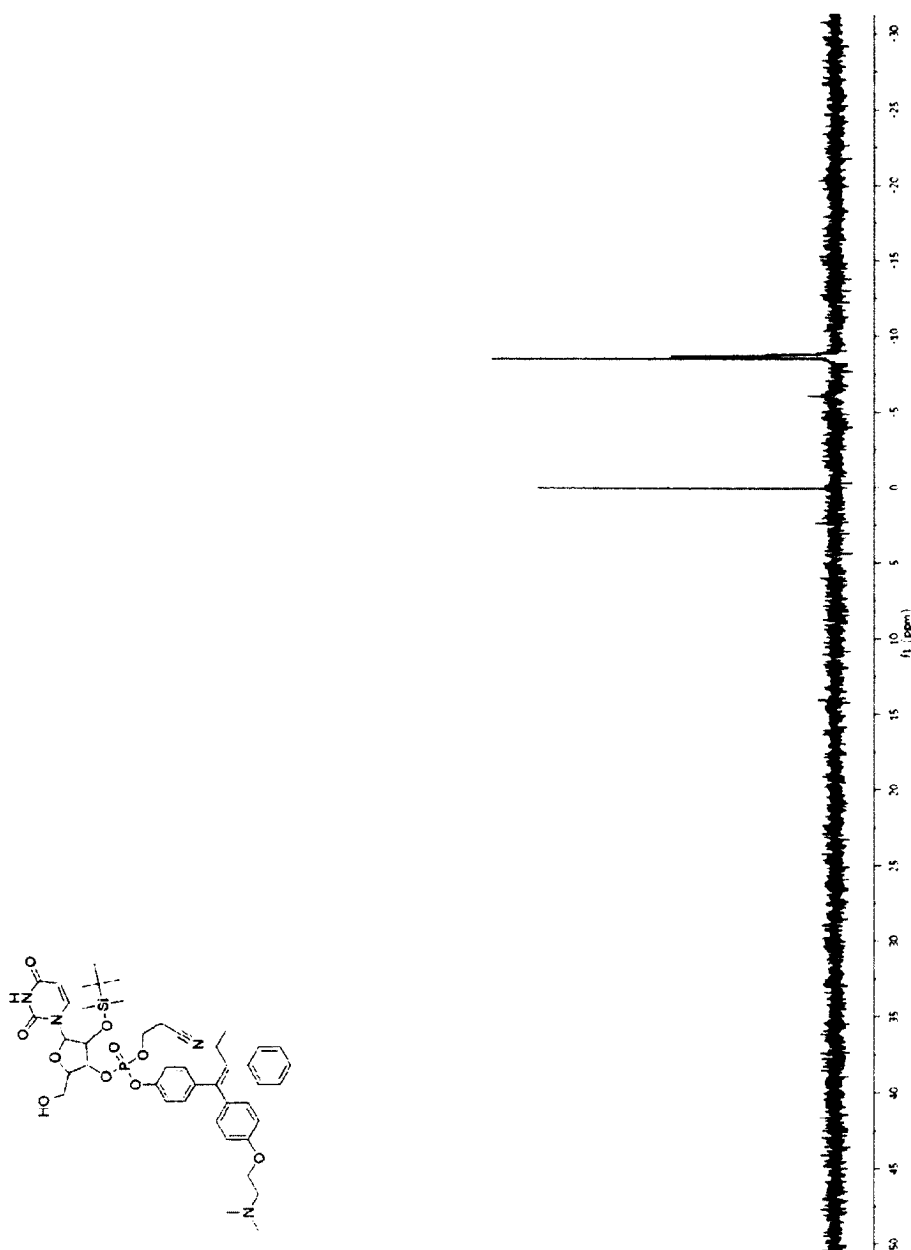


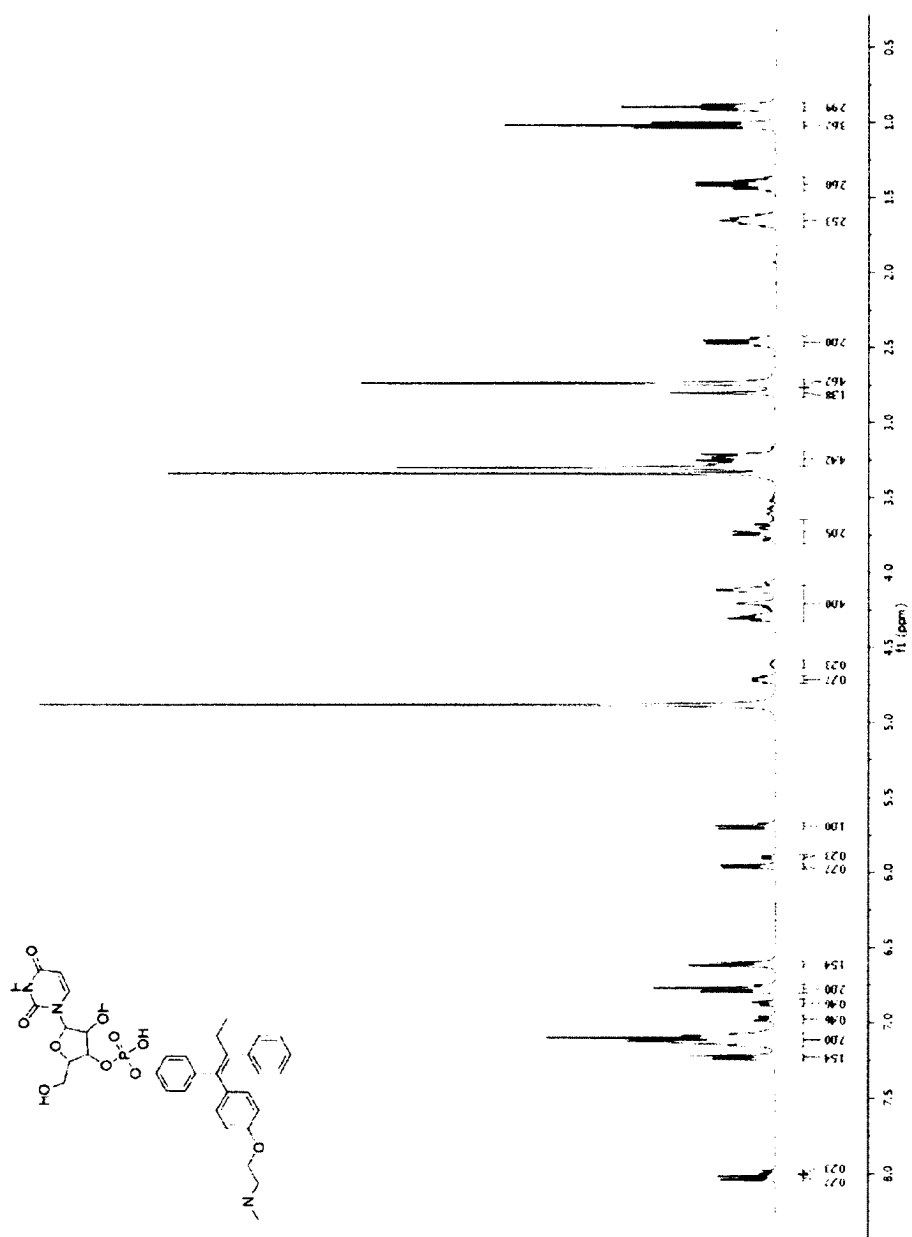


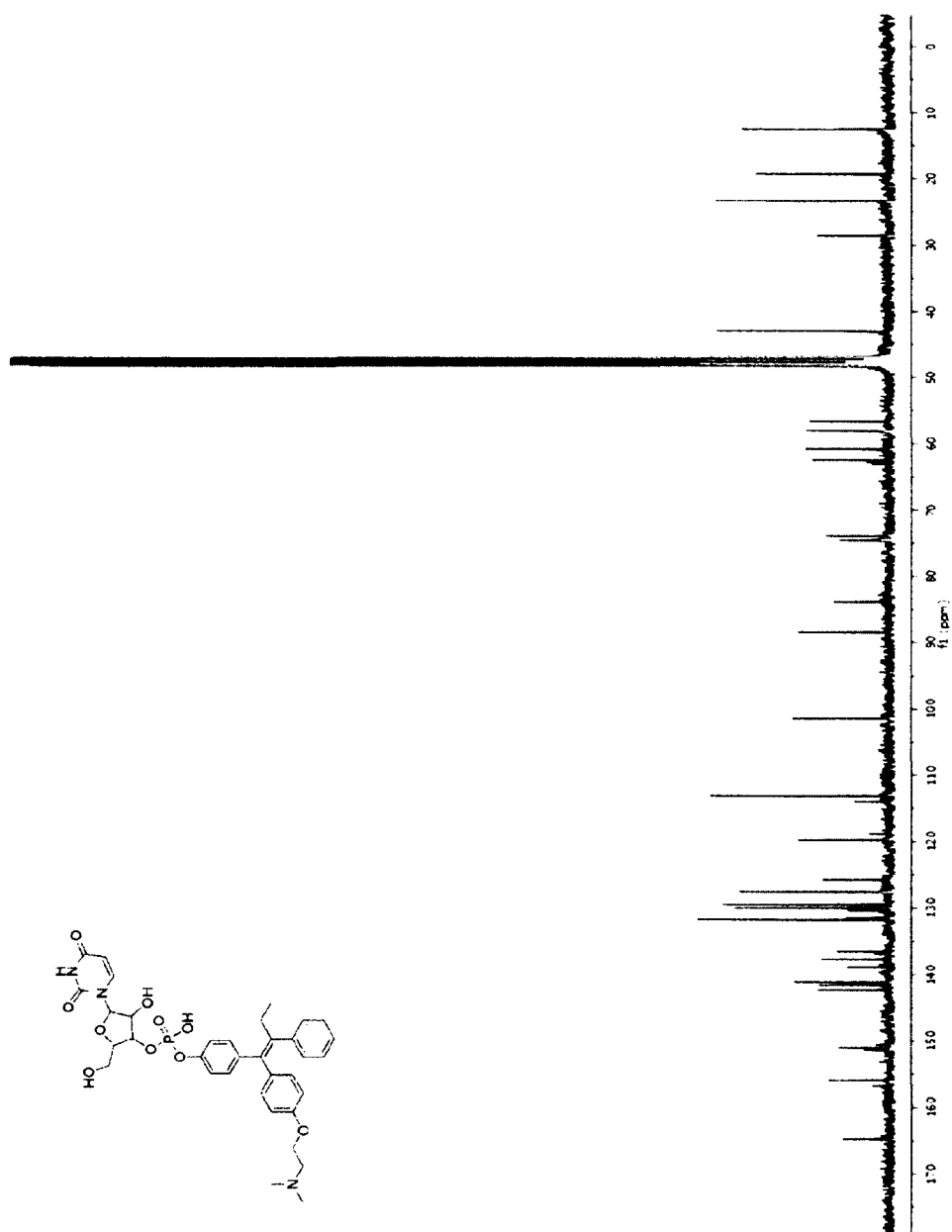
2.5.10.5 101 MHz  $^{13}\text{C}$  NMR spectrum of DMT-free 4-hydroxytamoxifen phosphate in  $\text{CD}_3\text{OD}$

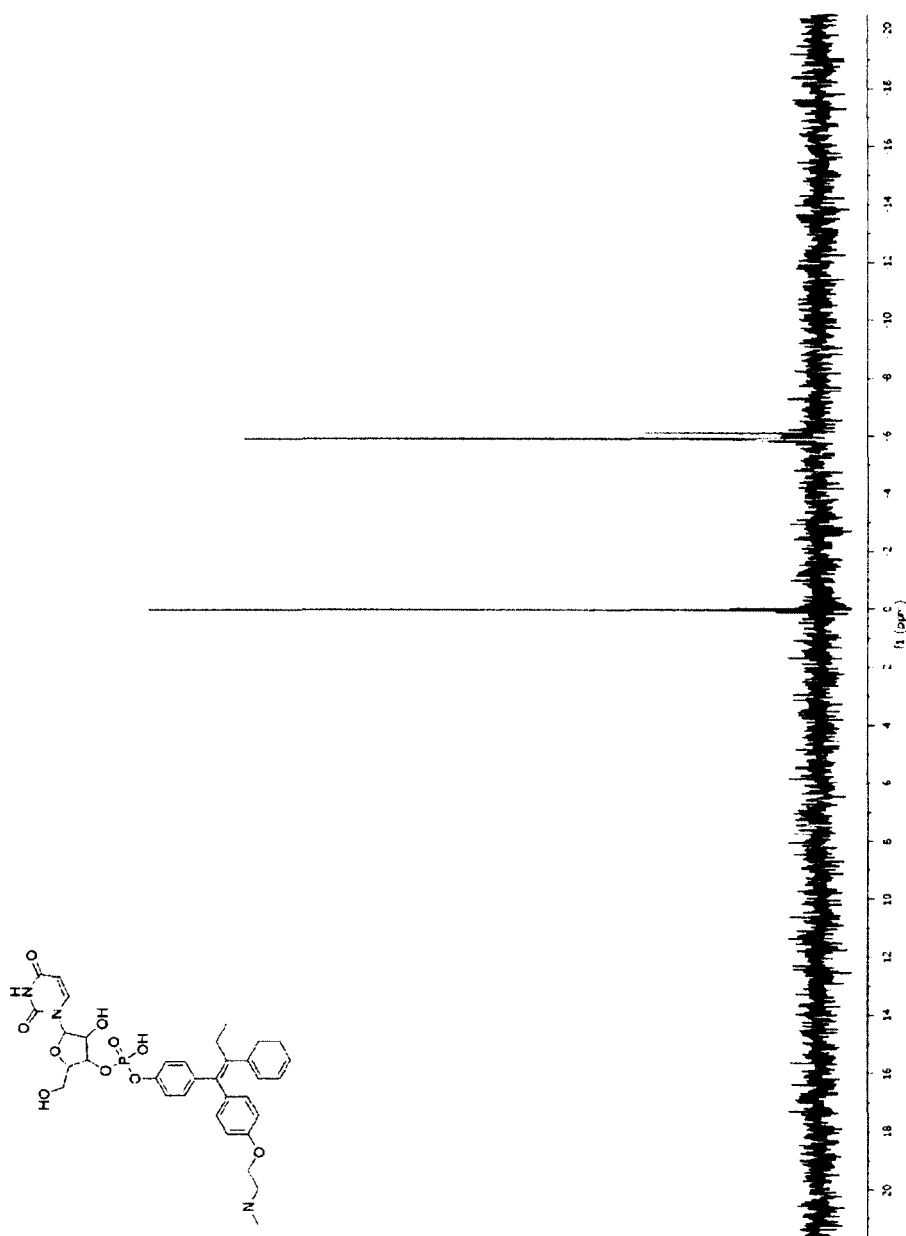


2.5.10.6 162 MHz  $^{31}\text{P}$  NMR spectrum of DMT-free 4-hydroxytamoxifen phosphate in  $\text{CD}_3\text{OD}$



2.5.10.7 400 MHz  $^1\text{H}$  NMR spectrum of 4-Hydroxytamoxifen prodrug in  $\text{CD}_3\text{OD}$ 





## 2.6 Acknowledgments

The authors acknowledge M. L. Hornung for early contributions, This work was supported by grant R01 CA073808 (NIH). N.A. McGrath was supported by the postdoctoral fellowship F32 GM096712 (NIH). M.J. Palte was supported by Molecular and Cellular Pharmacology Training Grant T32 GM008688 (NIH) and predoctoral fellowship 09PRE2260125 (American Heart Association). This study made use of the National Magnetic Resonance Facility at Madison, which is supported by NIH grants P41RR02301 (BRTP/ NCRR) and P41GM66326 (NIGMS). Additional equipment was purchased with funds from the University of Wisconsin, the NIH (RR02781, RR08438), the NSF (DMB-8415048, OIA-9977486, BIR-9214394), and the USDA.

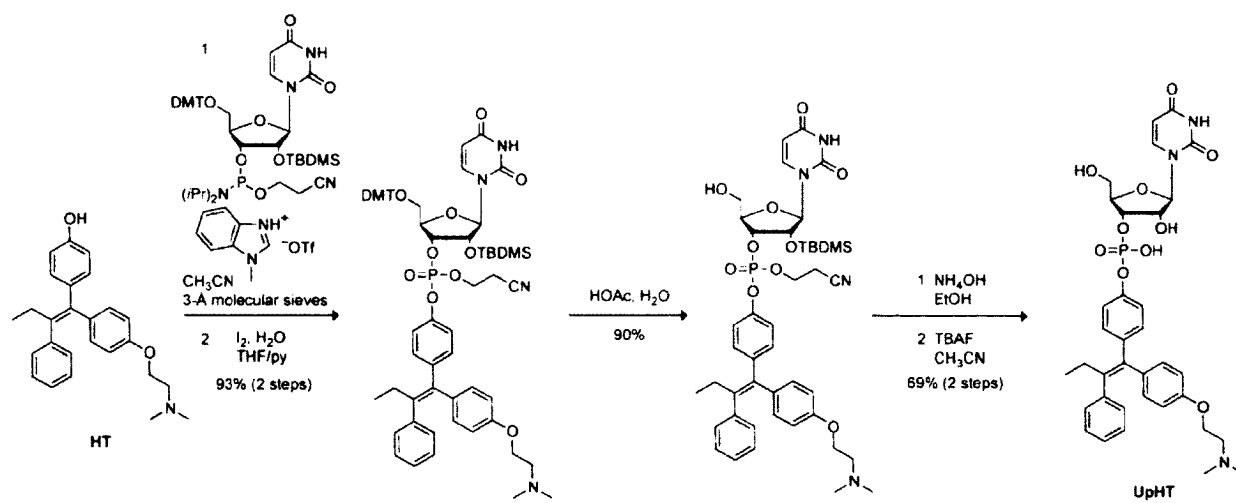
## 2.7 Contributions

Original idea for using ribonucleoside 3'-phosphate pro-moieties for timed-release was from M.J. Palte. Attempted syntheses of other drugs attached to uridine 3'-phosphate were first done by M.J. Palte and G.A. Ellis, then by N.A. McGrath and G.A. Ellis. First attempted synthesis of UpHT was done by G.A. Ellis; N.A. McGrath optimized conditions and synthesized UpHT synthesis in good yield. Final product was HPLC purified by G.A. Ellis. Full characterization of UpHT and intermediates was done by N.A. McGrath. Protein purification and characterization, LogP and LogD calculations, HPLC kinetic assays, and cytotoxicity experiments were done by G.A. Ellis.

**Table 2.1** Partition and distribution coefficients of HT and UpHT. These were calculated with the program MartinView (ChemAxon, Budapest, Hungary) (ChemAxon, 2011).

Coefficient	HT	UpHT
logP, non-ionized species	6.05	3.88
logP, ionized species	2.55	-2.00
logD (pH 7.4)	4.66	0.12
logD (pH = pI <sup>a</sup> )	5.69	-1.79

<sup>a</sup> HT, pI 9.01; UpHT, pI 5.00

**Scheme 2.1** Synthesis of UpHT



**Figure 2.1** Activation of prodrug by RNase 1. Prodrug (UpHT: uridine-3'-(4-hydroxytamoxifen phosphate) activation by RNase 1 should result in active drug (HT: 4-hydroxytamoxifen) and modified, inert pro-moiety (U>p: uridine-2',3'-cyclic phosphate ester).

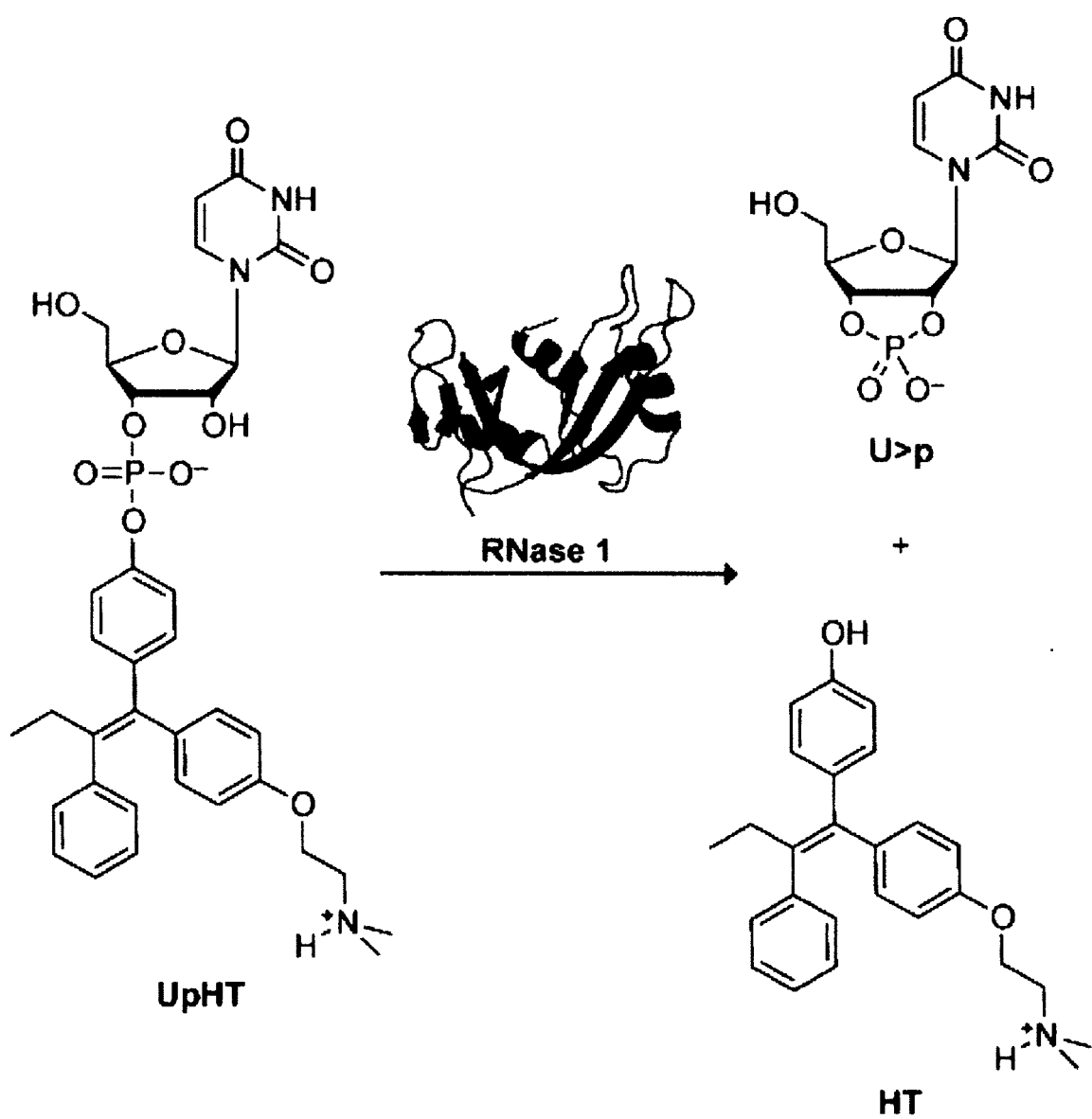


**Figure 2.2**    Compilation of HPLC traces from one UpHT activation experiment. Release of free HT by RNase 1 at 37 °C was monitored over time at 245 nm by the appearance of HT peaks at 3.3 and 3.9 min (presumably Z and E isomers). The baseline trace is prior to addition of RNase 1 and the final blue trace is after addition of excess RNase 1.

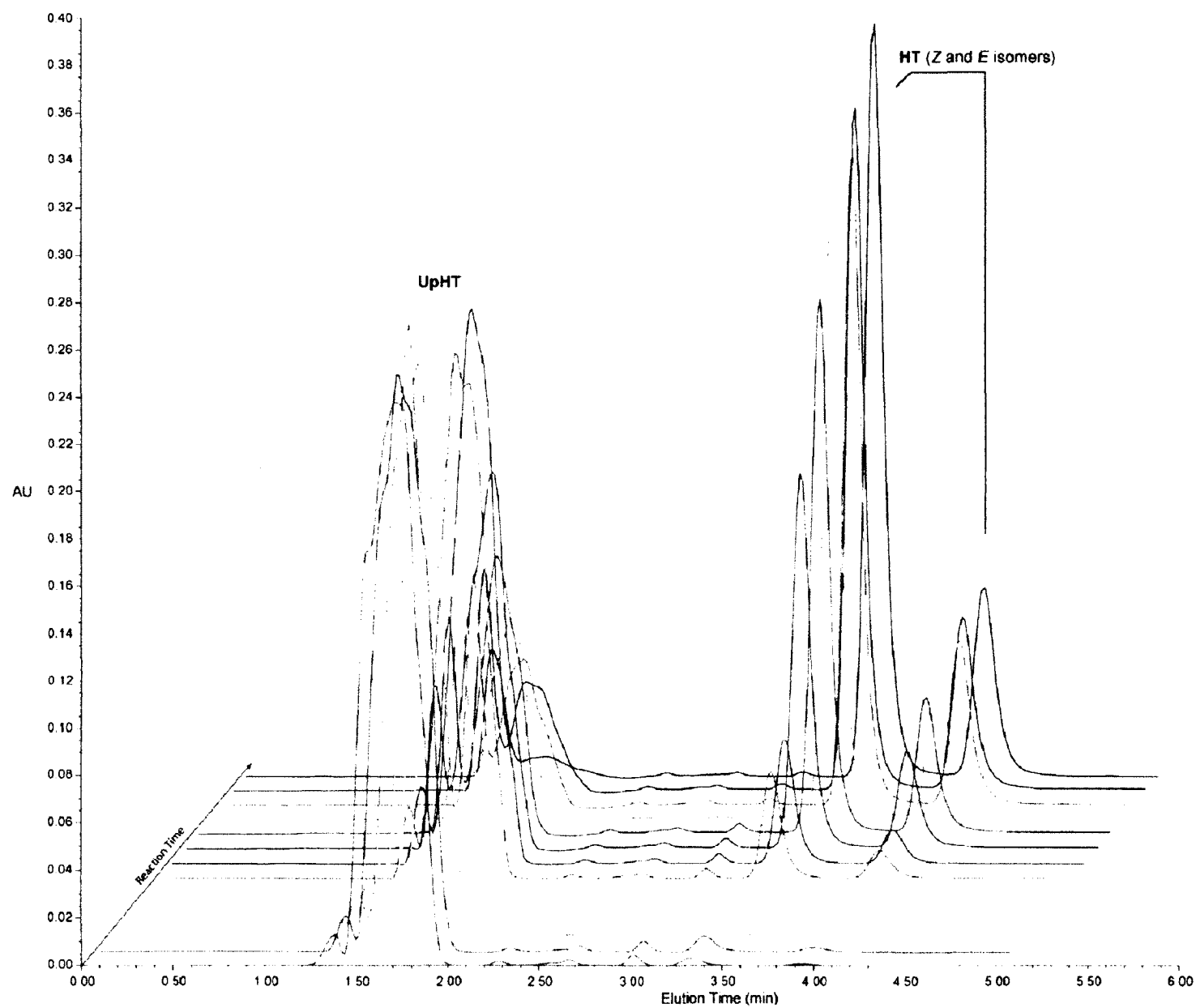


**Figure 2.3** Progress curve of UpHT activation by RNase 1. The half-life of the release of HT from UpHT (90.45  $\mu\text{M}$ ) by RNase 1 was approximately 4 h in the buffer 100 mM MES–NaOH, pH 6.0, containing NaCl (100 mM).

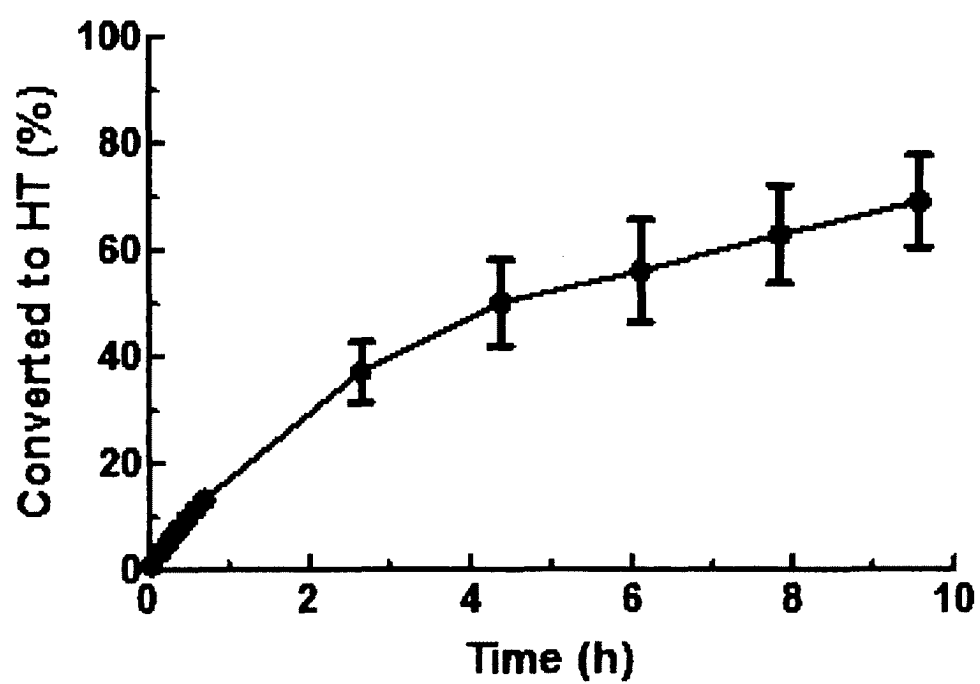
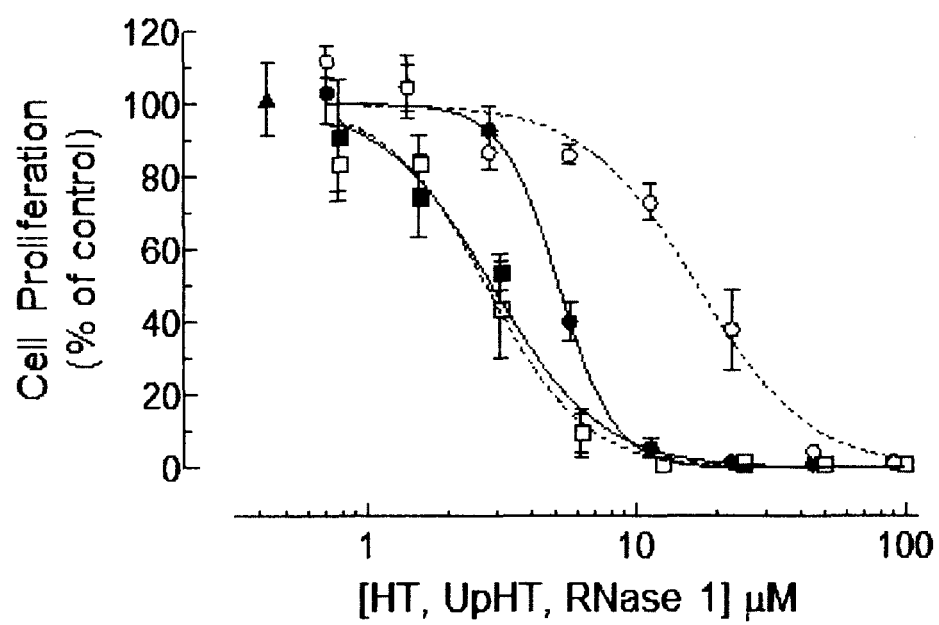


**Figure 2.4** MCF-7 cell proliferation upon UpHT activation by RNase 1. The anti-proliferative activity of UpHT (open circles, dashed line;  $IC_{50} = 16.7 \pm 0.8 \mu M$ ) is increased significantly upon incubation with added RNase 1 (closed circles, solid line;  $IC_{50} = 5.2 \pm 0.2 \mu M$ ). The anti-proliferative activity of control HT does not change significantly in the absence (open squares, dashed line;  $IC_{50} = 2.7 \pm 0.1 \mu M$ ) or presence (closed squares, solid line,  $IC_{50} = 2.7 \pm 0.4 \mu M$ ) of added RNase 1. Control RNase 1 treatment alone is represented as closed triangles. Error is calculated as standard error of the mean.





## **CHAPTER 3**

### **Boronate-mediated Drug Delivery**

This chapter was submitted for publication as:

Ellis, G.A.\*, Palte, M.J.\*, and Raines, R.T. (2011) Boronate-mediated drug delivery. (\* denotes equal contribution)

### 3.1 Abstract

Inefficient cellular delivery limits the landscape of macromolecular drugs. Boronic acids readily form boronate esters with the 1,2- and 1,3-diols of saccharides, such as those that coat the surface of cells. Here, pendant boronic acids are shown to enhance the delivery of a protein into cells (Figure 3.1).

### 3.2 Introduction

The utility of many biologic drugs is limited by inefficient cellular delivery (Patil, *et al.*, 2005; Malik, *et al.*, 2007; Shim and Kwon, 2010). Previous efforts to overcome this limitation have focused largely on the use of cationic domains—peptidic (*e.g.*, HIV-TAT, penetratin, and nonaarginine) or non-peptidic (*e.g.*, PAMAM dendrimers and polyethylimine)—to enhance the attraction between a chemotherapeutic agent and the anionic cell surface (Gao, *et al.*, 2008; Rapoport and Lorberboum-Galski, 2009; Sun and Zhang, 2010; Schmidt, *et al.*, 2010). Natural ligands (*e.g.*, folic acid, substance P, and the RGD tripeptide) and antibodies have also been used to facilitate cellular delivery by targeting agents to specific cell-surface receptors (Zhao, *et al.*, 2008; Rizk, *et al.*, 2009; Mohanty, *et al.*, 2011). Although some of these methods have had some success, additional delivery strategies are desirable.

The cell surface is coated with a dense forest of polysaccharides known as the glycocalyx (Varki, *et al.*, 2009). We anticipated that targeting therapeutic agents to the glycocalyx would enhance their cellular delivery, as has been demonstrated with lectin conjugates (Ishiguro, *et al.*, 2002). Boronic acids readily form boronate esters with the 1,2- and 1,3-diols of saccharides (James, *et al.*, 2006), including those in the glycocalyx (Vandenburg, *et al.*, 2000; Yang, *et al.*,

2004; Polsky, *et al.*, 2008; Matsumoto, *et al.*, 2009; Zhong, *et al.*, 2010; Matsumoto, *et al.*, 2010). In addition, boronate groups are compatible with human physiology, appearing in chemotherapeutic agents and other biological tools (Westmark and Smith, 1996; Jay, *et al.*, 2009; Barth, 2009; Wu, *et al.*, 2010; Peng, *et al.*, 2010; Kumar, *et al.*, 2011). Further, pendant boronic acids conjugated to polyethylenimine have been shown to enhance gene transfection (Peng, *et al.*, 2010). Herein, we demonstrate the first use of pendant boronic acids to mediate the delivery of a protein into mammalian cells.

Bovine pancreatic ribonuclease (RNase A) is a small, well-characterized enzyme that has been the object of much seminal work in protein chemistry (D'Alessio and Riordan, 1997; Raines, 1998; Marshall, *et al.*, 2008; Cuchillo, *et al.*, 2011). If this ribonuclease can gain access to the RNA that resides in the cytosol, then its prodigious catalytic activity can lead to cell death (Leland and Raines, 2001; Futami, *et al.*, 2001; Futami, *et al.*, 2002; Rutkoski, *et al.*, 2005; Futami, *et al.*, 2005; Rutkoski and Raines, 2008). Hence, RNase A can serve as an ideal model for assessing the delivery of a protein into the cytosol (rather than an endosome) because success can be discerned with assays of cytotoxic activity.

### 3.3 Results and Discussion

Initially, we quantified the affinity of simple boronic acids to relevant saccharides. Sialic acid is of particular interest because of its abundance in the glycocalyx of cancerous cells (Dube and Bertozzi, 2005). Phenylboronic acid (PBA) binds with higher affinity to sialic acid than to other pyranose saccharides (Springsteen and Wang, 2002; Otsuka, *et al.*, 2003; Djanashvili, *et al.*, 2005), suggesting that simple boronic acids could target chemotherapeutic agents selectively to

tumors. 2-Hydroxymethylphenylboronic acid (benzoboroxole) has among the highest reported affinities for boron binding to pyranose saccharides (Springsteen and Wang, 2002; Otsuka, *et al.*, 2003; Djanashvili, *et al.*, 2005; Dowlut and Dennis, 2006; Bérubé, *et al.*, 2008), which are abundant in the glycocalyx; hence, we reasoned that benzoboroxole could be an ideal boronate for drug delivery. We used  $^1\text{H}$  NMR spectroscopy to evaluate the affinity of PBA and benzoboroxole for fructose, glucose, and *N*-acetylneuraminic acid (Neu5Ac), which contains a sialic acid moiety, under physiological conditions. Our  $K_a$  values (Table 3.1) are in gratifying agreement with values determined by other workers using alternative assays (Table 3.2) (Springsteen and Wang, 2002; Djanashvili, *et al.*, 2005; Dowlut and Dennis, 2006; Bérubé, *et al.*, 2008). We found that both benzoboroxole and PBA have greater affinity for Neu5Ac than for glucose and that benzoboroxole has greater affinity than PBA for each saccharide in our panel. Accordingly, we chose benzoboroxole for our boronate-mediated delivery studies.

To display benzoboroxole moieties on RNase A, we conjugated 5-amino-2-hydroxymethylphenylboronic acid (Scheme 3.1, compound **1**) to protein carboxyl groups by condensation using a carbodiimide (Scheme 3.1). Of the 11 carboxyl groups of RNase A,  $7.5 \pm 2.0$  were condensed with boronate (Scheme 3.1, compound **1**), as determined by mass spectrometry (Figure 3.2).

Boronation should increase the affinity of a protein for oligosaccharides. To test this hypothesis qualitatively, we measured the retention of boronated and unmodified RNase A on a column of heparin, a common physiological polysaccharide. Boronated RNase A was indeed retained longer on the column (Figure 3.3). If the prolonged retention were due to boron–saccharide complexation, then fructose in the buffer should compete with immobilized heparin

for boron complexation. When these conditions were employed, the retention of boronated RNase A was indeed diminished (Figure 3.3).

To evaluate the enhanced affinity of boronated RNase A for oligosaccharides, we measured its affinity for ganglioside GD3 within a 1,2-dioleoyl-*sn*-glycero-3-phosphocholine (DOPC) liposome. This ganglioside has two sialic acid residues and is overexpressed on the surface of cancer cells (Malisan and Testi, 2005). By using fluorescence polarization/anisotropy to analyze binding of fluorescently-labeled proteins, we found that boronation increased the affinity of the protein for the ganglioside, an effect that was decreased by fructose (Figure 3.4). The  $K_d$  value of boronated protein for GD3 ganglioside liposomes was  $(53 \pm 11) \mu\text{M}$  as determined by fluorescence polarization and  $(28 \pm 8) \mu\text{M}$  as determined by fluorescence anisotropy (Figure 3.5). This affinity is ~439–831-fold greater than that for the binding of a single benzoboroxole to Neu5Ac (Table 3.1), consistent with a multivalent interaction between the boronated protein and the ganglioside.

Encouraged by the enhanced *in vitro* affinity of the boronated protein for oligosaccharides, we sought to test our hypothesis that boronate conjugation would increase its cellular uptake. To quantify cellular internalization, we used fluorophore-labeled protein and flow cytometry. To determine concurrently if the pendant boronates elicited selectivity for cells with higher quantities of cell-surface sialic acid, we employed a line of Chinese hamster ovary cells (Lec-2) that have lower levels of sialic acid in their glycocalyx than their progenitor line (Pro-5) (Stanley, *et al.*, 1975; Deutscher, *et al.*, 1984). We found that boronation of RNase A increased its cellular uptake by 4- to 5-fold (Figure 3.6). This enhancement was decreased by fructose. Cell-surface sialic acid-content did not affect uptake significantly, consistent with the modest

increase in the  $K_a$  value for benzoboroxole with sialic acid versus glucose (Table 3.1). Confocal microscopy of boronated protein demonstrated punctate staining (Figure 3.6, insert), which is consistent with uptake by endocytosis following complexation with cell-surface saccharides.

Although flow cytometry can quantify protein internalization into a cell, it does not differentiate between proteins in endosomes versus those in the cytosol. Delivery into the cytosol is essential for the efficacy of numerous putative chemotherapeutic agents. Boronated RNase A retained ( $17 \pm 3$ )% of its ribonucleolytic activity (the lost activity may be attributable in part to modification of aspartic acid 121 (Schultz, *et al.*, 1998)) and was modestly evasive to the ribonuclease inhibitor protein (Figure 3.7). Accordingly, boronated RNase A has the potential to be cytotoxic if it can enter the cytosol. We found that boronated RNase A inhibited the proliferation of a line of human erythroleukemia cells, with an  $IC_{50}$  value of ( $4.1 \pm 0.4$ )  $\mu$ M (K-562; Figure 3.8). The addition of fructose diminished cytotoxic activity, presumably by decreasing overall internalization. Chemically inactivated, boronated RNase A was much less cytotoxic, indicating that ribonucleolytic activity induced toxicity, not the pendant boronates. We conclude that boronation not only facilitates cellular uptake of an enzyme, but also allows for its delivery to the cytosol and the maintenance of its catalytic activity.

### 3.4 Conclusions

Boronates have attributes that make them attractive as mediators of drug delivery. First, endosomes become more acidic as they mature. In synergy, the affinity of boronates for saccharides typically decreases with decreasing pH (Springsteen and Wang, 2002). Moreover, the ensuing loss of complexation causes boronates to become more hydrophobic (Mothana, *et*

*al.*, 2010). These attributes could facilitate translocation to the cytosol. Second, boronates are not cationic (the  $\text{HOB}$  of benzoboroxole has  $\text{pK}_a$  7.2 (Bérubé, *et al.*, 2008), preserving most of the anionicity of a carboxyl group at pH 7.4), averting the non-specific Coulombic interactions elicited by cationic domains (Gao, *et al.*, 2008; Rapoport and Lorberboum-Galski, 2009; Sun and Zhang, 2010; Schmidt, *et al.*, 2010), which can lead to high rates of glomerular filtration and opsonization (Venturoli and Rippe, 2005; Owens and Peppas, 2006). Finally, we note that numerous diseases are associated with changes in cell-surface glycosylation (Dube and Bertozzi, 2005; Cheng, *et al.*, 2010), and we anticipate that boronic acids with specificity for particular glycans could serve as the basis for targeted delivery strategies (Pal, *et al.*, 2010).

### 3.5 Experimental Procedures

#### 3.5.1 Materials

*N*-Acetylneuraminic acid was from Carbosynth (Berkshire, UK). Phenylboronic acid, 2-hydroxymethylphenylboronic acid, and 5-amino-2-hydroxymethylphenylboronic acid were from Combi-Blocks (San Diego, CA). BODIPY<sup>®</sup> FL, STP ester was from Molecular Probes (Eugene, OR). *N*-(3-Dimethylaminopropyl)-*N'*-ethylcarbodiimide hydrochloride (EDC) and wild-type RNase A (Type III-A) were from Sigma–Aldrich (St. Louis, MO) and used without further purification. MES buffer was from Sigma–Aldrich and purified by anion-exchange chromatography to remove trace amounts of oligomeric vinylsulfonic acid (Smith, *et al.*, 2003). Spectra/Por<sup>®</sup> dialysis bags (3500 MWCO) were from Fisher Scientific (Thermo Fisher Scientific, Walham, MA). *Escherichia coli* BL21(DE3) cells were from Novagen (Madison, WI). [*methyl-*

$^3\text{H}$ ]Thymidine (6.7 Ci/mmol) was from Perkin–Elmer (Boston, MA). HiTrap Heparin HP columns for protein purification and analytical columns were from GE Biosciences (Piscataway, NJ). Ribonuclease substrate 6-FAM–dArUdAdA–6-TAMRA was from Integrated DNA Technologies (Coralville, IA). Non-binding surface (NBS) 96-well plates were from Corning (Corning, NY). Terrific Broth (TB) was from Research Products International Corp (Mt. Prospect, IL). Bovine Serum Albumin (BSA) was from Thermo Scientific (Rockfield, IL). SDS–PAGE gels were from Bio-Rad Laboratories (Hercules, CA). GD3 Ganglioside (bovine milk; ammonium salt), 1,2-dioleoyl-*sn*-glycero-3-phosphocholine (DOPC), and an extruder were from Avanti Polar Lipids (Alabaster, Alabama). 16S- and 23S-Ribosomal (rRNA) from *E. coli* MRE600 was from Roche Applied Science (Mannheim, Germany). Cell culture medium and supplements were from Invitrogen (Carlsbad, CA). Phosphate-buffered saline was either Dulbecco's PBS (DPBS) from Invitrogen or the same solution made in the laboratory (PBS), containing (in 1.0 L): 0.2 g KCl, 0.2g  $\text{KH}_2\text{PO}_4$ , 8 g NaCl, and 2.16 g  $\text{Na}_2\text{HPO}_4 \cdot 7\text{H}_2\text{O}$  at pH 7.4. Terrific Broth (TB) was from Research Products International (Mt. Prospect, IL), or was made by dissolving tryptone (12 g), yeast extract (24 g), glycerol (4 mL),  $\text{KH}_2\text{PO}_4$  (2.31 g), and  $\text{K}_2\text{HPO}_4$  (12.54 g) in  $\text{H}_2\text{O}$  (1.00 L). All other chemicals used were of commercial reagent grade or better, and were used without further purification.

### 3.5.2 *Analytical instruments and statistical calculations*

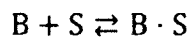
$^1\text{H}$  NMR spectra were acquired at the National Magnetic Resonance Facility at Madison at 298 K on an Avance III 500 MHz spectrometer with a TCI 500 H-C/N-D cryogenic probe from Bruker AXS (Madison, WI,  $^1\text{H}$ , 500 MHz). Protein absorbance values were measured on a



Varian Cary 50 UV–Vis Spectrometer (Agilent Technologies, Santa Clara, CA) and/or a NanoVue spectrometer (GE Healthcare, Piscataway, NJ). Confocal microscopy was carried out using an Eclipse C1 laser scanning confocal microscope from Nikon (Melville, NY). Flow cytometry was done using a LSRII (BD Biosciences, San Jose, CA) at the University of Wisconsin–Madison Carbone Cancer Center Flow Cytometry Facility. The mass of boronated RNase A conjugates were confirmed at the University of Wisconsin–Madison Biophysics Instrumentation Facility by matrix-assisted laser desorption/ionization time-of-flight (MALDI–TOF) mass spectrometry with a Voyager-DE-PRO Biospectrometry Workstation from Applied Biosystems (Foster City, CA). [*methyl*-<sup>3</sup>H]Thymidine incorporation into K-562 genomic DNA was quantified by scintillation counting using a Microbeta TriLux liquid scintillation and luminescence counter from Perkin–Elmer. Fluorescence measurements were made with an infinite M1000 plate reader from Tecan (Männedorf, Switzerland). Calculations for statistical significance were performed with GraphPad Prism version 5.02 software from GraphPad Software (La Jolla, CA), and a value of  $p < 0.05$  was considered to be significant.

### 3.5.3 *Determination of $K_a$ values by <sup>1</sup>H NMR spectroscopy*

Methodology to determine the values of  $K_a$  values for boronic acids and saccharides was adapted from work by Hall and coworkers (Dowlut and Dennis, 2006; Bérubé, *et al.*, 2008). A boronic acid (B) and a saccharide (S) were assumed to bind in one modality, B·S:



$$K_a = \frac{[B \cdot S]}{[B][S]}$$

The  $[B \cdot S]/[B]$  ratio was determined by the integration of aryl protons of the boronic acid·saccharide complex and the free boronic acid. The individual  $[B]$ ,  $[B \cdot S]$ , and  $[S]$  can be calculated from equations 3.1–3.3.

$$[B \cdot S] + [B] = [B_T]$$

$$\frac{[B \cdot S]}{[B]} + 1 = \frac{[B_T]}{[B]}$$

(3.1)

$$[B] = \frac{[B_T]}{\frac{[B \cdot S]}{[B]} + 1}$$

(3.2)

$$[B \cdot S] = \frac{[B \cdot S]}{[B]} [B], \text{ where } [B] \text{ is calculated from equation 3.1}$$

$$[B \cdot S] + [S] = [S_T]$$

(3.3)

$$[S] = [S_T] - [B \cdot S], \text{ where } [B \cdot S] \text{ is calculated from equation 3.2}$$

Each value of  $K_a$  arose from at least two independent experiments with freshly prepared solutions, and each experiment consisted of a titration with 6–9 different concentrations. All NMR spectra were analyzed with Topspin 3.0 software from Bruker AXS. NMR experiments

were done in a 0.10 M  $\text{NaH}_2\text{PO}_4$  buffer, pH 7.4, containing  $\text{D}_2\text{O}$  (2% v/v).  $^1\text{H}$  NMR experiments consisted of the first increment of a 2D NOESY with gradients for improved water suppression.

#### *3.5.3.1 Representative procedure for making a boronic acid solution*

$\text{NaH}_2\text{PO}_4$  (3.0g, 25mmol) and PBA (458mg, 3.75mmol) were dissolved in distilled, deionized water in a volumetric flask (~200 mL  $\text{H}_2\text{O}$ , 5 mL  $\text{D}_2\text{O}$ ). The pH was adjusted carefully to 7.4 using 10 M NaOH, and additional water was added for a final volume of 250 mL. Final solutions were 15 mM boronic acid (PBA = solution 1; benzoboroxole = solution 2) in 0.10 M sodium phosphate monobasic buffer, pH 7.4, containing  $\text{D}_2\text{O}$  (2% v/v).

#### *3.5.3.2 Determination of the value of $K_a$ for PBA and fructose*

To a 25-mL volumetric flask, D-fructose (674 mg, 3.75mmol) and ~20 mL of solution 1 was added. The solution was adjusted carefully to pH 7.4 by the addition of 10 M NaOH. (The volume of added NaOH was used in the calculation of the boronic acid concentration.) The volume was then increased to 25 mL by adding solution 1. This procedure resulted in a pH 7.4 solution of PBA (15 mM), D-fructose (150 mM),  $\text{NaH}_2\text{PO}_4$  (0.10 M), and  $\text{D}_2\text{O}$  (2% v/v) (solution A). Mixing various volumes of solution 1 and solution A generated fructose concentrations in the range of 4–14 mM. The  $[\text{B}\cdot\text{S}]/[\text{B}]$  ratio was determined as depicted in Figure 3.9D.

#### *3.5.3.3 Representative procedure for determining the chemical shifts of aryl protons in bound and free boronic acids*

A  $^1\text{H}$  NMR spectra of solution 1 (Figure 3.9A) and solution A (Figure 3.9B) were acquired. The two spectra were overlaid to determine which peaks belonged to the bound boronic acid and free boronic acid (Figure 3.9C). This analysis was used to interpret the spectra from the titrations with sugars (Figure 3.9D).

#### 3.5.3.4 *Determination of the value of $K_a$ for benzoboroxole and fructose*

To a 25-mL volumetric flask, D-fructose (674 mg, 3.75 mmol) and ~20 mL of solution 2 was added. The solution was adjusted carefully to pH 7.4 by the addition of 10 M NaOH. (The volume of added NaOH was used in the calculation of the boronic acid concentration.) The volume was then increased to 25 mL by adding solution 2. This procedure resulted in a pH 7.4 solution of benzoboroxazole (15 mM), D-fructose (150 mM),  $\text{NaH}_2\text{PO}_4$  (0.10 M), and  $\text{D}_2\text{O}$  (2% v/v) (solution B). Mixing various volumes of solution 2 and solution B generated fructose concentrations in the range of 4–14 mM. The  $[\text{B}\cdot\text{S}]/[\text{B}]$  ratio was determined as depicted in Figure 3.10. A value for  $K_a$  was calculated for every concentration as described above.

#### 3.5.3.5 *Determination of the value of $K_a$ for PBA and glucose*

To a 25-mL volumetric flask, D-glucose (2.25 g, 12.5 mmol) and ~20 mL of solution 1 was added. The solution was adjusted carefully to pH 7.4 by the addition of 10 M NaOH. (The volume of added NaOH was used in the calculation of the boronic acid concentration.) The volume was then increased to 25 mL by adding solution 1. This procedure resulted in pH 7.4 solution of PBA (15 mM), D-glucose (500 mM), 0.1M  $\text{NaH}_2\text{PO}_4$  (0.10 M), and  $\text{D}_2\text{O}$  (2% v/v) (solution C). Mixing various volumes of solution 1 and solution C generated glucose

concentrations in the range of 20–70 mM. The  $[B \cdot S]/[B]$  ratio was determined as depicted in Figure 3.11. A value for  $K_a$  was calculated for every concentration as described above.

#### 3.5.3.6 *Determination of the value of $K_a$ for benzoboroxole and glucose*

To a 25-mL volumetric flask, D-glucose (2.25 g, 12.5 mmol) and ~20 mL of solution 2 was added. The solution was adjusted carefully to pH 7.4 by the addition of 10 M NaOH. (The volume of added NaOH was used in the calculation of the boronic acid concentration.) The volume was then increased to 25 mL by adding solution 2. This procedure resulted in a pH 7.4 solution of benzoboroxazole (15 mM), D-glucose (500 mM),  $\text{NaH}_2\text{PO}_4$  (0.10 M), and  $\text{D}_2\text{O}$  (2% v/v) (solution D). Mixing various volumes of solution 2 and solution D generated glucose concentrations in the range of 20–70 mM. The  $[B \cdot S]/[B]$  ratio was determined as depicted in Figure 3.12. A value for  $K_a$  was calculated for every concentration as described above.

#### 3.5.3.7 *Determination of the value of $K_a$ for PBA and Neu5Ac*

To a 10-mL volumetric flask, Neu5Ac (1.53 g, 5.0 mmol) and ~20 mL of solution 1 was added. The solution was adjusted carefully to pH 7.4 by the addition of 10 M NaOH. (The volume of added NaOH was used in the calculation of the boronic acid concentration.) The volume was then increased to 25 mL by adding solution 1. This procedure resulted in a pH 7.4 solution of PBA (14.2 mM), Neu5Ac (500 mM),  $\text{NaH}_2\text{PO}_4$  (0.10 M), and  $\text{D}_2\text{O}$  (2% v/v) (solution E). Mixing various volumes of solution 1 and solution E, generated Neu5Ac concentrations in the range of 7–65 mM. The  $[B \cdot S]/[B]$  ratio was determined as depicted in Figure 3.13. A value for  $K_a$  was calculated for every concentration as described above.

#### 3.5.3.8 *Determination of the value of $K_a$ for benzoboroxole and Neu5Ac*

To a 10-mL volumetric flask, Neu5Ac (1.56 g, 5.0 mM) and ~20 mL of solution 2 was added. The solution was adjusted carefully to pH 7.4 by the addition of 10 M NaOH. (The volume of added NaOH was used in the calculation of the boronic acid concentration.) The volume was then increased to 25 mL by adding solution 2. This procedure resulted in a pH 7.4 solution of benzoboroxazole (14.2 mM), Neu5Ac (500 mM),  $\text{NaH}_2\text{PO}_4$  (0.10 M), and  $\text{D}_2\text{O}$  (2% v/v) (solution F). Mixing various volumes of solution 2 and solution F generated Neu5Ac concentrations in the range of 7–65 mM. The  $K_a$  value was calculated for every concentration as previously described. The  $[\text{B}\cdot\text{S}]/[\text{B}]$  ratio was determined as depicted in Figures 3.14 and 3.15. A value for  $K_a$  was calculated for every concentration as described above.

#### 3.5.4 *Preparation of boronated RNase A*

5-Amino-2-hydroxymethylphenylboronic acid (320 mg, 1.70 mmol) was added to 30 mL of distilled, deionized  $\text{H}_2\text{O}$ , and the resulting solution was adjusted to pH 5.0 with NaOH. To this solution was added RNase A (200 mg, 15  $\mu\text{mol}$ ), followed by EDC (640 mg, 3.30 mmol), and the pH was adjusted again to 5.0 with NaOH. The reaction mixture was incubated at ambient temperature overnight on a nutating mixer by BD (Franklin Lakes, NJ). Additional EDC (360 mg, 1.9 mmol) was added, and the solution was incubated at the same conditions for 3.5 h (24 h total). The solution was then subjected to centrifugation (5 min at 1000 rpm, and 5 min at 5000 rpm) to remove insoluble boronic acid, and dialyzed (3500 molecular weight cutoff) against distilled, deionized  $\text{H}_2\text{O}$  for 3 d at 4 °C, with daily water exchanges. The solution was

then passed through a 0.45- $\mu$ m filter and loaded onto a 5-mL HiTrap Heparin HP column. To prepare a high-salt buffer, NaCl (58.4 g, 1.00 mol) was added to 100 mL of a 10 $\times$  stock solution of PBS. This solution was diluted with distilled, deionized H<sub>2</sub>O to a final volume of 1 L, and adjusted to pH 7.4, making a buffer of approximately PBS plus an additional 1 M NaCl. The column was washed with 75 mL of PBS buffer, and protein was eluted with a linear gradient of 225 mL of additional NaCl (0.0–1.0 M) in PBS buffer. Fractions were collected, pooled, concentrated, stored at 4 °C, and analyzed by MALDI–TOF mass spectrometry. The mass spectrum between 13–16 kDa was fitted to a Gaussian curve with GraphPad Prism version 5.02 software to determine the average mass (Figure 3.2). Analysis of boronation of ribonuclease was also done in two addition ways. First, two samples (10  $\mu$ M) of unmodified and boronated ribonuclease was submitted for elemental analysis at the Soil and Plant Analysis Lab at the University of Wisconsin–Madison. Boron was at 1.40 and 0.79 ppm for unmodified and boronated ribonuclease, respectively. However, sulfur was at 1.99 and <1 ppm for unmodified and boronated ribonuclease, respectively; therefore, the relative amount of boron/protein (using sulfur as an internal control), could not be calculated. Second, unmodified and boronated ribonuclease were submitted to the Biotechnology Center at the University of Wisconsin–Madison for tryptic digest and MALDI spectroscopy (not 100% sequence coverage). Shifts corresponded to ~ 113.2 Da for some peptides. The expected shift was 148.954 Da (boronate) – 18.016 Da (water) = 130.938 Da. The difference in expected versus observed shift is 17.738 Da, close to hydroxyl (17.008 Da) or water (18.016 Da). We conclude that the boronate must lose a hydroxyl during mass spectrometry analysis from the analysis itself, or lose water by cyclizing onto other group in the peptide (e.g. a lysine amine or an aspartate/glutamate carboxylic acid).



Only very small peaks (or no peaks) were seen at a shift that would indicate an EDC by-product (O- or N-acylisourea). The activity of boronated RNase A was  $(1.6 \pm 0.2) \times 10^7 \text{ M}^{-1} \text{ s}^{-1}$ , which was ~ 17% of unmodified RNase A at  $(9.6 \pm 0.7) \times 10^7 \text{ M}^{-1} \text{ s}^{-1}$ . This value for unmodified RNase A is somewhat higher than reported previously,  $(5.2 \pm 0.4) \times 10^7 \text{ M}^{-1} \text{ s}^{-1}$  (Rutkoski, *et al.*, 2005).

### 3.5.5 *Preparation of inactivated, boronated RNase A*

RNase A (38mg, 2.8  $\mu\text{mol}$ ) was dissolved in 575.5  $\mu\text{L}$  of 0.10 M sodium acetate buffer, pH 4.9. In a separate solution, 2-bromoacetic acid (123 mg, 883  $\mu\text{mol}$ ) was dissolved in 9.2 mL of 0.10 M sodium acetate buffer, and the resulting solution was adjusted to pH 5.2. An aliquot (288  $\mu\text{L}$ ) of the 2-bromoacetic acid solution was added to the RNase A solution to generate a final concentration of 32 mM 2-bromoacetic acid and 3.2 mM RNase A. The reaction mixture was incubated at ambient temperature for 24 h on a nutating mixer, after which the reaction was dialyzed overnight against distilled, deionized  $\text{H}_2\text{O}$ . The inactivated RNase A was then loaded onto a Mono S HR 16/10 cation exchange FPLC column from Pharmacia. The column was washed with a 40-mL linear gradient of NaCl (0.00–0.05 M) in 10 mM sodium phosphate buffer, pH 6.0, and eluted with a 603-mL linear gradient of NaCl (0.05–0.40 M) in 10 mM sodium phosphate buffer, pH 6.0. Fractions were collected, pooled, and dialyzed overnight at 4 °C against 50 mM sodium acetate buffer, pH 5. Inactivated RNase A was then loaded onto a 5-mL HiTrap Heparin HP column. The column was washed with 10 mL of 50 mM sodium acetate buffer, pH 5.0, and eluted with a 200-mL linear gradient of NaCl (0.0–0.4 M) in 50 mM sodium acetate buffer, pH 5.0. Fractions were collected, and analyzed by MALDI–TOF mass spectrometry. Fractions with an molecular mass greater than that of wild-type RNase A were

pooled and dialyzed extensively with distilled, deionized H<sub>2</sub>O at 4 °C. 5-Amino-2-hydroxymethylphenylboronic acid was then conjugated as described above. Briefly, to 0.5 mL of chemically inactivated RNase A (6 mg, 400nmol) was added 5-amino-2-hydroxymethylphenylboronic acid (10 mg, 50μmol), and adjusted to pH 5. EDC was then added (19 mg, 100 μmol), and the resulting solution was adjusted to pH 5. The reaction mixture was incubated at ambient temperature for 20.5 h on a nutating mixer before adding additional EDC (11 mg, 56 μmol), and then incubated for an additional 3.5 h. Inactivated, boronated RNase A was dialyzed against distilled, deionized H<sub>2</sub>O and purified on a 1-mL HiTrap Heparin HP column similarly as described for boronated RNase A but approximately scaled for the 1-mL column (~15 mL PBS wash and eluted with a linear gradient of ~40–45 mL of additional NaCl (0.0–1.0 M) in PBS buffer. MALDI-TOF data was analyzed as for boronated RNase A, but with also taking into account the addition of BrAc – Br and unmodified RNase A standard. Specifically, the mass and standard deviation was (14576 ± 247.7) Da, minus bromoacetic acid and bromine to give (14517 ± 247.7) Da, which results in 6.4 ± 1.9 boronates/ribonuclease if all ribonuclease was inactivated once by bromoacetic acid. The activity of inactivated, boronated RNase A was (3.0 ± 0.2) × 10<sup>5</sup> M<sup>-1</sup> s<sup>-1</sup>, which was ~ 1.89% of boronated RNase A.

### 3.5.6 *Preparation of BODIPY FL-labeled ribonucleases*

Both unmodified and boronated RNase A were labeled with BODIPY FL. An aliquot (3.83mL) of a solution of ribonuclease (120 μM) was adjusted to pH 8.3. BODIPY FL STP ester (5 mg; 9 μmol) was dissolved in 0.5 mL of DMF. To the solution of ribonuclease was added 125 μL of the BODIPY FL STP ester solution. The reaction mixture was incubated at ambient

temperature on a nutating mixer for 4–6 h, and then incubated at 4 °C on a nutating mixer overnight. Labeled ribonuclease was loaded onto a 1-mL HiTrap Heparin HP column. The column was washed with 30 mL of 10 mM sodium phosphate buffer, pH 6.0. The protein was eluted with a 60-mL linear gradient of NaCl (0.0–1.5 M) and pH (6.0–7.4) in 10 mM sodium phosphate buffer, pH 7.4. Fractions were collected, pooled, concentrated, and analyzed by SDS–PAGE and MALDI–TOF mass spectrometry.

Labeled ribonucleases were dissolved in at least a 10× volume of DPBS, passed through a 0.45-μm syringe filter from Whatman (Piscataway, NJ), and re-concentrated before being used in assays. In this manner, the proteins were dissolved in solution that was largely DPBS. Concentrations of proteins were determined by UV spectroscopy (at  $A_{280\text{ nm}}$  to approximate  $A_{278\text{ nm}}$ ) using the extinction coefficient of RNase A at 278 nm ( $\epsilon = 0.72\text{ (mg}\cdot\text{mL}^{-1})^{-1}\cdot\text{cm}^{-1}$ ) (Sela, *et al.*, 1957). The absorbance of benzoboroxole was found to be negligible, contributing < 5% to the  $A_{278\text{ nm}}$  of the boronated ribonuclease (the 5-amino-2-hydroxymethylboronic acid may have higher absorbance). The concentration of labeled ribonucleases was corrected for fluorophore absorbance by using the manufacturer's protocol (<http://tools.invitrogen.com/content/sfs/manuals/mp00143.pdf>). Percent labeling was determined by UV spectrometry at 504 nm using the extinction coefficient of BODIPY FL ( $\epsilon = 68,000\text{ M}^{-1}\cdot\text{cm}^{-1}$ ) given in the manufacturer's protocol.

### 3.5.7 Heparin-affinity assays

The affinity of unmodified and boronated RNase A for heparin was assessed by retention on a 1-mL HiTrap Heparin HP column (GE Healthcare, Piscataway, NJ). Unmodified and

boronated RNase A were mixed in a 1:1 ratio (2.0 mg each) in DPBS, and the resulting solution was loaded onto the column. Buffers were made as specified for the preparation of boronated RNase A. The column was washed with 5 mL of PBS, followed by elution with 45 mL of a linear gradient of NaCl (0.0–1.0 M) in PBS. Elution was monitored by absorbance, and eluted proteins were identified by mass spectrometry. A small amount of unmodified RNase A was apparent in peak B (Figure 3.3). We hypothesize that boronated RNase A was able to complex to a small amount of unmodified RNase A and extend its elution time. The same assay was then repeated with 100 mM fructose in both buffers. To make fructose-supplemented buffers, fructose (18 g, 100 mmol) was added to 100 mL of a 10× stock solution of PBS, either no additional NaCl or NaCl (58.4 g, 1.00 mol) was added, and both buffers were diluted to a final volume of 1 L and adjusted to pH 7.4.

### 3.5.8 *Fluorescence polarization assays*

Liposomes were formed by transferring DOPC (dissolved in chloroform solution) and GD3 gangliosides (dissolved in 63:35:5 chloroform/methanol/water) to glass tubes and drying them under Ar(g) and then under vacuum. Lipids were re-suspended in 25 mM HEPES buffer, pH 7.0, containing NaCl (75 mM). The solution of lipids was mixed by vortexing for 2 min, and incubated at 37 °C for 1 h. For DOPC liposomes, DOPC was resuspended at a concentration of 5 mM. For GD3 ganglioside-labeled liposomes, DOPC and GD3 gangliosides were mixed at 3 mM and 2 mM concentrations, respectively. Large unilamellar vesicles were formed by extrusion through a 0.1-μm polycarbonate filter from Whatman (GE Healthcare, Piscataway, NJ). This process produces a population of vesicles of near uniform size (~100–150 nm diameter

as measured by dynamic light scattering). A portion of the DOPC lipids before extrusion were aliquoted as a control.

Fluorescence polarization assays were performed using 50 nM BODIPY FL-labeled unmodified and boronated RNase A in black NBS 96-well plates (Corning Costar, Lowell, MA). Ribonucleases were incubated with DOPC liposomes (625  $\mu$ M total lipid) or GD3 ganglioside-labeled liposomes (375  $\mu$ M DOPC, 250  $\mu$ M GD3 ganglioside = 625  $\mu$ M total lipid) in 25 mM HEPES buffer, pH 7.0, containing NaCl (75 mM) in the absence or presence of fructose (10 mM). In control wells, ribonucleases were incubated with non-extruded DOPC lipids. Fluorescence polarization at 470/535 nm with a *G*-factor of 1.257 was recorded after shaking the plate briefly and incubating at ambient temperature for 1 h. Control well polarization was subtracted from experimental well polarization for each ribonuclease. The assay was performed in triplicate. Note that at a 2 h timepoint, the polarization of unmodified ribonuclease with DOPC liposomes was negative, and the difference between this and unmodified ribonuclease with DOPC ganglioside liposomes was significant ( $p < 0.05$ ). The assay was also analyzed by anisotropy at the 2 h timepoint, and the control well used for subtraction was the protein free in solution, with no lipid added. For both polarization and anisotropy bar graphs, the total fluorescence intensity for boronated RNase A with fructose was lower, but this was not taken into account in analysis.

The affinity of boronated RNase A for GD3 ganglioside-labeled liposomes was assessed by using serially diluted liposomes. GD3 ganglioside-labeled liposomes were serially diluted in 25 mM HEPES, pH 7.0, containing 75 mM with dilutions of 62.5 nM–1250  $\mu$ M total lipid. Because the composition of these liposomes was 3:2 DOPC/GD3 ganglioside, this dilution

resulted in solutions containing GD3 ganglioside at 25 nM–500  $\mu$ M. Control DOPC liposomes (with no GD3 ganglioside) were likewise diluted in the same buffer, producing solutions of 62.5 nM–1250  $\mu$ M total lipid. Liposomes were then incubated with 50 nM BODIPY FL-labeled boronated RNase A in the same buffer in a black NBS 96-well plate. Fluorescence polarization was recorded after shaking the plate briefly and incubating at ambient temperature for 35 min. Fluorescence polarization from GD3 ganglioside-labeled liposomes was subtracted from that of DOPC-only liposomes, thereby correcting for binding to DOPC and for changes in solution viscosity. The assay was performed in duplicate. The fraction of labeled ribonuclease bound for each sample well was calculated by dividing its polarization from the polarization of ribonucleases incubated with the highest concentration of GD3 ganglioside (set at 100% bound). The value of  $K_d$  was calculated by plotting the fraction bound against the concentration of GD3 ganglioside and fitting the data to a binding isotherm (Roehrl, *et al.*, 2004). The data was reanalyzed using fluorescence anisotropy, and determining the fraction bound ( $F_{SB}$ ) using equation 3.4, where  $A_{OBS}$  is the anisotropy observed,  $A_F$  is the anisotropy of the protein free,  $A_B$  is the anisotropy of the protein totally bound by liposome, and  $Q$  is the fluorescence intensity of the bound species divided by the fluorescence intensity of the free species (Roehrl, *et al.*, 2004). Note that the free species here was the labeled protein free in solution, with no lipids (even non-extruded lipids) added. Also, the values for binding to DOPC-only liposomes were not subtracted out in this analysis.

$$F_{SB} = \frac{A_{OBS} - A_F}{(A_B - A_{OBS})Q + A_{OBS} - A_F} \quad (3.4)$$

### 3.5.9 *Cell culture*

Cell lines were obtained from American Type Culture Collection (Manassas, VA) and were maintained according to the recommended procedures. Cells were grown in a cell culture incubator at 37 °C under CO<sub>2</sub> (5% v/v) in flat-bottomed culture flasks. Cell medium was supplemented with GIBCO fetal bovine serum (FBS) (10% v/v), penicillin (100 units/mL), and streptomycin (100 µg/mL) in the appropriate cellular medium as follows: Pro-5, MEM  $\alpha$  + ribonucleosides + deoxyribonucleosides; Lec-2, MEM  $\alpha$  – ribonucleosides – deoxyribonucleosides; and K562, RPMI 1640. Cells were counted by hemocytometry for dispensing into 96-well plates (Nunc, Roskilde, Denmark), 12-well plates (Corning Costar, Lowell, MA), or 8-well chambered coverglass slides (Nunc Lab-Tek II, Thermo Scientific).

### 3.5.10 *Flow cytometry assays*

BODIPY-FL was excited with a 488 nm solid-state laser and the emission was collected with a 530/30 bandpass filter. To collect the most reproducible data, for every flow cytometry experiment, the sensitivity (voltage) of the photomultiplier tube was set for all data collections using mid-range Rainbow beads from Spherotech (Lake Forest, IL) to a predetermined fluorescence target value. At least 10,000 cellular events were acquired for each sample. Data were analyzed using FlowJo 8.1.3 (Treestar, Ashland, Oregon).

The day prior to an experiment, Pro-5 and Lec-2 cells (Stanley, *et al.*, 1975; Deutscher, *et al.*, 1984) were plated in 12-well plates at  $1 \times 10^5$  cells/well. The day of the experiment, the appropriate amount of fructose was dissolved into the cellular medium to obtain a final fructose concentration of 250 mM, and the medium was passed through a 0.45-µm syringe filter from

Whatman. Non-fructose-containing medium was filtered likewise. Stock solutions of fluorescently-labeled ribonucleases were diluted into the cell culture to a final concentration of 5  $\mu\text{M}$ . Ribonucleases were incubated with cells for 4 h. Then, the cells were rinsed with PBS ( $2 \times 400 \mu\text{L}$ ), removed from the cell culture plate with trypsin ( $400 \mu\text{L}$ , 0.05% (1 $\times$ ) with EDTA; Invitrogen, Carlsbad, California), placed in flow cytometry tubes containing 80  $\mu\text{L}$  of FBS, and incubated on ice until analyzed by flow cytometry. Final fluorescence values were divided by the percent fluorophore labeling of the ribonuclease to determine the corrected value of fluorescence. Experiments were run twice in triplicate.

### 3.5.11 *Confocal microscopy*

Pro-5 cells were plated on Nunc Lab-tek II 8-well chambered coverglass 24 h before use and grown to 80% confluency. Cells were incubated with 5  $\mu\text{M}$  BODIPY FL-labeled ribonucleases for 4 h. Cell nuclei were stained with Hoechst 33342 (Invitrogen,  $2\mu\text{g/mL}$ ) for the final 15 min of incubation. Cells were then washed twice with PBS, suspended in PBS, and examined using a Nikon Eclipse C1 laser scanning confocal microscope.

### 3.5.12 *Ribonucleolytic activity assays*

The ribonucleolytic activities of RNase A, boronated RNase A, and inactivated, boronated RNase A were determined by quantifying their ability to cleave 6-FAM-dArUdAdA-6-TAMRA, as described previously (Kelemen, *et al.*, 1999). Assays were carried out at ambient temperature in 2 mL of 0.10 M MES-NaOH buffer, pH 6.0, containing NaCl (0.10 M). Fluorescence data were fitted to equation 3.5, in which  $\Delta I/\Delta t$  is the initial reaction velocity,  $I_0$  is



the fluorescence intensity before addition of ribonuclease,  $I_f$  is the fluorescence intensity after complete substrate hydrolysis, and  $[E]$  is the total ribonuclease concentration. The assay was performed in triplicate.

$$k_{\text{cat}} / K_M = \frac{\Delta I / \Delta t}{(I_f - I_0)[E]} \quad (3.5)$$

### 3.5.13 Recombinant protein production

RNase A variants (G88R, DRNG, and A19C G88R) were produced as described previously (Ellis, *et al.*, 2011). A19C G88R RNase A was labeled with diethylfluorescein (DEF) iodoacetamide as described previously (Ellis, *et al.*, 2011). Human ribonuclease inhibitor was prepared in *E. coli* as described previously (Johnson, *et al.*, 2007b).

### 3.5.14 RI-RNase A competition assays

Competition assays were based on a previous RI-RNase competition assay (Lavis, *et al.*, 2007). Serial dilutions (2x) of boronated RNase A and G88R RNase A (control) in DPBS were prepared in Eppendorf Protein LoBind Tubes (Fisher Scientific). A master mix of A19C-DEF G88R RNase A (100 nM; 2x), RI (100 nM; 2x), DTT (10 mM; 2x), and BSA (0.1 mg/mL; 2x) was made and an aliquot (50  $\mu$ L) of this master mix was added to wells of a 96-well NBS plate. Aliquots of the serially-diluted ribonucleases (50  $\mu$ L) were then added to wells. The negative control contained no ribonuclease (PBS), and the positive control contained excess RNase A (20  $\mu$ M; 2x). The plate was shaken for 30 seconds and then incubated for 30 minutes at ambient

temperature, after which the fluorescence intensity was measured. The observed fluorescence intensity ( $I$ ) is described by equation 3.6:

$$I = f_F I_F + f_B I_B \quad (3.6)$$

where  $f_F$  and  $f_B$  are the fractions of the free and RI-bound form of the fluorescence conjugate, respectively, and  $I_F$  and  $I_B$  are the fluorescent intensities of the free and RI-bound states, respectively. The value of  $f_B$  was determined by linear regression analysis using the intensities of the positive and negative controls, which represent 0 and 75.9% bound, respectively, based on a  $K_d$  value of 1.4 nM for the fluorophore-labeled G88R variant of RNase A (Lavis, *et al.*, 2007). The fraction bound ( $f_B$ ) was then calculated by using equation 3.7:

$$f_B = \frac{I - I_F}{I_B - I_F} \quad (3.7)$$

The value of  $K_d$  was calculated by plotting  $f_B$  against the concentration of competing ribonuclease and fitting the data to the mathematical expression for complete competitive binding of two different ligands (Wang, 1995; Roehrl, *et al.*, 2004). Boronated RNase A data are reported as the average of two measurements (G88R RNase A control data were a single measurement), and the entire experiment was repeated in triplicate.

### 3.5.15 *Ribonuclease evasion gel*

Inhibition of ribonucleases by RI was visualized by using an agarose gel-based assay similar to previously described (Leland, *et al.*, 1998). Each reaction mixture contained 730 nM ribonuclease (~10 ng) and a serial dilution of ribonuclease inhibitor (0-, 5x-, or 10x-fold concentration relative to ribonuclease) in DPBS with 5 mM DTT. Reaction mixtures were allowed to incubate at ambient temperature for 30 min, followed by addition of rRNA (4 µg/mL) and an additional incubation of 30 min at ambient temperature (11 µL final). 2 µL of 6x loading dye (Blue/Orange Loading Dye, Promega, Madison, WI) was added to assays and this was immediately loaded onto a 1.5% wt/vol agarose gel containing ethidium bromide pre-incubated at 4 °C, which was then run and visualized.

### 3.5.16 *Cell-proliferation assays*

The effect of unmodified and boronated RNase A on the proliferation of K-562 cells was assayed similar to previously described (Leland, *et al.*, 1998). For assays, 5 µL of a solution of ribonuclease or PBS (control) was added to 95 µL of cells ( $5.0 \times 10^4$  cells/mL). For co-treatment assays with fructose, ribonucleases were first serially diluted at 2× concentration, followed by addition of an equal volume of 2 M fructose in PBS to each ribonuclease dilution, resulting in a 1× ribonuclease dilution as before but now containing 1 M fructose. Then, 5 µL of each dilution was added to cells as above, including a control of PBS containing 1 M fructose. Because 5 µL of samples were added to 95 µL of cells, the final concentration of fructose in each well was 50 mM. After a 44-h incubation, K-562 cells were treated with [*methyl*- $^3\text{H}$ ]thymidine for 4 h, and the incorporation of radioactive thymidine into cellular DNA was quantitated by liquid

scintillation counting. The results are shown as the percentage of [*methyl*-<sup>3</sup>H]thymidine incorporated relative to control cells treated with PBS. Data are the average of three measurements for each concentration, and the entire experiment was repeated in triplicate. Values for IC<sub>50</sub> were calculated by fitting the curves by nonlinear regression to equation 3.8, in which *y* is the total DNA synthesis following the [*methyl*-<sup>3</sup>H]thymidine pulse and *h* is the slope of the curve.

$$y = \frac{100\%}{1 + 10^{(\log(\text{IC}_{50}) - \log[\text{ribonuclease}])h}} \quad (3.8)$$

### 3.6 Acknowledgments

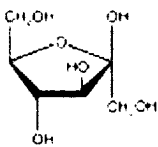
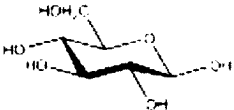
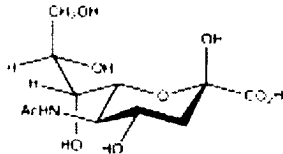
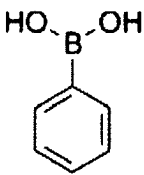
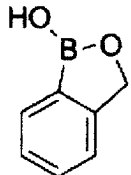
We are grateful to M.L. Hornung for preliminary experiments and to C.H. Eller for helpful guidance on liposome production and fluorescence polarization experiments. We are also grateful to B.R. Caes, N.A. McGrath, J. C. Lukesh, C. N. Bradford, and T. P. Smith for reviewing this chapter. Experiments made use of the Biophysics Instrumentation Facility, which was established by Grants BIR-9512577 (NSF) and S10 RR13790 (NIH). This work was supported by Grant R01 CA073808 (NIH).

### 3.7 Contributions

Original idea for using boronic acids for drug delivery was from M.J. Palte. Original idea to couple boronic acids to RNase A to demonstrate delivery was from G.A. Ellis. <sup>1</sup>H NMR assays were performed by M.J. Palte. Coupling conditions were determined jointly by G.A. Ellis and M.J. Palte. Protein purification and characterization was done by G.A. Ellis. Heparin affinity

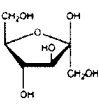
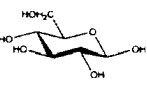
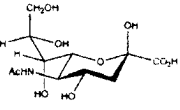
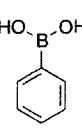
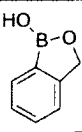
assays, fluorescence polarization assays, ribonucleolytic activity assays, RI-evasion assays, and cytotoxicity assays were performed by G.A. Ellis. Preliminary cytotoxicity assays were done by M.L. Hornung. Flow cytometry assays and confocal microscopy were performed by M.J. Palte.

**Table 3.1** Values of  $K_a$  ( $M^{-1}$ ) for boronic acids and saccharides.<sup>a</sup>

	 D-fructose	 D-glucose	 Neu5Ac
 $HO-B(OH)-C_6H_5$	128 ± 20	5 ± 1	13 ± 1
 $HO-B(O-C_6H_4-O)-C_6H_5$	336 ± 43	28 ± 4	43 ± 5

<sup>a</sup> Values are the mean (± SD) from ≥ 15 measurements in 0.10 M sodium phosphate buffer, pH 7.4, containing D<sub>2</sub>O (2% v/v).

**Table 3.2** Literature values of  $K_a$  ( $M^{-1}$ ) for boronic acids and saccharides. Reference A: (Springsteen and Wang, 2002). Reference B: (Dowlut and Dennis, 2006). Reference C: (Djanashvili, *et al.*, 2005). Reference D: (Mahalingam, *et al.*, 2011). Reference E: (Bérubé, *et al.*, 2008).

				Method	Reference
	D-fructose	D-glucose	Neu5Ac		
	$128 \pm 20$	$5 \pm 1$	$13 \pm 1$	$^1H$ NMR in $H_2O$ containing $D_2O$ (2% v/v) <sup>[a]</sup>	This work
	160	4.6	21	Competition with alizarin red S <sup>[a]</sup>	A
	79	0	—	$^1H$ NMR in $D_2O$ (100% v/v) <sup>[a]</sup>	B
	—	—	$11.6 \pm 1.9$	$^{11}B$ NMR in $H_2O/D_2O/MeOH$ mixture	C
	160	6	21	Competition with alizarin red S <sup>[a]</sup>	D
	$336 \pm 43$	$28 \pm 4$	$43 \pm 5$	$^1H$ NMR in $H_2O$ containing $D_2O$ (2% v/v) <sup>[a]</sup>	This work
	606	17	—	$^1H$ NMR in $D_2O$ (100% v/v) <sup>[a]</sup>	B
	664	21	160	Competition with alizarin red S <sup>[a]</sup>	D
	—	31	—	Competition with alizarin red S <sup>[a]</sup>	E

<sup>a</sup> Values were determined in 0.10 M sodium phosphate buffer, pH 7.4.

**Scheme 3.1** Boronation of RNase A and its putative mechanism for expediting cellular delivery. The location of each carboxyl group of RNase A is depicted in the ribbon diagram (PDB entry 7rsa (Wlodawer, *et al.*, 1988)).

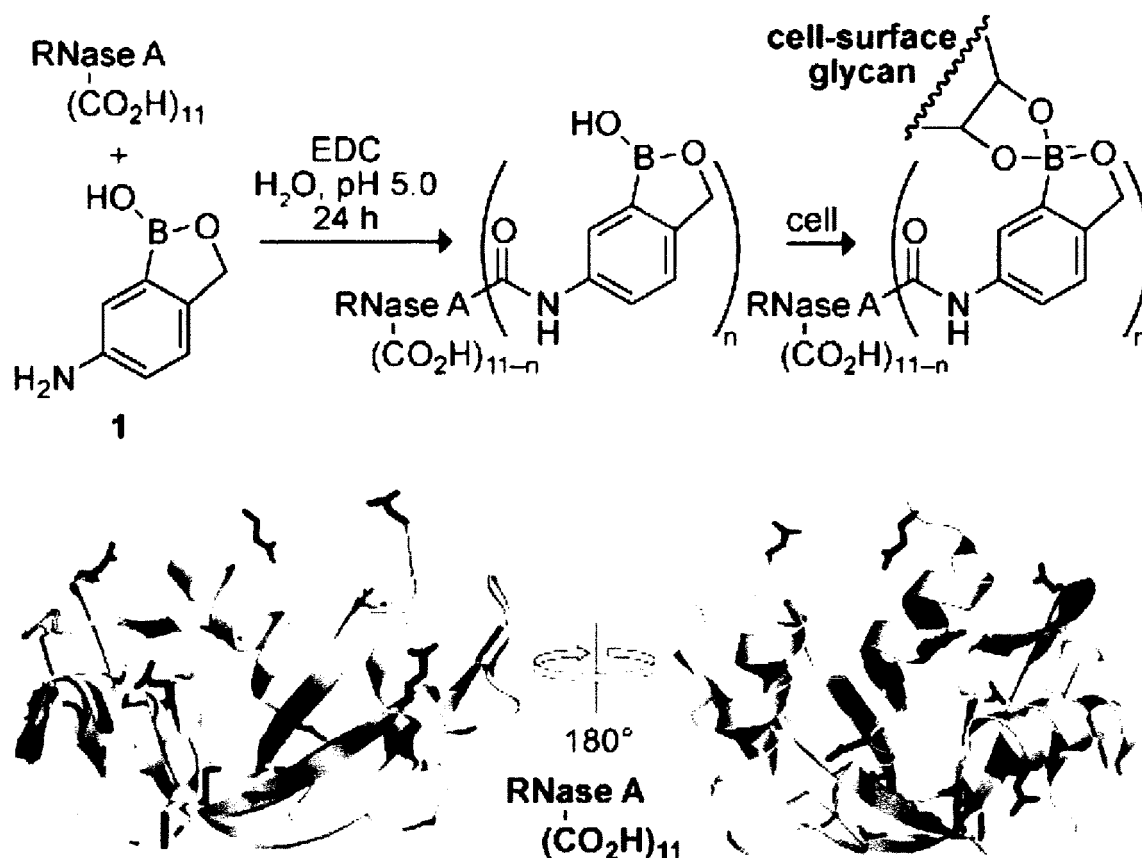




**Figure 3.1** Boronate-mediated drug delivery. Pendant boronic acids are shown to enhance the delivery of a protein into the cytosol of cells.

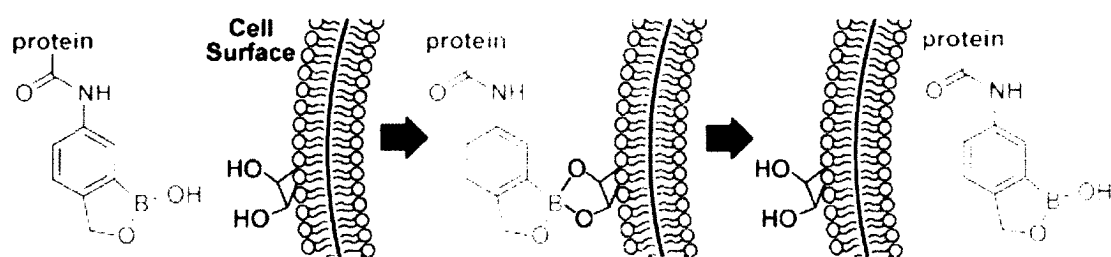
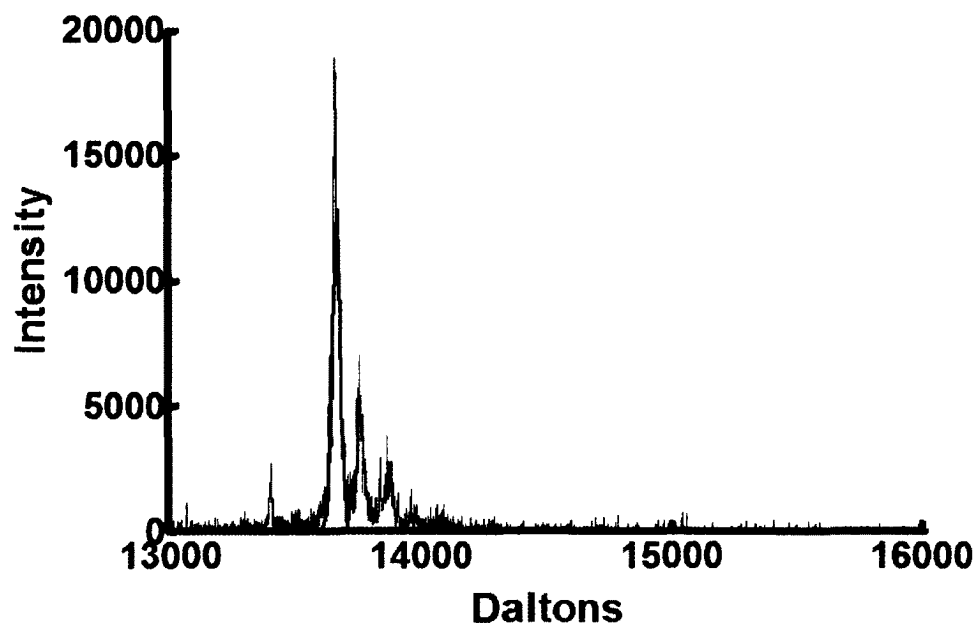


**Figure 3.2** MALDI-TOF spectrum of unmodified RNase A (top) and boronated RNase A (bottom) fit to a Gaussian curve (red line) with GraphPad Prism version 5.02. The mean molecular mass (14,641 Da) was corrected by adding the difference between the mean molecular mass of wild-type RNase A analyzed the same way (13659 Da) and the expected mass of wild-type RNase A (13,682) (correction factor = 23, corrected molecular mass = 14664 Da). This was subtracted from the molecular mass of unmodified RNase A (13,682 Da) to give 982 Da. This value was divided by the molecular mass of 5-amino-2-hydroxymethylphenylboronic acid ( $148.954 \text{ Da} - 18.016 \text{ Da} = 130.938 \text{ Da}$ ), corrected for the loss of water during conjugation, to give  $7.5 \pm 2.0$  boronic acids conjugated to RNase A, where SD = 2.0 arises from the SD of the Gaussian fit, 265.2 Da, divided by 130.938 Da.

Unmodified RNase A:



Boronated RNase A:

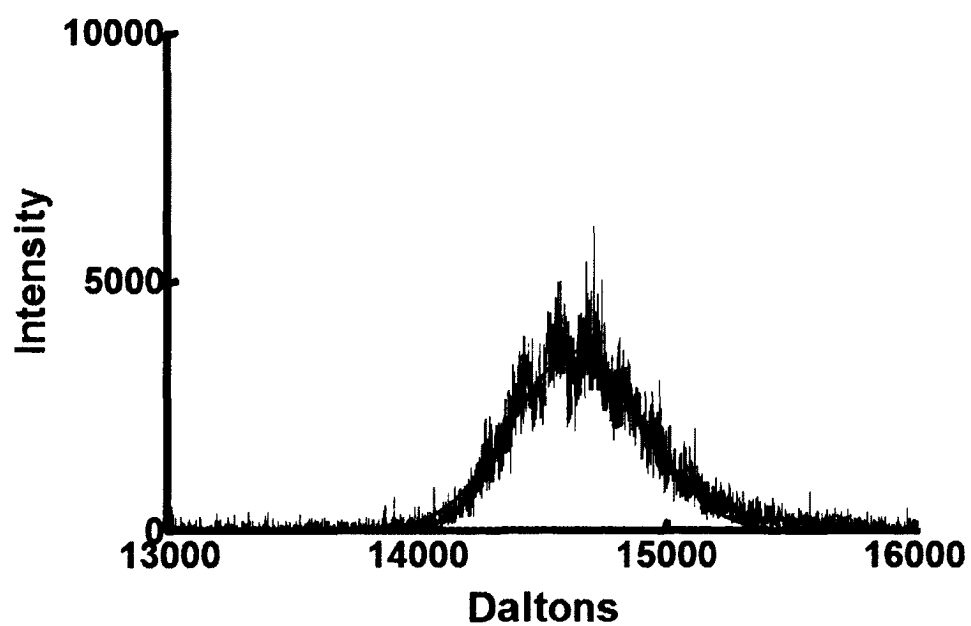


**Figure 3.3** Elution profile of a mixture of unmodified RNase A (eluting in region “A”) and boronated RNase A (eluting in region “B”) from a column of immobilized heparin in the absence (solid line) or presence (dashed line) of fructose (0.10 M).

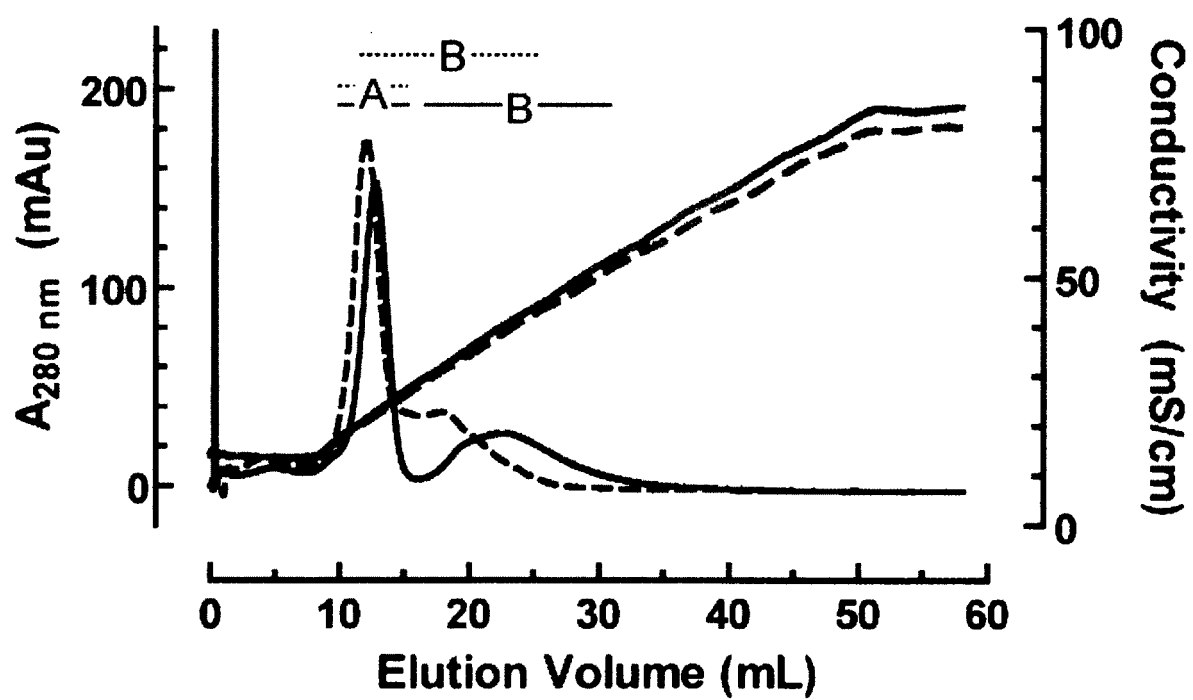
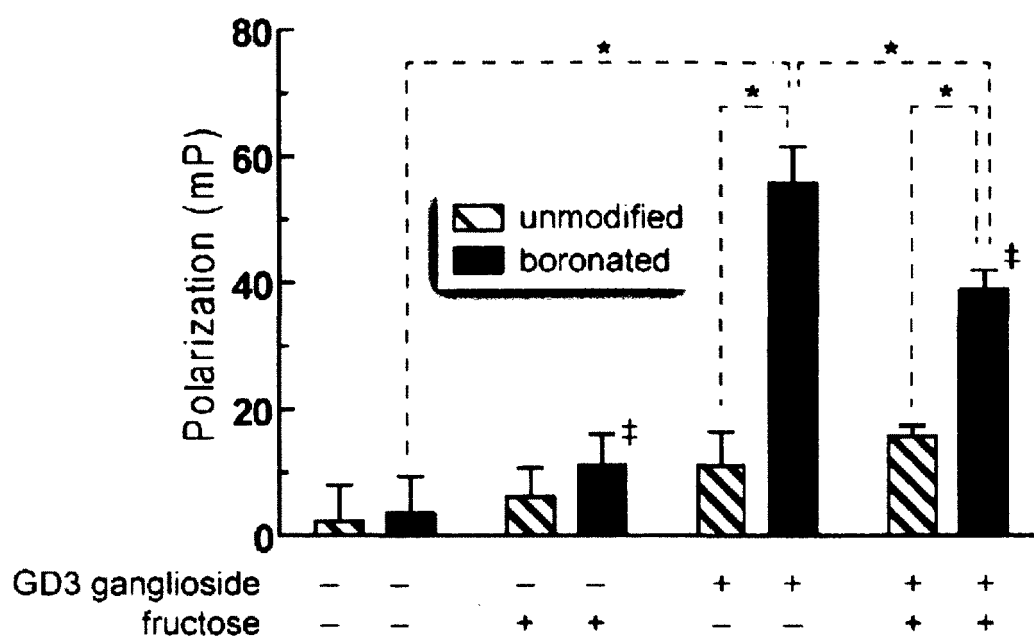


**Figure 3.4** Fluorescence polarization/anisotropy assay of ribonucleases binding ganglioside-labeled liposomes in the presence or absence of 10 mM fructose. Data was normalized to polarization of each ribonuclease incubated with non-extruded DOPC lipids. Data points represent the mean ( $\pm$  SD) of triplicate experiments. Asterisks indicate values with  $p < 0.05$ . The total fluorescence intensity lowered for boronated RNase A with fructose; this was not taken into account (double dagger).

Fluorescence polarization:



Fluorescence anisotropy:

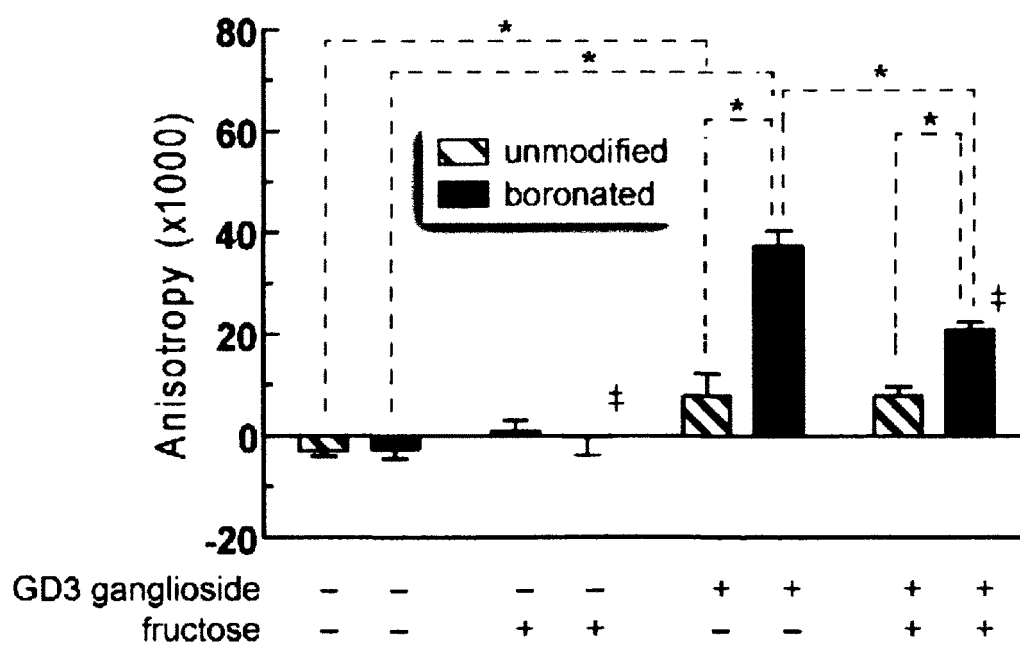
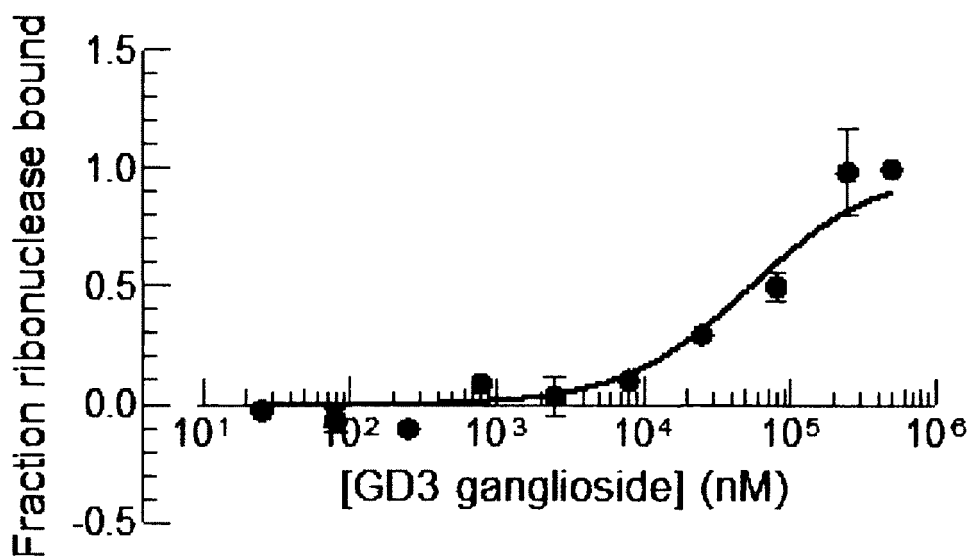




**Figure 3.5** Fluorescence polarization/anisotropy data for the binding of boronated RNase A to GD3 ganglioside in liposomes. BODIPY FL-labeled boronated RNase A was incubated with liposomes containing GD3 ganglioside in 25 mM HEPES buffer, pH 7.0, containing NaCl (75 mM). Data points represent the mean ( $\pm$  SE) of duplicate experiments. Polarization (top) and anisotropy (bottom) data were fitted to a binding isotherm (Roehrl, *et al.*, 2004) to give  $K_d = (53 \pm 11) \mu\text{M}$  and  $(28 \pm 8) \mu\text{M}$ , respectively.

Fluorescence polarization:



Fluorescence anisotropy:

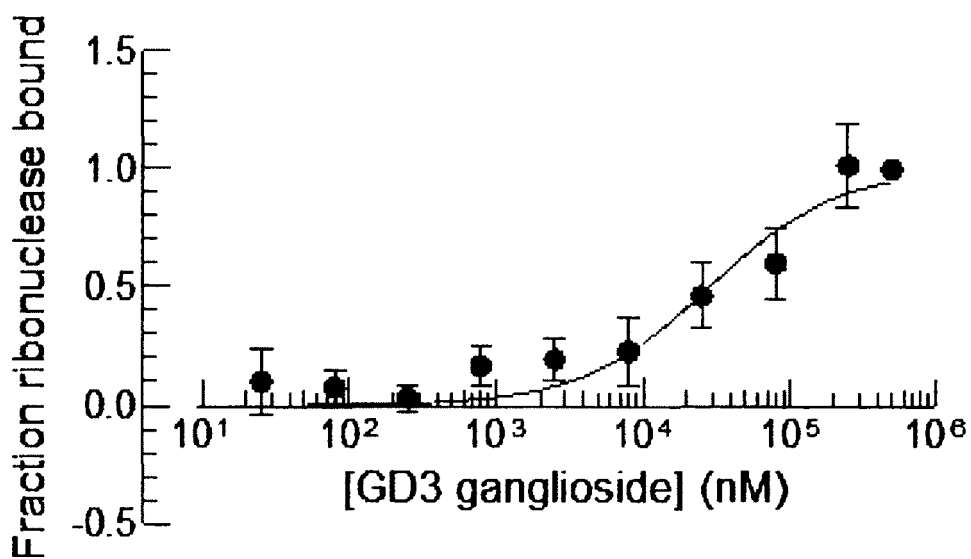


**Figure 3.6** Internalization of unmodified and boronated RNase A into Pro-5 and Lec-2 cells in the absence or presence of fructose (0.25 M). Flow cytometry data were normalized to the internalization of unmodified RNase A into Pro-5 cells. Error bars represent the SD. Insert: Confocal microscopy image of live Pro-5 cells incubated for 4 h with boronated RNase A (5  $\mu$ M) that had been labeled covalently with a green fluorophore. Nuclei were stained blue with Hoechst 33322 (2  $\mu$ g/mL). Scale bar:  $\sim$ 10  $\mu$ m.

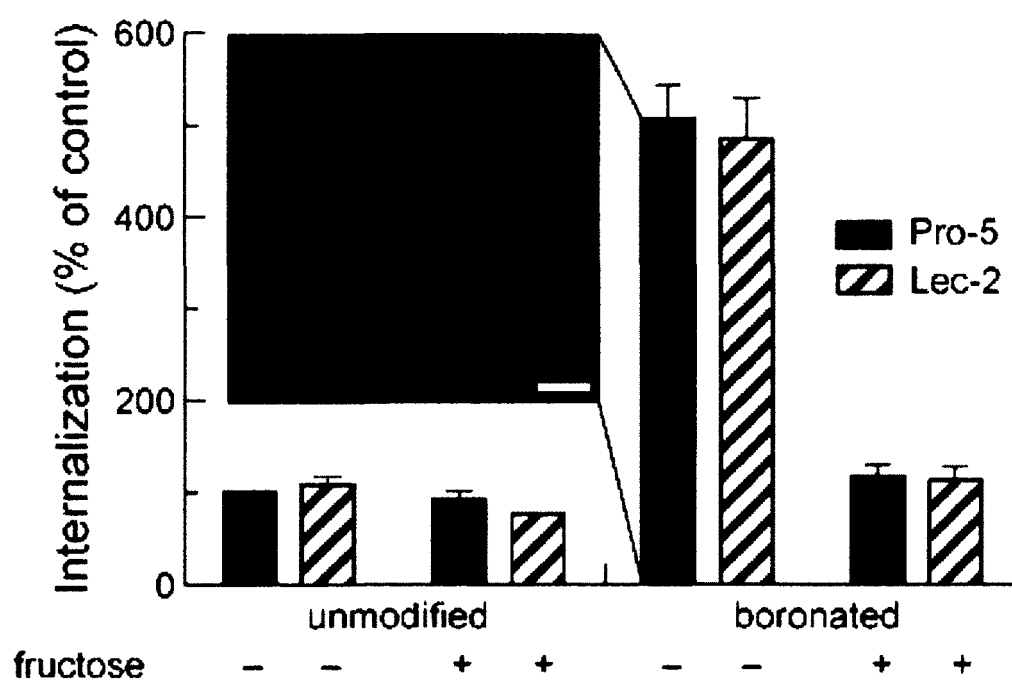
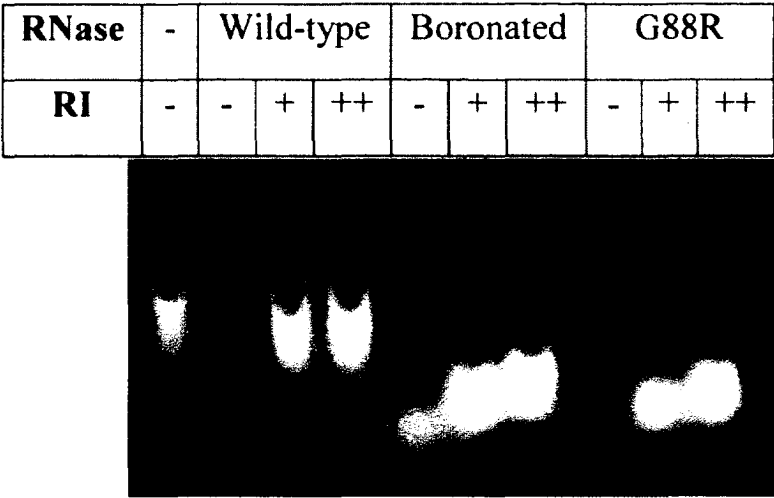


**Figure 3.7** Boronated RNase A evasion of ribonuclease inhibitor protein (RI). (A) Ribonucleases were pre-incubated with 0 (-), 5-fold (+), or 10-fold (++) concentrations of RI for 30 min then incubated with yeast ribosomal RNA for 30 min at room temperature. To samples was added loading dye (Promega, Madison, WI) and samples were subjected to 1.5% agarose gel electrophoresis. Less rRNA retention on the gel indicates degradation and therefore the lack of ribonuclease inhibition by RI. G88R RNase A was used as a RI-evasive positive control. (B) The  $K_d$  value for the RI–boronated RNase A complex was approximately  $(4 \pm 1)$  nM, determined by boronated RNase A (black) disrupting the interaction of RI with diethylfluorescein-labeled A19C G88R RNase A in PBS. G88R RNase A (gray) was used as a positive control. Error is calculated as standard error of the mean.

A



B

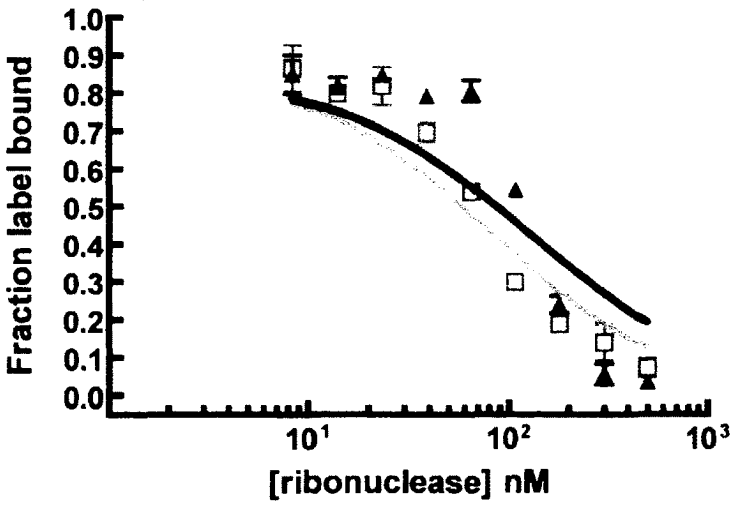


**Figure 3.8** Inhibition of K-562 cell proliferation by unmodified and boronated RNase A. Closed circles indicate unmodified RNase A ( $IC_{50} > 50 \mu M$ ); closed diamonds indicate boronated RNase A ( $IC_{50} 4.1 \pm 0.4 \mu M$ ); open diamonds indicate boronated RNase A in the presence of fructose (50 mM) ( $IC_{50} 9 \pm 3 \mu M$ ; dashed line); open squares indicate boronated RNase A alkylated with 2-bromoacetic acid (to decrease ribonucleolytic activity) ( $IC_{50} > 50 \mu M$ ). The proliferation of K-562 cells was measured by the incorporation of [*methyl*- $^3H$ ]thymidine. Data points represent the mean ( $\pm$  SEM) of three experiments containing triplicate measurements. Control DRNG RNase A (closed triangles)  $IC_{50}$  was ( $0.34 \pm 0.06$ )  $\mu M$ , slightly higher than reported previously ( $0.19 \pm 0.02$ )  $\mu M$  (Rutkoski, *et al.*, 2005). Addition of fructose increased DRNG RNase A  $IC_{50}$  to  $0.43 \mu M$  (open triangles, dashed line), though this was only one replicate.

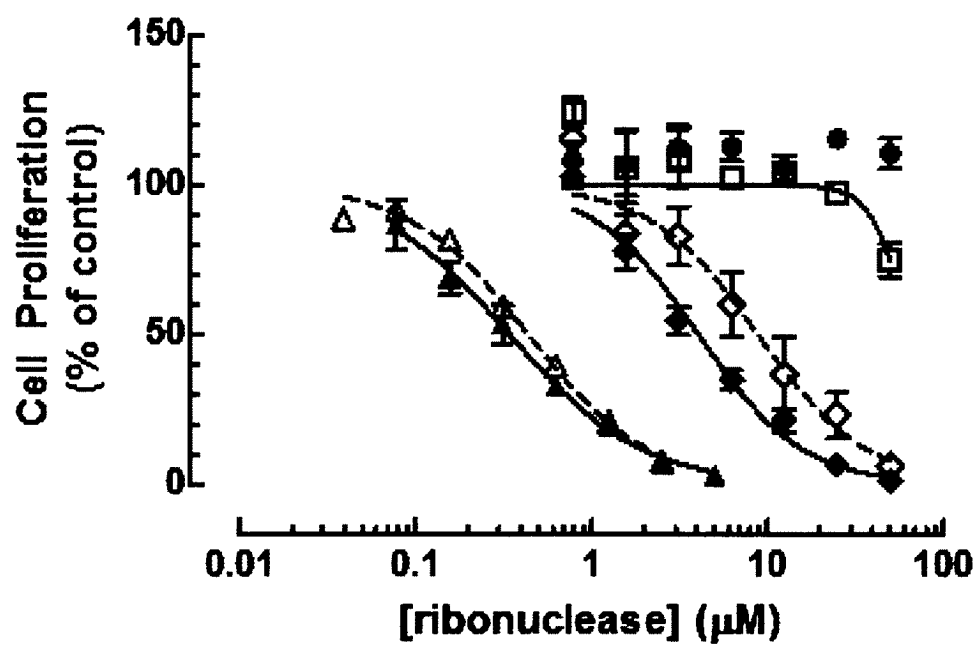




**Figure 3.9** Determination of the peaks corresponding to the aryl protons in bound and free boronic acid and example of the  $^1\text{H}$  NMR spectrum that was used to determine the  $K_a$  value for PBA and fructose. (A)  $^1\text{H}$  NMR spectrum of solution 1. (B)  $^1\text{H}$  NMR spectrum of solution A. (C) Overlay of aromatic region of spectra from panels A and B. (D) Example of a spectrum that was interpreted using the overlay from panel C, and used to determine the value of  $K_a$  for fructose with PBA. The  $[\text{B}\cdot\text{S}]/[\text{B}]$  ratio was calculated from the isolated peaks for the complex (3H, 7.01–7.11 ppm) and the isolated peaks for the free boronic acid (2H, 7.54–7.58 ppm).

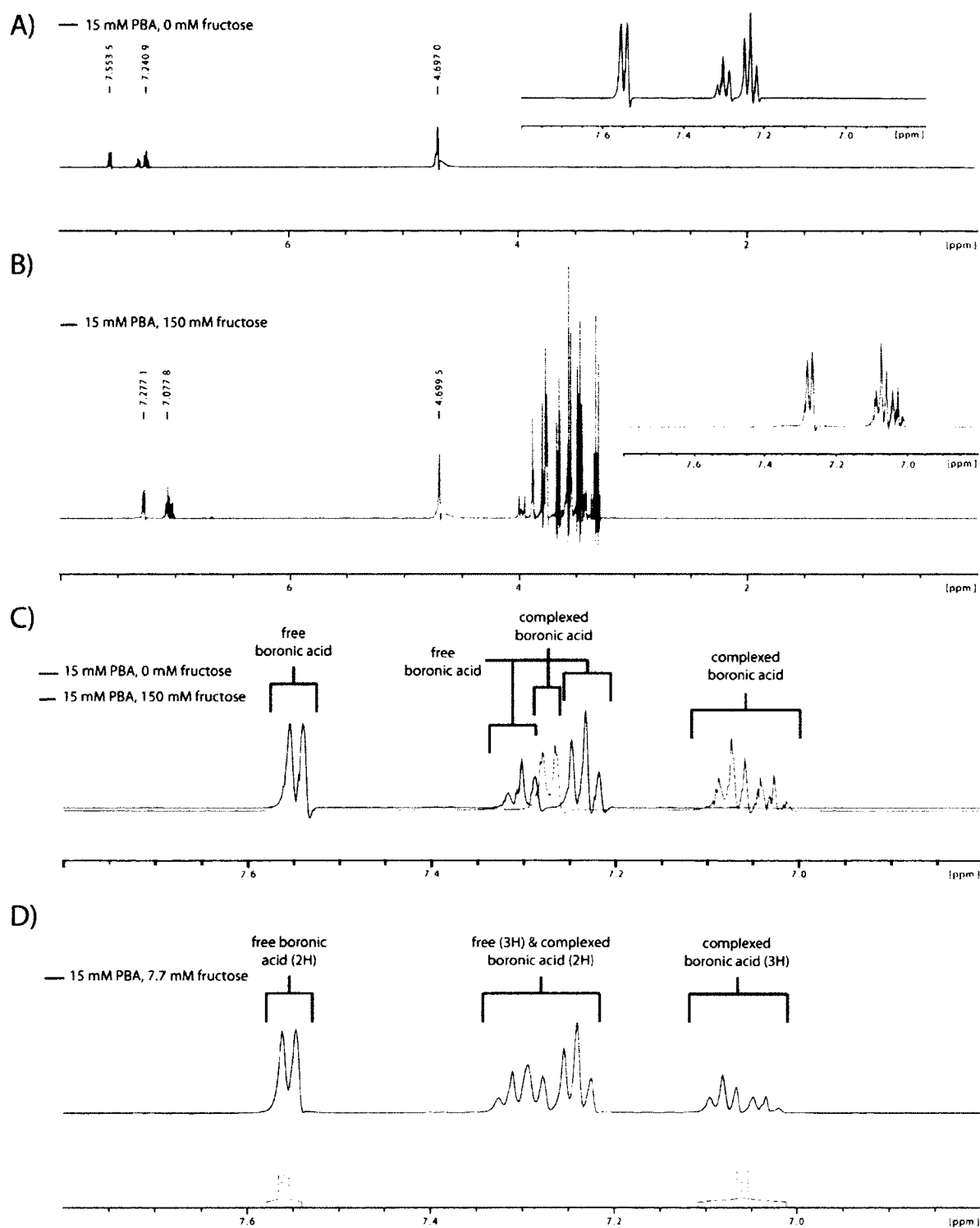


**Figure 3.10** Example of a  $^1\text{H}$  NMR spectrum that was used to determine the  $K_a$  value for benzoboroxole and fructose (10.3 mM). Peaks corresponding to the aryl protons in bound and free boronic acid were determined as described. The  $[\text{B}\cdot\text{S}]/[\text{B}]$  ratio was calculated from the isolated peaks for the complex (1H, 7.31–7.38 ppm, a mixture of isomeric species) and the isolated peaks for the free boronic acid (1H, 7.43–7.53 ppm, a mixture of isomeric species). Additional saccharide decreased the integration of the small peak at 7.44 ppm equally with that at 7.49 ppm, which arise from free boronic acid; and the shoulder peak at 7.31 ppm increased equally with that at 7.35 ppm, which arises from the complex.

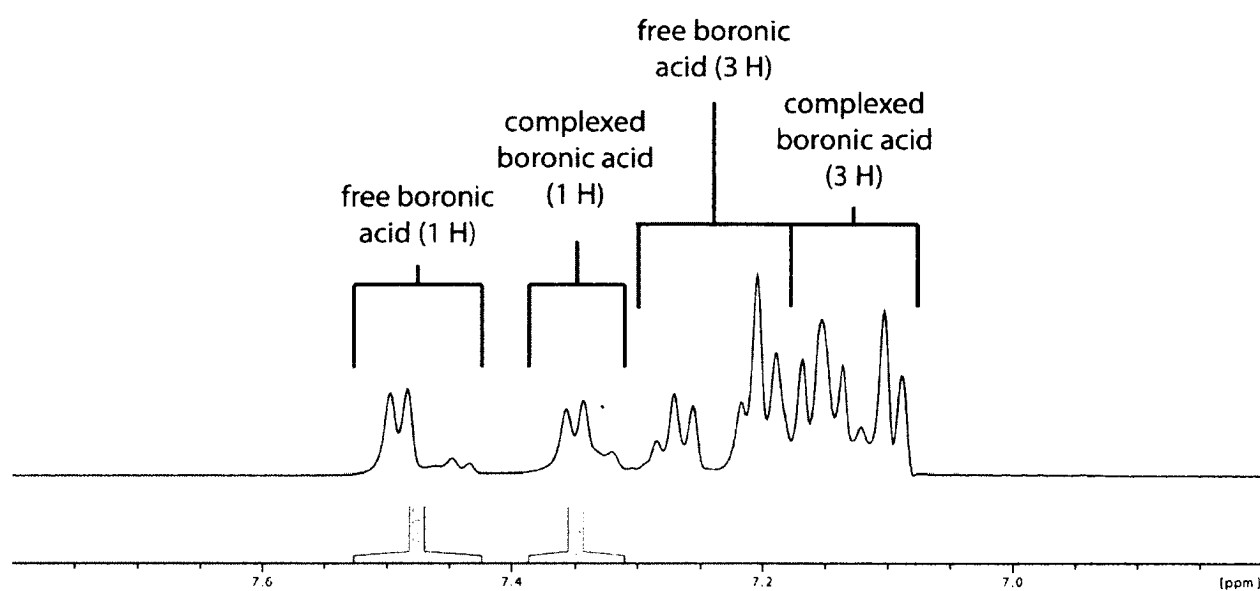


**Figure 3.11** Example of a  $^1\text{H}$  NMR spectrum that was used to determine the  $K_a$  value for PBA and glucose (44.9 mM). Peaks corresponding to the aryl protons in bound and free boronic acid were determined as described. The  $[\text{B}\cdot\text{S}]/[\text{B}]$  ratio was calculated from the isolated peaks for the complex (3H, 7.09–7.21 ppm) and the peaks for the free boronic acid (2H, 7.64–7.68 ppm).

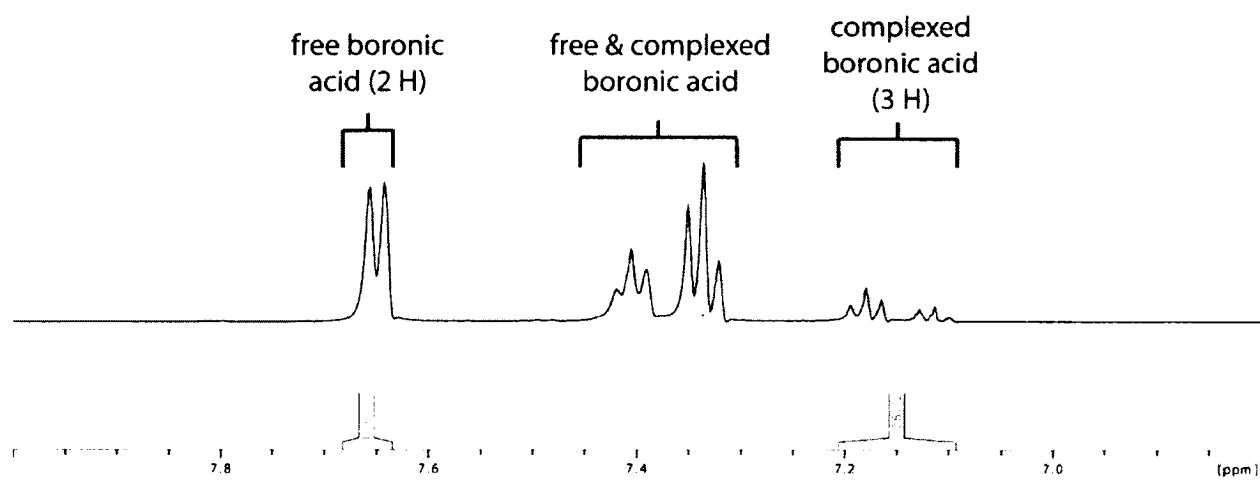


**Figure 3.12** Example of a  $^1\text{H}$  NMR spectrum that was used to determine the  $K_a$  value for benzoboroxazole and glucose (32.9 mM). Peaks corresponding to the aryl protons in bound and free boronic acid were determined as described. The  $[\text{B}\cdot\text{S}]/[\text{B}]$  ratio was calculated from the isolated peaks for the complex ( $^1\text{H}$ , 7.29–7.34 ppm) and the isolated peaks for the free boronic acid ( $^1\text{H}$ , 7.45–7.51 ppm). Note the broadening of the aryl protons, which had been reported for NMR spectra of boronic acids in the presence of pyranose sugars (Bérubé, *et al.*, 2008).

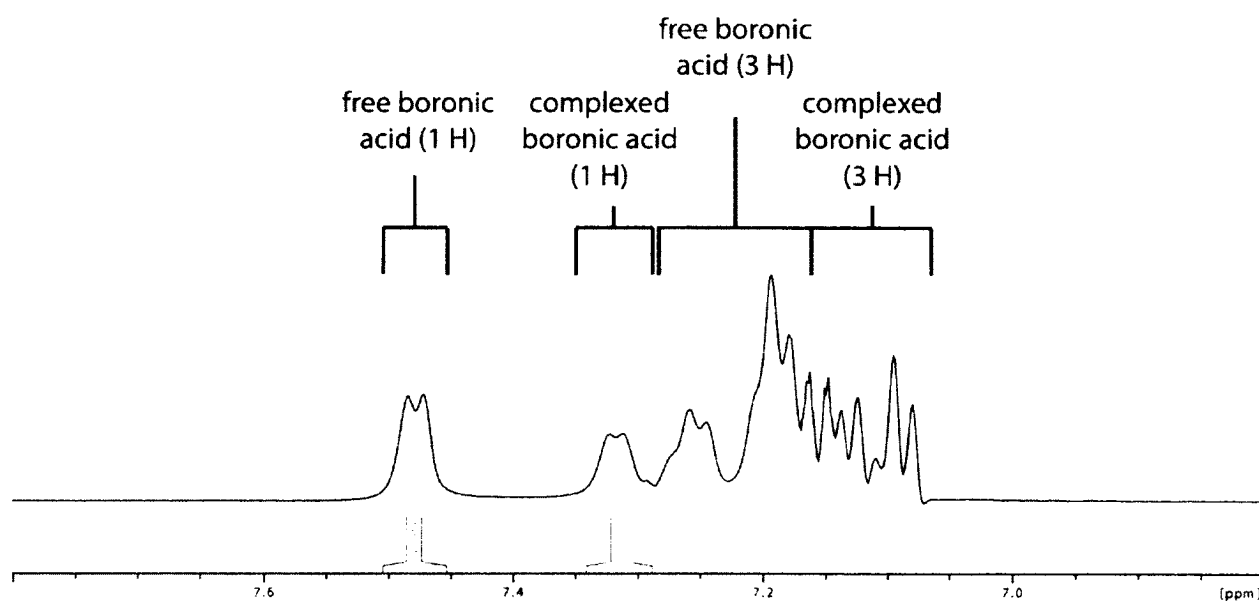




**Figure 3.13** Example of a  $^1\text{H}$  NMR spectrum that was used to determine the  $K_a$  value for PBA with Neu5Ac (35.4 mM). Peaks corresponding to the aryl protons in bound and free boronic acid were determined as described. The  $[\text{B}\cdot\text{S}]/[\text{B}]$  ratio was calculated from the isolated peaks for the complex (3H, 7.15–7.26 ppm) and the isolated peaks for the free boronic acid (2H, 7.6–7.69 ppm). Note that the aryl peaks have been broadened by the addition of the saccharide.

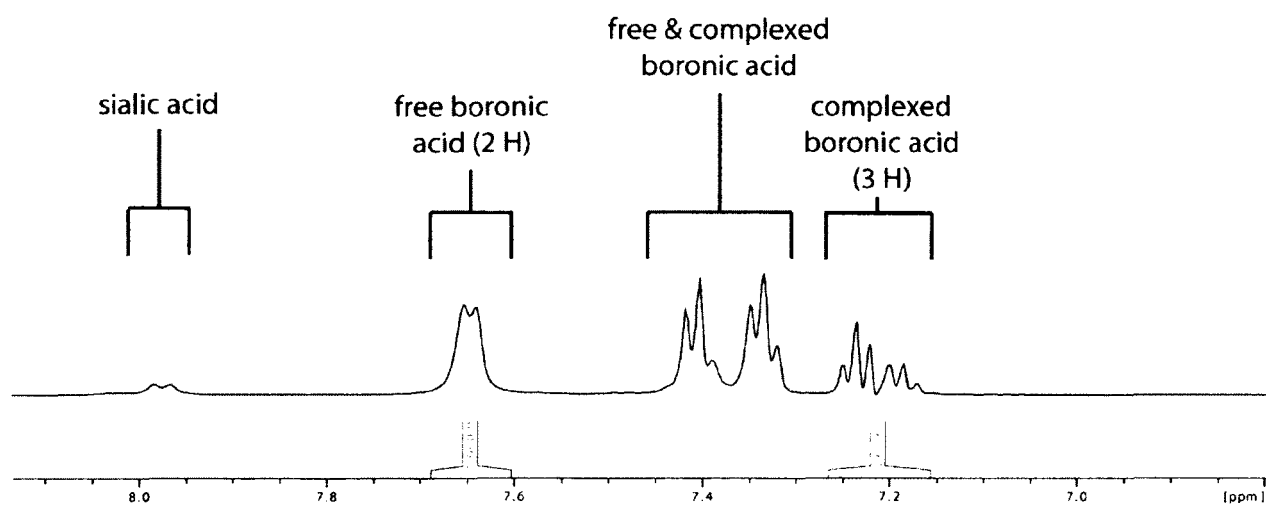


**Figure 3.14** Apparent in the  $^1\text{H}$  NMR spectrum of Neu5Ac is a small peak that overlapped with the aromatic regions of the boronic acids. This peak was subtracted out of all NMR spectra used to evaluate the interaction of benzoboroxazole and Neu5Ac.

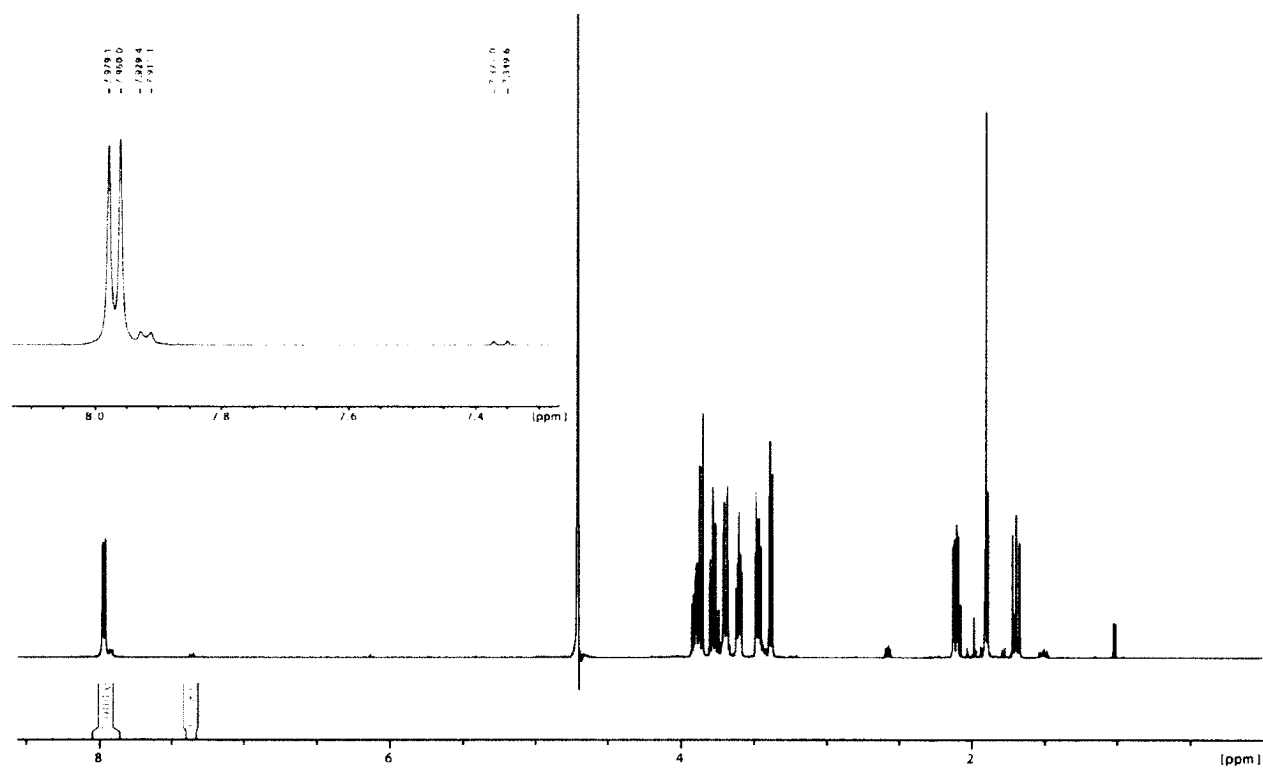
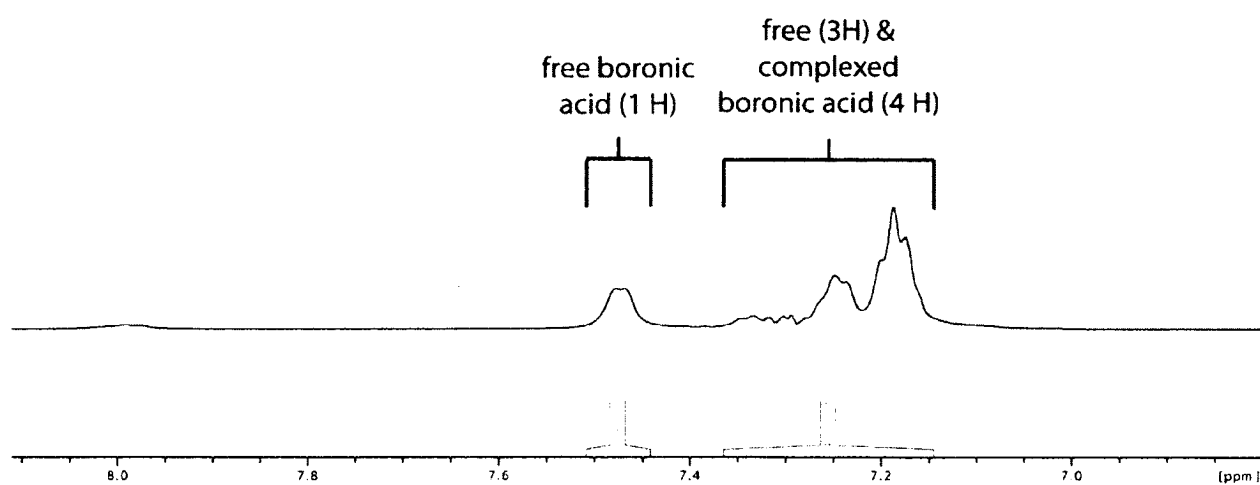


**Figure 3.15** Example of a  $^1\text{H}$  NMR spectrum that was used to determine the  $K_a$  value for benzoboroxazole with Neu5Ac (14.4 mM). Peaks corresponding to the aryl protons in bound and free boronic acid were determined as described. The  $[\text{B}\cdot\text{S}]/[\text{B}]$  ratio was determined from the isolated peaks for the free boronic acid (1H, 7.44–7.51 ppm) and the remainder of the aromatic region (7.15–7.36 ppm), which represented 3H from the free boronic acid and all 4 aromatic protons from the complex. Unlike fructose and glucose, the single isolated proton of the complexed species (7.33 ppm) was too broad to integrate accurately, and the entire region was used instead.



## CHAPTER 4

### Potentialiation of Ribonuclease Cytotoxicity by a Poly(amidoamine) Dendrimer

This chapter was published as:

Ellis, G.A., Hornung, M.L., and Raines, R.T. (2011) Potentialiation of ribonuclease cytotoxicity by a poly(amidoamine) dendrimer. *Bioorg. Med. Chem. Lett.* **21**, 2756-2758. (additions/corrections section 4.8)

## 4.1 Abstract

Variants of bovine pancreatic ribonuclease (RNase A) engineered to evade the endogenous ribonuclease inhibitor protein (RI) are toxic to human cancer cells. Increasing the basicity of these variants facilitates their entry into the cytosol and thus increases their cytotoxicity. The installation of additional positive charge also has the deleterious consequence of decreasing ribonucleolytic activity or conformational stability. Here, we report that the same benefit can be availed by co-treating cells with a cationic dendrimer. We find that adding the generation 2 poly(amidoamine) dendrimer *in trans* increases the cytotoxicity of RI-evasive RNase A variants without decreasing wild-type RNase A thermostability and with only modest effects on its activity. The increased cytotoxicity is likely not due to increased RI-evasion or cellular internalization, but likely results from improved translocation into the cytosol after endocytosis. These data indicate that co-treatment with highly cationic molecules could enhance the efficacy of ribonucleases as chemotherapeutic agents (Figure 4.1).

## 4.2 Introduction

Pancreatic-type ribonucleases can be toxic to cancerous cells (Matousek, 2001; Leland and Raines, 2001; Makarov and Ilinskaya, 2003; Benito, *et al.*, 2005; Arnold and Ulbrich-Hofmann, 2006). This cytotoxicity depends on the efficiency of their internalization into cells and subsequent translocation into the cytosol, their conformational stability, their ability to evade the endogenous ribonuclease inhibitor protein (RI) (Dickson, *et al.*, 2005), and their ability to catalyze the degradation of cellular RNA (Rutkoski and Raines, 2008). Although Onconase<sup>®</sup> (Lee and Raines, 2008), a ribonuclease from the Northern Leopard frog that naturally evades RI,



was in a Phase IIIb clinical trial as a treatment for malignant mesothelioma, its therapeutic potential was diminished by dose-limiting renal toxicity (Mikulski, *et al.*, 1993; Costanzi, *et al.*, 2005; Pavlakis and Vogelzang, 2006; Rutkoski and Raines, 2008; Ardelt, *et al.*, 2008; Beck, *et al.*, 2008). Mammalian pancreatic ribonucleases accumulate to a much lesser extent in the kidneys, but are strongly inhibited by RI (Vasandani, *et al.*, 1996; Rutkoski, *et al.*, 2005; Johnson, *et al.*, 2007b). Variants of both bovine (RNase A) (Raines, 1998) and human (RNase 1) pancreatic ribonuclease have been engineered to evade RI and are thereby endowed with cytotoxic activity (Leland, *et al.*, 1998; Leland, *et al.*, 2001; Rutkoski, *et al.*, 2005; Johnson, *et al.*, 2007b). An RNase 1 variant is in a Phase I clinical trial for patients having advanced, refractory, solid tumors.

Although ribonucleases show promise as cancer chemotherapeutic agents, their potency is limited by the bottleneck of cellular internalization and translocation into the cytosol. For example, RNase A has cytotoxicity at much lower (e.g., picomolar) concentrations when injected directly into cells (Saxena, *et al.*, 1991; Smith, *et al.*, 1999; Lotfi, *et al.*, 2007). RNase A and its homologues are cationic proteins (Figure 4.2). Internalization has been shown to correlate with ribonuclease cationicity (Johnson, *et al.*, 2007a), and efforts have been made to add positive charge and thereby enhance cytotoxicity. ‘Arginine-grafting’ and appending a nonaarginine tag do indeed increase the cytotoxicity of RI-evasive RNase A variants (Fuchs and Raines, 2005; Fuchs, *et al.*, 2007). These alterations, however, tend to diminish the conformational stability of the ribonuclease, abrogating some of the benefit from increased internalization. RNase A has also been modified by condensing the side chains of aspartate and glutamate residues with ethylenediamine or cationic polymers of poly(ethyleneimine) (Futami, *et al.*, 2001; Futami, *et*

*et al.*, 2005). Although these covalent modifications increase cytotoxicity, they diminish catalytic activity. We sought a means to increase ribonuclease-mediated cytotoxicity without compromising other desirable attributes.

To avoid the deleterious consequences of adding cationic groups to a ribonuclease, we hypothesized that ribonuclease cytotoxicity could be enhanced by adding a highly cationic molecule as a co-treatment, that is, *in trans*. This strategy was supported by the recent observation that co-treatment with a cationic peptide or PEI enhances the cellular uptake of proteins (Didenko, *et al.*, 2005; Loudet, *et al.*, 2008). As our co-treatment, we chose to use the generation 2 poly(amidoamine) (PAMAM) dendrimer, which has a high density of cationic charge (Figure 4.3). PAMAM dendrimers are monodisperse branched polymers that are available from numerous commercial vendors (Tomalia, *et al.*, 1985; Esfand and Tomalia, 2001). PAMAM dendrimers have been employed as drug and gene delivery vehicles, as they have the ability to transport encapsulated small molecules and enwrapped DNA into cells (Esfand and Tomalia, 2001; Cloninger, 2002; Guillot-Nieckowski, *et al.*, 2007; Navarro, *et al.*, 2010). We chose the relatively small generation 2 dendrimer due to its low inherent cytotoxicity compared to higher generation dendrimers and other highly cationic macromolecules, such as polyethylenimine (Roberts, *et al.*, 1996; Malik, *et al.*, 2000; Fischer, *et al.*, 2003). This dendrimer has 16 primary amino groups and 14 tertiary amino groups. Its net molecular charge is approximately  $Z = +16$  (Cakara, *et al.*, 2003), and could reach  $Z = +30$  in an acidic environment. The dendrimer is known to enter cells through endocytosis and then appears to disrupt endosomes through the 'proton sponge' effect (Sonawane, *et al.*, 2003). We reasoned that

dendrimers could elicit an adventitious increase in the translocation of ribonucleases into the cytosol and, thus, in their cytotoxic activity.

### 4.3 Results and Discussion

Ribonucleases tend to lose conformational stability (Fuchs and Raines, 2005; Fuchs, *et al.*, 2007) or catalytic activity (Futami, *et al.*, 2001; Futami, *et al.*, 2005) when modified covalently to be more cationic. Accordingly, we first sought to discern whether the dendrimer elicited any effects on these important attributes *in trans*. We found that the dendrimer at concentrations of 1 or 10  $\mu\text{M}$  has no discernable effect on the thermostability of RNase A (Table 4.1). Similarly, these concentrations had an insignificant effect on ribonucleolytic activity. Accordingly, we conclude that the dendrimer at a concentration of  $\leq 10 \mu\text{M}$  has no deleterious consequences.

Large cationic molecules antagonize the RI–RNase A interaction (Moenner, *et al.*, 1999). Hence, we next sought to determine whether the dendrimer is an antagonist of this interaction. Serial dilutions of a solution of dendrimer were used to compete with a 2',7'-diethylfluorescein-labeled variant of RNase A for binding to RI. Using this assay (Lavis, *et al.*, 2007), we determined that the RI-dendrimer complex in PBS has  $K_d = (3.1 \pm 0.5) \mu\text{M}$  (Figure 4.4), which is significantly greater than RI-evasive variants of RNase A (Rutkoski, *et al.*, 2005). This value, along with the known concentration of RI in the cytosol (4  $\mu\text{M}$ ) (Haigis, *et al.*, 2003), indicate that the dendrimer is unlikely to act by antagonizing the RI–RNase A interaction.

Having established that the dendrimer is inert *in vitro*, we sought to test our hypothesis *in cellulo*. Specifically, we determined the effect of the dendrimer on the cytotoxicity of wild-type RNase A and two RI-evasive variants. We did these experiments with K-562 cells, which are

nonadherent cells from a human myelogenous leukemia line. We choose dendrimer concentrations of 1 and 10  $\mu\text{M}$  because these concentrations did not compromise important attributes of the ribonucleases (Table 4.1) and allowed for the unrestricted proliferation of K-562 cells ( $97 \pm 3\%$  and  $95 \pm 3\%$ , respectively).

We found that wild-type RNase A showed no measurable cytotoxicity with or without dendrimer (Figure 4.5), as expected from its high affinity for RI. In contrast, both 1 and 10  $\mu\text{M}$  dendrimer potentiated the cytotoxicity of two RI-evasive ribonuclease variants, with 10  $\mu\text{M}$  being slightly more effective. At 10  $\mu\text{M}$  dendrimer, G88R RNase A, which is moderately evasive to RI, exhibited a decrease in  $\text{IC}_{50}$  value of fivefold. D38R/R39D/N67R/G88R (DRNG) RNase A, which is highly evasive to RI and hence more cytotoxic than the G88R variant (Rutkoski, *et al.*, 2005), likewise had its cytotoxicity potentiated by fivefold. Because the dendrimer evoked the same relative increase in cytotoxicity for both variants, we concluded that the dendrimer acts by enhancing either cellular internalization or translocation.

Ribonucleases enter the cytosol by first being internalized into endosomes and then translocating into the cytosol (Rutkoski and Raines, 2008). To discern whether the dendrimer affected internalization, we attached a fluorogenic label to RNase A, as described previously (Lavis, *et al.*, 2006). This label is not fluorescent until entering endosomes, which contain esterases that unmask its fluorescence. K-562 cells were incubated with or without dendrimer (1 or 10  $\mu\text{M}$ ), and ribonuclease internalization was measured by flow cytometry. Dendrimer did not increase internalization of the labeled ribonuclease into the cell (Table 4.1). Apparently, the dendrimer acts downstream of internalization, probably by increasing endosomal escape.

## 4.4 Conclusions

We conclude that a cationic dendrimer can potentiate the cytotoxicity of RI-evasive variants of RNase A *in trans*. This ability obviates the deleterious consequences that typically accompany chemical or mutagenic modification. Although it is unlikely that the particular strategy described here could be used in a clinical setting, our findings do encourage further exploration, both on the use of cationic dendrimers as co-treatments with chemotherapeutic agents and on the mechanism of their action in this context.

## 4.5 Experimental Procedures

### 4.5.1 Materials

*Escherichia coli* strain BL21(DE3) cells were from Novagen (Madison, WI). K-562 cells, which were derived from a continuous human chronic myelogenous leukemia line, were from the American Type Culture Collection (Manassas, VA). Cell culture medium and supplements, as well as Dulbecco's phosphate-buffered saline (DPBS) were from Invitrogen (Carlsbad, CA). [methyl-<sup>3</sup>H]Thymidine (6.7 Ci/mmol) was from Perkin–Elmer (Boston, MA). Protein purification columns were from GE Biosciences (Piscataway, NJ). Wild-type RNase A, PAMAM Generation 2 dendrimer, and 2-(N-morpholino)ethanesulfonic acid (MES) were from Sigma–Aldrich (St. Louis, MO). Dendrimers in methanol were placed under reduced pressure to remove methanol, then dissolved in DPBS; the pH of the resulting solution was adjusted to ~7.4. MES buffer was purified by anion-exchange chromatography to remove trace amounts of oligomeric vinylsulfonic acid (Smith, *et al.*, 2003). Ribonuclease substrate 6-FAM–dArUdAdA–

6-TAMRA was from Integrated DNA Technologies (Coralville, IA). Non-binding surface (NBS) 96-well plates were from Corning (Corning, NY). All other chemicals used were of commercial reagent grade or better, and were used without further purification. Terrific Broth (TB) was from Research Products International (Mt. Prospect, IL), or was made by dissolving tryptone (12 g), yeast extract (24 g), glycerol (4 mL),  $\text{KH}_2\text{PO}_4$  (2.31 g), and  $\text{K}_2\text{HPO}_4$  (12.54 g) in  $\text{H}_2\text{O}$  (1.00 L).

#### 4.5.2 *Analytical instruments and statistical calculations*

The incorporation of [*methyl*- $^3\text{H}$ ]thymidine into the genomic DNA of K-562 cells was quantified by scintillation counting using a Microbeta TriLux liquid scintillation and luminescence counter (Perkin–Elmer, Wellesley, MA). Fluorescence measurements were made with an Infinite M1000 plate reader (Tecan, Switzerland). Thermal denaturation data were collected with a Cary 3 double-beam spectrophotometer equipped with a Cary temperature controller (Varian, Palo Alto, CA). Molecular mass was determined by matrix-assisted laser desorption/ionization time-of-flight (MALDI–TOF) mass spectrometry using a Voyager-DE-PRO Biospectrometry Workstation (Applied Biosystems, Foster City, CA) at the campus Biophysics Instrumentation Facility. Flow cytometry data were collected by using a FACS Calibur flow cytometer equipped with a 488-nm argon-ion laser (Becton Dickinson, Franklin Lakes, NJ). Calculations for statistical significance were performed using the Student's *t*-test, and a value of  $p < 0.05$  was considered significant.

#### 4.5.3 Protein production

RNase A variants were produced as described previously (Rutkoski, *et al.*, 2005), but with the following exceptions. Phenylmethanesulfonyl fluoride (PMSF) was added during some preparations to minimize protein degradation. Ribonucleases were refolded for 24–72 h at room temperature or 4 °C. Following purification, proteins used in cytotoxicity assays were dialyzed against PBS. Protein concentration was determined by UV spectroscopy using an extinction coefficient at 278 nm of  $0.72 \text{ (mg/ml)}^{-1} \cdot \text{cm}^{-1}$  for RNase A and its variants. Variants with a cysteine residue at position 19 were protected by reaction with 5,5'-dithio-bis(2-nitrobenzoic acid) (DTNB) to form a mixed disulfide (Riddles, *et al.*, 1983; Lavis, *et al.*, 2006). Immediately prior to conjugation with a latent fluorophore or 2',7'-diethylfluorescein (DEF) (Lavis, *et al.*, 2006; Lavis, *et al.*, 2007), protected ribonucleases were treated with a 4-fold molar excess of dithiothreitol (DTT) and desalted by chromatography on a PD-10 desalting column (GE Biosciences, Piscataway, NJ). The deprotected ribonucleases were reacted for 2–4 h at 25 °C with a 10-fold molar excess of a thiol-reactive fluorophore (Lavis, *et al.*, 2006; Lavis, *et al.*, 2007). Conjugates were purified by chromatography using a HiTrap SP HP column. The concentration of labeled proteins was determined by using a bicinchoninic acid assay kit from Pierce (Rockford, IL) with wild-type RNase A as a standard. Human ribonuclease inhibitor (RI) was prepared in *E. coli* as described previously (Johnson, *et al.*, 2007b). Following their purification, the purity and molecular mass of the ribonucleases and RI were verified with SDS-PAGE.

#### 4.5.4 Conformational stability assay

The conformational stability of wild-type RNase A was determined by following the change in UV absorbance at 287 nm with increasing temperature, as described previously (Klink and Raines, 2000). Briefly, the temperature of PBS containing RNase A (25  $\mu$ M) with 1 or 10  $\mu$ M dendrimer, or without dendrimer (control), was heated from 25–80  $^{\circ}$ C at 0.15  $^{\circ}$ C/min. The  $A_{287}$  was followed at 1- $^{\circ}$ C intervals, and the absorbance change was fitted to a two-state model of denaturation, wherein the temperature of the midpoint of the transition curve corresponds to the value of  $T_m$ . Data are the average of three experiments.

#### 4.5.5 Ribonucleolytic activity assay

The ribonucleolytic activity of wild-type RNase A was determined by quantitating its ability to cleave 6-FAM–dArUdAdA–6-TAMRA, as described previously (Kelemen, *et al.*, 1999). Briefly, assays were carried out at ambient temperature in 2.00 mL of 0.10 M MES–NaOH buffer (pH 6.0) containing NaCl (0.10 M). Fluorescence data were fitted to equation 4.1, in which  $\Delta I/\Delta t$  is the initial reaction velocity,  $I_0$  is the fluorescence intensity before addition of ribonuclease,  $I_f$  is the fluorescence intensity after complete substrate hydrolysis, and  $[E]$  is the total ribonuclease concentration. Activity was measured without dendrimer (control) or in the presence of 1 or 10  $\mu$ M dendrimer. Data are the average of three experiments.

$$k_{\text{cat}}/K_M = \frac{\Delta I/\Delta t}{(I_f - I_0)[E]} \quad (4.1)$$



#### 4.5.6 RI-binding assay

Affinities for RI were determined by using a competition assay similar to one described previously (Lavis, *et al.*, 2007). Briefly, a serial dilution (2×) of the dendrimer in DPBS was prepared in Eppendorf Protein LoBind Tubes (Fisher Scientific). A stock solution of A19C–DEF G88R RNase A (20 nM; 2×), RI (24 nM; 2×), DTT (1 mM; 2×), and BSA (0.1 mg/mL; 2×) was made, and 50-μL aliquots of this stock solution were added to the wells of a 96-well NBS plate. Aliquots of the serially diluted solution of dendrimer were then added to the wells. The negative control contained no ribonuclease (PBS), and the positive control contained excess RNase A (0.2 μM; 2×). The plate was incubated for 30 min at ambient temperature, after which the fluorescence intensity was measured. The observed fluorescence intensity ( $I$ ) is described by equation 4.2:

$$I = f_F I_F + f_B I_B \quad (4.2)$$

where  $f_F$  and  $f_B$  are the fractions of the free and RI-bound form of the fluorescence conjugate, respectively, and  $I_F$  and  $I_B$  are the fluorescent intensities of the free and RI-bound states, respectively. The value of  $f_B$  was determined by linear regression analysis using the intensities of the positive and negative controls, which represent 0 and 75.9% bound, respectively, based on a  $K_d$  value of 1.4 nM for the fluorophore-labeled G88R variant of RNase A (Lavis, *et al.*, 2007). The fraction bound ( $f_B$ ) was then calculated by using equation 4.3:

$$f_B = \frac{I - I_F}{I_B - I_F} \quad (4.3)$$

The value of  $K_d$  was calculated by plotting  $f_B$  against the concentration of competing dendrimer and fitting the data to the mathematical expression for complete competitive binding of two different ligands (Wang, 1995; Roehrl, *et al.*, 2004). Data are the average of two measurements, and the entire experiment was repeated in triplicate.

#### 4.5.7 Cell-proliferation assay

The effect of RNase A, its variants, dendrimer, and co-treatment of dendrimer with ribonucleases on the proliferation of K-562 cells was assayed as described previously (Leland, *et al.*, 1998). Briefly, for assays with a single sample, 5  $\mu$ L of a serially diluted solution of ribonuclease, dendrimer, or PBS was added to 95  $\mu$ L of DPBS containing K-562 cells ( $5.0 \times 10^4$  cells/mL). For co-treatments, 10  $\mu$ L of a serially diluted solution of ribonuclease (2 $\times$ ) was premixed with 10  $\mu$ L of a solution of dendrimer (2 $\times$ ). Then, 5  $\mu$ L of this solution was added to 95  $\mu$ L of DPBS containing K-562 cells ( $5.0 \times 10^4$  cells/mL). After 44 h, the cells were treated with [*methyl*- $^3$ H]thymidine for 4 h, and the incorporation of radioactive thymidine into cellular DNA was quantified by liquid scintillation counting. Results were reported as the percentage of [*methyl*- $^3$ H]thymidine incorporated relative to control cells that had been treated with PBS. Data are the average of three measurements for each concentration, excluding those measurements that were determined to be outliers by the Grubb's test for outliers with  $p$  value = 0.05 (Grubbs, 1969). The entire experiment was repeated in triplicate. Values for  $IC_{50}$  were calculated by fitting the curves by nonlinear regression with equation 4.4, in which  $y$  is the total DNA synthesis following the [*methyl*- $^3$ H]thymidine pulse, and  $h$  is the slope of the curve.

$$y = \frac{100\%}{1 + 10^{(\log(IC_{50}) - \log[\text{ribonuclease}])h}} \quad (4.4)$$

#### 4.5.8 Flow cytometry assay

The internalization of ribonuclease variants with latent fluorophore attached was followed by monitoring the unmasking of fluorescence by intracellular esterases, as described previously (Johnson, *et al.*, 2007a). Briefly, K-562 cells were collected by centrifugation, washed with PBS, and resuspended at a density of  $1.25 \times 10^6$  cells/mL in fresh medium. Labeled ribonuclease (to 10  $\mu$ M) and dendrimer (to 0, 1, or 10  $\mu$ M) was added to 200  $\mu$ L of medium containing K-562 cells ( $1.25 \times 10^6$  cells/mL). Cells were allowed to incubate at 37 °C for 3 h. To quench internalization, cells were placed on ice, collected by centrifugation at 1000 rpm for 5 min at 4 °C, washed with 750  $\mu$ L of PBS, and collected again by centrifugation at 1000 rpm for 5 min at 4 °C. The cell pellets were suspended gently in ice-cold PBS (250  $\mu$ L). Samples remained on ice until analyzed by flow cytometry.

Fluorescence was detected through a 530/30-nm band-pass filter. Cell viability was determined by staining with propidium iodide, which was detected through a 660-nm long-pass filter. The mean channel fluorescence intensity of 20,000 viable cells was determined for each sample using CellQuest software and used for subsequent analysis. Data are the average of three measurements for each concentration, and the entire experiment was repeated in triplicate.

## 4.6 Acknowledgments

We are grateful to Drs. T. J. Rutkoski, L. D. Lavis, T.-Y. Chao, D. R. McCaslin, and R. W. Watkins, as well as J. E. Lomax for contributive discussions. Experiments made use of the Biophysics Instrumentation Facility, which was established by Grants BIR-9512577 (NSF) and S10 RR13790 (NIH). This work was supported by Grant R01 CA073808 (NIH).

## 4.7 Contributions

Original idea for exploring dendrimers for potentiating ribonuclease cytotoxicity was from R.T. Raines. Concluding idea that dendrimers were affecting ribonuclease translocation was from G.A. Ellis. Protein production, modification, and purification; thermostability measurements; and activity measurements were done by G.A. Ellis. Flow cytometry analysis and cell culture workup was done by G.A. Ellis with helpful guidance by T.-Y. Chao. Cytotoxicity experiments were done by G.A. Ellis and M.L. Hornung.

## 4.8 Additions/Corrections

The thermostability of RNase A with dendrimers was reanalyzed with regards to error and number of digits. Specifically, the values changed for the  $T_m$  (°C) of RNase A with no dendrimer to  $62.73 \pm 0.03$  from  $62.7 \pm 0.1$  and for RNase A with 1  $\mu\text{M}$  dendrimer to  $62.8 \pm 0.2$  from  $62.8 \pm 0.1$ . The effect of  $T_m$  of 10  $\mu\text{M}$  dendrimer with RNase A compared to no dendrimer with RNase A rounded to a  $p$  value of 0.05 instead of  $> 0.05$  for one t-test in Excel (1 tail, 2 sample equal variance (homoscedastic)), though it should be noted that the  $T_m$  increased, not decreased, so the dendrimer still does not seem to be significantly destabilizing RNase A.

The activity assay data of RNase A with dendrimers was re-analyzed. For 10  $\mu\text{M}$  dendrimer, a slight activity was seen before addition of RNase A for 2 of the 3 replicates. If this activity was not accounted for, then the activity of RNase A in the presence of 10  $\mu\text{M}$  dendrimer was  $(2.8 \pm 0.3) \times 10^7 \text{ M}^{-1} \text{ s}^{-1}$  versus the  $(2.8 \pm 0.2) \times 10^7 \text{ M}^{-1} \text{ s}^{-1}$  value that was published (and is significant for only 1 tailed t-test, paired). If the activity was corrected for, the activity of RNase A in the presence of 10  $\mu\text{M}$  dendrimer was  $(2.6 \pm 0.4) \times 10^7 \text{ M}^{-1} \text{ s}^{-1}$  (and is significant for 1 tailed t-test, paired and equals 0.052 for 2 tailed t-test, paired).

Further, there was less substrate range for the dendrimer-treated samples than non-treated samples. This could be due to dendrimer keeping the extra RNase A from degrading all the substrate, the dendrimer affecting the assay conditions (e.g. light scattering, pH), or something else. If the substrate range for RNase A alone is used for calculating the activity of RNase A in the presence of dendrimer (and the activity is corrected for dendrimer activity for the 10  $\mu\text{M}$  sample), then the values become: in the presence of 1  $\mu\text{M}$  dendrimer,  $(3.0 \pm 0.4) \times 10^7 \text{ M}^{-1} \text{ s}^{-1}$  (significant for 1 tailed t-test, paired) and in the presence of 10  $\mu\text{M}$  dendrimer,  $(2.2 \pm 0.4) \times 10^7 \text{ M}^{-1} \text{ s}^{-1}$  (significant for both 1 and 2 tailed t-test, paired). This becomes somewhat significant inhibition of RNase A, especially in the presence of 10  $\mu\text{M}$  dendrimer: more than arginine-grafted RNase A (Fuchs, *et al.*, 2007), about the same or more than sulfated RNase A (Futami, *et al.*, 2001) or nonaarginine-tagged RNase A (Fuchs and Raines, 2005), and less than ethylenediamine- or PEI- cationized RNase A (Futami, *et al.*, 2001; Futami, *et al.*, 2002; Futami, *et al.*, 2005).

The internalization was analyzed using the geometrical mean in the publication; the values as analyzed by the mean are:  $145 \pm 9$ ,  $139 \pm 2$ , and  $125 \pm 8$ , for none, 1  $\mu\text{M}$ , and 10  $\mu\text{M}$  dendrimer, respectively. The  $p$  value is still  $> 0.05$ .

For cytotoxicity, the cytotoxicity was measured as all three replicates together in GraphPad, but the error was miscalculated. To calculate the correct error, the  $\text{IC}_{50}$  value for each replicate was independently determined, and then averaged and the standard error determined. The published  $\text{IC}_{50}$  values of G88R RNase A with no, 1  $\mu\text{M}$ , and 10  $\mu\text{M}$  dendrimer were  $(8 \pm 1) \mu\text{M}$ ,  $(1.7 \pm 0.1) \mu\text{M}$ , and  $(1.6 \pm 0.1) \mu\text{M}$ , respectively. The published  $\text{IC}_{50}$  values of DRNG RNase A with no, 1  $\mu\text{M}$ , and 10  $\mu\text{M}$  dendrimer were  $(0.14 \pm 0.01) \mu\text{M}$ ,  $(0.030 \pm 0.002) \mu\text{M}$ , and  $(0.025 \pm 0.001) \mu\text{M}$ , respectively. The new  $\text{IC}_{50}$  values of G88R RNase A with no, 1  $\mu\text{M}$ , and 10  $\mu\text{M}$  dendrimer were  $(9 \pm 2) \mu\text{M}$ ,  $(1.7 \pm 0.3) \mu\text{M}$ , and  $(1.7 \pm 0.3) \mu\text{M}$ , respectively. The new  $\text{IC}_{50}$  values of DRNG RNase A with no, 1  $\mu\text{M}$ , and 10  $\mu\text{M}$  dendrimer were  $(0.14 \pm 0.03) \mu\text{M}$ ,  $(0.028 \pm 0.005) \mu\text{M}$ , and  $(0.026 \pm 0.003) \mu\text{M}$ , respectively.

**Table 4.1** Effect of dendrimers on RNase A thermostability, catalytic activity, and cellular internalization.

Additive	$T_m^a$ (°C)	$k_{cat}/K_M^b$ ( $10^6 \text{ M}^{-1} \text{ s}^{-1}$ )	Internalization (counts) <sup>c</sup>
None	$62.73 \pm 0.03^d$	$33 \pm 5$	$129 \pm 9^g$
+ 1 $\mu\text{M}$ Dendrimer	$62.8 \pm 0.2^d$	$34 \pm 4^e$	$125 \pm 1^g$
+ 10 $\mu\text{M}$ Dendrimer	$63.2 \pm 0.2$	$26 \pm 4^{e,1}$	$113 \pm 7^g$

<sup>a</sup> Values of  $T_m$  ( $\pm$  SE) were determined in PBS by UV spectrometry.

<sup>b</sup> Values of  $k_{cat}/K_M$  ( $\pm$  SE) were determined for catalysis of 6-FAM-dArUdAdA-6-TAMRA cleavage.

<sup>c</sup> Values of internalization represent the mean ( $\pm$  SE) from three separate experiments performed in triplicate in which K-562 cells were incubated with an esterase-activatable fluorogenic label for 3 h, and internalization was assessed with flow cytometry.

<sup>d</sup> Published values were  $62.7 \pm 0.1$  for none and  $62.8 \pm 0.1$  for 1  $\mu\text{M}$  dendrimer

<sup>e</sup> See section 4.8 for additions/corrections to these values, to as low as  $(30 \pm 4)$  and  $(22 \pm 4) \times 10^6 \text{ M}^{-1} \text{ s}^{-1}$  for + 1 and + 10  $\mu\text{M}$  dendrimer, respectively.

<sup>f</sup> Published value was  $28 \pm 2$

<sup>g</sup> Values calculated using geometrical means. Values calculated using means are  $145 \pm 9$ ,  $139 \pm 2$ ,  $125 \pm 8$  for none, + 1  $\mu\text{M}$  dendrimer, and + 10  $\mu\text{M}$  dendrimer, respectively

The effect of dendrimers was published as not significant ( $p > 0.05$ ), but some of the additional/corrected values are significant.

**Figure 4.1** The toxicity of a cationic ribonuclease for cancer cells is increased by co-treatment with a cationic dendrimer.



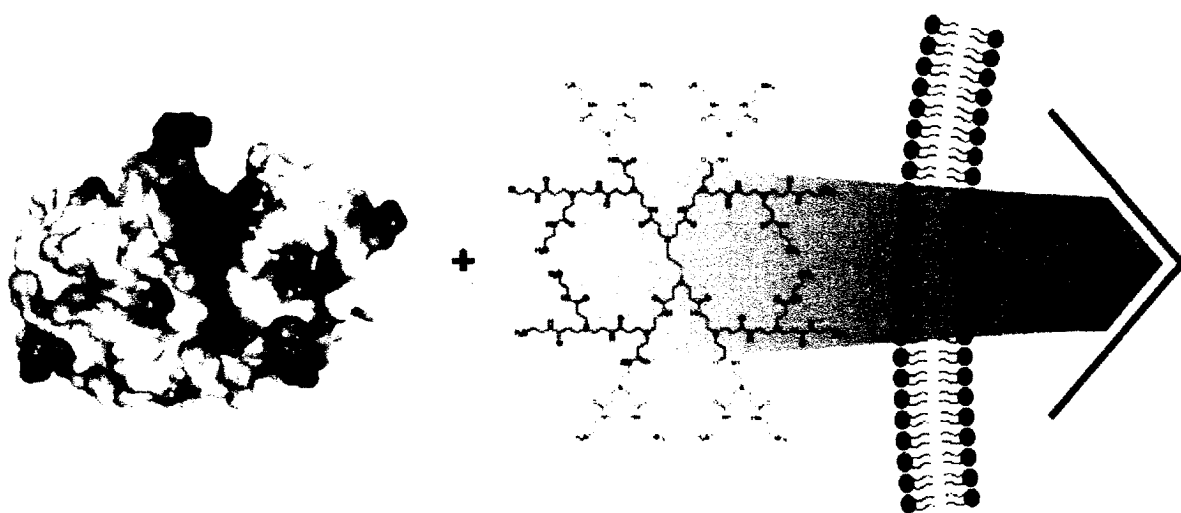


**Figure 4.2** Electrostatic potential map of the RNase A surface with positively charged surface in blue, negatively charged surface in red, and neutral surface in white. Images were created with PDB entry 7rsa (Wlodawer, *et al.*, 1988) and the program PYMOL (DeLano Scientific, San Francisco, CA, USA).

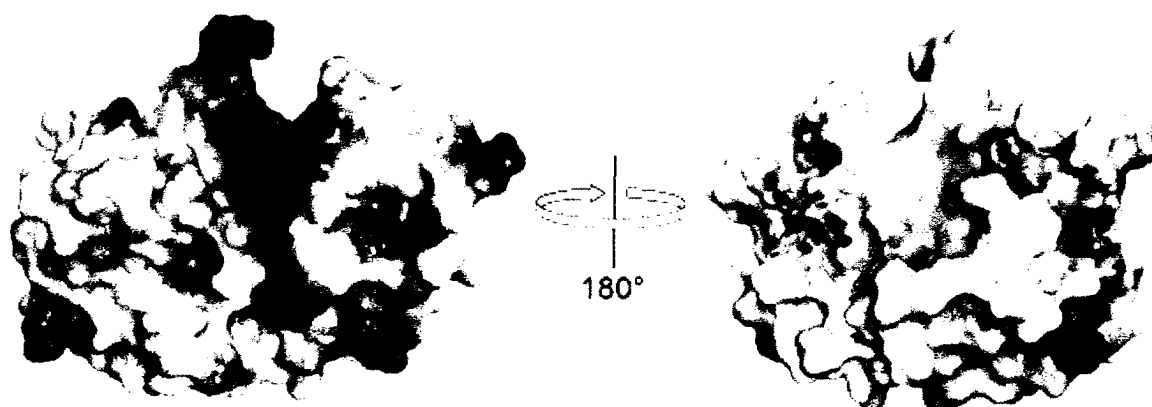


**Figure 4.3** Structure of the generation 2 poly(amidoamine) (PAMAM) dendrimer. The 30 amino nitrogens are in blue.

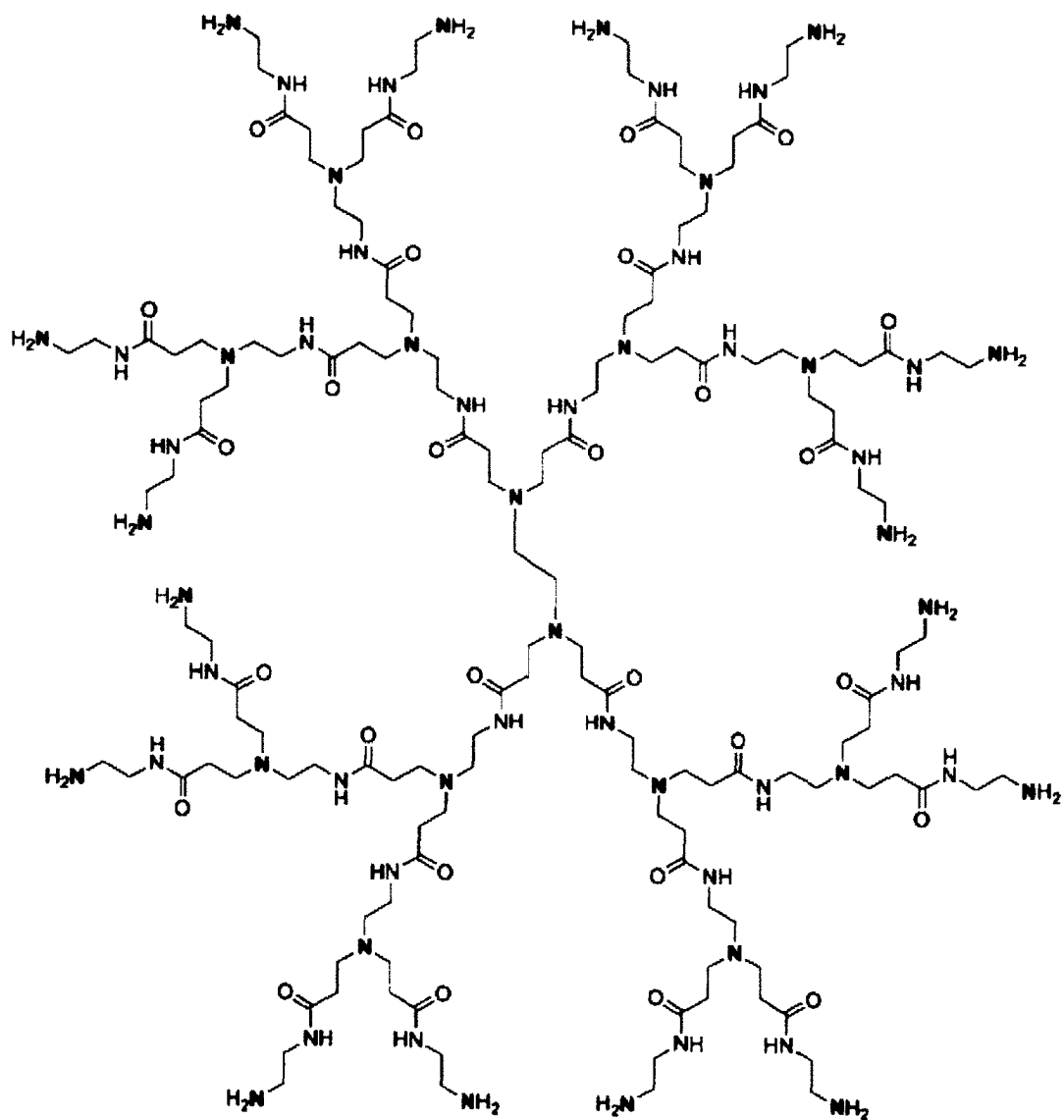


**Figure 4.4** Binding of the ribonuclease inhibitor protein to the generation 2 PAMAM dendrimer. The value of  $K_d = 3.1 \pm 0.5 \mu\text{M}$  for the RI-dendrimer complex (circles) was determined by disrupting the interaction of RI with DEF-labeled A19C G88R RNase A in PBS. The value of  $K_d = 0.79 \pm 0.06 \text{ nM}$  for the RI-G88R complex (squares) for control was analyzed the same way, though this value is less than that reported for the RI-G88R complex (1.2–1.3 nM) (Rutkoski, *et al.*, 2005; Lavis, *et al.*, 2007). Data are the mean ( $\pm$  SE) from three separate experiments.

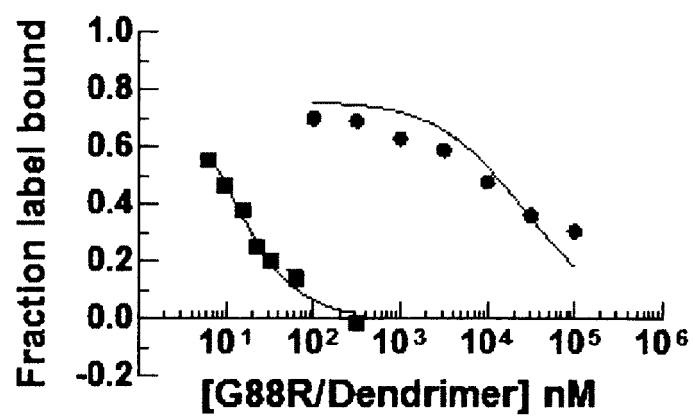
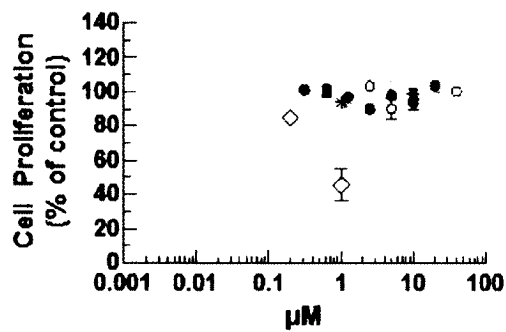


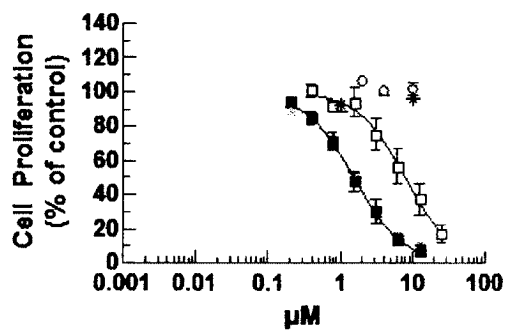
**Figure 4.5** Effect of generation 2 PAMAM dendrimer on the inhibition of cancer cell proliferation by ribonucleases. The proliferation of K-562 cells was measured by the incorporation of [*methyl*-<sup>3</sup>H]thymidine. Data points represent the mean ( $\pm$ SE) of three separate experiments performed in triplicate. The IC<sub>50</sub> values of G88R RNase A with no, 1  $\mu$ M, and 10  $\mu$ M dendrimer were  $(9 \pm 2) \mu$ M,  $(1.7 \pm 0.3) \mu$ M, and  $(1.7 \pm 0.3) \mu$ M, respectively. The IC<sub>50</sub> values of DRNG RNase A with no, 1  $\mu$ M, and 10  $\mu$ M dendrimer were  $(0.14 \pm 0.03) \mu$ M,  $(0.028 \pm 0.005) \mu$ M, and  $(0.026 \pm 0.003) \mu$ M, respectively.



Wild-type RNase A



G88R RNase A

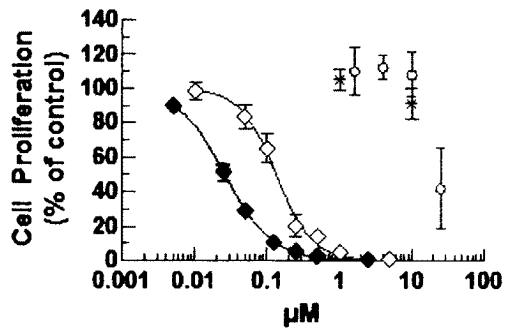


RNase A		[dendrimer] (μM)
○	Wild-type	0
◐	Wild-type	1
●	Wild-type	10
◻	G88R	0
◑	G88R	1
■	G88R	10
◊	DRNG	0
◒	DRNG	1
◆	DRNG	10

---

* *	Dendrimer control alone	
-----	-------------------------	--

DRNG RNase A



## **CHAPTER 5**

### **Future Directions**

## 5.1 Expanding the Repertoire and Use of Ribonucleotide Pro-moiety Timed-released Prodrugs

In CHAPTER 2, we demonstrated the attachment of the ribonucleoside uridine 3'-phosphate as a timed-release pro-moiety onto 4-hydroxytamoxifen and this prodrug's activation both *in vitro* and *in vivo* by human pancreatic ribonuclease (RNase 1).

This proof-of-concept research was crucial to lay the foundation for future research projects exploring the expanded use of this technology. First, the synthesis and characterization of timed-release prodrugs using all of the natural ribonucleoside 3'-phosphates as pro-moieties would define the ability to tune release kinetics. Second, the use of other drugs attached to these pro-moieties would demonstrate the breadth of this technology. Third, modifying the 5'-end of the pro-moiety by alkylation or PEGylation would demonstrate the ability to adjust the pharmacokinetics of the prodrug. Fourth, investigating these prodrugs in serum or *in vivo*, while technically challenging, would add further characterization to this technology, especially after the synthesis of a library of timed-release prodrugs. Finally, eosinophils are known to accumulate near tumor cells, indicating that the ribonucleases eosinophil-derived neurotoxin (RNase 2; EDN) and eosinophil cationic protein (RNase 3; ECP) may be at alleviated levels near tumors (Munitz and Levi-Schaffer, 2004; Cormier, *et al.*, 2006; Lotfi, *et al.*, 2007; Sorrentino, 2010). While ECP did not show any cleavage of the uridine 3'-(4-hydroxytamoxifen phosphate) prodrug, EDN was not tested. Testing whether these prodrugs were activated by EDN (assuming EDN is at a high enough level in tumors to significantly activate the prodrug compared to RNase 1 in serum) would indicate if this prodrug technology also imparts improved cancer specificity for modified chemotherapeutics.

## 5.2 Further Investigations of Boronate-mediated Drug Delivery

In CHAPTER 3, we demonstrated the use of pendant boronic acids to mediate the delivery of bovine pancreatic ribonuclease (RNase A) into mammalian cells. This research was the first demonstration of using boronic acids as an alternative to increased cationicity or attachment of ligands of cell-surface receptors to proteins as a means to deliver proteins into cells.

Investigating other means of conjugating boronic acids onto proteins is a next crucial step for using this technology on a broad range of proteins. Not all proteins will be amenable to attachment of pendant boronic acids by condensation onto multiple carboxyl groups using carbodiimide chemistry. Therefore, akin to nonaarginine and HIV-TAT tags, a peptidic tag of boronic acids attached site-specifically to a protein could facilitate internalization with only one point of modification to the protein. This would also lead to a more homogenous protein population, in comparison to random coupling to carboxyl groups. Further, the use of an esterase- or acid-cleavable linker attaching the boronic acid tag to the protein could release the native protein after endocytosis. This may be beneficial for the therapeutic activity of some proteins and may be a cleaner system for studying the cytosolic effects of native proteins. Other experiments on this system that warrant future investigation include studying the pharmacokinetic properties of a boronated protein *in vivo*.

## 5.3 Further Investigations of Poly(amidoamine) (PAMAM) Dendrimers

In CHAPTER 4, we demonstrated the use of PAMAM dendrimers *in trans* to potentiate the cytotoxicity of RNase A variants, possibly by increasing their translocation into the cytosol following endocytosis.

This research emphasized a major bottleneck in ribonuclease cytotoxicity: the inefficient translocation from endosomes into the cytosol. Currently, this translocation stage is difficult to measure. Some research in the Raines lab is dedicated to developing probes that are specifically activated in the cytosol but not in endosomes. When these probes are developed, future studies will investigate the mechanism of this fairly undefined stage. At that point, future studies can more clearly define the role that dendrimers play in potentiating ribonuclease cytotoxicity.

#### **5.4 Future Ribonuclease-specific Investigations**

In APPENDIX 1, we demonstrate the identification of a small molecule antagonist, triprolidine, of the interaction between a RNase A variant and the ribonuclease inhibitor protein (RI); in APPENDIX 2, we demonstrate the creation of a ribonuclease zymogen activated by urokinase. Both of these projects necessitate further engineering before realizing the full results of the research. Further characterization of triprolidine as an antagonist to the RNase A–RI interaction, including studies of the structure-activity relationships of triprolidine in this system, may lead to a more potent antagonist. However, the relative initial weakness of this antagonist will make these studies technically challenging. Alternate methods for producing a ribonuclease zymogen activated by urokinase (such as the small molecule approach discussed in APPENDIX 2), or the use of synergistic drugs, may result in a system which shows toxicity to cancer cells. Further, if a ribonuclease zymogen activated by urokinase that is toxic and selectively activated near cancer cells is developed, it may be used in synergy with ribonucleoside 3'-phosphate pro-moiety prodrugs (see above and CHAPTER 2). The ribonuclease zymogen would be activated

near cancer cells, and could then activate the prodrug near these cancer cells, leading to selective toxicity for the prodrug.

Further investigations of ribonucleases as biologic chemotherapeutics can extend in multiple directions. The investigation of the pharmacokinetics and pharmacodynamics of mammalian ribonucleases *in vivo*, such as through PET imaging or radioactive tracers, could answer several questions regarding how to improve the therapeutic index of these biologic chemotherapeutics. Specifically, is the efficacy of ribonucleases limited by retention time, as was suggested with the use of PEGylated ribonucleases (Rutkoski, *et al.*, 2011)? Are side effects (such as renal toxicity by Onconase (Costanzi, *et al.*, 2005; Pavlakis and Vogelzang, 2006; Rutkoski and Raines, 2008; Ardelt, *et al.*, 2008; Beck, *et al.*, 2008)) dependant on ribonucleolytic activity or just the accumulation of large amounts of protein in the kidneys? These future studies, among others, may lead to better understanding and improvements to the ribonuclease chemotherapeutic system.

## **APPENDIX 1**

### **Efforts Towards a Small Molecule Antagonist of the RI–Ribonuclease Interaction**

### A1.1 Abstract

Protein–protein interactions (PPIs) regulate many cellular processes, from signal transduction to cell growth. Among the tightest of all known PPIs are the interactions between human ribonuclease inhibitor (RI) and its ribonuclease ligands, which bind with femtomolar affinity even though these ribonucleases share only 20–68% protein sequence identity. Due to this high affinity, identifying antagonists of this interaction would be a novel advancement in the area of PPI inhibition.

The high affinity of RI for ribonucleases is thought to protect the cell from RNA degradation by invading ribonucleases. Ribonucleases that evade RI are selectively toxic to cancer cells, and the lack of affinity for RI is considered a primary determinant of ribonuclease toxicity. Therefore, it was hypothesized that inhibiting the RI–ribonuclease interaction with antagonists would potentiate the cytotoxic activity of modestly RI-evasive ribonucleases, possibly leading to extremely potent chemotherapeutics. Towards this goal, we optimized a high-throughput screening assay for identifying inhibitors of the RI–ribonuclease interaction and screened two compound libraries (4,160 compound Known Bioactives Library; 16,000 compound Chembridge Library). Initial hits were analyzed and screened in a secondary assay. While these compounds did not show utility *in cellulo*, future development of these hits could lead to more potent antagonists.

### A1.2 Introduction

Signal transduction, immune response, cell–cell recognition, cell division, and many other cellular processes depend upon protein–protein interactions (PPIs) (Toogood, 2002; Sidhu, *et al.*,



2003). Antagonists of these interactions can aid in the elucidation of their biological significance and lead to human therapeutics (Sidhu, *et al.*, 2003; Arkin and Wells, 2004). In contrast to enzyme inhibitors, PPI antagonists must overcome large buried surface areas (750–1,500 Å<sup>2</sup>/side), high affinities between protein partners, and the typically flat interfaces involved (Arkin and Wells, 2004). Despite these challenges, antagonists have been successfully developed against PPIs, partly due to the existence of small patches of residues, or “hot spots”, vital to the binding affinity of the interaction that provide smaller targets for antagonists to bind (Clackson and Wells, 1995; Arkin and Wells, 2004). Further, antagonists often do not need to completely inhibit PPIs to have significant biological effects (Toogood, 2002).

In addition to the use of PPI antagonists as biological tools, the inhibition of PPIs is also of therapeutic value. While vinca alkaloids were not known to inhibit tubulin polymerization until 1996, they have been effective anticancer treatments for nearly half a century (Gadek and Nicholas, 2003). In addition, the anticoagulant small-molecule tirofiban (Aggrastat) and peptide eptifibatide (Integrilin), which inhibit fibrinogen binding to its receptor on platelets, have been approved for patients undergoing angioplasty (Gadek and Nicholas, 2003). These prior successes portend the identification of additional antagonists of PPIs, demonstrate their usefulness to further understand PPIs, and make accessible a myriad of novel druggable targets.

We chose to investigate the PPI of bovine pancreatic ribonuclease (RNase A) with human ribonuclease inhibitor (RI). RNase A is a 13.7-kDa protein that catalyzes the degradation of RNA (Raines, 1998). RNase A is internalized by human cells but then is bound tightly and inhibited by RI. RI is found at a concentration of 4 μM in the cytosol of all mammalian cells studied, and binds to and inhibits both RNase A and human pancreatic ribonuclease (RNase 1) in

1:1 stoichiometric interactions (Dickson, *et al.*, 2005; Johnson, *et al.*, 2007b; Rutkoski and Raines, 2008). These interactions are among the tightest natural PPIs known, with femtomolar equilibrium dissociation constants ( $K_d$ ) (Kobe and Deisenhofer, 1995; Haigis, *et al.*, 2003; Dickson, *et al.*, 2005; Johnson, *et al.*, 2007b). A homologue of RNase A from *Rana pipiens*, Onconase® (ONC), is not highly inhibited by RI, allowing it to degrade cellular RNA which results in cytostatic and cytotoxic effects (Boix, *et al.*, 1996; D'Alessio and Riordan, 1997; Costanzi, *et al.*, 2005; Ardelt, *et al.*, 2008; Beck, *et al.*, 2008; Turcotte and Raines, 2008b; Ardelt, *et al.*, 2009). This toxicity led to the investigation of ONC in clinical trials, progressing to a Phase IIIb trial for unresectable malignant mesothelioma. Unfortunately, this trial resulted in mixed results (no improvement in the primary endpoint of survival), though ONC continues to be investigated for other indications (Alfacell, 2009). This limited clinical success was due in part to dose-limiting renal toxicity and a low catalytic activity that hinders its effectiveness (Costanzi, *et al.*, 2005; Pavlakis and Vogelzang, 2006; Rutkoski and Raines, 2008; Ardelt, *et al.*, 2008; Beck, *et al.*, 2008). RI-evasive variants of RNase A have been developed to overcome these disadvantages, since the renal retention of RNase A is 50–100 fold less than ONC and RNase A variants are considerably more active ( $10^2$ – $10^5$  fold) (Vasandani, *et al.*, 1996; Rutkoski and Raines, 2008; Ardelt, *et al.*, 2008). RI-evasive variants of RNase 1 have also been constructed (Leland, *et al.*, 2001; Johnson, *et al.*, 2007b; Johnson, *et al.*, 2007a), and one RNase 1 variant, QBI-139, is currently in a Phase I clinical trial for patients having advanced, refractory, solid tumors.

We hypothesized that small molecule antagonists of the RI–ribonuclease interaction, identified through a high-throughput screen (HTS), would potentiate the cytotoxicity of modestly

RI-evasive ribonucleases. These small molecule RI antagonists could augment the cytotoxicity of moderately RI-evasive RNase A or RNase 1 variants possessing desirable attributes for ribonuclease cytotoxicity, such as high stability (Klink and Raines, 2000) or enhanced ability to internalize into cells (Johnson, *et al.*, 2007a) (Figure A1.1). In addition to cytotoxicity, RNase A homologues have been implicated in other important biological processes, including neovascularization (ANG) and host defense (EDN) (D'Alessio and Riordan, 1997; Rosenberg, 1998; Dickson, *et al.*, 2005). Inhibitors of the RI–ribonuclease interaction could be used to probe the biological activities of these ribonucleases, and the role that RI plays in these processes. The identification of molecules that bind or inhibit RI is predicated by work demonstrating the affinity of immobilized kanamycin for RI (Wang, *et al.*, 2005b) and the inhibition of the angiogenin–RI interaction by basic proteins and protamines (Moenner, *et al.*, 1999). Herein, we optimized and performed a primary HTS assay for identifying inhibitors of the RI–ribonuclease interaction with two compound libraries totaling > 20,000 compounds. Secondary assays were performed that eliminated false hits. While the lead compound identified from these screens, triprolidine, did not show utility *in cellulo*, future development of this compound could lead to more potent antagonists.

### **A1.3 Results and Discussion**

A fluorescence intensity-based assay was previously developed in the Raines lab that can accurately and rapidly measure RI–RNase A binding (Abel, *et al.*, 2002). This assay measures the fluorescence decrease that occurs when fluorescein-labeled RNase A binds RI (~15%). Although this first generation assay could not be used to screen large libraries of compounds, as

its dynamic range was relatively small and the assay requires large volumes (2 mL/cuvette), it was chosen as the starting point for development of an assay format amenable to high-throughput screening (Abel, *et al.*, 2002).

The second generation of this assay utilizes 2',7'-diethylfluorescein-5-iodoacetamide (DEFIA; DEF post-conjugation) as a label for A19C/G88R RNase A (Lavis, *et al.*, 2007). The phenolic  $pK_a$  of DEFIA was tuned so that when labeled, cationic RNase A is bound by anionic RI, the  $pK_a$  of DEFIA increases, favoring protonation and lowering the brightness of the dye by 38%, approximately twice as much as in the previous assay (Lavis, *et al.*, 2007). When unlabeled ribonuclease competitively displaces the labeled RNase A, fluorescence is restored (Lavis, *et al.*, 2007). Due to this greater dynamic range, this second generation assay was successfully converted to a 96-well format. Addition of excess wild-type RNase A resulted in complete displacement of labeled RNase A and served as the positive control, and the negative control was addition of phosphate-buffered saline (PBS) (Lavis, *et al.*, 2007). To validate this assay the  $Z'$ -factor was determined, which takes into account both the dynamic range between positive and negative controls and the data variation of both controls of the assay (Zhang, *et al.*, 1999). A negative  $Z'$ -factor indicates no significant separation between controls, a positive  $Z'$ -factor of 0–0.5 indicates a feasible, small separation, and a  $Z'$ -factor of 0.5–1 indicates a large separation with low data variation of the controls (with 1 being ideal) (Zhang, *et al.*, 1999). The  $Z'$ -factor of this assay was determined to be 0.69, designating the assay as excellent to measure RNase A binding to RI (Lavis, *et al.*, 2007).

This assay was further optimized for high-throughput screening of small molecules by labeling the RNase A variant with one of the lowest affinities for RI, minimizing the assay to a

384-well microplate, and increasing its dynamic range. Due to the high affinity of RI for binding its ribonuclease ligands, identifying initial antagonists potent enough to disrupt a femtomolar affinity (wild-type RNase A) or even low nanomolar affinity (G88R RNase A, a RI-evasive RNase A variant with  $K_d = 1.2$  nM) (Rutkoski, *et al.*, 2005) interaction would be extremely unlikely. Therefore, to start with a more feasible target, K31A/D38R/R39D/N67R/G88R RNase A (KDRNG RNase A) was chosen because it has one of the lowest known affinities of a RNase A variant for RI ( $K_d = 2.5$   $\mu$ M; >2000-fold lower affinity than G88R RNase A) (Rutkoski, *et al.*, 2005). Also, the location of DEFIA attachment was shifted from Ala19, outside the RI–RNase A interface, to Gly88. Dye attachment to a cysteine substitution at position Gly88 places the dye directly at the RI–RNase A interface. By placing the DEFIA label closer to the anionic surface of RI, the DEFIA phenolic  $pK_a$  would shift, substantially increasing the dynamic range. However, it was not known if replacing the G88R substitution, which is important for the RI-evasion of KDRNG RNase A, with G88C-DEF would hinder RI-evasion.

A competition binding assay was performed to verify that the affinity of DEFIA-labeled KDRNG88C RNase A (herein KDRNG88C-DEF RNase A) for RI was still relatively low ( $K_d = 320 \pm 30$  nM, Figure A1.2), indicating that this assay was suitable for screening. Importantly, by moving the label the dynamic range of the assay in a microplate increased to 45%, which increased the accuracy of the assay and facilitated its miniaturization to a 384-well format. Further optimizations were required for high-throughput screening, including using a higher concentration of RI in the assay so that 80-90% of the labeled RNase A was bound. This concentration of RI was required to dramatically decrease the signal at the steepest region of the binding curve for compounds with weak inhibition. Also, a high concentration of DTT (10–15

mM) was necessary to combat the oxidative activity of DMSO, which is used as the vehicle for library compounds, to keep RI reduced and active (Figure A1.3).

The Small Molecule Screening Facility (SMSF) at the Keck-University of Wisconsin Comprehensive Cancer Center (UWCCC) enables high-throughput screening (HTS) of multiple chemical libraries with sophisticated robotics (Keck-UWCCC, 2011). Using the optimized assay we first screened a library of 4,160 molecules which included FDA approved drugs and other compounds with known biological activity (Keck-UWCCC, 2011). Each compound was screened at a concentration of 83  $\mu$ M and positive (RNase A) and negative (no addition) controls were included on each microplate. The best 24 compounds from each library microplate (7.5% of the library) were re-screened with controls. This re-screen resulted in a  $Z'$ -factor of 0.72, indicating that the assay was accurate. Data were analyzed as the percent of regained fluorescence, which reflects the ability of compounds to displace KDRNG88C-DEF RNase A from RI as compared to excess wild-type RNase A. There were two compounds identified with  $\geq 50\%$  of regained fluorescence, eight compounds with  $\geq 25\%$  regained fluorescence, and twenty-five compounds with  $\geq 12.5\%$  of regained fluorescence. The results of the assay and compounds with  $\geq 25\%$  of regained fluorescence, or “hits”, are identified in Figure A1.4.

One limitation of the primary screening assay is that small molecules with inherent fluorescence similar to that of diethylfluorescein ( $\lambda_{ex/em} = 501\text{ nm}/520\text{ nm}$ ) will increase the fluorescence signal. These potential false positives could even be of relatively low fluorescence intensity, since compounds are added in large excess over labeled RNase A. To identify these false positives, we developed secondary assays similar to the primary assay but instead using different fluorophores. The first secondary assay developed used the pH-sensitive label 4-

carboxyresorufin-C<sub>2</sub>-maleimide (CRCM; synthesized by L.D. Lavis). The excitation (570 nm) and emission (585 nm) maxima of CRCM are red-shifted to reduce fluorescence overlap of the false positives from the primary assay. KDRNG88C RNase A was labeled with CRCM (herein KDRNG88C-CR RNase A). The second secondary assay developed combined the idea of using a resorufin dye with the known benefits of modulating the  $pK_a$  of fluorescein through alkylation as seen for DEFIA (Lavis, *et al.*, 2007). Therefore, an alkylated derivative of carboxyresorufin, carboxyethylresorufin maleimide (CERM), was synthesized (under the guidance and collaboration of L.D. Lavis) in an effort to increase the  $pK_a$  of carboxyresorufin (resorufin  $pK_a \approx 6.5$ ) (Towne, *et al.*, 2004) and attached to KDRNG88C (herein KDRNG88C-CER). Finally, another secondary assay that was developed for some hits used dansyl attached to D38R/R39D/N67R/G88C RNase A (DRNG88C RNase A; labeled herein DRNG88C-dansyl RNase A) instead. This assay relied on Förster resonance energy transfer (FRET) between the tryptophans of RI and the dansyl dye.

Hits with  $\geq 25\%$  regained fluorescence from the primary screen were assessed in the CR-RNase A secondary assay and the  $Z'$ -factor for this assay was determined to be 0.30. Importantly, after reading the microplate at carboxyresorufin maxima ( $\lambda_{ex/em} = 570 \text{ nm}/585 \text{ nm}$ ) and verifying positive hits, the microplate was read again at diethylfluorescein maxima ( $\lambda_{ex/em} = 501 \text{ nm}/520 \text{ nm}$ ), which allowed for identification of compounds intrinsically fluorescent at this wavelength. The best compounds were defined as those resulting in a  $\geq 25\%$  of regained fluorescence for both the primary (KDRNG88C-DEF RNase A) and secondary (KDRNG88C-CR RNase A) assays, and those that were not fluorescent at the diethylfluorescein maxima.

Triprolidine·HCl was selected for further investigation as it was a hit in both assays, inexpensive, and commercially available in large quantities. To quantify the affinity of this antagonist, the second generation 96-well competitive binding assay described previously (Lavis, *et al.*, 2007) was performed; however, KDRNG88C-DEF RNase A was used to enhance the detection of low affinity antagonists as previously discussed. Using this assay, the estimated  $K_d$  value of triprolidine·HCl bound to RI was determined to be 210  $\mu$ M (Figure A1.5, single replicate). Note that preliminary experiments with A19C-DEF G88R RNase A were unable to confirm this, either due to the increased affinity of this variant for RI or perhaps ribonuclease variant specificity of the ability of triprolidine to inhibit the RI–ribonuclease interaction.

After identifying triprolidine as a initial hit, we applied for and received funding for primary and secondary screening of the ChemBridge Library (16,000 compounds) through the Lead Discovery Initiative (LDI) sponsored by the Wisconsin Alumni Research Foundation (WARF). The primary assay resulted in a  $Z'$ -factor of 0.38. It is unclear why this  $Z'$ -factor was lower than before. Two 384-well plates of the best hits were rescreened 3 times using the primary assay, the secondary assay with KDRNG88C-CER RNase A, and the secondary assay with DRNG88C-dansyl RNase A. A synergy cytotoxicity assay was performed by the SMSF, in which moderately RI-evasive G88R RNase A was added with co-treatment of 19 separate hits to test whether these hits inhibited cellular RI and potentiated the toxicity of the ribonuclease. Determination of the  $K_d$  values for the best compounds was also attempted. Unfortunately, no hits were verified from this library. Problems with the library compounds included that some were naturally highly fluorescent, some were non-polar and therefore had poor solubility, and



some had a charge that modified the pH of the assay solution, thereby affecting this assay which is highly dependent on pH.

Therefore, triprolidine was chosen as the lead compound. Synergy cytotoxicity experiments were performed with triprolidine, even though it is a relatively weak inhibitor ( $K_d$  value of 210  $\mu\text{M}$ ). Since DRNG RNase A and KDRNG RNase A are highly RI-evasive, they are thought to be at the upper limit of effective RI-evasiveness; in other words, inhibition of RI is not expected to increase their cytotoxicity (Rutkoski, *et al.*, 2005). Therefore, G88R RNase A, which is more moderately RI evasive, was used for synergy cytotoxicity assays, as was done with the ChemBridge library synergy cytotoxicity assay. Previously, RNAi-mediated of RI by ~ 55% was shown to increase the sensitivity of several cancer cell lines to G88R RNase A toxicity by more than 75% (Dickson and Raines, 2009); therefore, if triprolidine is as effective at knocking down RI activity, a similar increase in G88R RNase A toxicity could be expected. Cell proliferation effects were measured against K-562 cells. Triprolidine alone had an approximate  $\text{IC}_{50}$  value of 126  $\mu\text{M}$  (singlet), and G88R RNase A alone had an approximate  $\text{IC}_{50}$  value of  $4.4 \pm 0.4 \mu\text{M}$  (duplicate).

The toxicity curves of G88R RNase A with and without triprolidine overlap, making interpretation of any synergistic effect difficult; however, it appears that any synergy of triprolidine for G88R RNase A cytotoxicity is weak (Figure A1.6). At most, it appears that the addition of 75  $\mu\text{M}$  triprolidine, which causes significant toxicity alone (70% cell proliferation), only increases the  $\text{IC}_{50}$  value of G88R RNase A approximately 2.5-fold (to  $1.6 \pm 0.3 \mu\text{M}$ ). A similar effect is seen with DRNG RNase A, which would be unexpected if triprolidine was

working through a mechanism of inhibiting RI. Given the toxicity of triprolidine alone ( $IC_{50} < K_d$ ), the ability of triprolidine to inhibit RI *in cellulo* is inconclusive.

#### A1.4 Conclusions

Over 20,000 compounds were screened in an attempt to find inhibitors of the RI–RNase A interaction. The best inhibitor, triprolidine, had a fairly high  $K_d$  value with RI of approximately 210  $\mu$ M. Therefore, while triprolidine can inhibit the interaction of RI with modest to high RI-evasive RNase A variants, it is unlikely to do so with non to low RI-evasive variants (or wild-type RNase A) except at very high concentrations, possibly above its solubility limits. Synergy cytotoxicity experiments with G88R RNase A were inconclusive.

While the effectiveness of triprolidine for inhibiting the RI–RNase A interaction was disappointing, it is notable that an inhibitor was identified in this screen. PPI antagonists are notoriously difficult to identify, and the RI–RNase A interaction, with its large buried surface area, could be considered a very difficult target. Future modifications to triprolidine may increase its potency of inhibition. If so, then this compound may show future benefit for investigating the cellular interaction of ribonucleases with RI.

#### A1.5 Experimental Procedures

##### A1.5.1 Materials

*Escherichia coli* strain BL21(DE3) cells were from Novagen (Madison, WI). K-562 cells, which were derived from a continuous human chronic myelogenous leukemia line, were from the

American Type Culture Collection (Manassas, VA). Cell culture medium and supplements, as well as Dulbecco's phosphate-buffered saline (DPBS) were from Invitrogen (Carlsbad, CA). [methyl-<sup>3</sup>H]Thymidine (6.7 Ci/mmol) was from Perkin–Elmer (Boston, MA). Protein purification columns were from GE Biosciences (Piscataway, NJ). Wild-type RNase A, triprolidine, and 2-(N-morpholino)ethanesulfonic acid (MES) were from Sigma–Aldrich (St. Louis, MO). MES buffer was purified by anion-exchange chromatography to remove trace amounts of oligomeric vinylsulfonic acid (Smith, *et al.*, 2003). Ribonuclease substrate 6-FAM–dArUdAdA–6-TAMRA was from Integrated DNA Technologies (Coralville, IA). Non-binding surface (NBS) 96- and 384- well plates were from Corning (Corning, NY). All other chemicals used were of commercial reagent grade or better, and were used without further purification. Terrific Broth (TB) was from Research Products International (Mt. Prospect, IL), or was made by dissolving tryptone (12 g), yeast extract (24 g), glycerol (4 mL), KH<sub>2</sub>PO<sub>4</sub> (2.31 g), and K<sub>2</sub>HPO<sub>4</sub> (12.54 g) in H<sub>2</sub>O (1.00 L).

#### A1.5.2 Analytical instruments and statistical calculations

The incorporation of [methyl-<sup>3</sup>H]thymidine into the genomic DNA of K-562 cells was quantified by scintillation counting using a Microbeta TriLux liquid scintillation and luminescence counter (Perkin–Elmer, Wellesley, MA). Molecular mass was determined by matrix-assisted laser desorption/ionization time-of-flight (MALDI–TOF) mass spectrometry using a Voyager-DE-PRO Biospectrometry Workstation (Applied Biosystems, Foster City, CA) at the campus Biophysics Instrumentation Facility. Fluorescent measurements for  $K_d$  determination were made on an Envision plate reader (PerkinElmer, Waltham, MA). All

equipment for high-throughput screening, including robotics and plate readers, was from the Small Molecule Screening Facility (SMSF) at the Keck-University of Wisconsin Comprehensive Cancer Center (UWCCC).

#### *A1.5.3 High-throughput screening libraries*

The Known Bioactives Library consisted of 880 compounds from Prestwick Chemical, 2000 compounds from the Spectrum Chemical Collection, and 1280 compounds from Sigma, LOPAC (for 4,160 compounds total). The ChemBridge library compounds totaled 16,000 compounds. All compound libraries were from and maintained by the SMSF.

#### *A1.5.4 Protein production*

RNase A variants were produced as described previously (Rutkoski, *et al.*, 2005; Lavis, *et al.*, 2007; Ellis, *et al.*, 2011). Protein concentration was determined by UV spectroscopy using an extinction coefficient at 278 nm of  $0.72 \text{ (mg/ml)}^{-1} \cdot \text{cm}^{-1}$  for RNase A and its variants or typically with a bicinchoninic acid assay kit from Pierce (Rockford, IL) for fluorescently-labeled proteins. Variants with a cysteine residue at position 19 were protected by reaction with 5,5'-dithio-bis(2-nitrobenzoic acid) (DTNB) to form a mixed disulfide. Labeling of proteins was done similarly as described previously (Rutkoski, *et al.*, 2005; Lavis, *et al.*, 2007). Human ribonuclease inhibitor (RI) was prepared in *E. coli* as described previously (Rutkoski, *et al.*, 2005; Lavis, *et al.*, 2007).

#### A1.5.5 High-throughput screening assay

The high-throughput screening assay was based on previous assays (Abel, *et al.*, 2002; Lavis, *et al.*, 2007). All high-throughput screening was done at the SMSF. A master mix was made by first adding 10 mM DTT and 20  $\mu$ g/mL BSA (final concentrations) to DPBS. Then, to this was added 50 nM KDRNG88C-DEF RNase A and 1.5  $\mu$ M RI final. For screening the Known Bioactives Library, the robot dispensed 15.5  $\mu$ L then 14  $\mu$ L (29.5  $\mu$ L total), then paused for manual addition of the positive control to positive control wells (5  $\mu$ M wild-type RNase A final), and then the robot dispensed 0.5  $\mu$ L of 5 mM compound (83  $\mu$ M final) in DMSO over time. The plate was quickly read at 501/520 nm, to minimize oxidation of RI by DMSO. For the ChemBridge library screen, only 28.5  $\mu$ L of master mix was used, and the concentration of DTT was increased to 15 mM. Secondary assays were performed similarly. To quantify hits, the percent regained fluorescence was quantitated. This was determined from the fluorescence of compound wells compared to the range between negative and positive controls.

#### A1.5.6 $K_d$ value determination

The determinations for  $K_d$  values were done similar to those described previously (Lavis, *et al.*, 2007). A serial dilution (2 $\times$ ) of triprolidine or DRNG RNase A in DPBS was prepared. Importantly, the stock of triprolidine for serial dilutions was pH adjusted very close to the pH of the DPBS to minimize pH effects on the assay. A stock solution of KDRNG88C-DEF RNase A (100 nM; 2 $\times$ ), RI (3  $\mu$ M; 2 $\times$ ), DTT (10 mM; 2 $\times$ ), and BSA (0.1 mg/mL; 2 $\times$ ) was made, and 50- $\mu$ L aliquots of this stock solution were added to the wells of a 96-well NBS plate. Aliquots of the serially-diluted solution of triprolidine or DRNG RNase A were then added to the wells. One negative control contained no ribonuclease (PBS), another negative control contained extra RI

(5–6.5  $\mu\text{M}$  final including RI from master mix, to bind  $\sim 100\%$  of KDRNG88C-DEF RNase A) and the positive control contained excess RNase A (10  $\mu\text{M}$ ; 2 $\times$ ). The fluorescence intensity was then measured. The fraction bound at each concentration of competitor was determined by (the fluorescence of the competitor well minus the fluorescence of the RNase A positive control) divided by (the fluorescence of the extra RI negative control minus the fluorescence of the RNase A positive control). This is different from the linear regression approach used previously (Lavis, *et al.*, 2007). The data was then fit to an equation for competitive binding (Roehrl, *et al.*, 2004). For triprolidine  $K_d$  determination, the assay was duplicated in the same plate with master mix not containing RI to identify any trends in changes in fluorescence with triprolidine concentration (there should be none). This was done to certify that the pH of the solution was not changing upon addition of increasing amounts of triprolidine, thereby biasing the assay. The triprolidine  $K_d$  determination data were the average of three measurements but only one experiment. The KDRNG88C-DEF RNase A  $K_d$  determination data (using DRNG RNase A as a competitor) were the average of three measurements, and the entire experiment was repeated in triplicate.

#### A1.5.7 Cell-proliferation assay

The effect of RNase A, its variants, triprolidine, and co-treatment of triprolidine with G88R RNase A on the proliferation of K-562 cells was assayed as described previously (Leland, *et al.*, 1998; Rutkoski, *et al.*, 2005). Briefly, for assays with a single sample, 5  $\mu\text{L}$  of a serially diluted solution of ribonuclease, triprolidine, or PBS was added to 95  $\mu\text{L}$  of media containing K-562 cells ( $5.0 \times 10^4$  cells/mL). For co-treatments, 10  $\mu\text{L}$  of a serially-diluted solution of G88R RNase

A (2×) was premixed with 10 µL of a solution of triprolidine (2×, 75 µM final in wells). Then, 5 µL of this solution was added to 95 µL of media containing K-562 cells ( $5.0 \times 10^4$  cells/mL). After 44 h, the cells were treated with [*methyl*- $^3\text{H}$ ]thymidine for 4 h, and the incorporation of radioactive thymidine into cellular DNA was quantified by liquid scintillation counting. Results were reported as the percentage of [*methyl*- $^3\text{H}$ ]thymidine incorporated relative to control cells that had been treated with PBS. Each experiment consisted of three wells (measurements) for each condition which were averaged, and this mean was used as one replicate when calculating  $\text{IC}_{50}$ s and errors. The triprolidine alone experiment was done once, the G88R RNase A alone experiment was repeated in duplicate, and the triprolidine co-treatment with G88R RNase A was repeated in triplicate. Values for  $\text{IC}_{50}$  were calculated by fitting the curves by nonlinear regression with equation A1.1, in which  $y$  is the total DNA synthesis following the [*methyl*- $^3\text{H}$ ]thymidine pulse, and  $h$  is the slope of the curve.

$$y = \frac{100\%}{1 + 10^{(\log(\text{IC}_{50}) - \log[\text{ribonuclease}])h}} \quad (\text{A1.1})$$

## A1.6 Acknowledgements

The authors would like to acknowledge the SMSF for helping to run the high-throughput screening. In particular, the authors would like to acknowledge Noël Peters for her guidance, patience, and friendly and open personality. L.D. Lavis was instrumental in synthesizing carboxyethylresorufin maleimide, and G.A. Ellis is grateful for his mentorship in this area. Experiments made use of the Biophysics Instrumentation Facility, which was established by

Grants BIR-9512577 (NSF) and S10 RR13790 (NIH). This work was supported by Grant R01 CA073808 (NIH) and two grants from the Wisconsin Alumni Research Foundation (WARF).

### **A1.7 Contributions**

Original idea for project was from R.T. Raines. Assay optimization for 384-well plate high-throughput screening was done by G.A. Ellis. High-throughput screening was initially run by the SMSF and G.A. Ellis, then was done by G.A. Ellis under the guidance of the SMSF. All  $K_d$  determinations were done by G.A. Ellis. Cytotoxicity assays on 19 ChemBridge compounds were done by the SMSF with protein supplied by G.A. Ellis. Cell-proliferation assays with [*methyl*- $^3\text{H}$ ]thymidine incorporation were done by G.A. Ellis and M.L. Hornung. Protein production was done by G.A. Ellis. DEFIA and CRCM were synthesized by L.D. Lavis. CERM was synthesized by L.D. Lavis with G.A. Ellis.



**Figure A1.1** Putative mechanism of ribonuclease cytotoxicity. A) Ribonucleases reversibly bind to the anionic cell surface. This binding is needed to facilitate B) endocytosis. Following endocytosis, ribonucleases C) translocate from endosomes into the cytosol where they D) encounter RI. Ribonucleases are either E) bound and inhibited by RI, maintaining cell status, or F) able to evade RI and degrade cellular RNA, causing cell death. The figure is partially adapted from a previous publication (Rutkoski and Raines, 2008).

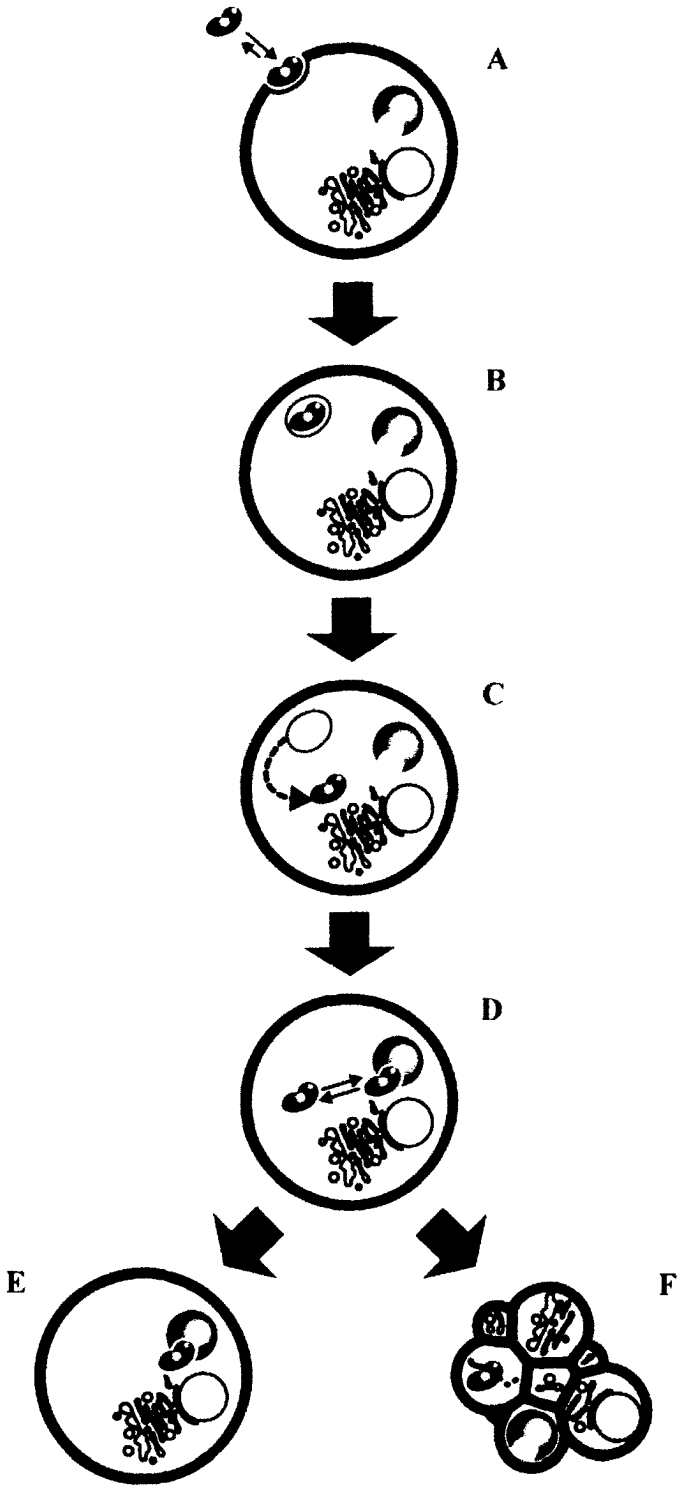


**Figure A1.2** Determination of the  $K_d$  value of KDRNG88C-DEF RNase A for RI.

KDRNG88C-DEF RNase A was mostly bound by RI, then competed away from RI with DRNG RNase A, which has a known  $K_d$  for RI of 510 nM (Rutkoski, *et al.*, 2005). The  $K_d$  of KDRNG88C-DEF RNase A for RI was determined to be  $320 \pm 30$  nM. Data points represent the mean from triplicate experiments  $\pm$  standard error of the mean.

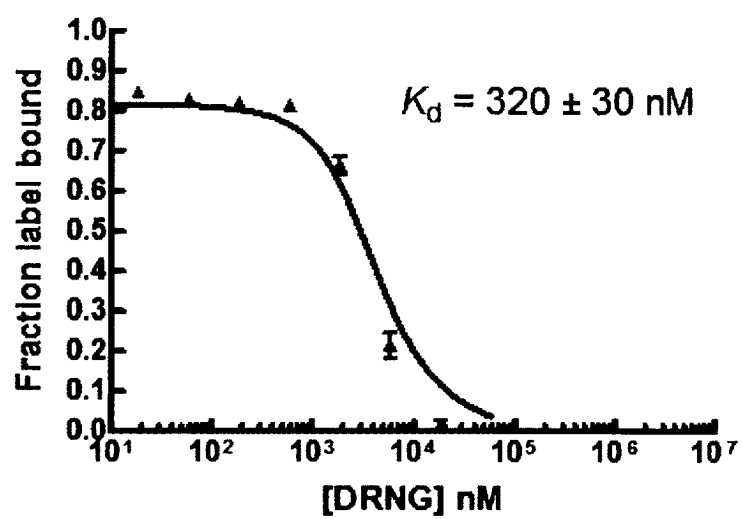


**Figure A1.3** Development of a high-throughput RI–RNase A binding assay. The RI–RNase A competitive binding assay was optimized from previous assays (Abel, *et al.*, 2002; Lavis, *et al.*, 2007) for increased signal window (SW) and high-throughput screening conditions.

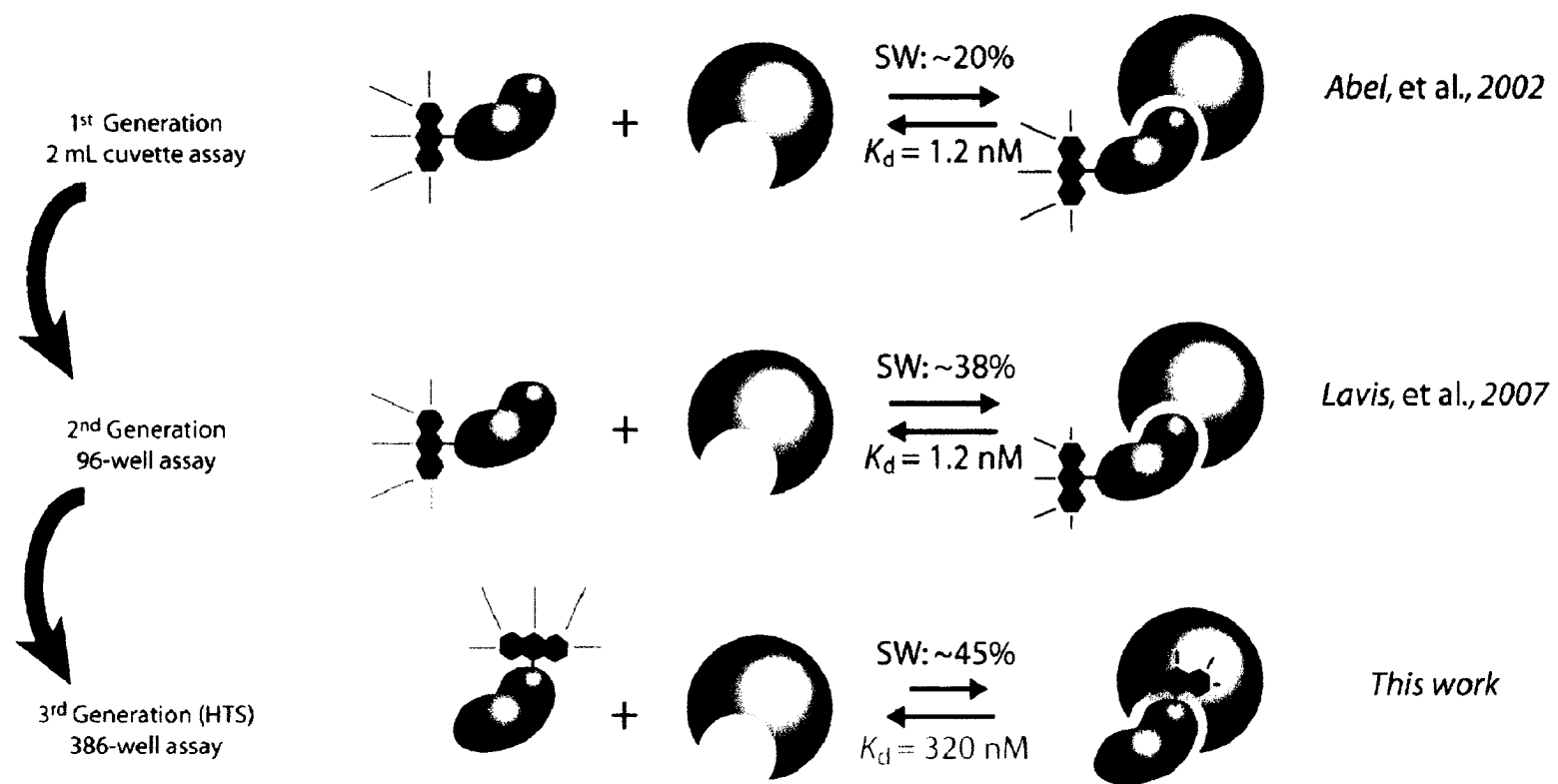
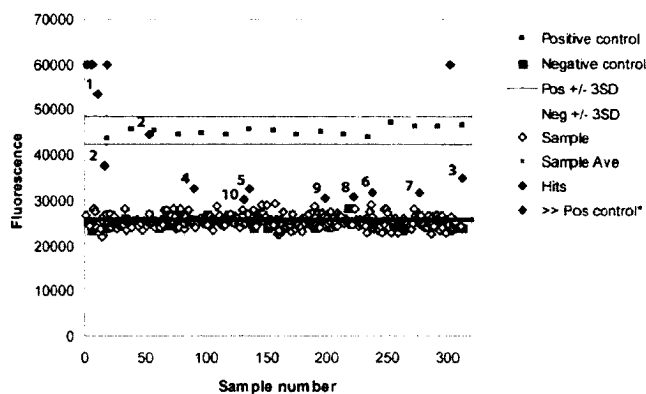
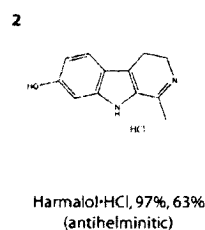
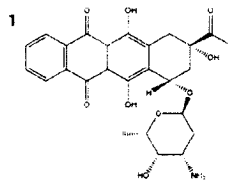


**Figure A1.4** Results of the Known Bioactives Library screen. Results from the assay indicate a good separation between controls. Five compounds (>> pos control\*) were overly fluorescent and later determined to be fluorescent dyes, likely false positives. Structures, names, percent of regained fluorescence in the primary assay, and known biological activities of compounds  $\geq 25\%$  of regained fluorescence are designed as preliminary “hits.” Triprolidine and tobramycin were determined to be the most likely true hits after secondary assays.



**Hits  $\geq 50\%$ :**



**Hits  $\geq 25\%$ :**

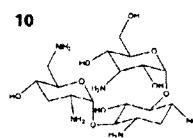
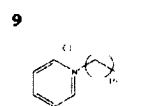
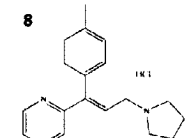
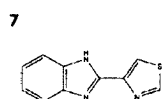
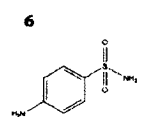
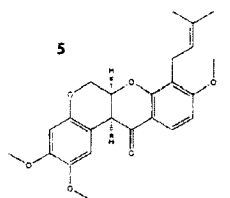
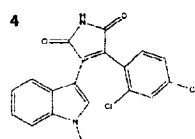
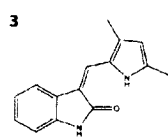




**Figure A1.5** Determination of  $K_d$  of triprolidine for inhibiting the interaction of KDRNG88C-DEF RNase A with RI. KDRNG88C-DEF RNase A was mostly bound by RI and then competed away from RI with triprolidine. The  $K_d$  of triprolidine for inhibiting the interaction of KDRNG88C-DEF RNase A with RI was determined to be 210  $\mu\text{M}$ . Data points represent a single experiment.

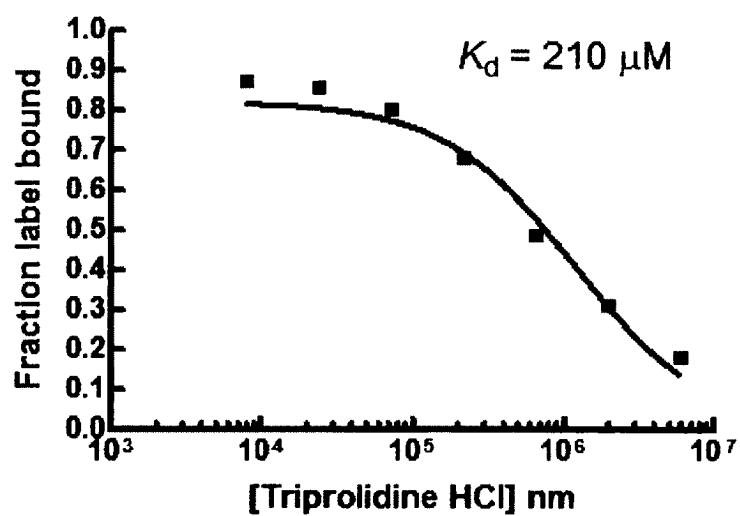
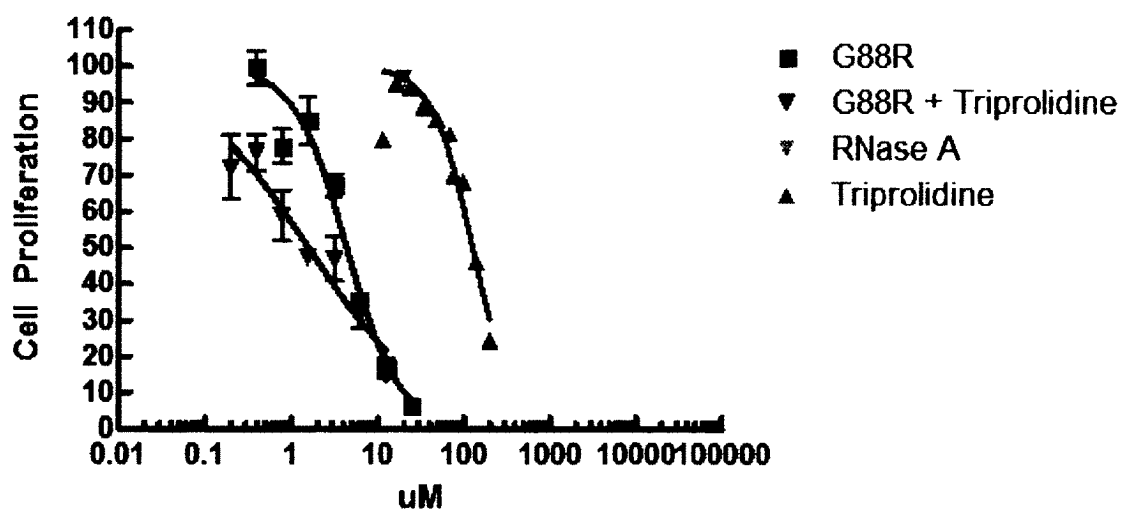


**Figure A1.6** Investigations of whether triprolidine and G88R RNase A are synergistically cytotoxic. The cytotoxicity of triprolidine alone (singlet), G88R RNase A alone (duplicate), and G88R RNase A with 75  $\mu$ M triprolidine (triplicate) was measured for K-562 cells. The  $IC_{50}$  values were 126  $\mu$ M for triprolidine alone,  $4.4 \pm 0.4$   $\mu$ M for G88R alone, and  $1.6 \pm 0.3$   $\mu$ M for triprolidine and G88R RNase A. However, at 75  $\mu$ M, triprolidine was toxic itself, with 70% cell proliferation. Further, the curves overlap of G88R and triprolidine toxicity. Therefore, the data is inconclusive. Error is represented as standard error of the mean.



## **APPENDIX 2**

### **Engineering a Ribonuclease Zymogen Activated by Urokinase for Selective Toxicity**

## **A2.1 Abstract**

Cells often express proteases as inactive zymogens to protect them from their proteolytic activity. Herein, we use a similar method to create a RNase A zymogen activated by urokinase. Urokinase is a protease overexpressed and secreted by many cancer cells and this overexpression is a marker of potential malignancy and poor prognosis. The RNase A zymogen constructed herein carries mutations which should endow it with evasiveness to a cellular ribonuclease inhibitor protein. Therefore, upon activation, this RNase A zymogen would hypothetically be able to enter cells and degrade RNA, ultimately leading to preferential cell death of cancer cells. A RNase A zymogen was produced that is activated 26-fold by urokinase. While this zymogen was not toxic to cancer cells, additional engineering of it or other zymogen constructs may lead to augmented selective killing of cancer cells with ribonucleases.

## **A2.2 Introduction**

A crucial issue for the body in the design of proteases is how to produce them without significant off-target activity leading to toxicity. One evolved solution is the use of zymogens: precursor enzymes that are inactive until a region is cleaved by another protease, activating the enzyme at its needed site of action (Khan and James, 1998). Typically, this region extends from the N-terminus and works by either orchestrating a peptide loop to form and block the active site or by mimicking the substrate and binding into the active site to inhibit the enzyme (Khan and James, 1998).

Nature's use of zymogens was the basis for the creation of three classes of engineered zymogens using bovine pancreatic ribonuclease (RNase A) by the Raines laboratory (Plainkum,

*et al.*, 2003; Johnson, *et al.*, 2006; Turcotte and Raines, 2008a). These zymogens were engineered using circular permutation, where new N- and C- termini were created and a peptide linker spanned the old N- and C- terminus, blocking the active site. The RNase A zymogens were relatively inactive until the linker regions were cleaved by disease-associated proteases: plasmepsin II from *Plasmodium falciparum*, the organism responsible for most cases of malaria; NS3 protease from the hepatitis C virus; or the HIV-1 protease (Plainkum, *et al.*, 2003; Johnson, *et al.*, 2006; Turcotte and Raines, 2008a). RNase A variants that have been engineered to evade a cellular ribonuclease inhibitor protein (RI) are toxic to cells. Therefore, zymogens of RI-evasive ribonuclease variants could be used as biologic therapeutics for multiple diseases; all cells would internalize the ribonuclease zymogen, but only in those cells harboring the disease protease would the ribonuclease zymogen be activated, leading to the degradation of cellular RNA and consequently cell death.

While ribonuclease zymogens produced by the Raines Lab have been effective *in vitro*, none have been effective *in cellulo* (Raines, R.T., personal communication). This could be for a number of reasons. First, the thermostability of these RNase A zymogens is considerably lower than wild-type RNase A (Plainkum, *et al.*, 2003; Johnson, *et al.*, 2006; Turcotte and Raines, 2008a), and as stability has been shown to be a determinate of cytotoxicity (Klink and Raines, 2000), this could hinder potency. Second, even after activation by the protease, these RNase A zymogens do not regain 100% of wild-type ribonucleolytic activity (Plainkum, *et al.*, 2003; Johnson, *et al.*, 2006; Turcotte and Raines, 2008a). Third, these RNase A zymogens are notoriously difficult to fold, leading to low yields and making optimization of cellular conditions for toxicity difficult (R.J. Johnson, R.F. Turcotte, and R.T. Raines, personal communication).

Finally, developing and optimizing cellular models for the disease states, and their associated proteases, is difficult (R.F. Turcotte, personal communication).

In this study we chose to engineer a novel RNase A zymogen activated by urokinase-type plasminogen activator (uPA or urokinase). Urokinase is a serine protease secreted by cells as a zymogen itself (pro-uPA) (Blasi and Carmeliet, 2002; Sidenius and Blasi, 2003; Huai, *et al.*, 2006). Following secretion, it binds its cell-surface receptor (uPAR) with nanomolar affinity. The urokinase zymogen is proteolytically activated by many proteases, including plasmin. (Andreasen, *et al.*, 1997; Huai, *et al.*, 2006). Urokinase, bound to its receptor, proteolytically activates plasminogen into plasmin, thereby completing a putative positive-feedback loop (Andreasen, *et al.*, 1997; Nozaki, *et al.*, 2006; Smith and Marshall, 2010). After activation, plasmin activates growth factors and zymogen matrix metalloproteases (MMPs) (Figure A2.1) (Sidenius and Blasi, 2003; Nozaki, *et al.*, 2006; Smith and Marshall, 2010). This cascade, along with signaling from uPAR, results in the degradation of the extracellular matrix and increased cellular migration (Sidenius and Blasi, 2003; Nozaki, *et al.*, 2006). Importantly, both urokinase and uPAR are overexpressed in many cancer cells, and their overexpression is linked to malignancy (i.e. metastasis) and poor prognosis (Andreasen, *et al.*, 1997; Blasi and Carmeliet, 2002; Sidenius and Blasi, 2003; Nozaki, *et al.*, 2006; Smith and Marshall, 2010). Therefore, it was hypothesized that a RI-evasive RNase A zymogen activated by urokinase would more preferentially kill cancer cells over normal cells.

Using urokinase to activate cytotoxins is predicated by previous systems (Liu, *et al.*, 2001; Abi-Habib, *et al.*, 2004; Chung and Kratz, 2006). One of the most similar systems is based on anthrax toxin (Liu, *et al.*, 2001). Anthrax toxin is composed of protective antigen, lethal factor,



and edema factor (Liu, *et al.*, 2001). Protective antigen binds to the cell surface and upon cleavage by a furin-like protease, facilitates the internalization of lethal factor and edema factor, which kill the cell (Liu, *et al.*, 2001). The protective antigen was engineered so that the furin cleavage site was replaced by a urokinase-specific cleavage site (Liu, *et al.*, 2001). Therefore, only when the engineered protective antigen is activated by urokinase are edema factor and lethal factor internalized, causing cell death (Liu, *et al.*, 2001). This system showed specific toxicity to cancer cells overexpressing urokinase/pro-uPA and uPAR (Liu, *et al.*, 2001; Abi-Habib, *et al.*, 2006). Additionally, this system has shown specificity for cancer cells in mouse models (Liu, *et al.*, 2003; Rono, *et al.*, 2006; Su, *et al.*, 2007).

In the current study, RNase A zymogens activated by urokinase were engineered to have the urokinase-cleavable site SGR↓SA. This site has been shown through phage display to be readily and specifically cleaved by urokinase ( $k_{\text{cat}}/K_{\text{M}} = 1200 \text{ M}^{-1} \text{ s}^{-1}$ ) (Ke, *et al.*, 1997). This sequence was also used for the urokinase-activated anthrax toxin system (Ke, *et al.*, 1997; Liu, *et al.*, 2001; Liu, *et al.*, 2003; Rono, *et al.*, 2006; Abi-Habib, *et al.*, 2006; Su, *et al.*, 2007). A circular-permuted RNase A zymogen activated by urokinase was produced and analyzed both *in vitro* and *in cellulo*. While the zymogen was activated by urokinase *in vitro*, it did not demonstrate *in cellulo* toxicity. Two other methods novel to the Raines laboratory of producing a RNase A zymogen were also attempted, and while they did not produce any viable zymogen, they are discussed as future options in section A2.5. Hopefully, additional engineering will lead to a zymogen that is specifically toxic to cancer cells overexpressing urokinase.

### A2.3 Results and Discussion

A RNase A zymogen activated by urokinase was designed based on previous successful RNase A zymogens (Plainkum, *et al.*, 2003; Johnson, *et al.*, 2006; Turcotte and Raines, 2008a). The zymogen had new N- and C-termini at positions 89 and 88, respectively, and a linker was placed between the previous N- and C- termini with two urokinase cleavage sites: GSGR↓SAGMSGR↓SAG (Figure A2.2). Four residues, including the new N- and C-termini, were mutated to cysteines (A4C, G88C, S89C, V118C; wild-type numbering) to form additional disulfide bonds for increased stability (Plainkum, *et al.*, 2003). Two residues were mutated (R38D, D39R) to endow the zymogen with RI evasion so that the activated zymogen could potentially kill cancer cells (Rutkoski, *et al.*, 2005). Production of the zymogen resulted in two main groups of fractions from the cation exchange column, herein denoted low-salt and high-salt zymogen.

The RNase A zymogen (15 kDa) should be cleaved in the presence of urokinase, and under denaturing and reducing conditions should dissociate into two main fragments of 10 kDa and 4.3 kDa, and a smaller 0.7 kDa fragment from the linker (assuming the linker is cleaved twice). The two purified fractions of the traditional zymogen, low-salt and high-salt, were incubated with urokinase (1 unit/μL, 100 units total) in PBS buffer at 37 °C. Cleavage was detected by a shift of the zymogen band to a lower molecule weight (the 10 kDa fragment) on a SDS-PAGE gel. Gratifyingly, most of the zymogen was cleaved quickly by urokinase (Figure A2.3). Cleavage was not tested with other proteins to ensure specificity, though some cleavage may have occurred with cells detached by trypsin treatment (data not shown).

One of the most important aspects of a zymogen is that it is less catalytically inactive until cleaved. To test this in our system, the zymogen was incubated with 100 units of urokinase in PBS at 37 °C for 1 h. This reaction was diluted into RNase A activity buffer, and the activity of the activated and unactivated zymogen was compared. The activity of low-salt zymogen was increased by 26-fold after activation with urokinase. The activity of high-salt zymogen, however, was only increased by 3-fold (Table A2.1). Notably, the activity of the activated zymogens was still low compared to wild-type RNase A. The 26-fold activation of the low-salt zymogen indicates that this zymogen does work successfully, so it was chosen for further investigation.

A critical issue for ribonuclease zymogens produced in the Raines laboratory has been activation and toxicity *in cellulo*. To test activation, the low-salt zymogen was incubated with the prostate cancer cell line DU-145. DU-145 cells are known to express both uPAR and urokinase, and this cell line was able to unleash the cytotoxicity of the engineered urokinase-activated anthrax toxin (Abi-Habib, *et al.*, 2006). The ribonuclease zymogen was incubated with DU-145 cells for 0, 24, and 48 hours. Media was removed from cells, followed by removal of cells from plates. Zymogen activation was analyzed by running samples on a SDS-PAGE gel. It did not appear that much zymogen, if any, was activated *in cellulo* (Figure A2.4). This corresponded with a lack of significant cytotoxicity of the zymogen against DU-145 cells (data not shown).

## A2.4 Conclusions

A RNase A zymogen was produced that is activated by urokinase *in vitro*, with a 26-fold change in activity. This is slightly below but on-par with previous RNase A zymogens (Plainkum, *et al.*, 2003; Johnson, *et al.*, 2006; Turcotte and Raines, 2008a). Two zymogen

constructs novel to the Raines laboratory were also constructed but did not yield usable protein. The urokinase system remains an attractive target for ribonuclease-based zymogens. Hopefully, with further engineering of RNase A zymogens activated by urokinase, a cytotoxic ribonuclease can be produced.

### **A2.5 Ribonuclease Constructs Necessitating Additional Engineering**

In addition to the ribonuclease zymogen studied here, two additional RNase A zymogen methods novel to the Raines laboratory were engineered to be activated by urokinase. DNA sequences for these zymogens were constructed, but neither produced viable protein. First, a RNase A zymogen (alternate frame zymogen) was designed to have a false partial active site before a urokinase cleavage site, and a long, flexible linker attached to a true partial active site was constructed on the opposite side of the enzyme (Figure A2.5). Hypothetically, when urokinase cleaved the false partial active site, this region would dissociate, allowing the linker and true partial active site to loop around, fit into the now empty space, and reconstitute the active enzyme. In an attempt to accomplish this, a loop region of RNase A from residues 18–22 was mutated to a urokinase cleavage site (SGR↓SA). An active site residue between the N-terminus and this cleavage site, H12, was mutated to alanine, which is known to significantly reduce the activity of RNase A (Raines, 1998). A flexible peptide linker was added to the C-terminus, and residues 1–15 were added to the end of this linker, with a wild-type His12 (wild-type numbering) (Figure A2.5). Unfortunately, after production of this zymogen, mass spectrometry analysis indicated a mass that corresponded to the zymogen minus residues 1–13. Upon further analysis, after mutation of H12A, a site similar to the pelB cleavage site (Ala-Met-

Asp) was produced; this *E. Coli* protease is used often in ribonuclease synthesis to remove a leader sequence. Presumably, this protease was cleaving away residues 1–13 during production in *E. Coli*. Concurrently, a report from the Loh laboratory described a similar system with the bacterial ribonuclease barnase, although they used opposite ends of the enzyme (Mitrea, *et al.*, 2010). This report also indicated that the zymogen was not highly stable (Mitrea, *et al.*, 2010). Given that this was a problem for previous Raines Lab zymogens (Plainkum, *et al.*, 2003; Johnson, *et al.*, 2006; Turcotte and Raines, 2008a), the alternate frame zymogen method was abandoned.

Second, a RNase A zymogen activated by urokinase (inhibitor zymogen) was designed to have a flexible linker attached to the C-terminus, followed by a urokinase cleavage site, followed by part of a known peptide inhibitor of RNase A (Figure A2.5) (Smith and Raines, 2008). This inhibitor should loop around to bind and inactivate the enzyme tightly due to intramolecular interactions until urokinase cleaves the protein, at which point the inhibitor should dissociate, allowing for a more active RNase A / less inhibition (intermolecular interaction). Unfortunately, this construct did not produce any detectable protein at the correct mass, and the inhibitor zymogen method was abandoned.

Other constructs for ribonucleases activated by urokinase or proteases that are activated by urokinase, such as matrix metalloproteases (MMP), are possible. One construct that was briefly investigated was based on the activatable cell-penetrating peptide system (Jiang, *et al.*, 2004). Briefly, a cell-penetrating peptide, Arg<sub>9</sub>, which has been shown to increase the internalization and cytotoxicity of RI-evasive RNase A variants (Fuchs and Raines, 2005), was appended onto the C-terminus of an RI-evasive RNase A variant (D38R/R39D/G88R RNase A). To the end of

this was added a MMP cleavage site. Attached to the end of this was Glu<sub>9</sub>, which is thought to fold over, bind, and inactivate the Arg<sub>9</sub> tag (Jiang, *et al.*, 2004), eliminating the beneficial effect for ribonuclease cytotoxicity. When the MMP site was cleaved, Glu<sub>9</sub> would dissociate, allowing Arg<sub>9</sub> to help internalize ribonuclease into the cell (Figure A2.5). Unfortunately, preliminary attempts to produce usable protein from this construct failed.

Finally, a zymogen may be produced using a chemical biology approach. Specifically, a peptide attached to a self-immolative linker (Dubowchik, *et al.*, 2002) that mimics diethylpyrocarbonate (DEPC) may be able to be attached semi-specifically to a RNase A active-site histidine, if the conjugation is done at the correct pH. Upon cleavage of the peptide, the self-immolative linker would cleave from the histidine, reconstituting an active ribonuclease. This system may need to be thoroughly engineered with different length linkers to ensure that the protease can cleave the peptide.

## A2.6 Experimental Procedures

### A2.6.1 Materials

*Escherichia coli* strain BL21(DE3) cells were from Novagen (Madison, WI). DU-145 prostate cells were from a Raines laboratory stock presumably originally from the American Type Culture Collection (Manassas, VA). Cell culture medium and supplements, as well as Dulbecco's phosphate-buffered saline (DPBS) were from Invitrogen (Carlsbad, CA). [methyl-<sup>3</sup>H]Thymidine (6.7 Ci/mmol) was from Perkin-Elmer (Boston, MA). Protein purification columns were from GE Biosciences (Piscataway, NJ). Wild-type RNase A was from Sigma-

Aldrich (St. Louis, MO). MES buffer was purified by anion-exchange chromatography to remove trace amounts of oligomeric vinylsulfonic acid (Smith, *et al.*, 2003). Ribonuclease substrate 6-FAM–dArUdAdA–6-TAMRA was from Integrated DNA Technologies (Coralville, IA). All other chemicals used were of commercial reagent grade or better, and were used without further purification. Terrific Broth (TB) was from Research Products International (Mt. Prospect, IL), or was made by dissolving Tryptone (12 g), yeast extract (24 g), glycerol (4 mL),  $\text{KH}_2\text{PO}_4$  (2.31 g), and  $\text{K}_2\text{HPO}_4$  (12.54 g) in  $\text{H}_2\text{O}$  (1.00 L).

#### A2.6.2 *Analytical instruments and statistical calculations*

The incorporation of [*methyl*- $^3\text{H}$ ]thymidine into the genomic DNA of K-562 cells was quantified by scintillation counting using a Microbeta TriLux liquid scintillation and luminescence counter (Perkin–Elmer, Wellesley, MA). Molecular mass was determined by matrix-assisted laser desorption/ionization time-of-flight (MALDI–TOF) mass spectrometry using a Voyager-DE-PRO Biospectrometry Workstation (Applied Biosystems, Foster City, CA) at the campus Biophysics Instrumentation Facility. Fluorescent measurements for activity assays were made on a QuantaMaster1 photon-counting fluorometer (Photon Technology International) equipped with sample stirring.

#### A2.6.3 *Design of zymogens*

The RNase A zymogen investigated most was designed similar to previously described (Plainkum, *et al.*, 2003; Johnson, *et al.*, 2006; Turcotte and Raines, 2008a). The plasmid used was previously used for the NS3 protease zymogen, which contained the mutations described

above and in Figure A2.2 (Johnson, *et al.*, 2006). The RNase A zymogen activated by urokinase construct was made using overlapping PCR.

The other two zymogen constructs and the ACPP construct were also made using overlapping PCR. The sequences for these constructs are described in Figure A2.5.

#### A2.6.4 *Protein production*

RNase A zymogen was produced as described previously (Plainkum, *et al.*, 2003; Johnson, *et al.*, 2006; Turcotte and Raines, 2008a) and some preps may have contained phenylmethane sulfonyl fluoride (PMSF). Protein concentration was determined with a bicinchoninic acid assay kit from Pierce (Rockford, IL) for RNase A zymogens.

#### A2.6.5 *Activation of RNase A zymogen by urokinase*

The activation of RNase A zymogen by urokinase was measured as described previously for other RNase A zymogens using a SDS-PAGE gel assay (Plainkum, *et al.*, 2003; Johnson, *et al.*, 2006; Turcotte and Raines, 2008a). Briefly, separate tubes of zymogen alone, urokinase alone, or zymogen with urokinase were incubated at 37 °C. The concentration of zymogen was 10 µM, the concentration of urokinase was 1 unit / µL (100 units total), and both were in DPBS. At various timepoints, some of the reaction was removed and placed into sample loading buffer at a lower temperature to stop cleavage. Samples were run on a SDS-PAGE gel. The RNase A zymogen is approximately 15 kDa, and the cleaved products should be approximately 10 kDa, 4.3 kDa, and 0.7 kDa, with the 10 kDa fragment being retained on the gel. Urokinase is larger (52 kDa) (Blasi and Carmeliet, 2002; Sidenius and Blasi, 2003; Huai, *et al.*, 2006) and therefore runs as a light



band above ribonucleases. Cleavage was measured by the disappearance of the band corresponding to the intact RNase A zymogen standard, and the appearance of a lower molecular weight band.

For *in cellulo* activation assays, the same technique was used to measure cleavage. RNase A zymogen was incubated with DU-145 cells for the indicated times. Importantly, DU-145 cells were initially transferred either with EDTA, or were washed with media after being transferred and adhered with media, to eliminate any trypsin (initial experiments may have indicated cleavage due to trypsin). Following RNase A zymogen incubation, media was removed and run as “media” samples. Cells were detached and run as “cell” samples. Both were frozen at -20 °C until the gel was run.

#### A2.6.6 *Ribonucleolytic activity assay*

The ribonucleolytic activity of the activated and unactivated RNase A zymogen was determined by quantitating its ability to cleave 6-FAM-dArUdAdA-6-TAMRA, as described previously for wild-type RNase A (Kelemen, *et al.*, 1999). Briefly, assays were carried out at ambient temperature in 2.00 mL of 0.10 M MES–NaOH buffer (pH 6.0) containing NaCl (0.10 M). Fluorescence data were fitted to equation A2.1, in which  $\Delta I/\Delta t$  is the initial reaction velocity,  $I_0$  is the fluorescence intensity before addition of ribonuclease,  $I_f$  is the fluorescence intensity after complete substrate hydrolysis, and  $[E]$  is the total ribonuclease concentration. For measuring the activity of activated zymogen, the zymogen was activated with 100 units of urokinase in PBS at 37 °C for 1 h. This reaction was diluted into RNase A activity buffer, and

the activity measured. Data are the average of triplicate measurements in three experiments for low-salt zymogen, and triplicate measurements in two experiments for high-salt zymogen.

$$k_{\text{cat}}/K_{\text{M}} = \frac{\Delta I/\Delta t}{(I_{\text{f}} - I_0)[\text{E}]} \quad (\text{A2.1})$$

#### A2.6.7 Cell-proliferation assay

The effect of RNase A and RNase A zymogen on the proliferation of DU-145 cells was assayed similarly to previously described for measuring cell proliferation of K-562 cells after treatment with RNase A variants (Leland, *et al.*, 1998; Rutkoski, *et al.*, 2005). Briefly, 5  $\mu\text{L}$  of a serially-diluted solution of RNase A, RNase A zymogen, or PBS was added to 95  $\mu\text{L}$  of media containing DU-145 cells. After 44 h, the cells were treated with [*methyl*- $^3\text{H}$ ]thymidine for 4 h, and the incorporation of radioactive thymidine into cellular DNA was quantified by liquid scintillation counting. Results were reported as the percentage of [*methyl*- $^3\text{H}$ ]thymidine incorporated relative to control cells that had been treated with PBS. Values for  $\text{IC}_{50}$  were calculated by fitting the curves by nonlinear regression with equation A2.2, in which  $y$  is the total DNA synthesis following the [*methyl*- $^3\text{H}$ ]thymidine pulse, and  $h$  is the slope of the curve.

$$y = \frac{100\%}{1 + 10^{(\log(\text{IC}_{50}) - \log[\text{ribonuclease}])h}} \quad (\text{A2.2})$$

## **A2.7 Acknowledgments**

The authors would like to acknowledge M.L. Hornung for help with preliminary cytotoxicity experiments and J.E. Lomax for helpful discussions. Experiments made use of the Biophysics Instrumentation Facility, which was established by Grants BIR-9512577 (NSF) and S10 RR13790 (NIH). This work was supported by Grant R01 CA073808 (NIH).

## **A2.8 Contributions**

Original idea for constructing a RNase A zymogen activated by urokinase was from R.T. Raines. Original idea for constructing the alternate frame zymogen, the inhibitor zymogen, and the activatable cell-penetrating peptide zymogen was from G.A. Ellis. Original plasmids came from R.J. Johnson and S.M. Fuchs, but were modified into the zymogens studied here extensively by G.A. Ellis. All experiments were conducted by G.A. Ellis, with the exception of preliminary cytotoxicity experiments by M.L. Hornung.

**Table A2.1** Catalytic efficiency of RNase A zymogen activated by urokinase.

Zymogen	$(k_{\text{cat}}/K_{\text{M}})_{\text{unactivated}}$ $10^4 \text{ M}^{-1} \text{ s}^{-1}$	Percent wt activity	$(k_{\text{cat}}/K_{\text{M}})_{\text{activated}}$ $10^4 \text{ M}^{-1} \text{ s}^{-1}$	Percent wt activity	$\frac{(k_{\text{cat}}/K_{\text{M}})_{\text{activated}}}{(k_{\text{cat}}/K_{\text{M}})_{\text{unactivated}}}$
Low-salt	1.8 +/- 0.1	0.03	47 +/- 2	0.9	26
High-salt	47 +/- 2	0.9	130 +/- 20	2.5	3

**Figure A2.1** Urokinase and uPAR pathway. After secretion, pro-urokinase (pro-uPA) binds its receptor, uPAR, and is proteolytically activated by plasmin into urokinase (uPA). Urokinase proteolytically activates plasminogen into plasmin, completing the putative positive-feedback loop. Plasmin can activate pro-matrix metalloproteases, and these active enzymes can then degrade the extracellular matrix. Plasmin can also activate growth factors (GFs). Integrins are also thought to play a role in uPAR signaling. Both urokinase and uPAR are overexpressed in many tumors, and together, this pathway helps facilitate cellular migration and cancer metastasis (Nozaki, *et al.*, 2006). Figure is from a previous publication (Nozaki, *et al.*, 2006).

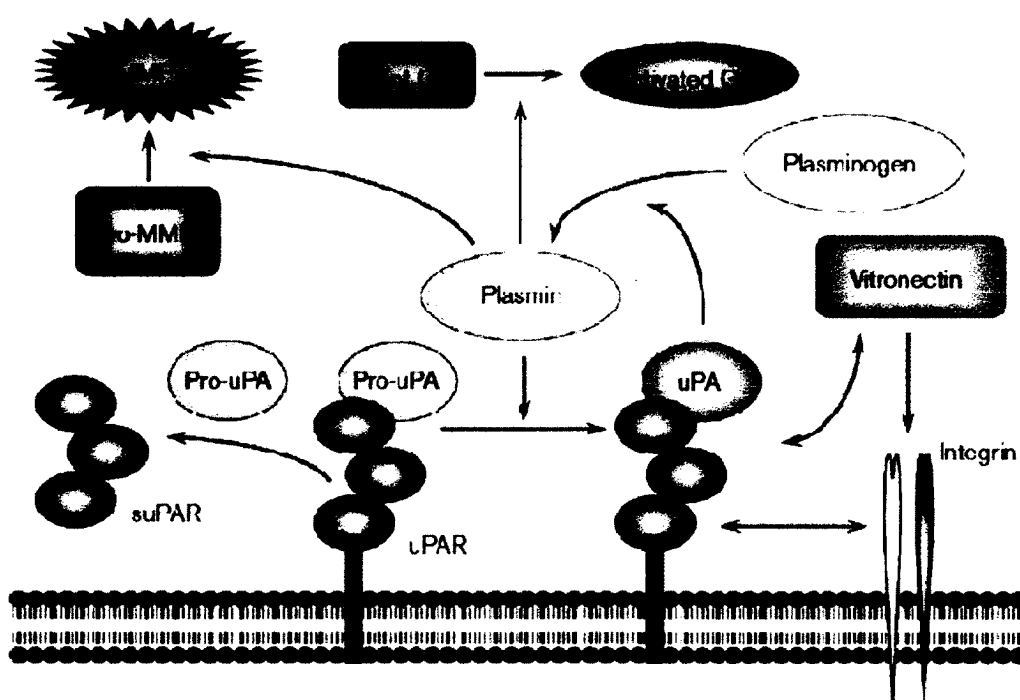


**Figure A2.2** Construction of RNase A zymogen activated by urokinase. The zymogen was constructed based on the RNase A sequence (top). Underlines are similar/same sequences in a different position. Light blue represents mutations. Bold red letters indicate urokinase cleavage sites. A cartoon model of the zymogen is depicted (below). Black represents the linker, red represents the cleavage sites, and magenta represents the histidine active site residues.

## Sequences of wild-type RNase A and zymogen

	1	20	30	40	50	60	70	80	90	100	110	120	124
RNase A	KELAAAKLGRDHMLSSLSAASSSSYCSOMMASRNLTKDRCKPASTLVHLSLADYDAVCSQKRYACKNBDINCYQSSIMSLLDRLTGSRYENCARKLTHANKHLLVALTGNSSPYRLDASS												
Zymogen	KSAVSENAVALQANNTLLAAGLCSNCAVPHHDAAYQSLRNVOMSGSNVQKELCAAKLEKQHMDSLSAASSSSYCSOMMASRNLTKDRCKPASTLVHLSLADYDAVCSQKRYACKNBDINCYQSSIMSLLDRLTGS												

*bridge over active site*  
 mutated residues  
 urokinase cleavage site



RNase A Zymogen Activated by Urokinase  
*bridge with cleavage sites (red) over active site histidines (magenta)*



**Figure A2.3** Activation of RNase A zymogen by urokinase *in vitro*. Both low-salt and high-salt zymogen at 10  $\mu$ M were activated when incubated with 100 units of urokinase (1 unit/ $\mu$ L final concentration) in PBS at 37 °C, and afterwards reactions were run on SDS-PAGE gel. “L” indicates ladder lane, “U” indicates 100 units of urokinase only, “Z” indicates 10  $\mu$ M zymogen only, and numbers 0–60 indicate the number of minutes zymogen was incubated with urokinase.

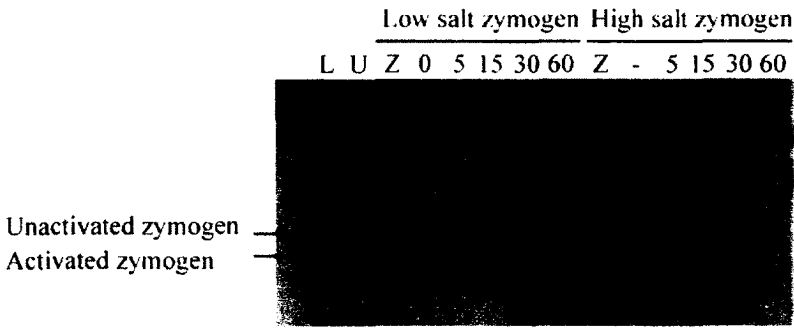


**Figure A2.4** Extent of Activation of RNase A zymogen by urokinase *in vitro* and *in cellulo*.

Low-salt zymogen activation *in vitro* was run again for comparison to *in cellulo* activation. Low-salt zymogen was incubated with urokinase and afterwards reactions were run on SDS-PAGE gel. “L” indicates ladder lane, “Z” indicates 10  $\mu$ M zymogen only, and numbers 0–120 indicate the number of minutes zymogen was incubated with urokinase. Low-salt zymogen was also incubated with DU-145 cells, and samples were loaded onto the gel of the cells “cells” or the media incubated with cells “media”. “C” indicates DU-145 cells only. Numbers 0–48 indicate hours of zymogen incubation *in cellulo*. It does not appear that significant zymogen activation occurred *in cellulo*.

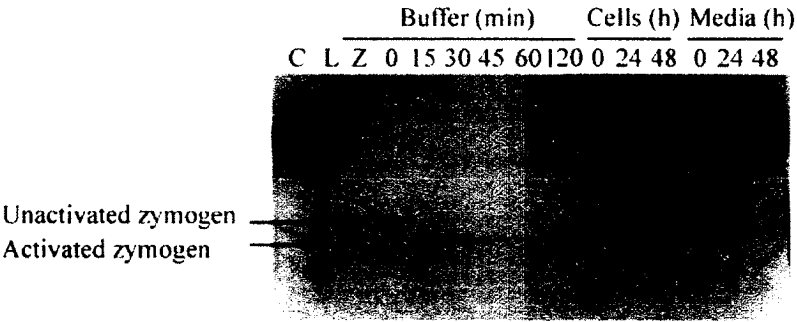


**Figure A2.5** Construction of genes for other RNase A zymogens and ACPD RNase A. The zymogens and activatable cell-penetrating peptide (ACPD) RNase A were constructed based on the RNase A sequence (top). Underlines are similar/same sequences in a different position. Light blue represents mutations. Bold red letters indicate cleavage sites. Cartoon models of the zymogens are depicted (below). Black represents linkers, red represents cleavage sites, orange represents an inhibitor peptide, dark blue represents cationic and anionic tags, and magenta represents the histidine active site residues.



## **REFERENCES**

### List of References

- Abel, R. L., Haigis, M. C., Park, C., Raines, R. T. (2002). Fluorescence assay for the binding of ribonuclease A to the ribonuclease inhibitor protein. *Anal. Biochem.* **306**, 100-107.
- Abi-Habib, R. J., Liu, S., Bugge, T. H., Leppla, S. H., Frankel, A. E. (2004). A urokinase-activated recombinant diphtheria toxin targeting the granulocyte-macrophage colony-stimulating factor receptor is selectively cytotoxic to human acute myeloid leukemia blasts. *Blood* **104**, 2143-2148.
- Abi-Habib, R. J., Singh, R., Liu, S., Bugge, T. H., Leppla, S. H., Frankel, A. E. (2006). A urokinase-activated recombinant anthrax toxin is selectively cytotoxic to many human tumor cell types. *Mol. Cancer Ther.* **5**, 2556-2562.
- Alfacell (2009). Annual Report 2009. [www.alfacell.com/annualreport2009.pdf](http://www.alfacell.com/annualreport2009.pdf)
- Andreasen, P. A., Kjoller, L., Christensen, L., Duffy, M. J. (1997). The urokinase-type plasminogen activator system in cancer metastasis: a review. *Int. J. Cancer* **72**, 1-22.
- Andresen, T. L., Jensen, S. S., Jorgensen, K. (2005). Advanced strategies in liposomal cancer therapy: problems and prospects of active and tumor specific drug release. *Prog. Lipid Res.* **44**, 68-97.
- Anfinsen, C. B. (1973). Principles that govern the folding of protein chains. *Science* **181**, 223-230.
- Angeles-Boza, A. M., Erazo-Oliveras, A., Lee, Y. J., Pellois, J. P. (2010). Generation of endosomolytic reagents by branching of cell-penetrating peptides: tools for the delivery of bioactive compounds to live cells in cis or trans. *Bioconjug. Chem.* **21**, 2164-2167.
- Ardelt, W., Ardelt, B., Darzynkiewicz, Z. (2009). Ribonucleases as potential modalities in anticancer therapy. *Eur. J. Pharmacol.* **625**, 181-189.
- Ardelt, W., Mikulski, S. M., Shogen, K. (1991). Amino acid sequence of an anti-tumor protein from *Rana pipiens* oocytes and early embryos. Homology to pancreatic ribonucleases. *J. Biol. Chem.* **266**, 245-251.
- Ardelt, W., Shogen, K., Darzynkiewicz, Z. (2008). Onconase and amphinase, the antitumor ribonucleases from *Rana pipiens* oocytes. *Curr. Pharm. Biotechnol.* **9**, 215-225.



- Arkin, M. R., Wells, J. A. (2004). Small-molecule inhibitors of protein-protein interactions: progressing towards the dream. *Nat. Rev. Drug Discov.* **3**, 301-317.
- Arnold, U., Ulbrich-Hofmann, R. (2006). Natural and engineered ribonucleases as potential cancer therapeutics. *Biotechnol. Lett.* **28**, 1615-1622.
- Barth, R. F. (2009). Boron neutron capture therapy at the crossroads: challenges and opportunities. *Appl. Radiat. Isot.* **67**, S3-6.
- Beaucage, S. L., Caruthers, M. H. (1981). Deoxynucleoside Phosphoramidites - a New Class of Key Intermediates for Deoxypolynucleotide Synthesis. *Tetrahedron Lett.* **22**, 1859-1862.
- Beck, A. K., Pass, H. I., Carbone, M., Yang, H. (2008). Ranpirinase as a potential antitumor ribonuclease treatment for mesothelioma and other malignancies. *Future Oncol.* **4**, 341-349.
- Benito, A., Ribó, M., Vilanova, M. (2005). On the track of antitumor ribonucleases. *Mol. Biosyst.* **1**, 294-302.
- Benito, A., Vilanova, M., Ribo, M. (2008). Intracellular routing of cytotoxic pancreatic-type ribonucleases. *Curr. Pharm. Biotechnol.* **9**, 169-179.
- Bergman, L., Beelen, M. L., Gallee, M. P., Hollema, H., Benraadt, J., van Leeuwen, F. E. (2000). Risk and prognosis of endometrial cancer after tamoxifen for breast cancer. Comprehensive Cancer Centres' ALERT Group. Assessment of Liver and Endometrial cancer Risk following Tamoxifen. *Lancet* **356**, 881-887.
- Bérubé, M., Dowlut, M., Hall, D. G. (2008). Benzoboroxoles as Efficient Glycopyranoside-Binding Agents in Physiological Conditions: Structure and Selectivity of Complex Formation. *J. Org. Chem.* **73**, 6471-6479.
- Bildstein, L., Dubernet, C., Couvreur, P. (2011). Prodrug-based intracellular delivery of anticancer agents. *Adv. Drug Deliv. Rev.* **63**, 3-23.
- Blasi, F., Carmeliet, P. (2002). uPAR: a versatile signalling orchestrator. *Nat. Rev. Mol. Cell Biol.* **3**, 932-943.

- Boix, E., Leonidas, D. D., Nikolovski, Z., Nogues, M. V., Cuchillo, C. M., Acharya, K. R. (1999). Crystal structure of eosinophil cationic protein at 2.4 Å resolution. *Biochemistry* **38**, 16794-16801.
- Boix, E., Wu, Y., Vasandani, V. M., Saxena, S. K., Ardel, W., Ladner, J., Youle, R. J. (1996). Role of the N terminus in RNase A homologues: differences in catalytic activity, ribonuclease inhibitor interaction and cytotoxicity. *J. Mol. Biol.* **257**, 992-1007.
- Bosslet, K., Straub, R., Blumrich, M., Czech, J., Gerken, M., Sperker, B., Kroemer, H. K., Gesson, J. P., Koch, M., Monneret, C. (1998). Elucidation of the mechanism enabling tumor selective prodrug monotherapy. *Cancer Res.* **58**, 1195-1201.
- Braschoss, S., Hirsch, B., Dubel, S., Stein, H., Durkop, H. (2007). New anti-CD30 human pancreatic ribonuclease-based immunotoxin reveals strong and specific cytotoxicity in vivo. *Leuk. Lymphoma* **48**, 1179-1186.
- Brown, D. M., *Drug delivery systems in cancer therapy*. Humana Press: Totowa, N.J., 2004; p 390.
- Cakara, D., Kleimann, J., Borkovec, M. (2003). Microscopic protonation equilibria of poly(amidoamine) dendrimers from macroscopic titrations. *Macromolecules* **36**, 4201-4207.
- Cao, H., Chen, J., Awoniyi, M., Henley, J. R., McNiven, M. A. (2007). Dynamin 2 mediates fluid-phase micropinocytosis in epithelial cells. *J. Cell Sci.* **120**, 4167-4177.
- Chang, K. C., Lo, C. W., Fan, T. C., Chang, M. D., Shu, C. W., Chang, C. H., Chung, C. T., Fang, S. L., Chao, C. C., Tsai, J. J., Lai, Y. K. (2010). TNF-α mediates eosinophil cationic protein-induced apoptosis in BEAS-2B cells. *BMC Cell Biol.* **11**,
- Chao, T. Y., Lavis, L. D., Raines, R. T. (2010). Cellular uptake of ribonuclease A relies on anionic glycans. *Biochemistry* **49**, 10666-10673.
- Chao, T. Y., Raines, R. T. (2011). Mechanism of Ribonuclease A Endocytosis: Analogies to Cell-Penetrating Peptides. *Biochemistry*

- ChemAxon (2011). Calculator Plugins were used for structure property prediction and calculation, Marvin 5.4.1.1, 2011, ChemAxon (<http://www.chemaxon.com>).
- Cheng, Y. F., Li, M. Y., Wang, S. R., Peng, H. J., Reid, S., Ni, N. T., Fang, H., Xu, W. F., Wang, B. H. (2010). Carbohydrate biomarkers for future disease detection and treatment. *Sci. China. Chem.* **53**, 3-20.
- Cho, S., Beintema, J. J., Zhang, J. (2005). The ribonuclease A superfamily of mammals and birds: identifying new members and tracing evolutionary histories. *Genomics* **85**, 208-220.
- Chung, D. E., Kratz, F. (2006). Development of a novel albumin-binding prodrug that is cleaved by urokinase-type-plasminogen activator (uPA). *Bioorg. Med. Chem. Lett.* **16**, 5157-5163.
- Clackson, T., Wells, J. A. (1995). A hot spot of binding energy in a hormone-receptor interface. *Science* **267**, 383-386.
- Cloninger, M. J. (2002). Biological applications of dendrimers. *Curr. Opin. Chem. Biol.* **6**, 742-748.
- Coezy, E., Borgna, J. L., Rochefort, H. (1982). Tamoxifen and metabolites in MCF7 cells: correlation between binding to estrogen receptor and inhibition of cell growth. *Cancer Res.* **42**, 317-323.
- Conner, S. D., Schmid, S. L. (2003). Regulated portals of entry into the cell. *Nature* **422**, 37-44.
- Cormier, S. A., Taranova, A. G., Bedient, C., Nguyen, T., Protheroe, C., Pero, R., Dimina, D., Ochkur, S. I., O'Neill, K., Colbert, D., Lombardi, T. R., Constant, S., McGarry, M. P., Lee, J. J., Lee, N. A. (2006). Pivotal Advance: eosinophil infiltration of solid tumors is an early and persistent inflammatory host response. *J. Leukoc. Biol.* **79**, 1131-1139.
- Costanzi, J., Sidransky, D., Navon, A., Goldsweig, H. (2005). Ribonucleases as a novel pro-apoptotic anticancer strategy: review of the preclinical and clinical data for ranpirnase. *Cancer Invest.* **23**, 643-650.

- Cuchillo, C. M., Nogues, M. V., Raines, R. T. (2011). Bovine Pancreatic Ribonuclease: 50 Years of the First Enzymatic Reaction Mechanism. *Biochemistry*
- D'Alessio, G., Di Donato, A., Parente, A., Piccoli, R. (1991). Seminal RNase: a unique member of the ribonuclease superfamily. *Trends Biochem. Sci.* **16**, 104-106.
- D'Alessio, G., Riordan, J. F., *Ribonucleases: Structures and Functions*. Academic Press: New York, 1997.
- Davis, A. M., Regan, A. C., Williams, A. (1988). Experimental charge measurement at leaving oxygen in the bovine ribonuclease A catalyzed cyclization of uridine 3'-phosphate aryl esters. *Biochemistry* **27**, 9042-9047.
- De Lamirande, G. (1961). Action of deoxyribonuclease and ribonuclease on the growth of Ehrlich ascites carcinoma in mice. *Nature* **192**, 52-54.
- De Lorenzo, C., Arciello, A., Cozzolino, R., Palmer, D. B., Laccetti, P., Piccoli, R., D'Alessio, G. (2004). A fully human antitumor immunoRNase selective for ErbB-2-positive carcinomas. *Cancer Res.* **64**, 4870-4874.
- Decensi, A., Robertson, C., Viale, G., Pigatto, F., Johansson, H., Kisanga, E. R., Veronesi, P., Torrisi, R., Cazzaniga, M., Mora, S., Sandri, M. T., Pelosi, G., Luini, A., Goldhirsch, A., Lien, E. A., Veronesi, U. (2003). A randomized trial of low-dose tamoxifen on breast cancer proliferation and blood estrogenic biomarkers. *J. Natl. Cancer Inst.* **95**, 779-790.
- delCardayré, S. B., Ribo, M., Yokel, E. M., Quirk, D. J., Rutter, W. J., Raines, R. T. (1995). Engineering Ribonuclease A: production, purification and characterization of wild-type enzyme and mutants at Gln11. *Protein Eng.* **8**, 261-273.
- Desta, Z., Ward, B. A., Soukhova, N. V., Flockhart, D. A. (2004). Comprehensive evaluation of tamoxifen sequential biotransformation by the human cytochrome P450 system in vitro: prominent roles for CYP3A and CYP2D6. *J. Pharmacol. Exp. Ther.* **310**, 1062-1075.
- Deutscher, S. L., Nuwayhid, N., Stanley, P., Briles, E. I., Hirschberg, C. B. (1984). Translocation across Golgi vesicle membranes: a CHO glycosylation mutant deficient in CMP-sialic acid transport. *Cell* **39**, 295-299.

- Dickson, K. A., Haigis, M. C., Raines, R. T. (2005). Ribonuclease inhibitor: Structure and function. *Prog. Nucleic Acid Res. Mol. Biol.* **80**, 349-374.
- Dickson, K. A., Raines, R. T. (2009). Silencing an inhibitor unleashes a cytotoxic enzyme. *Biochemistry* **48**, 5051-5053.
- Didenko, V. V., Ngo, H., Baskin, D. S. (2005). Polyethyleneimine as a transmembrane carrier of fluorescently labeled proteins and antibodies. *Anal Biochem* **344**, 168-173.
- Djanashvili, K., Frullano, L., Peters, J. A. (2005). Molecular recognition of sialic acid end groups by phenylboronates. *Chem. Eur. J.* **11**, 4010-4018.
- Dowlut, M., Dennis, G. (2006). An improved class of sugar-binding boronic acids, soluble and capable of complexing glycosides in neutral water. *J. Am. Chem. Soc.* **128**, 4226-4227.
- Dube, D. H., Bertozzi, C. R. (2005). Glycans in cancer and inflammation--potential for therapeutics and diagnostics. *Nat. Rev. Drug Discovery* **4**, 477-488.
- Dubowchik, G. M., Firestone, R. A., Padilla, L., Willner, D., Hofstead, S. J., Mosure, K., Knipe, J. O., Lasch, S. J., Trail, P. A. (2002). Cathepsin B-labile dipeptide linkers for lysosomal release of doxorubicin from internalizing immunoconjugates: model studies of enzymatic drug release and antigen-specific in vitro anticancer activity. *Bioconjug. Chem.* **13**, 855-869.
- Ellis, G. A., Hornung, M. L., Raines, R. T. (2011). Potentiation of ribonuclease cytotoxicity by a poly(amidoamine) dendrimer. *Bioorg. Med. Chem. Lett.* **21**, 2756-2758.
- Erickson, H. A., Jund, M. D., Pennell, C. A. (2006). Cytotoxicity of human RNase-based immunotoxins requires cytosolic access and resistance to ribonuclease inhibition. *Protein Eng. Des. Sel.* **19**, 37-45.
- Esfand, R., Tomalia, D. A. (2001). Poly(amidoamine) (PAMAM) dendrimers: from biomimicry to drug delivery and biomedical applications. *Drug Discov. Today* **6**, 427-436.
- Findlay, D., Herries, D. G., Mathias, A. P., Rabin, B. R., Ross, C. A. (1961). The active site and mechanism of action of bovine pancreatic ribonuclease. *Nature* **190**, 781-784.

- Fischer, D., Li, Y., Ahlemeyer, B., Krieglstein, J., Kissel, T. (2003). In vitro cytotoxicity testing of polycations: influence of polymer structure on cell viability and hemolysis. *Biomaterials* **24**, 1121-1131.
- Fischer, S., Nishio, M., Dadkhahi, S., Gansler, J., Saffarzadeh, M., Shibamiyama, A., Kral, N., Baal, N., Koyama, T., Deindl, E., Preissner, K. T. (2011). Expression and localisation of vascular ribonucleases in endothelial cells. *Thromb. Haemost.* **105**, 345-355.
- Fisher, B., Costantino, J. P., Wickerham, D. L., Cecchini, R. S., Cronin, W. M., Robidoux, A., Bevers, T. B., Kavanah, M. T., Atkins, J. N., Margolese, R. G., Runowicz, C. D., James, J. M., Ford, L. G., Wolmark, N. (2005). Tamoxifen for the prevention of breast cancer: current status of the National Surgical Adjuvant Breast and Bowel Project P-1 study. *J. Natl. Cancer Inst.* **97**, 1652-1662.
- Fredens, K., Dahl, R., Venge, P. (1991). In vitro studies of the interaction between heparin and eosinophil cationic protein. *Allergy* **46**, 27-29.
- Fuchs, S. M., Raines, R. T. (2004). Pathway for polyarginine entry into mammalian cells. *Biochemistry* **43**, 2438-2444.
- Fuchs, S. M., Raines, R. T. (2005). Polyarginine as a multifunctional fusion tag. *Protein Sci.* **14**, 1538-1544.
- Fuchs, S. M., Raines, R. T. (2006). Internalization of cationic peptides: the road less (or more?) traveled. *Cell Mol. Life. Sci.* **63**, 1819-1822.
- Fuchs, S. M., Raines, R. T. (2007). Arginine grafting to endow cell permeability. *ACS Chem. Biol.* **2**, 167-170.
- Fuchs, S. M., Rutkoski, T. J., Kung, V. M., Groeschl, R. T., Raines, R. T. (2007). Increasing the potency of a cytotoxin with an arginine graft. *Protein Eng. Des. Sel.* **20**, 505-509.
- Futami, J., Kitazoe, M., Maeda, T., Nukui, E., Sakaguchi, M., Kosaka, J., Miyazaki, M., Kosaka, M., Tada, H., Seno, M., Sasaki, J., Huh, N. H., Namba, M., Yamada, H. (2005). Intracellular delivery of proteins into mammalian living cells by polyethylenimine-cationization. *J. Biosci. Bioeng.* **99**, 95-103.

- Futami, J., Maeda, T., Kitazoe, M., Nukui, E., Tada, H., Seno, M., Kosaka, M., Yamada, H. (2001). Preparation of potent cytotoxic ribonucleases by cationization: enhanced cellular uptake and decreased interaction with ribonuclease inhibitor by chemical modification of carboxyl groups. *Biochemistry* **40**, 7518-7524.
- Futami, J., Nukui, K., Maeda, T., Kosaka, M., Tada, H., Seno, M., Yamada, H. (2002). Optimum modification for the highest cytotoxicity of cationized ribonuclease. *J. Biochem. (Tokyo)* **132**, 223-228.
- Futami, J., Seno, M., Ueda, M., Tada, H., Yamada, H. (1999). Inhibition of cell growth by a fused protein of human ribonuclease 1 and human basic fibroblast growth factor. *Protein Eng. Des. Sel.* **12**, 1013-1019.
- Futami, J., Yamada, H. (2008). Design of cytotoxic ribonucleases by cationization to enhance intracellular protein delivery. *Curr. Pharm. Biotechnol.* **9**, 180-184.
- Gadek, T. R., Nicholas, J. B. (2003). Small molecule antagonists of proteins. *Biochem. Pharmacol.* **65**, 1-8.
- Gao, Y., Gao, G., He, Y., Liu, T., Qi, R. (2008). Recent advances of dendrimers in delivery of genes and drugs. *Mini Rev. Med. Chem.* **8**, 889-900.
- Gennaro, A. R., *Remington: The Science and Practice of Pharmacy, 20th Edition*. Lippincott Williams & Wilkins: Baltimore, MD, 2000; p 2077.
- Greenway, M. J., Andersen, P. M., Russ, C., Ennis, S., Cashman, S., Donaghy, C., Patterson, V., Swingler, R., Kieran, D., Prehn, J., Morrison, K. E., Green, A., Acharya, K. R., Brown, R. H., Jr., Hardiman, O. (2006). ANG mutations segregate with familial and 'sporadic' amyotrophic lateral sclerosis. *Nat. Genet.* **38**, 411-413.
- Grubbs, F. E. (1969). Procedures for Detecting Outlying Observations in Samples. *Technometrics* **11**, 1-21.
- Guillot-Nieckowski, M., Eisler, S., Diederich, F. (2007). Dendritic Vectors for Gene Transfection. *New J. Chem.* **31**, 1111.

- Gutte, B., Merrifield, R. B. (1969). The total synthesis of an enzyme with ribonuclease A activity. *J. Am. Chem. Soc.* **91**, 501-502.
- Haigis, M. C., Kurten, E. L., Raines, R. T. (2003). Ribonuclease inhibitor as an intracellular sentry. *Nucleic Acids Res.* **31**, 1024-1032.
- Haigis, M. C., Raines, R. T. (2003). Secretory ribonucleases are internalized by a dynamin-independent endocytic pathway. *J. Cell Sci.* **116**, 313-324.
- Hayakawa, Y., Kawai, R., Hirata, A., Sugimoto, J. I., Kataoka, M., Sakakura, A., Hirose, M., Noyori, R. (2001). Acid/azole complexes as highly effective promoters in the synthesis of DNA and RNA oligomers via the phosphoramidite method. *J. Am. Chem. Soc.* **123**, 8165-8176.
- Hirs, C. H., Moore, S., Stein, W. H. (1960). The sequence of the amino acid residues in performic acid-oxidized ribonuclease. *J. Biol. Chem.* **235**, 633-647.
- Hoshimoto, S., Ueda, M., Jinno, H., Kitajima, M., Futami, J., Seno, M. (2006). Mechanisms of the growth-inhibitory effect of the RNase-EGF fused protein against EGFR-overexpressing cells. *Anticancer Res.* **26**, 857-863.
- Huai, Q., Mazar, A. P., Kuo, A., Parry, G. C., Shaw, D. E., Callahan, J., Li, Y., Yuan, C., Bian, C., Chen, L., Furie, B., Furie, B. C., Cines, D. B., Huang, M. (2006). Structure of human urokinase plasminogen activator in complex with its receptor. *Science* **311**, 656-659.
- Ishiguro, M., Hisako, T., Sakakibara, R., Yamaguchi, J., Aso, Y. (2002). A ricin B chain-ribonuclease A hybrid protein - (A new tool for introduction of a foreign protein into targeted cells). *J. Fac. Agric. Kyushu Univ.* **46**, 367-379.
- Iyer, S., Holloway, D. E., Kumar, K., Shapiro, R., Acharya, K. R. (2005). Molecular recognition of human eosinophil-derived neurotoxin (RNase 2) by placental ribonuclease inhibitor. *J. Mol. Biol.* **347**, 637-655.
- James, T. D., Phillips, M. D., Shinkai, S., *Boronic Acids in Saccharide Recognition*. Royal Society of Chemistry: 2006.



- Jay, J. I., Lai, B. E., Myszka, D. G., Mahalingam, A., Langheinrich, K., Katz, D. F., Kiser, P. F. (2009). Multivalent benzoboroxole functionalized polymers as gp120 glycan targeted microbicide entry inhibitors. *Mol. pharmaceutics* **7**, 116-129.
- Jiang, T., Olson, E. S., Nguyen, Q. T., Roy, M., Jennings, P. A., Tsien, R. Y. (2004). Tumor imaging by means of proteolytic activation of cell-penetrating peptides. *Proc. Natl. Acad. Sci. USA* **101**, 17867-17872.
- Johnson, R. J., Chao, T. Y., Lavis, L. D., Raines, R. T. (2007a). Cytotoxic ribonucleases: the dichotomy of Coulombic forces. *Biochemistry* **46**, 10308-10316.
- Johnson, R. J., Lin, S. R., Raines, R. T. (2006). A ribonuclease zymogen activated by the NS3 protease of the hepatitis C virus. *FEBS J.* **273**, 5457-5465.
- Johnson, R. J., McCoy, J. G., Bingman, C. A., Phillips, G. N., Jr., Raines, R. T. (2007b). Inhibition of human pancreatic ribonuclease by the human ribonuclease inhibitor protein. *J. Mol. Biol.* **368**, 434-449.
- Jones, A. T. (2007). Macropinocytosis: searching for an endocytic identity and role in the uptake of cell penetrating peptides. *J. Cell Mol. Med.* **11**, 670-684.
- Jones, W. (1920). The action of boiled pancreas extract on yeast nucleic acid. *J. Am. Physiol.* **52**, 203-207.
- Kartha, G. (1967). Tertiary structure of ribonuclease. *Nature* **214**, 234 passim.
- Ke, S. H., Coombs, G. S., Tachias, K., Corey, D. R., Madison, E. L. (1997). Optimal subsite occupancy and design of a selective inhibitor of urokinase. *J. Biol. Chem.* **272**, 20456-20462.
- Keck-UWCCC (2011). Small Molecule Screening Facility. [www.hts.wisc.edu](http://www.hts.wisc.edu)
- Kelemen, B. R., Klink, T. A., Behlke, M. A., Eubanks, S. R., Leland, P. A., Raines, R. T. (1999). Hypersensitive substrate for ribonucleases. *Nucleic Acids Res.* **27**, 3696-3701.

- Kelemen, B. R., Schultz, L. W., Sweeney, R. Y., Raines, R. T. (2000). Excavating an active site: the nucleobase specificity of ribonuclease A. *Biochemistry* **39**, 14487-14494.
- Khan, A. R., James, M. N. (1998). Molecular mechanisms for the conversion of zymogens to active proteolytic enzymes. *Protein Sci.* **7**, 815-836.
- Kim, J. S., Soucek, J., Matousek, J., Raines, R. T. (1995a). Catalytic activity of bovine seminal ribonuclease is essential for its immunosuppressive and other biological activities. *Biochem. J.* **308** ( Pt 2), 547-550.
- Kim, J. S., Soucek, J., Matousek, J., Raines, R. T. (1995b). Structural basis for the biological activities of bovine seminal ribonuclease. *J. Biol. Chem.* **270**, 10525-10530.
- Klink, T. A., Raines, R. T. (2000). Conformational stability is a determinant of ribonuclease A cytotoxicity. *J. Biol. Chem.* **275**, 17463-17467.
- Kobe, B., Deisenhofer, J. (1995). A structural basis of the interactions between leucine-rich repeats and protein ligands. *Nature* **374**, 183-186.
- Korostelev, A., Trakhanov, S., Laurberg, M., Noller, H. F. (2006). Crystal structure of a 70S ribosome-tRNA complex reveals functional interactions and rearrangements. *Cell* **126**, 1065-1077.
- Kratz, F., Muller, I. A., Ryppa, C., Warnecke, A. (2008). Prodrug strategies in anticancer chemotherapy. *ChemMedChem* **3**, 20-53.
- Krauss, J., Arndt, M. A., Dubel, S., Rybak, S. M. (2008). Antibody-targeted RNase fusion proteins (immunoRNases) for cancer therapy. *Curr. Pharm. Biotechnol.* **9**, 231-234.
- Kumar, A., Hozo, I., Wheatley, K., Djulbegovic, B. (2011). Thalidomide versus bortezomib based regimens as first-line therapy for patients with multiple myeloma: a systematic review. *Am. J. Hematol.* **86**, 18-24.
- Kunitz, M., McDonald, M. R., *Biochemical Preparations*. John Wiley & Sons: New York, 1953; p 128.

- Lagos-Quintana, M., Rauhut, R., Lendeckel, W., Tuschl, T. (2001). Identification of novel genes coding for small expressed RNAs. *Science* **294**, 853-858.
- Langer, R. (1990). New methods of drug delivery. *Science* **249**, 1527-1533.
- Lavis, L. D., Chao, T. Y., Raines, R. T. (2006). Fluorogenic label for biomolecular imaging. *ACS Chem. Biol.* **1**, 252-260.
- Lavis, L. D., Rutkoski, T. J., Raines, R. T. (2007). Tuning the pK(a) of fluorescein to optimize binding assays. *Anal Chem* **79**, 6775-6782.
- Layek, B., Mukherjee, B. (2010). Tamoxifen Citrate Encapsulated Sustained Release Liposomes: Preparation and Evaluation of Physicochemical Properties. *Sci. Pharm.* **78**, 507-515.
- Ledoux, L. (1955a). Action of ribonuclease on certain ascites tumours. *Nature* **175**, 258-259.
- Ledoux, L. (1955b). Action of ribonuclease on two solid tumours in vivo. *Nature* **176**, 36-37.
- Ledoux, L., Baltus, E. (1954). The effects of ribonuclease on cells of Ehrlich carcinoma. *Experientia* **10**, 500-501.
- Lee, J. E., Raines, R. T. (2008). Ribonucleases as novel chemotherapeutics : the ranpirnase example. *BioDrugs* **22**, 53-58.
- Lee, Y. J., Erazo-Oliveras, A., Pellois, J. P. (2010). Delivery of macromolecules into live cells by simple co-incubation with a peptide. *Chembiochem* **11**, 325-330.
- Leich, F., Stohr, N., Rietz, A., Ulbrich-Hofmann, R., Arnold, U. (2007). Endocytotic internalization as a crucial factor for the cytotoxicity of ribonucleases. *J. Biol. Chem.* **282**, 27640-27646.
- Leland, P. A., Raines, R. T. (2001). Cancer chemotherapy—ribonucleases to the rescue. *Chem. Biol.* **8**, 405-413.

- Leland, P. A., Schultz, L. W., Kim, B. M., Raines, R. T. (1998). Ribonuclease A variants with potent cytotoxic activity. *Proc. Natl. Acad. Sci. USA* **95**, 10407-10412.
- Leland, P. A., Staniszewski, K. E., Kim, B. M., Raines, R. T. (2001). Endowing human pancreatic ribonuclease with toxicity for cancer cells. *J. Biol. Chem.* **276**, 43095-43102.
- Liu, S., Aaronson, H., Mitola, D. J., Leppla, S. H., Bugge, T. H. (2003). Potent antitumor activity of a urokinase-activated engineered anthrax toxin. *Proc. Natl. Acad. Sci. USA* **100**, 657-662.
- Liu, S., Bugge, T. H., Leppla, S. H. (2001). Targeting of tumor cells by cell surface urokinase plasminogen activator-dependent anthrax toxin. *J. Biol. Chem.* **276**, 17976-17984.
- Lotfi, R., Lee, J. J., Lotze, M. T. (2007). Eosinophilic granulocytes and damage-associated molecular pattern molecules (DAMPs): role in the inflammatory response within tumors. *J. Immunother.* **30**, 16-28.
- Loudet, A., Han, J., Barhoumi, R., Pellois, J. P., Burghardt, R. C., Burgess, K. (2008). Non-covalent delivery of proteins into mammalian cells. *Org. Biomol. Chem.* **6**, 4516-4522.
- Lu, D. R., Oie, S., *Cellular Drug Delivery: Principles and Practice*. Humana: Totowa, New Jersey, 2004; p 392.
- Luzio, J. P., Pryor, P. R., Bright, N. A. (2007). Lysosomes: fusion and function. *Nat. Rev. Mol. Cell Biol.* **8**, 622-632.
- Mack, D. J., Brichacek, M., Plichta, A., Njardarson, J. T. (2009). Top 200 Pharmaceutical Prodrugs by Worldwide Sales in 2009; Source: Midas World Review, IMS Health Incorporated. *Journal*
- Mahalingam, A., Geonnotti, A. R., Balzarini, J., Kiser, P. F. (2011). Activity and Safety of Synthetic Lectins Based on Benzoboroxole-Functionalized Polymers for Inhibition of HIV Entry. *Mol. Pharm.*
- Makarov, A. A., Ilinskaya, O. N. (2003). Cytotoxic ribonucleases: Molecular weapons and their targets. *FEBS Lett.* **540**, 15-20.

- Malik, D. K., Baboota, S., Ahuja, A., Hasan, S., Ali, J. (2007). Recent advances in protein and peptide drug delivery systems. *Curr. Drug Deliv.* **4**, 141-151.
- Malik, N., Wiwattanapatapee, R., Klopsch, R., Lorenz, K., Frey, H., Weener, J. W., Meijer, E. W., Paulus, W., Duncan, R. (2000). Dendrimers: relationship between structure and biocompatibility in vitro, and preliminary studies on the biodistribution of 125I-labelled polyamidoamine dendrimers in vivo. *J. Control. Release* **65**, 133-148.
- Malisan, F., Testi, R. (2005). The ganglioside GD3 as the Greek goddess Hecate: several faces turned towards as many directions. *IUBMB Life* **57**, 477-482.
- Marshall, G. R., Feng, J. A., Kuster, D. J. (2008). Back to the future: ribonuclease A. *Biopolymers* **90**, 259-277.
- Matousek, J. (2001). Ribonucleases and their antitumor activity. *Comp. Biochem. Physiol.* **129C**, 175-191.
- Matousek, J., Soucek, J., Slavik, T., Tomanek, M., Lee, J. E., Raines, R. T. (2003). Comprehensive comparison of the cytotoxic activities of onconase and bovine seminal ribonuclease. *Comp. Biochem. Physiol. C Toxicol. Pharmacol.* **136**, 343-356.
- Matsumoto, A., Cabral, H., Sato, N., Kataoka, K., Miyahara, Y. (2010). Assessment of tumor metastasis by the direct determination of cell-membrane sialic acid expression. *Angew. Chem. Int. Ed.* **49**, 5494-5497.
- Matsumoto, A., Sato, N., Kataoka, K., Miyahara, Y. (2009). Noninvasive Sialic Acid Detection at Cell Membrane by Using Phenylboronic Acid Modified Self-Assembled Monolayer Gold Electrode. *J. Am. Chem. Soc.* **131**, 12022-12023.
- Merrifield, B. (1986). Solid phase synthesis. *Science* **232**, 341-347.
- Mikulski, S., Grossman, A., Carter, P., Shogen, K., Costanzi, J. (1993). Phase-I human clinical-trial of onconase(r) (p-30 protein) administered intravenously on a weekly schedule in cancer-patients with solid tumors. *Int. J. Oncol.* **3**, 57-64.

- Mitreá, D. M., Parsons, L. S., Loh, S. N. (2010). Engineering an artificial zymogen by alternate frame protein folding. *Proc. Natl. Acad. Sci. USA* **107**, 2824-2829.
- Moenner, M., Chauviere, M., Chevaillier, P., Badet, J. (1999). Basic homopolyamino acids, histones and protamines are potent antagonists of angiogenin binding to ribonuclease inhibitor. *FEBS Lett.* **443**, 303-307.
- Mohanty, C., Das, M., Kanwar, J. R., Sahoo, S. K. (2011). Receptor mediated tumor targeting: an emerging approach for cancer therapy. *Curr. Drug Deliv.* **8**, 45-58.
- Moore, S., Stein, W. H. (1973). Chemical structures of pancreatic ribonuclease and deoxyribonuclease. *Science* **180**, 458-464.
- Mosimann, S. C., Ardelt, W., James, M. N. (1994). Refined 1.7 Å X-ray crystallographic structure of P-30 protein, an amphibian ribonuclease with anti-tumor activity. *J. Mol. Biol.* **236**, 1141-1153.
- Mothana, S., Grassot, J. M., Hall, D. G. (2010). Multistep Phase Switch Synthesis by Using Liquid-Liquid Partitioning of Boronic Acids: Productive Tags with an Expanded Repertoire of Compatible Reactions. *Angew. Chem. Int. Ed.* **49**, 2883-2887.
- Mukherjee, S., Ghosh, R. N., Maxfield, F. R. (1997). Endocytosis. *Physiol. Rev.* **77**, 759-803.
- Munitz, A., Levi-Schaffer, F. (2004). Eosinophils: 'new' roles for 'old' cells. *Allergy* **59**, 268-275.
- Murphy, C. S., Langan-Fahey, S. M., McCague, R., Jordan, V. C. (1990). Structure-function relationships of hydroxylated metabolites of tamoxifen that control the proliferation of estrogen-responsive T47D breast cancer cells in vitro. *Mol. Pharmacol.* **38**, 737-743.
- Nakase, I., Niwa, M., Takeuchi, T., Sonomura, K., Kawabata, N., Koike, Y., Takehashi, M., Tanaka, S., Ueda, K., Simpson, J. C., Jones, A. T., Sugiura, Y., Futaki, S. (2004). Cellular uptake of arginine-rich peptides: roles for macropinocytosis and actin rearrangement. *Mol. Ther.* **10**, 1011-1022.
- Navarro, G., Maiwald, G., Haase, R., Rogach, A. L., Wagner, E., de Ilarduya, C. T., Ogris, M. (2010). Low generation PAMAM dendrimer and CpG free plasmids allow targeted and

- extended transgene expression in tumors after systemic delivery. *J. Control. Release* **146**, 99-105.
- Navarro, S., Aleu, J., Jimenez, M., Boix, E., Cuchillo, C. M., Nogues, M. V. (2008). The cytotoxicity of eosinophil cationic protein/ribonuclease 3 on eukaryotic cell lines takes place through its aggregation on the cell membrane. *Cell. Mol. Life Sci.* **65**, 324-337.
- Notomista, E., Mancheno, J. M., Crescenzi, O., Di Donato, A., Gavilanes, J., D'Alessio, G. (2006). The role of electrostatic interactions in the antitumor activity of dimeric RNases. *FEBS J.* **273**, 3687-3697.
- Nozaki, S., Endo, Y., Nakahara, H., Yoshizawa, K., Ohara, T., Yamamoto, E. (2006). Targeting urokinase-type plasminogen activator and its receptor for cancer therapy. *Anticancer Drugs* **17**, 1109-1117.
- O'Regan, R. M., Jordan, V. C. (2002). The evolution of tamoxifen therapy in breast cancer: selective oestrogen-receptor modulators and downregulators. *Lancet Oncol.* **3**, 207-214.
- Otsuka, H., Uchimura, E., Koshino, H., Okano, T., Kataoka, K. (2003). Anomalous binding profile of phenylboronic acid with N-acetylneuraminic acid (Neu5Ac) in aqueous solution with varying pH. *J. Am. Chem. Soc.* **125**, 3493-3502.
- Owens, D. E., 3rd, Peppas, N. A. (2006). Opsonization, biodistribution, and pharmacokinetics of polymeric nanoparticles. *Int. J. Pharm.* **307**, 93-102.
- Pal, A., BÈrubÈ, M., Hall, D. G. (2010). Design, Synthesis, and Screening of a Library of Peptidyl Bis (Boroxoles) as Oligosaccharide Receptors in Water: Identification of a Receptor for the Tumor Marker TF Antigen Disaccharide. *Angew. Chem. Int. Ed.* **49**, 1492-1495.
- Papageorgiou, A. C., Shapiro, R., Acharya, K. R. (1997). Molecular recognition of human angiogenin by placental ribonuclease inhibitor--an X-ray crystallographic study at 2.0 Å resolution. *EMBO J* **16**, 5162-5177.
- Park, C., Raines, R. T. (2000). Origin of the 'inactivation' of ribonuclease A at low salt concentration. *FEBS Lett.* **468**, 199-202.

- Parkinson-Lawrence, E. J., Shandala, T., Prodoehl, M., Plew, R., Borlace, G. N., Brooks, D. A. (2010). Lysosomal storage disease: revealing lysosomal function and physiology. *Physiology (Bethesda)* **25**, 102-115.
- Patil, S. D., Rhodes, D. G., Burgess, D. J. (2005). DNA-based therapeutics and DNA delivery systems: a comprehensive review. *AAPS J.* **7**, E61-77.
- Pavlakakis, N., Vogelzang, N. J. (2006). Ranpirnase--an antitumour ribonuclease: its potential role in malignant mesothelioma. *Expert Opin. Biol. Ther.* **6**, 391-399.
- Peng, Q., Chen, F., Zhong, Z., Zhuo, R. (2010). Enhanced gene transfection capability of polyethylenimine by incorporating boronic acid groups. *Chem. Commun.* **46**, 5888-5890.
- Plainkum, P., Fuchs, S. M., Wiyakrutta, S., Raines, R. T. (2003). Creation of a zymogen. *Nat. Struct. Biol.* **10**, 115-119.
- Polsky, R., Harper, J. C., Wheeler, D. R., Arango, D. C., Brozik, S. M. (2008). Electrically Addressable Cell Immobilization Using Phenylboronic Acid Diazonium Salts. *Angew. Chem. Int. Ed.* **120**, 2671-2674.
- Potenza, N., Salvatore, V., Migliozi, A., Martone, V., Nobile, V., Russo, A. (2006). Hybridase activity of human ribonuclease-1 revealed by a real-time fluorometric assay. *Nucleic Acids Res.* **34**, 2906-2913.
- Powles, T. J. (2003). Anti-oestrogenic chemoprevention of breast cancer-the need to progress. *Eur. J. Cancer* **39**, 572-579.
- Psarras, K., Ueda, M., Tanabe, M., Kitajima, M., Aiso, S., Komatsu, S., Seno, M. (2000). Targeting activated lymphocytes with an entirely human immunotoxin analogue: human pancreatic RNase1-human IL-2 fusion. *Cytokine* **12**, 786-790.
- Raines, R. T. (1998). Ribonuclease A. *Chem. Rev.* **98**, 1045-1065.
- Rapoport, M., Lorberboum-Galski, H. (2009). TAT-based drug delivery system--new directions in protein delivery for new hopes? *Expert Opin. Drug Deliv.* **6**, 453-463.



- Rautio, J., Kumpulainen, H., Heimbach, T., Oliyai, R., Oh, D., Jarvinen, T., Savolainen, J. (2008). Prodrugs: design and clinical applications. *Nat. Rev. Drug Discovery* **7**, 255-270.
- Rawat, A., Vaidya, B., Khatri, K., Goyal, A. K., Gupta, P. N., Mahor, S., Paliwal, R., Rai, S., Vyas, S. P. (2007). Targeted intracellular delivery of therapeutics: an overview. *Pharmazie* **62**, 643-658.
- Richard, J. P., Melikov, K., Brooks, H., Prevot, P., Lebleu, B., Chernomordik, L. V. (2005). Cellular uptake of unconjugated TAT peptide involves clathrin-dependent endocytosis and heparan sulfate receptors. *J. Biol. Chem.* **280**, 15300-15306.
- Riddles, P. W., Blakeley, R. L., Zerner, B. (1983). Reassessment of Ellman's reagent. *Methods Enzymol.* **91**, 49-60.
- Rizk, S. S., Luchniak, A., Uysal, S., Brawley, C. M., Rock, R. S., Kossiakoff, A. A. (2009). An engineered substance P variant for receptor-mediated delivery of synthetic antibodies into tumor cells. *Proc. Natl. Acad. Sci. USA* **106**, 11011-11015.
- Roberts, J. C., Bhalgat, M. K., Zera, R. T. (1996). Preliminary biological evaluation of polyamidoamine (PAMAM) Starburst dendrimers. *J. Biomed. Mater. Res.* **30**, 53-65.
- Roehrl, M. H., Wang, J. Y., Wagner, G. (2004). A general framework for development and data analysis of competitive high-throughput screens for small-molecule inhibitors of protein-protein interactions by fluorescence polarization. *Biochemistry* **43**, 16056-16066.
- Rono, B., Romer, J., Liu, S., Bugge, T. H., Leppla, S. H., Kristjansen, P. E. (2006). Antitumor efficacy of a urokinase activation-dependent anthrax toxin. *Mol. Cancer Ther.* **5**, 89-96.
- Rosenberg, H. F. (1998). The eosinophil ribonucleases. *Cell. Mol. Life Sci.* **54**, 795-803.
- Rosenberg, H. F. (2008). Eosinophil-derived neurotoxin / RNase 2: connecting the past, the present and the future. *Curr. Pharm. Biotechnol.* **9**, 135-140.
- Rothenberg, M. E., Hogan, S. P. (2006). The eosinophil. *Annu. Rev. Immunol.* **24**, 147-174.

- Rudolph, B., Podschun, R., Sahly, H., Schubert, S., Schroder, J. M., Harder, J. (2006). Identification of RNase 8 as a novel human antimicrobial protein. *Antimicrob. Agents Chemother.* **50**, 3194-3196.
- Rutkoski, T. J., Kink, J. A., Strong, L. E., Raines, R. T. (2011). Site-specific PEGylation endows a mammalian ribonuclease with antitumor activity. *Cancer Biol. Ther.* **12**, 208-214.
- Rutkoski, T. J., Kink, J. A., Strong, L. E., Schilling, C. I., Raines, R. T. (2010). Antitumor activity of ribonuclease multimers created by site-specific covalent tethering. *Bioconjug. Chem.* **21**, 1691-1702.
- Rutkoski, T. J., Kurten, E. L., Mitchell, J. C., Raines, R. T. (2005). Disruption of shape-complementarity markers to create cytotoxic variants of ribonuclease A. *J. Mol. Biol.* **354**, 41-54.
- Rutkoski, T. J., Raines, R. T. (2008). Evasion of ribonuclease inhibitor as a determinant of ribonuclease cytotoxicity. *Curr. Pharm. Biotechnol.* **9**, 185-189.
- Sashital, D. G., Venditti, V., Angers, C. G., Cornilescu, G., Butcher, S. E. (2007). Structure and thermodynamics of a conserved U2 snRNA domain from yeast and human. *RNA* **13**, 328-338.
- Saxena, S. K., Rybak, S. M., Winkler, G., Meade, H. M., McGray, P., Youle, R. J., Ackerman, E. J. (1991). Comparison of RNases and toxins upon injection into *Xenopus* oocytes. *J. Biol. Chem.* **266**, 21208-21214.
- Schmidt, N., Mishra, A., Lai, G. H., Wong, G. C. (2010). Arginine-rich cell-penetrating peptides. *FEBS Lett.* **584**, 1806-1813.
- Schultz, C. (2003). Prodrugs of biologically active phosphate esters. *Bioorg. Med. Chem.* **11**, 885-898.
- Schultz, L. W., Quirk, D. J., Raines, R. T. (1998). His...Asp catalytic dyad of ribonuclease A: structure and function of the wild-type, D121N, and D121A enzymes. *Biochemistry* **37**, 8886-8898.

- Sela, M., Anfinsen, C. B., Harrington, W. F. (1957). The correlation of ribonuclease activity with specific aspects of tertiary structure. *Biochim. Biophys. Acta.* **26**, 502-512.
- Shapiro, R., Riordan, J. F., Vallee, B. L. (1986). Characteristic ribonucleolytic activity of human angiogenin. *Biochemistry* **25**, 3527-3532.
- Shim, M. S., Kwon, Y. J. (2010). Efficient and targeted delivery of siRNA in vivo. *FEBS J.* **277**, 4814-4827.
- Shogen, K., Yoan, W. K. (1973). Antitumor activity in extracts of Leopard frog (*Rana pipiens*) embryos. *Journal*
- Sidenius, N., Blasi, F. (2003). The urokinase plasminogen activator system in cancer: recent advances and implication for prognosis and therapy. *Cancer Metastasis Rev.* **22**, 205-222.
- Sidhu, S. S., Fairbrother, W. J., Deshayes, K. (2003). Exploring protein-protein interactions with phage display. *Chembiochem* **4**, 14-25.
- Smith, B. D., Higgin, J. J., Raines, R. T. (2011). Site-specific folate conjugation to a cytotoxic protein. *Bioorg. Med. Chem. Lett.* **21**, 5029-5032.
- Smith, B. D., Raines, R. T. (2008). Genetic selection for peptide inhibitors of angiogenin. *Protein Eng. Des. Sel.* **21**, 289-294.
- Smith, B. D., Soellner, M. B., Raines, R. T. (2003). Potent inhibition of ribonuclease A by oligo(vinylsulfonic acid). *J. Biol. Chem.* **278**, 20934-20938.
- Smith, H. W., Marshall, C. J. (2010). Regulation of cell signalling by uPAR. *Nat. Rev. Mol. Cell Biol.* **11**, 23-36.
- Smith, M. R., Newton, D. L., Mikulski, S. M., Rybak, S. M. (1999). Cell cycle-related differences in susceptibility of NIH/3T3 cells to ribonucleases. *Exp. Cell. Res.* **247**, 220-232.
- Smyth, D. G., Stein, W. H., Moore, S. (1963). The sequence of amino acid residues in bovine pancreatic ribonuclease: revisions and confirmations. *J. Biol. Chem.* **238**, 227-234.

- Sonawane, N. D., Szoka, F. C., Jr., Verkman, A. S. (2003). Chloride accumulation and swelling in endosomes enhances DNA transfer by polyamine-DNA polyplexes. *J. Biol. Chem.* **278**, 44826-44831.
- Soncin, F., Strydom, D. J., Shapiro, R. (1997). Interaction of heparin with human angiogenin. *J. Biol. Chem.* **272**, 9818-9824.
- Sorrentino, S. (2010). The eight human "canonical" ribonucleases: molecular diversity, catalytic properties, and special biological actions of the enzyme proteins. *FEBS Lett.* **584**, 2194-2200.
- Sorrentino, S., Libonati, M. (1994). Human pancreatic-type and nonpancreatic-type ribonucleases: a direct side-by-side comparison of their catalytic properties. *Arch. Biochem. Biophys.* **312**, 340-348.
- Springsteen, G., Wang, B. (2002). A detailed examination of boronic acid-diol complexation. *Tetrahedron* **58**, 5291-5300.
- Stanley, P., Caillibot, V., Siminovitch, L. (1975). Selection and characterization of eight phenotypically distinct lines of lectin-resistant Chinese hamster ovary cell. *Cell* **6**, 121-128.
- Stella, V. J., Nti-Addae, K. W. (2007). Prodrug strategies to overcome poor water solubility. *Adv. Drug Delivery Rev.* **59**, 677-694.
- Su, A. I., Wiltshire, T., Batalov, S., Lapp, H., Ching, K. A., Block, D., Zhang, J., Soden, R., Hayakawa, M., Kreiman, G., Cooke, M. P., Walker, J. R., Hogenesch, J. B. (2004). A gene atlas of the mouse and human protein-encoding transcriptomes. *Proc. Natl. Acad. Sci. USA* **101**, 6062-6067.
- Su, Y., Ortiz, J., Liu, S., Bugge, T. H., Singh, R., Leppla, S. H., Frankel, A. E. (2007). Systematic urokinase-activated anthrax toxin therapy produces regressions of subcutaneous human non-small cell lung tumor in athymic nude mice. *Cancer Res.* **67**, 3329-3336.

- Sun, X., Zhang, N. (2010). Cationic polymer optimization for efficient gene delivery. *Mini Rev. Med. Chem.* **10**, 108-125.
- Suzuki, M., Saxena, S. K., Boix, E., Prill, R. J., Vasandani, V. M., Ladner, J. E., Sung, C., Youle, R. J. (1999). Engineering receptor-mediated cytotoxicity into human ribonucleases by steric blockade of inhibitor interaction. *Nat. Biotechnol.* **17**, 265-270.
- Tada, H., Onizuka, M., Muraki, K., Masuzawa, W., Futami, J., Kosaka, M., Seno, M., Yamada, H. (2004). Insertional-fusion of basic fibroblast growth factor endowed ribonuclease 1 with enhanced cytotoxicity by steric blockade of inhibitor interaction. *FEBS Lett.* **568**, 39-43.
- Taylorson, C. J., Eggelte, H. J., Tarragona-Fiol, A., Rabin, B. R., Boyle, F. T., Hennam, J. F., Blakey, D. C., Marsham, P. R., Heaton, D. W., Davies, D. H., Slater, A. M., Hennequin, L. F. A. Chemical compounds. Patent 5985281, Nov. 16, 1999.
- Terzyan, S. S., Peracaula, R., de Llorens, R., Tsushima, Y., Yamada, H., Seno, M., Gomis-Ruth, F. X., Coll, M. (1999). The three-dimensional structure of human RNase 4, unliganded and complexed with d(Up), reveals the basis for its uridine selectivity. *J. Mol. Biol.* **285**, 205-214.
- Testa, B., Mayer, J. M., *Hydrolysis in drug and prodrug metabolism : chemistry, biochemistry, and enzymology*. Wiley-VCH: Zürich ; Weinheim, 2003; p 780.
- Thompson, J. E., Kutateladze, T. G., Schuster, M. C., Venegas, F. D., Messmore, J. M., Raines, R. T. (1995). Limits to Catalysis by Ribonuclease A. *Bioorg. Chem.* **23**, 471-481.
- Thompson, J. E., Raines, R. T. (1994). Value of general acid-base catalysis to Ribonuclease A. *J. Am. Chem. Soc.* **116**, 5467-5468.
- Tomalia, D. A., Baker, H., Dewald, J., Hall, M., Kallos, G., Martin, S., Roeck, J., Ryder, J., Smith, P. (1985). A New Class of Polymers: Starburst-Dendritic Macromolecules. *Polym. J.* **17**, 117-132.
- Toogood, P. L. (2002). Inhibition of protein-protein association by small molecules: approaches and progress. *J. Med. Chem.* **45**, 1543-1558.

- Torchilin, V. P. (2006). Recent approaches to intracellular delivery of drugs and DNA and organelle targeting. *Annu. Rev. Biomed. Eng.* **8**, 343-375.
- Towne, V., Will, M., Oswald, B., Zhao, Q. (2004). Complexities in horseradish peroxidase-catalyzed oxidation of dihydroxyphenoxazine derivatives: appropriate ranges for pH values and hydrogen peroxide concentrations in quantitative analysis. *Anal. Biochem.* **334**, 290-296.
- Tsuji, T., Sun, Y., Kishimoto, K., Olson, K. A., Liu, S., Hirukawa, S., Hu, G. F. (2005). Angiogenin is translocated to the nucleus of HeLa cells and is involved in ribosomal RNA transcription and cell proliferation. *Cancer Res.* **65**, 1352-1360.
- Turcotte, R. F., Raines, R. T. (2008a). Design and characterization of an HIV-specific ribonuclease zymogen. *AIDS Res. Hum. Retroviruses* **24**, 1357-1363.
- Turcotte, R. F., Raines, R. T. (2008b). Interaction of onconase with the human ribonuclease inhibitor protein. *Biochem. Biophys. Res. Commun.* **377**, 512-514.
- Ui, N. (1971). Isoelectric points and conformation of proteins. I. Effect of urea on the behavior of some proteins in isoelectric focusing. *Biochim. Biophys. Acta.* **229**, 567-581.
- Vandenburg, Y. R., Zhang, Z. Y., Fishkind, D. J., Smith, B. D. (2000). Enhanced cell binding using liposomes containing an artificial carbohydrate-binding receptor. *Chem. Commun.* 149-150.
- Varki, A., Cummings, R. D., Esko, J. D., Freeze, H. H., Stanley, P., Bertozzi, C. R., Hart, G. W., *Essential of Glycobiology, second edition.* Cold Spring Harbor Laboratory Press, New York. 2009.
- Vasandani, V. M., Wu, Y. N., Mikulski, S. M., Youle, R. J., Sung, C. (1996). Molecular determinants in the plasma clearance and tissue distribution of ribonucleases of the ribonuclease A superfamily. *Cancer Res.* **56**, 4180-4186.
- Venturoli, D., Rippe, B. (2005). Ficoll and dextran vs. globular proteins as probes for testing glomerular permselectivity: effects of molecular size, shape, charge, and deformability. *Am. J. Physiol. Renal Physiol.* **288**, F605.

- Veronesi, U., Maisonneuve, P., Decensi, A. (2007). Tamoxifen: an enduring star. *J Natl Cancer Inst* **99**, 258-260.
- Vink, H., Duling, B. R. (1996). Identification of distinct luminal domains for macromolecules, erythrocytes, and leukocytes within mammalian capillaries. *Circ. Res.* **79**, 581-589.
- Vitseva, O., Flockhart, D. A., Jin, Y., Varghese, S., Freedman, J. E. (2005). The effects of tamoxifen and its metabolites on platelet function and release of reactive oxygen intermediates. *J. Pharmacol. Exp. Ther.* **312**, 1144-1150.
- Voet, D., Voet, J. G., *Biochemistry*. John Wiley & Sons: 2004; p 1178.
- Wang, B., Siahaan, T., Soltero, R., *Drug Delivery: Principles and Applications*. John Wiley & Sons, Inc.: 2005a; p 464.
- Wang, Z., Zhang, L., Lu, J. (2005b). Analysis of the interactions of ribonuclease inhibitor with kanamycin. *J. Mol. Model.* **11**, 80-86.
- Wang, Z. X. (1995). An exact mathematical expression for describing competitive binding of two different ligands to a protein molecule. *FEBS Lett* **360**, 111-114.
- Weickmann, J. L., Olson, E. M., Glitz, D. G. (1984). Immunological assay of pancreatic ribonuclease in serum as an indicator of pancreatic cancer. *Cancer Res.* **44**, 1682-1687.
- Westmark, P. R., Smith, B. D. (1996). Boronic acids facilitate the transport of ribonucleosides through lipid bilayers. *J. Pharm. Sci.* **85**, 266-269.
- Witmer, M. R., Falcomer, C. M., Weiner, M. P., Kay, M. S., Begley, T. P., Ganem, B., Scheraga, H. A. (1991). U-3'-BCIP: a chromogenic substrate for the detection of RNase A in recombinant DNA expression systems. *Nucleic Acids Res.* **19**, 1-4.
- Wlodawer, A., Svensson, L. A., Sjolín, L., Gilliland, G. L. (1988). Structure of phosphate-free ribonuclease A refined at 1.26 Å. *Biochemistry* **27**, 2705-2717.

- Wolf, P. L., Horwitz, J. P., Freisler, J., Vazquez, J., Von der Muehl, E. (1968). Application of the indigogenic principle for the histochemical demonstration of ribonuclease. *Experientia* **24**, 1290-1291.
- Wu, W., Mitra, N., Yan, E. C., Zhou, S. (2010). Multifunctional hybrid nanogel for integration of optical glucose sensing and self-regulated insulin release at physiological pH. *ACS Nano* **4**, 4831-4839.
- Yamamura, T., Ueda, M., Psarras, K., Suwa, T., Watanaabe, Y., Kameyama, N., Tanabe, M., Imamura, H., Kitajima, M. (2002). Immunosuppressive and anticancer effect of a mammalian ribonuclease that targets high-affinity interleukin-2-receptors. *Eur. J. Surg.* **168**, 49-54.
- Yang, W., Fan, H., Gao, X., Gao, S., Karnati, V. V., Ni, W., Hooks, W. B., Carson, J., Weston, B., Wang, B. (2004). The first fluorescent diboronic acid sensor specific for hepatocellular carcinoma cells expressing sialyl Lewis X. *Chem. Biol.* **11**, 439-448.
- Zhang, J., Dyer, K. D., Rosenberg, H. F. (2003). Human RNase 7: a new cationic ribonuclease of the RNase A superfamily. *Nucleic Acids Res.* **31**, 602-607.
- Zhang, J. H., Chung, T. D., Oldenburg, K. R. (1999). A Simple Statistical Parameter for Use in Evaluation and Validation of High Throughput Screening Assays. *J. Biomol. Screen.* **4**, 67-73.
- Zhao, X., Li, H., Lee, R. J. (2008). Targeted drug delivery via folate receptors. *Expert Opin. Drug Deliv.* **5**, 309-319.
- Zheng, A., Kallio, A., Harkonen, P. (2007). Tamoxifen-induced rapid death of MCF-7 breast cancer cells is mediated via extracellularly signal-regulated kinase signaling and can be abrogated by estrogen. *Endocrinology* **148**, 2764-2777.
- Zhong, X., Bai, H. J., Xu, J. J., Chen, H. Y., Zhu, Y. H. (2010). A Reusable Interface Constructed by 3 Aminophenylboronic Acid Functionalized Multiwalled Carbon Nanotubes for Cell Capture, Release, and Cytosensing. *Adv. Funct. Mater.* **20**, 992-999.